Towards the Design of Highly Selective Molecularly Imprinted Hydrogels for Biosensor Applications

by

Lorena R. Padró Cortés

A thesis submitted in partial fulfillment of the requirements for the degree of

DOCTOR OF PHILOSOPHY
in
CHEMICAL ENGINEERING

UNIVERSITY OF PUERTO RICO
MAYAGÜEZ CAMPUS
2009

Approved by:

_____	_____
Carlos Rinaldi, PhD Member, Graduate Committee	Date
_____	_____
Juan Lopez Garriga, PhD Member, Graduate Committee	Date
_____	_____
Eduardo Juan, PhD Member, Graduate Committee	Date
_____	_____
Madeline Torres Lugo, PhD President, Graduate Committee	Date
_____	_____
Maria Aponte, PhD Representative of Graduate Studies	Date
_____	_____
David Suleiman, PhD Chairperson of the Department and Member, Graduate Committee	Date

ABSTRACT

Robust molecular recognition is essential to enhance the accuracy of diagnostic devices aiming for a better efficacy in the clinical treatment of patients. The molecular imprinting technique has gained attention to generate novel biosensor and clinical diagnostic devices with high sensitivity and specificity, which demonstrated affinities compared to their natural counterparts. A method for the rational design of biomimetic sensors based on molecularly imprinted polymer for the detection of hydrocortisone is described and applied. The thermodynamic of the association between hydrocortisone and the functional monomer, methacrylic acid (MAA) was investigated by nuclear magnetic resonance (NMR) spectroscopy. Dissociation constants for the complex formation between hydrocortisone and a functional monomer analogue, acetic acid, as a function of solvent nature were estimated by NMR titration. The results demonstrate lower affinity using ethanol as solvent (K=0.5814±0.0.1163 M). However, the formation of adduct was confirmed, which suggested creation of MAA-Hydrocortisone at the pre-polymeric mixture. The stoichiometry of the complex formation between hydrocortisone and an acetic acid on each solvent was evaluated by the Job method of continuous variation. Dimethyl sulfoxide and ethanol were selected as porogens to assess solvent effect. The dissociation constants obtained for ethanol-d_6 reflected a greater proximity of interaction between solution adducts compared to dimethyl sulfoxide-d_6. It is

consequently associated by the dielectric constant of the solvents. Job plot results suggested a complex mole ratio of 1.5:1 and 1:2 for dimethyl sulfoxide-d_6 and ethanol-d_6, respectively. The collective analysis of NMR titration and Job plot method indicated the extent of shift displacement is proportional to the proximity to the interaction site that is not apparently associated with its stoichiometric capabilities of complex formation. To evaluate synthesis condition, *in situ* free radical copolymerization was monitored by ATR-FTIR spectroscopy with methacrylic acid (MAA) as the functional monomer and tetra(ethylene glycol) dimethacrylate (TEGDMA) as the crosslinking agent in different solvents. The synthesis was performed in presence and absence of the template molecule. The combined set of analysis allowed a better understanding of the recognition events giving rise to the imprinting effect during MIP synthesis and to ligand-MIP binding events. In situ polymerization results demonstrated a delay of the auto-acceleration during the imprinting process. In essence, the propagation kinetic was reduced by the decrease of monomer mobility, which suggested the functional monomer-template complexation already confirmed by the NMR spectroscopic studies. Consequently, the information was to be applied for the design of thin films MIP. It can be for seen that using this information, the collapse-swelling transition of MIPs could be programmed to promote binding capabilities and enhance template diffusion. To these aims, hydrocortisone imprinted polymers were synthesized in aqueous media. The feasibility of hydrogel-based MIPs was evaluated by measuring equilibrium

swelling, structural parameters (e.g. mesh size, ξ) and template permeation as function of pH and copolymer composition. The MIP characterization results demonstrated an increase of template permeation directly influenced by mesh size at pH equal to 5.5 at 37°C and ionic strength of 0.1M. A different behavior was shown for the characterization at pH equal to 6.0 at 37°C and ionic strength of 0.1M. A reduction was observed on the permeability coefficient for MIP with a MAA/EGDMA ratio of 17:1. It suggested the influence of MIP-ligand binding on hydrocortisone transport through the polymeric network synthesized by molecular imprinting technique based on the permeation reduction. In order to confirm this hypothesis, the binding constant (b) was estimated from the slope (15.17309 M^{-1}) of linear regression of the Langmuir isotherm and the saturation capacity (q_s = 0.09128) from its intercept (1.385). In addition, the hydrocortisone rebinding to 17:1 MIP was confirmed with the electroconductivity results of MIP 17:1, which demonstrated higher sensitivity toward hydrocortisone in comparison to non-MIP. Overall, this work reported the evaluation of the principal factors affecting the stabilization of functional monomer-template complex before and during the imprinting process, which provides essential information for the rational design of molecularly imprinted polymers. In addition, the sensitivity of imprinted gels confirmed the presence of binding sites.

RESUMEN

El reconocimiento molecular es esencial para mejorar la precisión de equipos para el diagnóstico mejorando así la eficacia del tratamiento clínico de los pacientes. La técnica de impresión molecular ha ganado la atención para el desarrollo de biosensores y sistemas de diagnostico clínico. Los mismos se caracterizan por tener alta sensitividad y especificidad que demuestran tener afinidades comparables con los anticuerpos. El diseño racional de un biosensor basado en polímeros de impresión molecular es descrito y fue demostrado. La asociación termodinámica entre hidrocortisona y el monómero funcional ácido metacrílico fue investigada utilizando espectroscopia de resonancia magnética nuclear (NMR). La constante de disociación para el complejo formado por hidrocortisona y el monómero análogo, ácido acético, como función de la naturaleza de solvente fue estimado por titilación de NMR. Los resultados demostraron menor afinidad al utilizar etanol como solvente ($K=0.5814\pm0.0.1163/M$). Aun así, los resultados sugieren es la formación de los complejos MAA-hidrocortisona en la solución pre-polimérica al utilizar etanol como solvente. Esto es favorable para utilizar etanol eventualmente para la síntesis de estos polímeros. La estequiometría de la formación del complejo se estimó con el método de variación continua. Los solventes evaluados fueron sulfóxido de dimetilo y etanol. La constante de disociación evaluada para etanol refleja menor proximidad entre los grupos funcionales durante la formación del complejo de MAA-hidrocortisona. Los gráficos de Job sugieren la formación de los complejos cuya

razón son de 2:1 y de 1:2 para sulfóxido de dimetilo y etanol, respectivamente. La evaluación de la síntesis de impresión molecular se efectuó monitoreando la polimerización por radical libre utilizando espectroscopia de infrarrojo. La polimerización de ácido metacrílico con dimetacrilato de glicol de etileno fue evaluada en varios solventes y en la presencia de la molécula modelo, hidrocortisona. La evaluación de los resultados demuestra un retraso en la auto-aceleración con la presencia de la molécula modelo en la síntesis del polímero. Esto sugiere que el complejo se mantiene ya que la movilidad del monómero funcional (MAA) es reducida al estar interactuando con la molécula modelo (hidrocortisona) lo cual fue confirmado con los estudios de espectroscopia de resonancia magnética nuclear. Esta información fue utilizada para diseñar polímeros de impresión molecular de tipo capa fina programados para promover capacidades de enlace con la molécula modelo y de esta misma forma mejorar su difusión a través de la membrana. Con este propósito, se sintetizaron polímeros de impresión molecular para la detección de hidrocortisona en fase acuosa. Para evaluar la viabilidad de los polímeros, estos se caracterizaron para determinar su capacidad de hinchamiento, tamaño de poro (ξ) y capacidad de permeabilidad como función de pH y composición del polímero. La caracterización de los polímeros de impresión molecular demostró que aumento en la permeabilidad de la molécula modelo el cual fue influenciado por el tamaño del poro y el ambiente químico observado a pH igual a 5.5 y 6.0 con fuerza iónica de 0.1 M. Por otro lado, un comportamiento diferente

fue observado a pH 6.0. El coeficiente de permeabilidad se redujo al utilizar el polímero de impresión molecular con una razón de MAA/EGDMA de 17:1. Los resultados sugieren la influencia del enlace entre el ligando (hidrocortisona) y el polímero de impresión molecular en el transporte de hidrocortisona a través de la membrana. Esto debido a la creación de lugares de reconocimiento molecular luego de la síntesis utilizando la técnica de impresión molecular. Con el propósito de confirmar la hipótesis, la constante de enlace y la capacidad de saturación del polímero de impresión molecular 17:1 fueron estimadas realizando experimentos de enlaces. Los datos de estos experimentos fueron ajustados al modelo de Langmuir lineal para obtener de la pendiente la constante de enlace (15.17309 M^{-1}) y del intercepto calcular la capacidad de saturación (0.09128). La hipótesis de que la permeabilidad se redujo debido a la interacción de hidrocortisona con el polímero de impresión molecular fue confirmada con las pruebas electroconductividad donde el polímero de impresión molecular 17:1 que demostraron mayor sensitividad a hidrocortisona al compararla con los polímeros de referencia. En conclusión, este trabajo reporta el avalúo de los principales factores que afectan la estabilización del complejo de MAA-hidrocortisona antes y durante la síntesis de impresión molecular. Esta información es vital para el diseño racional de polímeros de impresión molecular con el objetivo de mejorar su selectividad y sensitividad en fase acuosa.

.

To our Lord who gave me the gift of life and different talents in order to serve my community.
To my family (aunts, grandmothers, grandfathers, cousin, uncles, friends, and more) who have always encouraged me.
To my mother, Sara and my father, Lorenzo who showed me the value of love, work and service.
To my sisters, Mayra and Sara; and my brother, Omar, who inspired my desire of living in community.
To my daughter, Kamille Isabel and my son, Yosef Isaías, who increased my hope in humanity and my need to contribute.
To my beloved husband, David, who chose to share with me his adventure of life and gave me the strength to succeed and to become a better human being.

ACKNOWLEDGEMENTS

I express my appreciation to Dr. Madeline Torres-Lugo, my advisor for her appraisal and guidance. I am thankful for all the suggestions and comments received from my graduate committee: Dr. David Suleiman, Dr. Carlos Rinaldi, Dr. Lopez Garriga, Dr. Eduardo Juan and Dr. María Aponte. I also appreciate the collaboration of Dr. Meléndez and his technical discussion during the NMR studies. It is also necessary to mention the support given by Dr. José Colluci during the beginning of my doctoral career. Thank you for your professional and enthusiastic counseling. I am proud to acknowledge the extended technical discussion with Maria Gabriela, Omar Viera, Magally Arocho, Margarita Licha, Julio Cartagena, Nilmarie Santos, Rafael Mendez, Aracelis Cardona, Milton Rivera, Hector Luis Rodríguez, Celimar Valentin, Carlos Ortega, Victoria Calero, Nilmarie Santos, Ramón, and Brenda. I express my appreciation to Celimar Valentin for exploring science and motivating my critical thinking. I'd like to acknowledge Ramón, Bedalin, Frances Gratacós, Adriana Reyes, Tania, and David Jiménez. All of them were undergraduate students that worked within the scope of this project and proposed ideas for the success of this research. I owe a major debt of gratitude to Aixa Lebrón and Sindia Rivera who supported me and encouraged my role as enthusiastic mother and a professional woman.

I gratefully thank Juan Carlos Saez Miranda for his encouragement and professional advice during the development of this dissertation. I will also like to thank LifeScan Products, LLC and the Web Printing team for the opportunity to participate in the Technology Transfer of One Touch® Ultra™ Strip and his support at the final stage of this project. I owe a major debt of gratitude to Myrna who gave me words of hope during the correction process of this dissertation.

Finally, I greatly thank my husband David, my daughter Kamille Isabel and my son Yosef Isaías for their tolerance, faith, sympathy, and patience during the accomplishment of our goal to complete this PhD.

Puerto Rico, 2009

Lorena Padro-Cortes

Table of Contents

Table List

Tables **Page**

Figure List

Figures **Page**

CHAPTER 1

1 Introduction

Biosensor technology has emerged significantly within the fields of drug discovery, clinical diagnostics, environmental analysis, food analysis, and production monitoring [1]. Its convenience for self-testing, small size, fast response, sensitivity and specificity are key factors for the continuous development of biosensors[2]. A biosensor is a self-contained integrated device, which is capable of providing specific quantitative and semi-quantitative analytical information when employing a biological receptor in combination with a transducer. Molecular imprinting has been an essential technique to generate novel high affinity materials that are employed as recognition elements for biosensor devices. Chemical sensors based on molecularly imprinted polymers (MIP) were developed for the detection of pesticides, sugars, nucleic acids, amino acid derivatives, drugs, toxins, steroids, proteins, and cells [3, 4].

Although the idea behind molecular imprinting may be simple in terms of sequential stages, it is a complex phenomenon involved in the formation of selective and stable recognition abilities within the imprinted material. Significant effort has been devoted to optimize MIP design. One of the challenges is the extensive and iterative characterization required to understand the binding affinity and selectivity abilities of MIP. Technical reports have shown that MIP affinity and selectivity are strongly influenced by functional group orientation toward the template molecule and the shape of the recognition site formed during the synthesis of the imprinted

material[5]. Consequently, the imprinting conditions (e.g. type of monomer, porogen, monomer/crosslinker ratio, initiation methodology, synthesis temperature and pressure) employed during the synthesis in order to incorporate the template molecule whithin the imprinted material have shown to play an important role in the generation of MIP-ligand selective recognition. Several examples of the approaches that have been proposed to optimize MIP performance are: a) enhance the MIP-ligand binding process[6], b) MIP production automation[7], and c) major insight to the molecular imprinting phenomena[8]. The above mentioned approach requires that the scientific research be focused towards the better understanding of the main mechanisms underlying MIP formation and/or MIP-ligand binding. Combinatorial chemistry, computational simulation, chemometrics and spectroscopic assessments (e.g. ^{1}H NMR spectroscopy, UV spectroscopy, and FTIR spectroscopy) have demonstrated to be vital tools on this regard [7, 9-11] [10, 12]. The intention is to predict the MIP-ligand binding abilities during MIPs design to rapidly screen the most critical parameters (e.g., monomer/crosslinker ratio, template/functional monomer ratio, porogen selection, synthesis condition, MIP-ligand rebinding condition) to achieve the desired affinity and selectivity during their applications. These research findings suggest the need to rationally design imprinted materials by the correlation of MIP formation with MIP-ligand rebinding.

To this aim a method for the rational design of a biomimetic sensor based on molecularly imprinted polymers is described and applied using hydrocortisone as a

model template. This method focuses on the optimization of imprinting conditions in terms of template/functional monomer ratio, monomer/crosslinker ratio, porogen properties (i.e. the characteristics of the solvent employed during the MIP synthesis), and synthesis kinetics[13]. For this purpose, a combination of spectroscopic techniques (e.g. NMR spectroscopy and ATR-FTIR spectroscopy) was utilized to monitor the molecular imprinting process starting with the complex formation through MIP synthesis (Chapter 4). In addition, the MIPs were synthesized and characterized to evaluate the MIP-ligand binding process (Chapter 5).

The main objective of this dissertation is to establish a basis for molecular imprinting rational design that will be employed in an aqueous environment. Recently a widespread interest in MIP technology has emerged and is reflected in the increasing number of publications. The diverse applications of the molecular imprinted material make them prominent for the market of separation, catalysis, sensor and assay. The applications were extended to tissue engineering, drug delivery system, drug discovery and drug targeting, which required the rational design of MIP for an aqueous media. The essential advances that have been done in each application are discussed in Chapter 2. This chapter will also discuss the fundamental aspect of the molecular imprinting technique, which includes the critical factors to optimize the synthesis of imprinted polymers. The chapter 2 will finish pointing out the challenges that tend to encourage researchers for the innovation within the molecular imprinting technique. The subsequent chapter 3 will present the

research scope and the specific objectives to achieve the principal research goal. Overall, Chapters 4 and 5 will present the characterization of the imprinting process starting with the functional monomer-template complex formation, followed by the MIP synthesis and ending with the evaluation of MIP-ligand binding. A conclusion and future prospective for the molecular imprinting is presented on Chapter 6.

It is induced from the topic discussion that the technique includes aspects of chemical equilibrium, molecular recognition theory, thermodynamics, polymer science, enzyme kinetics, and transport phenomena. Consequently, the interdisciplinary contribution of several disciplines such as chemistry, chemical engineering, material science, biomedical engineering, biotechnology and bioengineering will emerge in the commercialization of the imprinted material in the near future.

The principal aspects associated with molecular imprinting are reviewed in the following sections.

CHAPTER 2

2 BACKGROUND

Molecular recognition has demonstrated to be an essential event in biochemical processes that follow highly specific pathways. Enzyme catalyzed reactions and antibody-antigen systems reveal how the biomolecules proceed in an organized sequence in biochemical processes using their functionalized properties. As a consequence, they control and regulate essential bioprocesses. Metabolic pathways are highly coordinated due to the formation of supramolecular complexes. These complexes are generated by the contribution of various ionic, hydrogen-bonding, hydrophobic and van der Waals interactions[14].

A particular interest has emerged on the development of biomaterials capable of molecular recognition. Prominent research activities have focused on optimizing the synthesis conditions of advanced materials with similar affinity and specificity compared to natural ligands[15]. Molecular imprinting (MI) has become an important technique for the assembly of polymeric artificial receptors, which mimics antibody-antigen or enzyme mechanisms[16]. Imprinted polymers have demonstrated to be robust and stable thus making them suitable and effective in acid or organic environments and in extreme conditions of temperature and pressure. In addition, they are easily produced, restored and reused.[17].

Although the molecular imprinting process involves simple sequences, it is influenced by several factors that have a direct impact on MIP performance.

Imprinted materials should possess structural stiffness, high structural flexibility, and good accessibility to the binding sites in order to promote the MIP-ligand rebinding. The monomer/crosslinker ratio, amount of porogen and initiator, synthesis conditions (e.g. temperature, pressure), reaction time, initiation mechanism (i.e. photochemical or thermal), and other factors are considered and investigated during the optimization of MIP selectivity and its affinity [13]. Certainly, the evaluation of the physical mechanism underlying MIP formation and MIP-ligand binding will assist in the design and application of new and improved MIP systems.

In order to understand the wide range of possibilities that exist during the MIPs design, the following sections will review the fundamental aspects of molecular imprinting and its potential applications.

2.1 Principles of Molecular Imprinting

Molecular imprinting (MI) has emerged as a technique to develop high affinity materials. The affinity produced by MI can be compared to those of the antibody-antigen systems denoting them as antibody or enzyme mimics[18]. Consequently, the formation of an active site on the MIP should contain essential characteristics to achieve binding affinity similar to those reported by natural counterparts. The recognition sites are complemented by a defined shape and the presence of functional moieties to provide a suitable catalytic active environment. Accordingly, the synthesis of imprinted material is performed in the presence of target molecules to promote the assembly of functional monomer-template complexes. Functional

monomers orient the functional groups toward the template molecules by a self-assembly technique (i.e. non covalent approach) or pre-organized mechanism (i.e. covalent approach). The spatial orientation and the solution adduct between the functional monomer and the template molecule are fixed by the utilization of a crosslinking agent during the imprinting process. The eventual removal of the template molecule after the synthesis will generate recognition sites with binding affinity towards the template molecule [19] (see Figure 2.1). Certainly, the imprinting technique has induced a stereo-specific characteristic, which makes the imprinted material versatile for drug discovery, catalytic reaction, drug targeting, and therapeutic diagnostics.

The molecular imprinting technique found its beginnings in the 1940s when silica gels were prepared by procedures analogous to the formation of antibodies. Dickey polymerized sodium silicate in the presence of a dye. The dye was subsequently removed, and a rebinding experiment demonstrated that the patterned molecule bound in preference to other dyes[20]. In 1972, the research group of Klotz and Wulff[21] introduced independently the formation of synthetic polymers through covalent interactions. Non-covalent and metal mediated complexes are examples of subsequent self-assembly approaches utilized to diversify the synthesis of molecularly imprinted polymers.

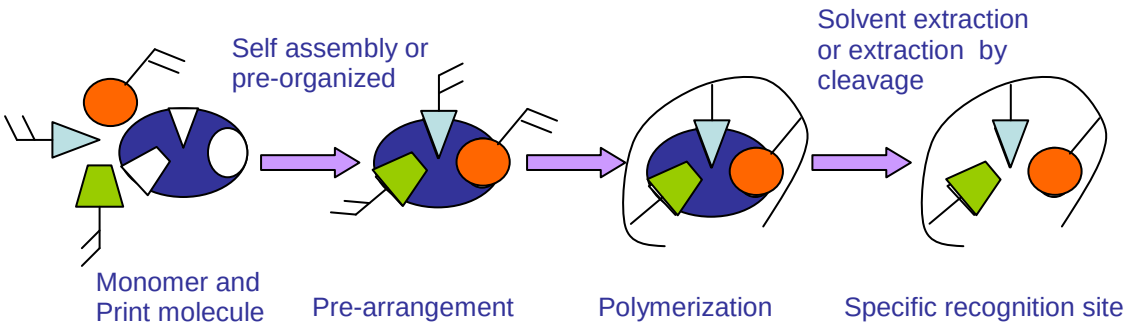

Figure 2.1 Schematic representation of molecular imprinting procedure

Non-covalent imprinting was introduced by Mosbach et al[22] as a potential technique to develop MIP in the early 1980s. Mosbach and collaborators fabricated phenylalanine ethyl ester selective polymers that demonstrated high affinity toward the template molecule. Belokon and collaborators pioneered the MIP synthesis based in metal coordination[23]. The study used A-bis[N-(5-methacryloylamino)salicylidene-S-norsalinate] Co(III) complexes as the metal complexing monomer. After several decades of studies, covalent imprinting has demonstrated to generate more homogenous binding sites. However, non-covalent imprinting is more attractive because of the simplicity of its preparation and that MIP applications are expanded to several template molecules. [24-26]. In recent years, non-covalent and covalent imprinting have been combined to achieve the fortitude of each mechanism.

The major advantage of imprinted polymers relies on their good thermal, chemical and mechanical stability compared to natural biomolecules that are not effective under extreme conditions (e.g. organic solvents, acidic/basic solutions, and high temperature)[27]. Furthermore, MIP has demonstrated long shelf life. Certainly, it is crucial to rationally design their morphology to obtain imprinted structures with good accessibility, integrity and stability of the recognition sites. The catalytic efficiency is influenced by the ability of the template molecule to access the binding sites. Equally important is to obtain stable binding cavities to maintain the integrity of the functional monomer-template assembly. Eventually, the binding abilities of the

material are also affected by the degree of swelling of the material and polymer porosity. Both properties are defined by the morphology that results from the imprinting synthesis.

In order to understand the factors that influenced the MIP binding properties, a more in depth discussion relating the synthesis and the role of the functional monomer-template during MIP fabrication is further developed (Refer to section 2.5, 2.6 and 2.7).

2.2 Applications of Molecularly Imprinted Polymers

Certainly, molecularly imprinted materials have increased their forthcoming usage due to their high affinity and selectivity, chemical and physical stability, in addition to the reproducibility and simplicity of their preparation method [3]. They have been relevant to the development of separation systems, immunoassay, artificial catalysts, artificial enzymes, and sensors. The following sections discuss the actual and further potential applications for molecularly imprinted materials.

2.2.1 Enantiomers and Drug Separations

Molecular imprinting was introduced in 1949 by Dickey's experiments with silica gels[20] in search of an alternative absorption material. Dickey's findings motivated Curti et al [28] to employ imprinted silicas as a solid phase in the chromatographic separation of mandelic acid and camphorsulphonic acid

enantiomers. Furthermore, the application of molecular imprinting in synthetic organic polymers has provided the means for the development of a novel stationary phase systems with high adsorption selectivity. Liquid chromatography, capillary electrophoresis, capillary electrochromatography, and solid phase extraction are typical examples where MIPs have been used as selective stationary phases [29, 30].

A series of enantioselective imprinted polymers were prepared for the resolution of L- and D-isomers of CBz-Asp in polar and organic eluents[31]. A selection of sugar-containing vinyl monomers, such as methyl-α-D-glucopyranoside-6-acrylate, was considered for the synthesis of MIP using dimethylformamide (DMF) as the solvent. The recognition capabilities were evaluated by high performance liquid chromatography (HPLC). Higher retention values of the imprinted template reflected the binding strength and the complementary size of the imprinted site on the stationary phase. The results demonstrated significant selectivity toward the imprinted L- and D-isomers of CBz-Asp. An increment of the interaction within the template and the MIP, which is directly proportional with the separation factor (α), was observed using acetonitrile as the eluent. It was demonstrated that the nature of the eluent and the amount of imprinted sites in the stationary phase have a direct impact on the effectiveness of the separation. Molecular modeling confirmed that the binding ability of the sugar and the CBz-Asp was strongly influenced by hydrogen bonding interactions.

Molecularly imprinted polymers for 2-L-phenylalanylamino-pyridine, 3-L phenylalanylamino-pyridine, and 4-L-phenylalanylamino-pyridine were prepared using methacrylic acid and ethylene glycol dimethacrylate as functional and crosslinker monomers, respectively[32]. A higher polymerization temperature with a non-covalent approach was employed during the MIP synthesis. Polymers were evaluated by liquid chromatography using an isocratic scheme. Electrostatic and hydrogen bond interactions were proposed as the mechanism underlying the retention of the template molecule using acetonitrile as eluent.

Li and collaborators[9] optimized the chromatographic conditions by changing the mobile phase composition and the hydrogen bond capacity. The selectivity of the imprinted polymer was not reduced by the increase of water content on the mobile phase. In order to understand the diffusion capabilities of the material, pore analysis was performed. Results demonstrated a wide distribution of pore sizes (i.e., heterogeneous MIP), which was reflected in mass transfer limitations.

Another interesting example was presented by Baggiani and collaborators [33]. They evaluated the performance of MIP using the herbicide 2,4,5-trichlorophenoxyacetic acid as the template. The polymers were prepared in aqueous media with 4-vinylpyridine and ethylene glycol dimethacrylate as functional monomer and crosslinker monomers, respectively. The effect of the mobile phase on the imprinted polymer was investigated. Solvents with a different dielectric constant (i.e. directly related with hydrogen bond capabilities) were considered (e.g

acetonitrile, ethanol, tetrahydrofuran, and isopropanol). The investigation revealed the binding kinetics were mostly impacted by the accessibility of the imprinted cavities than by the nature of the porogen used during the study. The template diffusion through the imprinted material was significantly affected by the MIP composition, which defines the MIP structure. In addition, an un-stabilized recognition site was revealed by the template leakage during the chiral separation.

Further investigation was achieved by Baggiani and coworkers[25]. They explored the utilization of methanol and water as a porogens to imprint the herbicide, 2,4,5-trichlorophenoxyacetic acid (2,4,5-T). The functional monomer and crosslinker were again 4-vinylpyridine and ethylene glycol dimethacrylate, respectively. Liquid chromatography was used as the characterization method to evaluate the effect of the template/monomer ratio on the binding properties and selectivity of the imprinted polymers. The effectiveness of the imprinting process was evaluated by the analysis of column capacity (k'), column selectivity and imprinting factor (k_{MIP}/k_{nonMIP}). The work illustrated that the ion pairing and the hydrophobic interactions between the template and the stationary phase controlled the imprinting effect.

In recent work, Yang et al. [34] evaluated the feasibility of using molecularly imprinted solid phase extraction (MISPE) of cotinine, (S)-(−)-1-methyl-5-(3-pyridyl)-2-pyrrolidinone, (the main metabolite of nicotine) from human urine. Methacrylic acid and ethylene glycol dimethacrylate were employed as functional and crosslinker monomers, respectively. Binding isotherms revealed a higher cotinine affinity

toward the imprinted polymer in aqueous solutions. Furthermore the apparent dissociation constant (K_{diss}) and the binding sites (Q_{sites}) comparison between MIP and non-MIP confirmed the presence of specific sites formed by the imprinting effect. Higher affinity toward the template molecule was observed through the resolution of nicotine and its metabolites (cotinine, nicotine, N-nitrosonornicotine). The complementary effect of the size and shape of the imprinted site to the recognition mechanism of the MIP was demonstrated by the selectivity factor results.

Table 2.1 summarizes selected separation applications and their realization with molecular imprinting materials. These examples demonstrated the potential of imprinted polymers to become broadly applicable within separation systems. It reveals the importance of solvent selection to promote interactions (e.g. hydrogen bonding, ion pairing, hydrophobic) that will enhance the analytes affinity. It also shows the effect of MIP heterogeneity on the diffusion through the imprinted material. The size and shape of imprinted sites were identified as contributors to the MIP rebinding effect. The importance of studying the MIP mechanism is especially remarkable in order to correlate the MIP synthesis and MIP-ligand binding for the preparation of a robust material capable of higher template affinity and selectivity. Further discussion will identify the challenges associated with the development of MIP-related applications such as the stationary separation phase.

TABLE 2.1 Selective examples of studies related for MIP application as separation phase

Template molecule	Monomer	Reference
(S)-nilvadipine	4-vinylpyridine	[35]
propanolol, tyrosine, dihydroxyphenylalanine, 2,2,2-trifluoro-1-(9-anthryl) ethanol	Organosilanes (TMOS, PTMOS, MTMOS)	[36]
cinchonidine, cinchonine	dibenzyl-(2R, 3R)-O-mono-acryl tartrate	[37]
Tamoxifen	Methacrylic acid	[38]
Phenylalanylamino-pyridine	Methacrylic acid	[32]
[Sar, Alas] Angiotensin II	Sodium acrylate	[39]
Phenylalanine	Cu(II)-N-(4-vinyl benzyl)iminodiacetic acid	[40]

2.2.2 Immunoassay

Clinical and research laboratories frequently employ antibodies as reagents for analytical procedures. Immunoassays, immunoaffinity chromatography, and immunosensors must be aided by molecular recognition through the formation of an epitode (i.e. the site on an antigen that is recognized by an antibody) between the antigen and the antibody. The molecular imprinting technique has emerged as producer of possible antibody counterparts due to its stability and durability in extreme conditions where antibodies will not usually endure. Molecularly imprinted sorbent assays (MIA) have shown binding strength at nanomolar and micromolar range compared to antibodies[16]. Moreover, the imprinted assay has the advantage over natural antibodies that can be stored preserving their recognition abilities[41].

An interesting example was reported by Mosbach and coworkers that applied the imprinting technique for the development of MIA to detect theophylline or diazepam in human serum[42]. A radio-labeled ligand-binding assay was prepared by using methacrylic acid as the functional monomer and ethylene glycol dimethacrylate as the crosslinker. Assays were performed under optimized conditions using organic solvents (e.g, acetonitrile, acetone, and tetrahydrofurane). The results revealed a good correlation of the MIA detection when compared to the traditional immunoassay technique. Also, satisfactory results were found for the therapeutic monitoring of the drug over a range of 14-224 μM.

In a similar approach, Andersons et al.[43] reported the preparation of imprinted particles employed for the selective adsorption of S-propanol. The group evaluated the effect of crosslinker structure on the MIP performance by making the copolymerization of methacrylic acid, with two different crosslinking agents. The influence of crosslinker morphology was evaluated by comparing MIP synthesized using MAA and ethylene glycol dimethacrylate (EGDMA), and MAA and trimethylolpropane trimethacrylate (TRIM). The polymerization was performed in toluene containing 0.5% (v/v) of acetic acid. Ligand binding analyses were carried out in an organic solvent and an aqueous buffer. The results demonstrated that the loading capacity was improved by employing TRIM as the crosslinking agent. Certainly, the non-linear structure of TRIM compared to EGDMA should produce a polymeric morphology with higher adsorption capabilities. However, the enantioselective ability was reduced. In addition, the report demonstrated a higher selectivity toward propanol using an aqueous buffer-based assay relative to a toluene-based assay.

Mosbach et al. developed artificial antibody-binding mimics based on methacrylic acid copolymerized with ethylene glycol dimethacrylate for the following template molecules: diazepam, theophylline, morphine, S-propanolol, methyl-α-D-glucoside and hydrocortisone.[44] The non-covalent approach was selected to develop the MIA. Specifically, the porogens employed for the polymerization were chloroform, acetonitrile, and tetrahydrofuran. The results demonstrated that the cross-reactivities

of MIA were comparable with the magnitudes of natural antibodies. However, direct evidence revealed the heterogeneity of MIAs. Their saturation capacity was inherently correlated with binding sites of higher affinity. Consequently, it demonstrated the role of the stability and uniformity of the solution adduct formed during the molecular imprinting process.

Attempts to develop an assay for 2,4-dichlorophenoxyacetic acid with imprinted microparticles have also been published by Haupt et al.[45] Bulk polymers were synthesized by dissolving the template molecule, 4-vinylpyridine, with ethylene glycol dimethacrylate in a mixture of methanol and water. The investigation confirmed the potential of using the molecular imprinting technique in a polar protic solvent. In this work, the rebinding conditions were optimized. Naturally, the mechanisms of template complexation and MIP-ligand binding have to be better understood to advance MIA applications.

Takeuchi and collaborators[30] reported the copolymerization of methacrylic acid and ethylene glycol dimethacrylate in chloroform for the formation of biotin methyl ester (B-Me) imprinted cavities. A continuous variation method revealed the stoichiometric ratio of the functional monomer-template complex (1:1). Results indicated that the imprinted affinity was induced by hydrogen bond interactions between the carboxylic acid moiety and the template molecule. Additionally, 2-(trifluromethyl) acrylic acid (TFMAA) was evaluated as a potential functional monomer expecting to be a stronger acid. However, the experiments demonstrated

lower affinity when TFMAA was substituted by MAA. In particular, MAA was observed to promote higher affinity compared to TFMAA showing it can interact as a hydrogen donor and acceptor.

In view of the recent developments obtained in MIA technology, it has been considered to develop MIA as a substitute for antibodies in immunoassay. The above-mentioned studies revealed that MIA exhibit highly selective molecular recognition, in many instances compared to biological systems (affinity nM-μM range). The simplicity of their preparation, their mechanical and chemical robustness are essential characteristics that allow MIA to emerge as an assay alternative for small molecules.

2.2.3 Catalyst and Artificial Enzymes

Over the past decades, the development and use of catalysts has increased yield and selectivity of chemical reactions specifically on fermentation or enzymatic processes. Imprinted materials have been applied for the substitution of enzymatic systems with the purpose of removing toxic compounds formed in the course of biochemical reactions and to shift reaction equilibrium towards product formation. The molecular imprinting studies for catalyst applications have focused on acid-base and metal complex catalysts [46]. Molecularly imprinted beads are frequently used and have demonstrated acceleration of product formation as a consequence of the reduction in the activation energy due to the presence of imprinted active sites.

Nevertheless, imprinted surfaces have also demonstrated to be a prominent alternative to develop catalyst[47]. Further discussion provides details regarding the more frequent configuration utilized as molecular imprinted materials (e.g. beads, monoliths, thin films, particles, surface) [48]. It is necessary to provide a brief overview of the scientific inquiry within the application of the molecular imprinting technique for the transformation of recognition sites into an enzyme mimic systems.

Enzymatic polymers were synthesized by Furusaki and coworkers[49]. A metal mediated imprinted polymer was prepared by producing a complex between a cobalt ion and an imidazole molecule. The substrate analog, N-α-*t*-boc-L-histidine was introduced to enhance the enzymatic properties of the MIP to catalyze the hydrolysis reaction of the amino acid ester. Bulk polymerization was performed in a water/organic emulsion. Toluene was selected as the organic phase and acetic acid-sodium acetate buffer was utilized as the base of the aqueous solution. The performance of the imprinted polymer was evaluated by the Michaelis-Menten analysis. A lower k_M value was observed for the imprinted polymer, which indicates high affinity of MIP toward the target substrate. The substrate recognition sites were also confirmed by the apparent V_{max} (6.25 x 10^{-2} mM/min). The reactivity of the substrate was enhanced as a consequence of the molecular arrangement of the functional molecules that creates a catalytic site generated during the imprinting synthesis. Furthermore, the substrate specificity was investigated by comparing the relative reactivities (i.e. initial rated catalyzed by MIP/ initial rated catalyzed by

nonMIP) of four different substrates (e.g. N-*t*-boc-l-alanine *p*-nitrophenyl ester, N-*t*-boc-l phenylalanine, *p*-nitrophenyl ester, N-*t*-boc-l-leucine *p*-nitrophenyl ester, and *p*-nitrophenyl acetate). Imprinted polymer demonstrated higher catalytic activity toward the amino acid ester during the hydrolysis reaction. In addition, results revealed the complementary interaction between the binding abilities of the recognition site and its shape on the selectivity of the imprinted polymers.

In another approach, Nicholls and collaborators [50] developed a transaminase imprinted polymer to catalyze a sigmatropic shift reaction (i.e., pericyclic reaction wherein the transition state of the molecule has a cyclic geometry that often has a transition metal catalyst that forms intermediates in analogous reaction) in aqueous media. Methacrylic acid crosslinked with ethylene glycol dimethacrylate was synthesized using a transition state analogue (TSA) as the template. Results demonstrated a 15-fold enhancement of the apparent reaction rate in an aqueous environment. Additionally, the results estimated the amount of recognition sites ($n=11.9 \pm 2$ $\mu mol\ g^{-1}$). Moreover, MIP selectivity was demonstrated by running the reactions relative to the substrate and products. Results revealed that the imprinted polymer has a marginal effect on the initial reaction rate as compared to non-imprinted polymer. The low selectivity was attributed to the fact that the recognition sites have less detection capability due to the smaller size of the substrate.

In a subsequent study, Meng and Sode et al.[51] attempted to catalyze the transesterification of p-nitrophenyl acetate and hexanol with imprinted microspheres

to demonstrate the benefits offered by enzyme mimics material. Itaconic acid and imidazole were copolymerized with trimethylpropanol trimethacrylate (TRIM). Results demonstrated a 3-fold improvement on the catalytic activity of the process due to the presence of imprinted spheres. However, the imprinted polymer did not show specificity towards the target template. This suggests that the lack of flexibility of the imprinting sites did not contribute to the substrate recognition via an induced-fitting mechanism. Although traditional MIPs morphologies are characterized as rigid structures to reduce the rotational entropy changes during the rebinding process, the above finding suggests the rational design of a new generation of imprinted materials with MIP-based catalysis exhibiting an induce-fitting mechanism. Thus, the recognition site's flexibility combined with the fortitude of their interaction makes imprinting synthesis an attractive approach to enhance the specificity of the transesterification process.

To this date significant findings have been reported on the formation of MIP-based catalysts. MIP has demonstrated higher tolerance to organic media and harsh physical treatment when compared with their natural counterparts. Their ability to provide binding sites that can restrict conformations essential for stereochemical and regiochemical control certainly confirmed that the imprinting technique is making a significant contribution to the development of new artificial enzymes.

2.2.4 Sensor Technology

Sensors are analytical devices capable of molecular recognition with significant selectivity and sensitivity[17]. A recent interest has involved the scientific activity on the development of sensors that assist in clinical diagnostics, environmental analysis, food analysis, drug screening, production monitoring, detection of illicit drugs, genotoxicity and chemical warfare agents[1]. In this context, the specific quantitative or semi-quantitative analytical information is obtained during the interaction of an analyte with the recognition element. Consequently a chemical signal is produced and is measured with the conversion of an electrical signal by a transducer.[52] Essentially, the recognition element encompassed high affinity abilities, specificity toward the template molecule, significant binding capacity, and stability. Actually, several exciting materials are already capable of sensing target molecules. However, it has been required to control and to monitor processes in harsh environments such as high temperatures, high pressure, in presence of acids, bases, and in organic solvents. As a consequence, imprinted materials have emerged as an attractive alternative to obtain more robust and stable multisensors. [3].

MIP sensors can be classified as: affinity sensors, receptor sensors, and catalyst sensors. The affinity sensor provides a response based on the accumulation of the electroactive template on the MIP surface. The receptor sensor

generates a response based on the transformation of polymer characteristic induced by the interaction of MIP and the template. The response of the catalyst sensor is promoted by modifying its environment as a consequence of MIP-catalyzed reaction[53]. Conventional network polymers have been used more frequently for sensor design. Membranes are particularly suitable for this application and have been prepared as imprinted thin films. A great diversity of techniques have been followed to produce biomimetic sensors based on molecular imprinting. It is necessary to perform a brief overview of the recent progress toward the development of imprinted sensors.

An interesting example was presented by Karube et al [54] that developed a highly specific polymer to detect testosterone using the MI technique. In order to assess the efficacy of the covalent and non-covalent method, synthetic receptors were prepared by the polymerization of the functional monomer, methacrylic acid (MAA) and the crosslinker, ethylene glycol dimethacrylate (EGDMA). Higher affinity was observed with the imprinted material synthesized with the covalent approach produced which suggests the formation of a more homogenous morphology. However, a small percentage of the template was removed from the microcavities therefore reducing the binding capacity of the imprinted polymer. Further studies demonstrated an increment of 4-fold on the retention factor of the imprinted polymer as a result of the binding affinity toward testosterone. Moreover, the selectivity

studies indicated the formation of imprinted sites complementary in shape and functional moiety to the target molecule.

Mosbach and collaborators[55] developed a conductometric sensor for the detection of the benzyltriphenylphosphonium ion with a recognition element based on P(MAA-co-EGMA). The binding characteristics of the imprinted polymer were observed by adding an incremental amount of benzyltriphenylphosphonium chloride. It should be mentioned that the MIP demonstrated a higher binding ratio than the reference polymer. Conversely, the conductometric evaluation demonstrated that after saturation, the template binding was non-specific in nature and produced a conductometric response similar to non-imprinting sensor. Results from this study revealed the need of incrementing the loading capacity of imprinted polymers.

One severe problem identified by Kriz et al[56] was the long response time involved in the measurement which must be overcome by improving the binding kinetics. Modifying the polymer morphology to smaller particles and membranes has been suggested in order to enhance the binding kinetics based on the diffusion limitations.

Willner and collaborators[57] described the preparation of imprinted sites on acrylamide-acryl aminophenyl boronate thin membranes and TiO_2 film. Impedance spectroscopy was employed to estimate the thickness of chemically assembled thin film on the gate surface (85±10μm). Moreover, gate potential measured upon the binding of the template molecule showed significant sensitivity toward the nucleotide.

The specificity of the imprinted material was attributed to the cooperative binding of non-covalent and covalent interactions. More efforts are still required to optimize the polymer morphology (i.e. crosslinker degree) to enhance template recognition.

Early attempts to develop polyurethane films as a recognition element for a Quartz crystal microbalance (QCM) were performed by Dickert and coworkers[58]. This sensor was developed to detect erythrocytes. AFM images demonstrated the formation of imprinted cavities on the polyutherane surface. Imprinted polymers were synthesized in the presence of blood group AB and blood group O. Results revealed a remarkable selectivity towards the template cell. Furthermore, the author acknowledges that the recognition of the target cell by the imprinted polymer is fully reversible. Certainly, the polymer would be produced and regenerated for multiple usages.

The fabrication of an imprinted QCM odor sensor based on poly(methacrylic acid-co ethylene glycol dimethacrylate) for the detection of formaldehyde was developed. The selectivity of the MIP was characterized by monitoring the resonant frequency. The author estimated the dissociation constant between the template molecule and the MIP to evaluate the sensor sensitivity. This example demonstrates the potential of imprinted material to detect templates in the gaseous phase.

Of particular relevance is the work of Wu et al[59] and its insight on the in situ polymerization of polyethylene glycol (PEG) as a functional monomer with γ-glycidoxypropyltrimetoxysilane (GPTMS) to fabricate organic-inorganic hybrid

membranes. Chitosan imprinted membranes were synthesized through covalent approach and characterized by FTIR spectroscopy, X-ray diffraction, scanning electron microscopy (SEM), swelling studies and binding experiments. Results revealed that the surface morphology of the membrane was controlled by the molecular weight and weight fraction of PEG employed during the imprinting process. The membranes prepared with PEG 20,000 as a porogen demonstrated a low degree of swelling and higher adsorption. It was observed that a hierarchical structured-in morphology (i.e., *levels-of-structure* that build from small-scale structure to large-size-scale structure through discrete *levels-of-morphology*) enhanced the protein adsorption capacity and its property of high metal chelating.

Finally, essential examples were mentioned, which demonstrated the utility of combining molecularly imprinted materials with transducers to produce highly sensitive and selective sensors with the potential of commercialization.

TABLE 2.2 Selective examples of studies related for MIP application as sensor

Template	Monomer	Reference
Viruses	Methacrylic acid, styrene	[4]
Uric acid	Acrylic acid-acrylonitrile	[60]
chloramphenicol	Methacrylic acid	[61]
Albuterol	Poly(vinylidine fluoride hexafluopropylene)	[62]
Adrenaline	Acrylic acid	[63]
Atrazine	Methacrylic acid, diethyl aminoethyl methacrylate	[64]
Propanolol, ephedrine, benzylamine, cyclohexylamine	Methacrylic acid	[65]

2.2.5 Other applications

Today, research efforts are focused on creating new strategies to extend MIP applications. Certainly, the significant enhancement of molecular imprinting performance in an aqueous media will extend the applications with the intention to advance tissue engineering scaffolds development[52]. Imprinting of living cells has served as a structural support for the oriented proliferation of cell growth. The imprinted polymeric network was designed to degrade with a releasing growth factor allowing living cell growth through the macromolecule pores[66].

In addition, imprinted materials are appealing as drug delivery devices (refer to Figure 2.2). Allender and coworkers[67] have studied the imprinting of theopylline with the idea to develop selective transcutaneous monitoring devices. Permeability and binding capacity studies have revealed template flux control provided a useful means of extending the delivery profile of the device.

In an effort to prepare MIP for a drug delivery application, Ciardelli and coworkers[60] employed the approach of making nanospheres with theophylline imprinted cavities. The study evaluated the effect of the functional monomer ‘s nature to release theophylline produced by MIP-ligand rebinding. Methacrylic acid (MAA), methylmethacrylate (MMA) and trimethylolpropanol trimethacrylate (TRIM) were employed as the monomers during the polymerization in acetonitrile solution. The binding capacity of imprinted nanospheres was determined. The release ability of theophylline was also estimated. Results revealed the release properties of the

MIP and rebinding capacity were modulated by changing the ratio of MAA and MMA present during polymerization. Evidence of selectivity towards the template molecule was observed by the evaluation of the imprinted nanospheres' affinity to caffeine-theophylline solution.

Another approach for the development of imprinted hydrogels for medical and pharmaceutical applications was performed by Peppas and collaborators[68]. Their research focused in the synthesis of imprinted star polymers based on the tethered chains of long poly(ethylene glycol) (PEG) chains on poly(acryl acid) (PAA) for drug delivery systems. The idea was to increase the bioactive surface to enhance the binding ability of MIP. Glucose and theophylline were employed as template molecules. It was shown that the morphology of star polymers promoted higher concentration of functionalities in a small volume. The resulting MIP has different functionalities, which provided ionic, metal coordination, hydrophilic and hydrophobic interactions. The study used a molecular theory to calculate the structure of the layer-tethered polymers on gel surface. It was evisioned that the calculations would aid further experimental design.

The rational design of imprinted hydrogels will advance their potential application as drug delivery devices. Most MIP relay upon a high crosslinking structure. However for drug delivery systems, it is usually an advantage to prepare imprinted hydrogels with a flexible morphology, which permits the controlled release of a therapeutic agent[69]. The imprinted hydrogel demonstrated the complementary

characteristic of affinity and its ability of acting as a drug reservoir. Eventually, the drug release was modulated by the swelling characteristic of the imprinted gel. Furthermore, the specificity of the imprinted gel allowed to identify a target in the cell with the final purpose of producing stimuli. Specifically, the imprinted drug delivery device released the therapeutic agent when the MIP bound to the target, a competitive displacement of the drug by a structurally related cross reactant. Finally both stimuli are combined with the internalization of an MIP- drug complex (see Figure 2.2)[70].

In conclusion, imprinted polymers need to be designed as engineered materials that control their binding abilities and their eventual response. Consequently, a new generation of MIP has emerged with the purpose of expanding the molecular imprinting technique in a range of exciting applications in the near future.

2.3 Challenges in Molecular Imprinting

The performance of molecularly imprinted polymers will be influenced by the accessibility, integrity, stability and affinity of the recognition sites. In order to understand the challenges faced by the imprinting community, it is necessary to identify the different types of binding sites in MIPs. The polymer will have a wide distribution of pore sizes. The MIP consists of binding sites located at macropores (>20 Å) and micropores (<20 Å) regions that affect the template diffusion through the

imprinting system. Within those regions, different interaction modes are created based on the pre-arrangement process in self-assembly of the template molecule and the functional group prior to polymerization. Binding modes of high affinity, low affinity, and with no selectivity have been observed as the results of this self-assembly phenomena (see Figure 2.3). It is evident that several drawbacks must be overcome to enhance MIP affinity and binding kinetic. This section will provide an insight into the technical challenges that have been addressed for new and commercially attractive MIP applications in the near future.

Withcombe[71], Takeguchi[29], and Wulff[14] identified the need to design a new generation of functional monomers capable of stronger interactions with the template molecules, specially in an aqueous media. The idea is to improve the ratio between specific and non-specific binding sites. As a result, increment in this ratio will enhance the specificity and efficiency of the imprinted polymer[72]. More work has been devoted towards polymer synthesis with a homogeneous population of binding sites [41, 72-75]. It has been affirmed the requirement for the development and validation of general protocols for MIP design[53, 76]. Therefore, optimization of MIP morphology by its characterization during imprinting design will aid to reduce the following limitations: template leakage[15, 73, 74, 77, 78], slow mass transfers during template removal[77, 78] and rebinding process [73]; and reduced loading capacity[72-74]. A better insight of the functional monomer-template complex formation and its role on

the polymerization kinetics will enhance the MIP morphology to improve the MIP-ligand rebinding.

Several authors indicate the needs of creating novel polymer morphology that will allow the imprinting of macromolecules such as peptides, proteins and cells[44, 45, 74, 79]. To this end, a greater effort is required to generate imprinted materials capable of molecular recognition in an aqueous media[15, 44, 53, 75, 77-79].

A possible solution to the abovementioned limitations is the understanding of the peculiarity of MIP formation and MIP-ligand binding to design imprinted material with optimal morphology for specific transport and recognition abilities. Therefore, an extended discussion will be given in section 2.8 that presents the protocols of approaches used by several authors to design recognition elements.

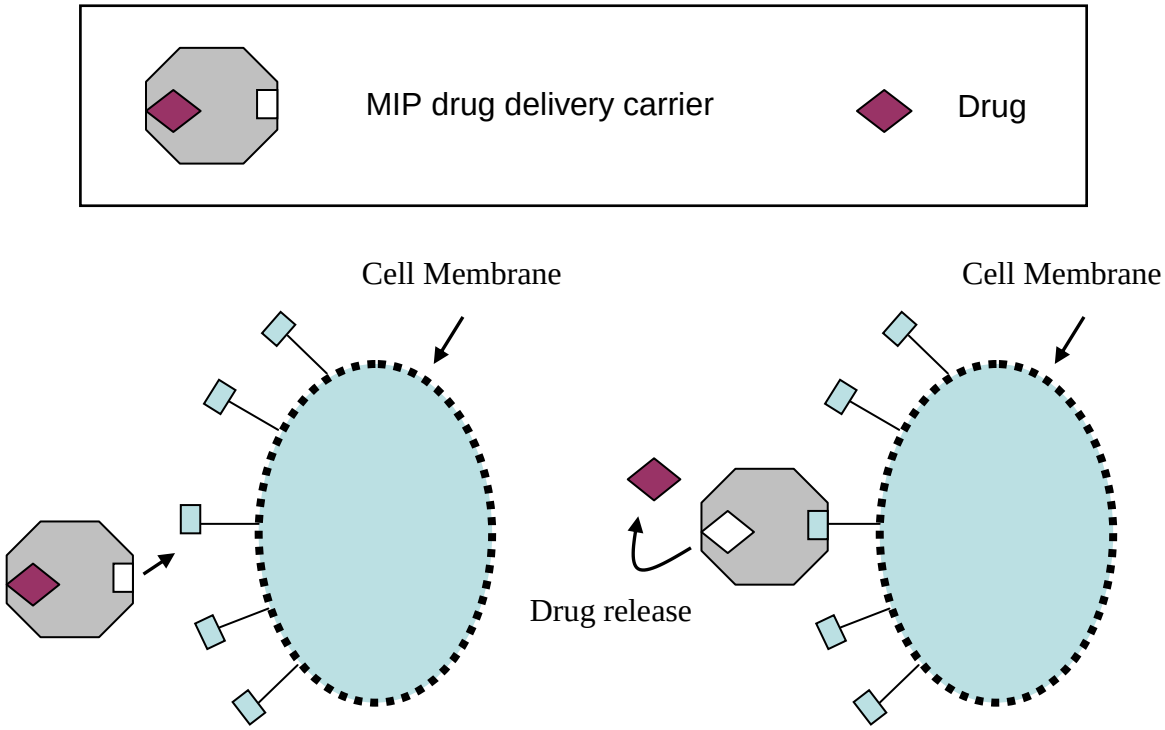

Figure 2.2 MIP Drug Delivery System

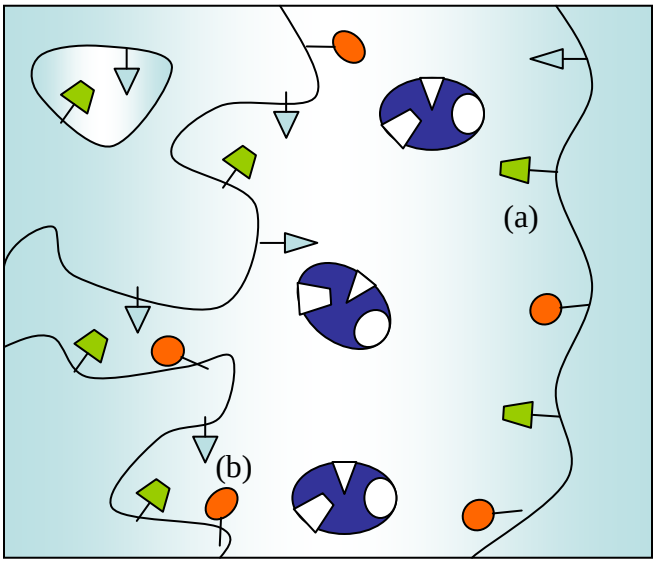

Figure 2.3 Representation of different types of binding sites containing recognition sites with non-specificity (a) and high affinity/selectivity (b)

2.4 Molecular Imprinting within Hydrogels

Although the development of molecular imprinting began with silica gels[20], inorganic matrixes (e.g., metal and semi-metal oxides) were found to have recognition properties. Moreover, highly crosslinked polymeric networks have played a key role to advance creating remarkable imprinting materials. As a drawback, the highly crosslinked polymeric networks have an adverse effect if the MIP will have further use on biomedical system (e.g., drug delivery, microfluidics drug device, artificial tissues). Consequently, an interest to develop intelligent-imprinted hydrogels with recognition abilities has emerged in order to combine their oscillatory swelling properties with their binding capacity to obtain an intelligent drug delivery system and analyte sensing micro-valves[80]. This section will review recent effort on molecular imprinting within hydrogels and their principles.

Hydrogels are defined as three-dimensional polymeric networks that contain physical or chemical crosslinks and are hydrophilic in nature. Therefore, they can imbibe water or biological fluid rendering them biocompatible and immunotolerant, an essential property for biomedical applications such as tissue engineering, sensor, controlled drug delivery, and separations[81].

Hydrogels are chemically or physically crosslinked. The chemical crosslinked hydrogels refer to the process of covalently linking chains within the polymeric network. In contrast, physical crosslinked hydrogels refer to the connection of

polymeric chains by molecular entanglements and or secondary forces including ionic, H-bonding or hydrophobic forces[66] .

Hydrogels are classified as neutral, anionic or cationic. They have demonstrated to be sensitive to environmental changes such as external pH, temperature, ionic strength, nature of swelling agent, or electromagnetic radiation[82]. The principal hydrogel properties are the correlation length or network mesh size (ξ), number-average molecular weight between crosslinks (Mc), and the swelling ratio(Q). The mesh size is indicative of the linear distance between two consecutive junctions. The M_c represents the degree of cross-linking. The swelling ratio is associated with the equilibrium polymer volume fraction in the gel[83]. The evaluation of the structural properties' relationship will provide significant information for the design of molecularly imprinted polymers.

Several conditions influence the synthesis of imprinted gels. A rational methodology is required to develop hydrogels based-MIPs with binding conformation and environmental stimulus capabilities. It is necessary to understand the reversible and transient behavior of an intelligent imprinted gel, which influences the MIP affinity and selectivity. In recent work, Tanaka et al[84] have observed the reversible self-organized conformation of hydrogels between their swelled and collapsed states. Imprinted gels were prepared using methacrylamido-propyl-trimethyl-ammonioum chloride (MAPTAC) as the functional monomer. N-isopropylacrylamide (NIPA) was chosen as the thermoresponsive monomer that allows the swelling and shrinking of

the imprinting network. The crosslinkers employed during the imprinting synthesis were N, N' – methylene-bis-acrylamide (BIS) and N-(2-S-acetylthio)ethyl acrylamide. The imprinted gels were characterized at their collapsed and swelling state by determining the binding affinity of pyridine, the template molecule. Results reveal the absorption of the imprinting gel was represented by Langmuir type adsorption isotherm. The absorption was reduced during the collapsed state. It was also demonstrated that the MAPTAC complex can be restored showing the imprinting capacity of environmental stimulus gels. Thus, an obvious target is to create MIP morphology that maintains the imprinted cavities in the absence of the template, but that also has enough flexibility to facilitate a fast equilibrium between the release and the uptake of the template molecule. The current challenge for the MIP rational design is to determine the optimal crosslinking ratio that will produce an effective recognition. The idea is to predict the optimal synthesis condition to reduce the time employed in the MIP development based on a trial and error approach[85].

In a subsequent study, Kofinas and collaborators[86] synthesized molecular imprinted hydrogels for the detection of glucose. Poly(allylamine hydrochloride) (PAA·HCl) were produced by the non-covalent imprinting approach. The affinity and selectivity of MIP was evaluated by equilibrium binding capacity studies in buffer solution. Results revealed the MIP recognition toward glucose in a water-swollen state. In addition, imprinted gels demonstrated five to seven-fold specificity toward glucose over fructose. The studies showed molecular recognition was achieved

even in swollen gels. However, optimal synthesis condition was not rationally designed.

Another interesting example was the work by Peppas et al.[87], which demonstrated the ability of using imprinted star polymers for glucose recognition. The star morphology was designed to be a responsive recognition element. The poly(ethylene glycol) (PEG) stars with 75 and 31 arms were crosslinked by EGDMA with an ethylene glycol chain of molecular nominal weight of 600. The MIP synthesis was performed in an aqueous media. The imprinted polymers were characterized by binding and permeability studies using water as a solvent. The polymer synthesized with 31 arms exhibited a higher binding capability. Imprinted stars showed selectivity toward the template molecule when glucose uptake was compared to fructose uptake. The imprinted stars were not specific when the glucose uptake was compared to galactose uptake, which has a chemical structure similar to glucose. Furthermore, the morphology has to be optimized to enhance its binding capacity.

A subsequent study performed by Peppas et al[88] revealed that an increment of the template feed concentration in the MIP synthesis demonstrated a higher binding capacity and better recognition selectivity. Network polymeric films of poly(HEMA-co-PEG600DMA) were synthesized using glucose as the template molecule. In addition, the selectivity behavior was confirmed using proxyphyline, another hydrophilic compound, as the template molecule. The imprinted network demonstrated higher uptake capacity toward proxyphyline over theophyline. The

crosslinking ratio of the imprinted gels was varied in order to to obtain suitable binding abilities. Nevertheless, the synthesis enhancements were based in a trial and error approach. Additionally, the optimal template:monomer:crosslinking ratio was not established.

More recently, attempts to develop an imprinted polymer based in poly(N-tert-butylacrylamide-co-acylamide/maelic acid) [P(TBA-co-AAm/MA)] for protein application were performed by Caykara and collaborators[89]. In this study the authors presented the approach of combining strong and weak interactions to create binding abilities on pH-temperature sensitive hydrogels toward bovine serum albumin (BSA). Template absorption was estimated as a function of pH and temperature. The results indicated the imprinted polymers have an optimum absorption at a pH equal to 5.0, near the isoelectric point of BSA (4.8), which resulted from the ionic interaction between the imprinted polymer and the protein. However, during the binding experiments the effect of temperature was evaluated. The binding results showed a reduction in the absorption capacity of the imprinted material as a consequence of an increment in temperature. It was suggested that the absorption difference was modified by the swelling characteristics of the polymer, which was in the collapsed state at higher temperatures. Further selectivity analysis indicated the existence of a high affinity site towards BSA. Competitive binding between BSA and casein demonstrated the high specificity of the imprinted polymer. It was suggested

that the selectivity was influenced not only by the complementary interactions at the binding site, but also by the shape of the recognition site.

In a subsequent study, Alvarez-Lorenzo and coworkers[85] developed a molecularly imprinted contact lens to uptake and control the norfloxacin release (NRF). A copolymerization of hydroxyethyl methacrylate (HEMA), acrylic acid (AA), and vinyl pyridine (VP) in the presence of ethylene glycol dimethacrylate (EGDMA) was performed to obtain hydrogel discs. Preliminary screenings within non-imprinted gels suggested that the acrylic acid monomer permitted a greater loading of the NRF. Further characterization of poly(AA-co-EGDMA) demonstrated an increase in the hydrogel's loading capabilities by the incorporation of AA. The effect of template/functional monomer ratio was also investigated. An optimal molar ratio was identified suggesting that higher stabilization of the functional monomer-template complex.

This research assists on the rational designs of a hydrogel based-MIP. It employed the most common hydrogels used during molecular imprinting synthesis (MAA and EGDMA). An attractive approach to enhance the selective recognition and binding affinity in an aqueous solvent consists of introducing a strong hydrogen bond donor and acceptor, and strong ionic directed recognition sites. Conceivably, the utilization of MAA during MIP design potentially generates binding sites for a large variety of template structures with recognition abilities in an aqueous media. In fact, MAA exhibits selective recognition and good affinity in organic and aqueous solvents.

MAA also demonstrated evidence of syndiotacticity (i.e. alternate sequence of the asymmetric centers along the polymer chain)[90]. The syndiotactic characteristic of MAA influences the recognition properties of MIP due to the chain flexibility.

Equally important is the selection of the crosslinker for the MIP synthesis. The functional monomer-crosslinker system determines the morphology of the polymer matrix. The relative reactivity of the crosslinker with the functional monomer during polymer propagation influenced the secondary structure on the polymer chain growth. EGDMA appears to be a superior crosslinker recognizing the production of polymer chains flexible enough for fast template splitting and rebinding. Higher MIP selectivity was observed when EGDMA was chosen as the crosslinking agent[91, 92]. Consequently, the EGDMA-MAA based system provides good recognition properties. It is important to note that the EGDMA-MAA system encourages the rapid mass transfer of the template molecule. Another important aspect of the crosslinker functionality is the fact that it also assists on the stabilization of the recognition sites. The EGDMA imparts good mechanical stability to the polymeric matrix, which helps in the MIP recognition process[93].

In summary, highly crosslinked materials have been employed to create efficient molecularly imprinted polymers, which demonstrated great binding abilities in several applications (separation, immunoassay, sensors, and artificial enzymes). Nevertheless, a great effort is actually dedicated to extend MIP application towards smart medical devices. To this end, the following challenges have to be overcome in

order to form recognition capabilities in hydrogels: a) to sustain the stability of the functional monomer-template complex, b) to ensure the integrity of the recognition site is stable during MIP-ligand rebinding process, c) to promote interaction favorable for the MIP-ligand rebinding. Particularly important is the rational design of material morphology to envision the discovery of controlled release imprinted gels[70,80].

2.5 Synthesis of Imprinted Polymers

A preferential tacticity must be induced on the polymeric structure during imprinting synthesis, which eventually influences the molecular recognition properties. Various alternatives have been reported for the synthesis of imprinted polymers[61, 94]. Free radical polymerization is frequently used for the fabrication of a molecularly imprinted polymer. It offers advantages during the design of imprinted polymers recognizing that the imprinting synthesis is performed in several solvents or porogens because the reaction has less impact by the presence of acid, bases, or by changes in solvent polarity[95].

In addition, copolymerization is often employed to prepare imprinted polymers. The polymer structure is formed by the incorporation of two monomers. The functional monomer has complementary groups for the recognition mechanism; and the crosslinked agent promotes structural stiffness in the imprinted network. The sequence in which the monomers interact depends on the relative reactivity within these monomers. Consequently, the formation of the structure is produced by the

copolymers randomization, by alternating copolymers or block copolymers. Reports showed more effective molecular recognition in the design of imprinted polymers with a random incorporation of monomers. The stability of the template molecule, the functional monomers and the crosslinker before and during the imprinting synthesis have intrinsic impact on the recognition capacity of the polymer. Therefore, the functional monomer, crosslinker, and the porogen selection are key parameters in the design of a molecularly imprinted system. The rational design will advance the MIP manufacturing process by eliminating the trial and error method. Finally, it will assist to determine the suitable MIP synthesis parameters by improving the effectiveness of fabrication protocols to enhance the imprinted polymer's sensitivity and selectivity. An extended discussion of the critical factors associated with successful imprinting was provided on section 2.6. This section focuses on the description of recent reports that demonstrate the synthesis and physical configuration of MIPs.

An interesting example was reported by Mayes et al[96] who assess the influence of imprinted methods (i.e. bulk polymerization, suspension polymerization, two-step swelling polymerization, precipitation polymerization, emulsion core-shell polymerization) on the recognition properties of MIP. A ligand assay characterization was performed to compare the difference in the recognition properties produced by the selected synthesis method. Results revealed the polymerization method affected the MIP-ligand rebinding. The binding characteristic of the imprinted polymer

synthesized by precipitation was higher if the porogen used during ligand rebinding was organic in nature. If the porogen was changed to an aqueous solution the specificity was reduced. Two-step swelling demonstrated a greater imprinted affinity when an aqueous solution was utilized during MIP-ligand rebinding. Finally, the author identifies the importance of selecting a polymerization method that produces recognition at the imprinted polymer based on the desired application.

TABLE 2.3. Summary of typical configuration employed to produce MIP[48]

Physical forms of Molecularly Imprinted Polymers
Crushed monoliths
Soluble microgels
Nano and microdots
Nanostructured surfaces
Porous microbeads
Nanobeads, nanofibers, nanotubes, and nanowires
Porous films

Imprinted materials demand distinct characteristics (e.g. specificity, capacity, and configuration) for their feasible applications. Nowadays, research on MIP provides a variety of configurations to prepare MIP (see Table 2.2). Bulk polymers or monoliths are most widely synthesized. The bulk polymer is crushed and sieved to obtain particles of irregular size and shape, which influence the efficiency of template separation. The reduction in yield of recognition sites by losing material as a consequence of removing fine particles from the usable remains has been identified as a drawback of this procedure. Evidently, some binding sites are partially destroyed by the procedure. To overcome these problems several other attempts to prepare a different alternative of MIP configuration have been reported.

Mosbach and Kempe [97] reported surface imprinting of proteins on silica particles. Imprinting effectiveness was compared by using methacrylic acid and 4-vinylpyridine as functional monomers. Trimethylolpropaten trimethacrylate and ethylene glycol dimethacrylate were used as crosslinker agents. Higher affinity for RNase A was showed in the imprinted stationary phase compared to the reference phase.

An elegant approach is to employ in situ preparation of imprinted columns to optimize the conditions of molecular imprinting. Zou et al.[98] performed in situ molecular imprinting to create monolithic polymers as the stationary phase of a chromatographic column for separation applications. The imprinting polymerization was completed in a column filled with a functional monomer (MAA, 4-VP), a

crosslinker (EGDMA), a free-radical initiator (AIBN) and the corresponding porogen (i.e. solvent). Subsequently, the template molecule was extracted and the imprinted material was directly utilized for the enantiomer separation. The principal advantage was to eliminate the procedures of grinding, sieving, and column packing. Consequently, the possibility of destroying imprinted sites was removed from the preparation stages. Polymerization conditions, solvent composition (toluene and dodecanol) and monomer-template ratio (1:2, 1:3, 1:4) were evaluated to optimize the MIP synthesis. Amino acid derivatives and diastereomers were effectively resolved with good performance. Results reveal large through-pores which led to low back pressure (1.76 MPa) with a mobile phase flow rate of 2.0 ml/min. The recognition mechanism was proposed to be driven by hydrophobic interaction, ionic, and/or hydrogen bonding interactions.

In a recent publication, a direct rapid synthesis method had been developed by Mayes et al. [94]. MIP beads were synthesized by *in situ* polymerization using methacrylic acid, acrylic acid, vinyl pyridine, and hydroxyethyl methacrylate as functional monomers. The study evaluated the nature of the functional monomer (e.g. methacrylic acid, acrylic acid, hydroxyethyl methacrylate, 2-vinylpyridine) and the effect of functional monomer/cross linker ratio for the imprinting of propanol and morphine. EGDMA was selected as the crosslinker agent. The percentage of template rebinding was estimated through a radioligand binding assay. Results demonstrated that imprinted polymers based in methacrylic acid produce higher

binding affinity. In addition, it was observed that a 3-fold reduction in the functional monomer/crosslinker ratio diminished the percentage of rebinding in the case of MAA.

In another approach, Dickert and collaborators[4] conducted the surface imprinting of cells and proteins for nano and micro structured sensing elements. The key intention was to solve the typical problems associated with bulk polymerization such as (i) reduction or destruction of imprinting cavities by the grinding and sieving step and (ii) diffusion of biological target molecules. Methacrylic acid, styrene, and divinylbenzene were polymerized to coat the quartz crystal microbalance transducer. The image obtained using atomic force microscopy (AFM) showed imprinted sites at the polyurethane surface with a size dimension similar to the size distribution of cells. Additionally, enzyme crystallization was observed when exposing an imprinted surface to lysozyme solution. It was proposed that the imprinted site provided a nucleation center that favored the eventual crystal growth.

An additional attempt was performed by Flores et al [99] to synthesize divinylbenzene-based beads. The effect of solvent volume was evaluated based on polymer composition. Moreover, the imprinted beads were characterized by the kinetic uptake of the cholesterol. Results revealed the influence of the MIP configuration in the template re-binding. An increase in product yield was demonstrated by the production of monodisperse microbeads.

Conversely, thin films are employed on the development of membranes for sensor applications. The transport of the template molecule on synthetic membranes is controlled by channels with non-porous, microporous or macroporous characteristics. Microporous and macroporous membranes have demonstrated different transport properties. A report by Marx and collaborators[100] described the spin coating of a sol gel film imprinted polymer for the enantioselective absorption of propanol and other enantiomers. A silane monomer was employed for the synthesis. The chirial discrimination of the imprinted sol gels was evaluated by a fluorescence method. Results demonstrated the presence of non-specific and specific adsorption on the imprinted stage. The selectivity studies demonstrated a substantial adsorption of both enantiomers. Consequently, the cavity shape directly influenced the specificity of the imprinted matrix, which is associated to the final morphology.

Piletsky et al. [101] adopted a different approach by adding a plasticizer to improve the mechanical and transport properties of the thin imprinted membrane. Oligourethane acrylate and a porogen were added as part of the component in the copolymerization of methacylic acid (MAA) and tri(ethyl glycol) dimethacrylate. This process resulted in the formation of atrazine-imprinted membranes with higher porosity to increase the template's permeability. The recognition properties of the membranes were characterized by the adsorption assessment of atrazine in an aqueous media. The result revealed high binding capacity as a consequence of better accessibility to the binding sites in a porous MIP morphology. Selectivity

studies demonstrated that atrazine imprinted films have low nonspecific binding when compared to triazine, and triazinone herbicides. In context, it is interesting to note the MIP-ligand binding efficiency was dictated by pore size distribution. These careful studies illustrate the requirement for a rational design of imprinted polymers to enhance the mass transfer process among the many desirable properties associated with the imprinting mechanism.

From the preceding discussion, it is evident that a range of configuration alternatives can be chosen for the synthesis of molecularly imprinted polymers. The configuration selection of the imprinted material influenced its intended use. None of the techniques already mentioned are precise. However, further evaluation of the imprinted morphology and the effect of imprinting technique during the material synthesis can advance on the convenient production of enhanced MIP.

2.6 Critical Factors for Successfully Imprinting Design

Although molecular imprinting is simple in terms of sequential stages, it is complex in nature. Consequently, methodological approaches are required to produce state of the art MIPs. Essential key parameters need to be evaluated during the design of a molecularly imprinted system including the composition and the nature of the functional monomer, crosslinker, and porogen (i.e. solvent employed during the MIP synthesis) employed during MIP synthesis. The first consideration to be taken during the rational design is the selection of chemical groups which

promote the motif (i.e., a distinct folding pattern for elements of secondary structure) for molecular recognition. Consequently, the selection of the functional monomer is based on this requirement. Table 2.4 illustrates an example of functional monomers frequently used during molecular imprinting synthesis. They are classified as acid, basic, or neutral. The most prominent monomer employed toward preparing polymeric receptors is methacrylic acid(MAA). MAA demonstrated to has complementary binding properties. The carboxylic acid group in MAA provides complementary binding sites, which serve as hydrogen bond, hydrogen bond acceptor, or proton donor. The strength of the association depends on the polarity of the porogen used during the synthesis.

The crosslinker selection is essential by designing macromolecular architecture of the imprinted polymer. It also establishes the mechanical stability of the polymeric network. Table 2.5 listed several well-known crosslinkers used in the molecularly imprinted field. The influence of the nominal crosslinker ratio and the volume of the porogen over the imprinted morphology can be seen on figure 2.4. Several regions are observed depending on the percentage of the crosslinker and solvent utilized during polymerization. High cross-linker ratios are generally preferred. However, low crosslinked systems have recently been examined as possible intelligent controlled release imprinted gels[80]. Consequently, the functional monomer-crosslinker ratio is optimized during the MIP design recognizing it influences the final structure that preserves the binding sites. Another aspect to be

considered is the effect of the crosslinking density to the MIP-ligand binding kinetics. The crosslinker should not disrupt the interaction within the template and the functional group. It should also offer enough flexibility to the polymer structure for fast template rebinding.

TABLE 2.4 Selection of functional monomers used in molecular imprinting[102]

Acidic

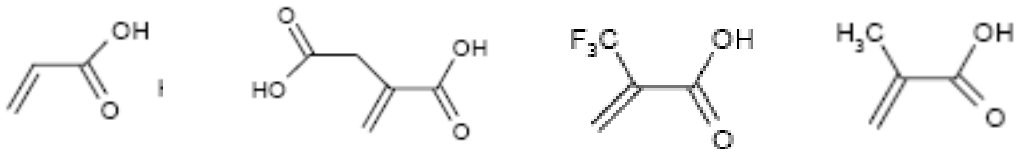

Basic

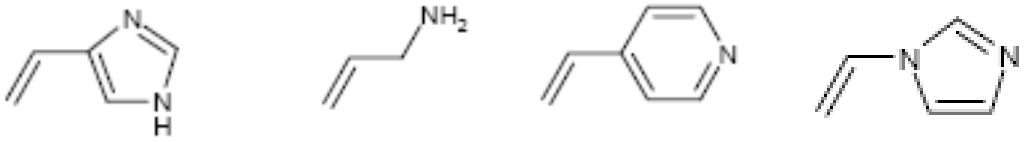

Neutral

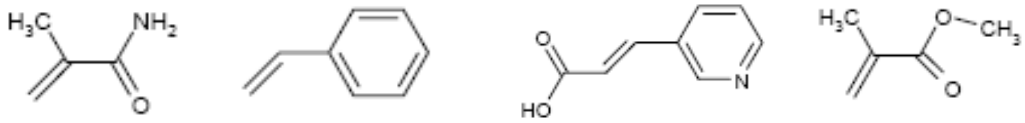

TABLE 2.5 Selection of crosslinkers used in molecular imprinting[102]

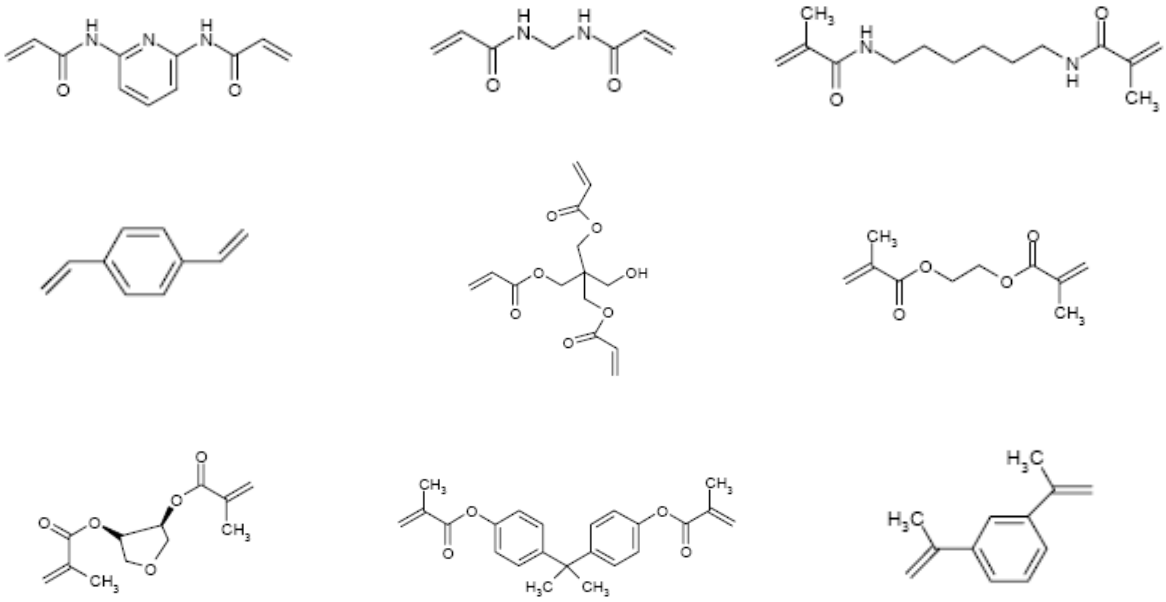

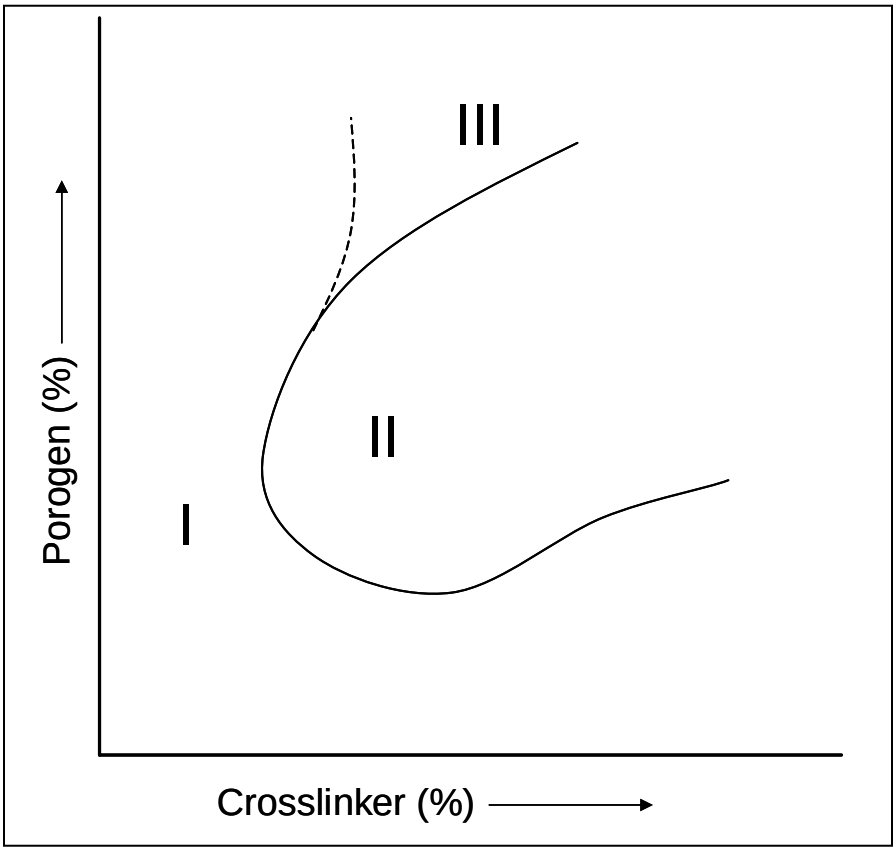

Figure 2.4 Polymer pseudo-phase diagram which demonstrates the effect of crosslinking ratio and percentage of solvent on the resulting morphology (I = gel type polymers, II= macroporous polymer, III = microgel powder.[103]

The solvent plays an important role in MIP design. In practice, it influences the interaction's strength during the equilibrium of functional monomer-template complex and the polymer morphology in terms of surface area and pore size. Therefore, the solvent is usually referred to as a porogen, recognizing its role in pore formation. The pore size has a direct impact on the recognition's kinetics. The most frequent porogens used during the molecular imprinting technique are those with low dielectric constant, such as acetone, tetrahydrofuran, and chloroform. The principal objective is to reinforce the hydrogen bond and ionic interactions. However, porogens with higher dielectric constant have been utilized (e.g acetonitrile, ethanol, and methanol). Other examples of porogens used during the synthesis of molecular imprinted polymers are dimethyl sulfoxide, toluene, and water. There are no obvious conclusions to be drawn from the selection of the type of solvent that will promote the polymer morphology with a structural integrity and good accessibility during MIP-ligand binding. Moreover, it is understood that MIP morphology is influenced by the stabilization of the functional monomer-template complex. As a consequence, the rational design of MIP has to include the effect of solvent nature to optimize MIP performance.

Conversely, the initiator selection depends on the conditions that the imprinted material will be synthesized in. Table 2.6 shows the initiator selection typically used for radical polymerization. Azobisisobutyronitrile (AIBN) is frequently used for imprinting fabrication. For applications using thin films, additional initiators

have been selected. An example is reported by Haupt and collaborators[104] in which 2,2-dimethoxy-2-phenylacetophenone (DPAP) was employed due to its ability of curing films quicker, resulting in more porous morphologies. Spin-coating was utilized to develop thin films by polymerizing methacrylic acid (MAA) and trimethylolpropane trimethacylate(TRIM) as the functional and crosslinking monomers, respectively. The results demonstrated that imprinted films have chiral memory towards the model template, S-propanolol. It also described a simplistic technique to control the porous morphology and the film thickness.

From the preceding discussion, it can be concluded that the MIP's performance is determined by the design conditions of MIP synthesis. Therefore, strategies for the rational design of imprinted polymers will assist in their optimization to enhance their affinity and selectivity. Much effort is still required to understand the mechanism underlying the formation of a binding site and its influence in the MIP-ligand binding. Furthermore, interesting research is in progress to evaluate the possibility of new polymerization conditions which would result in a wide spread of molecular imprinting techniques in the near future.

TABLE 2.6. Selection of initiators typically used for radical polymerization[102]

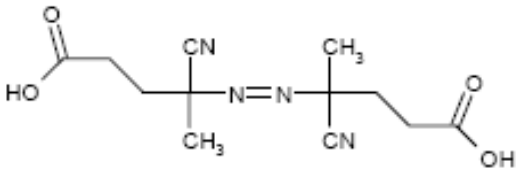

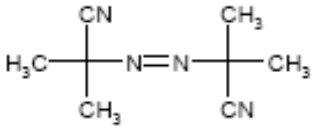

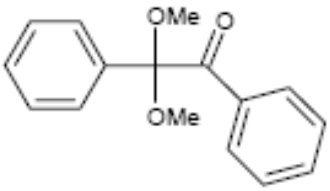

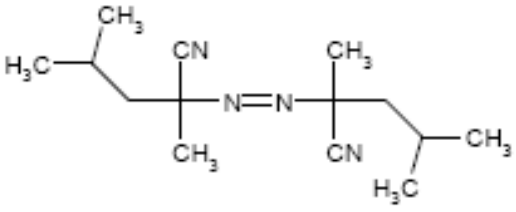

2.7 The role of functional monomer-template complex

In order to establish the strategies to select the optimal conditions for the MIP synthesis, it is important to ponder the thermodynamic considerations that occur during the functional monomer-template complex formation and MIP-ligand binding recognition. From analog to biological systems, the molecular recognition occurs by the combination of several complementary interactions between the binding sites and the template molecule. The phenomenon will be governed by the enthalpic and entropic contributions, which result in Gibbs free energy changes for the complex formation and rebinding recognition. This overview identifies the factors influencing the stabilization of a functional monomer-template complex to obtain an effective MIP-ligand binding.

It is interesting to note that the nature of the functional monomer-template complex is established by the quantity and the type of binding sites on molecularly imprinted polymers. It is also defined by the site's heterogeneity. The fidelity of the MIP binding sites depends on the extent and the stability of the functional monomer-template complex[105]. Consequently, it is critical to understand the functional monomer-template complex and its stabilization to achieve a rational design of MIPs. The thermodynamic equilibrium of MIP formation is defined by the Gibbs free energy changes of complex formation (ΔG_{bind})[106]:

$$\Delta G_{bind} = \Delta G_{t+r} + \Delta G_r + \Delta G_h + \Delta G_{vib} + \sum \Delta G_p + \Delta G_{conf} + \Delta G_{vdw} \quad (1)$$

Where the changes of Gibbs free energy are associated to complex formation (ΔG_{bind}) are: translational and rotational free energy (ΔG_{t+r}), internal rotation free energy (ΔG_r), hydrophobic interactions (ΔG_h), residual soft vibrational modes (ΔG_{vib}), the sum of interacting polar group contributions ($\Sigma\Delta G_p$), adverse conformational changes (ΔG_{conf}), and unfavorable van der Waals' interactions (ΔG_{vdW}). The translational and rotational terms are related to the order of complex that may be formed. The greater the number of components associated to the complex formation reduces the stability of the complex. The internal rotation free energy term indicates the importance of reducing the number of possible solution conformation by forming a more rigid structure. The sum of interacting polar group contributions implies that the stability of solution adducts depends on the number and the strength of functional monomer-template interaction created during the complex formation. The hydrophobic effect has been considered on the ΔG_h term, which indicates that a balance between the hydrophobic portions of the template structure and functional monomers enhances the stability of complex formation. The ΔG_{vdW} terms and the ΔG_{conf} term reflect that an effective solvation and the need for compromise of template conformation encourage the formation of solution adducts.

It is interesting to note that each thermodynamic contribution influences the ΔG_{bind}. The assessment of the extent of the functional monomer–template complexation will allow the optimization of MIP through the non-covalent approach. Sellergren et al.[107] pioneered the evaluation of the complex formation between

methacrylic acid (MAA) and phenylalanine anilide (PA) by NMR titration. The results are evidence of the MAA-PA complex formation with the apparent chemical shift. In another elegant approach, Nicholls and collaborators[10] employed UV spectroscopy to estimate the apparent change of Gibbs free energy at the prepolymerization stage. N-acetyl-Lphenylalaninyl-L-tryptophanyl methyl ester, yohimbine and cinchonidine were studied as template molecules for the imprinted crosslinked network based on methacrylic acid and ethylene glycol dimethacrylate. The method provided a valuable tool for the rapid screening of new molecular imprinting systems. However, the concentration range that can be assessed with UV studies is often below the traditional concentrations employed during MIP synthesis. In a recently published study, Karlsson et al.[11] performed ^{1}H-NMR studies to propose a model for the molecular basis of a functional monomer-template complex utilizing bupivacaine as a template molecule in poly(methacrylic acid-co-ethylene glycol) dimethacrylate. The results also suggested the possibility of preserving the electrostatic interactions during MIP polymerization. Subsequent studies by Mizaikoff and collaborators[108] applied FTIR and ^{1}H-NMR spectroscopy to study the complex formation of the template 2,4-dichlorophenoxyacetic acid with the functional monomer 4-vinylpyridine. Results confirmed the formation of a functional monomer-template complex based on hydrogen bonding interactions and hydrophobic interactions such as π–π stacking. Regardless, additional efforts have to be focused toward the characterization of the pre-polymeric stage. Peppas and collaborators[109] performed dynamic studies of

molecular imprinting polymerization by employing ATR-FTIR spectroscopy and differential photocalorimetry. Copolymers of 2-hydroxylethyl methacrylate and poly(ethylene glycol) dimethacrylate were investigated for the imprinting of glucose. Results showed an early lag period followed by a late auto-acceleration process during MIP synthesis.

To consider the physical principles underlying the MIP-ligand rebinding, equation (1) is simplified to equation (2) assuming the template populations will neither possess conformational strain nor adverse van der Waals interactions.

$$\Delta G_{bind} = \Delta G_{t+r} + \Delta G_r + \Delta G_h + \Delta G_{vib} + \sum \Delta G_p \quad (2)$$

Extensive studies should be performed to assess the relationship between the self-assembly and the MIP-ligand rebinding. However, several authors have executed thermodynamic experiments to comprehend the MIP-ligand binding kinetics. A typical example was reported by Sellergren and Shea[110]. Several elution conditions were evaluated by Van't Hoff analyses showing the effect on the enthalpic-entropy compensation during the binding of L-phylalanine anilide (D,L-PA). The pH of the solvent and several additives were included during the studies to select the optimal condition that enhanced the MIP-ligand rebinding. Consequently, the rebinding process was optimized to balance the electrostatic and hydrophobic interactions resulting in the entropy-enthalpy compensation. In another report, Mosbach et al. [79] attempted to develop an alternative fluorescence assay based on MIP. The imprinted polymers were synthesized by employing 2,4-

dichlorophenoxyacetic acid, 4-vinylpyridine (4-VP), and ethylene glycol dimethacryalte (EDMA) as the template molecule, the functional monomer and crosslinking agent, respectively. The specificity and selectivity of the assay were evaluated in an organic and aqueous solvent. Results demonstrated the contribution of the sum of polar and hydrophobic interaction that produced different specificities in organic and aqueous solvents.

In terms of understanding the MIP-ligand binding, Baggiani and collaborators prepared imprinted polymers for the binding of 2,4,5-tricholorphenoxyacetic acid (2,4,5-T) in an aqueous media. The mobile phase composition was optimized by different organic solvents, which provided variable polarity and hydrogen bond donor/acceptor properties. Retention factors were estimated for the elution of 2,4,5-T using acetonitrile, methanol, ethanol, propanol, isopropanol, tetrahydrofuran, 2-methoxyethanol, and 1,2-dimethoxyethanol. Results revealed that the molecular recognition mechanism was dependent on the combination of ion pairs and hydrophobic interactions.

Although progress to increase the knowledge of MIP formation and MIP-ligand binding has been made, a more extensive research is still required to rationally design MIPs. The impact of synthesis conditions in the self-assembly of a functional monomer-template complex, and the stability of the complex during the polymerization stage need to be elucidated through spectroscopic and

thermodynamic studies. Relevant information is essential to improve the MIP performance in aqueous systems.

2.8 Strategies for MIP Design

The synthesis and design of novel materials with high affinity and selectivity by employing the molecular imprinting technique have been a focal research area. The optimization strategies have been addressed by the assessment of the pre-polymerization stage or the post-polymerization stage[73].

Pre-polymerization stage assessment foresees the understanding of the functional monomer-template complex stabilization or the development of a method capable of simultaneous characterization of several significant factors on MIP synthesis. Takeuchi and collaborators[7] demonstrated a semiautomatic system to screen an MIP receptor through a combinatorial molecular imprinting method. Preliminary results were obtained from a first screening and a second regular screening was performed to provide detailed information. Results demonstrated that one way to design high performance MIPs is through the examination of thousands of various polymers prepared with different combinations and amounts of agents under diverse polymerization conditions. The study evaluated monomer acidity through the selection of MAA and TFMAA as functional monomers and the template/monomer ratio. Factors concerning crosslinking and solvents were fixed.

El-Toufaili and collaborators[111] enhanced the abovementioned approach by proposing a membrane module to cast the imprinted material simplifying the requirement of an automated system. The optimal solvent (porogen) and template to crosslinker ratio were investigated. 4-vinylpyridene (4-VPy) was chosen as the functional monomer. Three crosslinkers were investigated: ethylene glycol dimethacrylate (EGDMA), TRIM, and divynilbenzene (DVB). Quantitative screening was achieved by optimizing the thickness of the cast MIP layer and using fluorescence spectroscopy.

Davis et al.[112] described a chemometric approach to optimize the MIPs for sulfonamides. Chemometrics is the application of statistical methods to chemical data in order to extract the maximum relevant information to design or optimize experimental parameters. A methacrylic acid/ ethylene glycol dimethacrylate MIP was used as the model imprinted receptor. The molar ratio between the functional monomer, crosslinker, and template were the factors selected for evaluation. By using chemometric models with the selected significant factors, the study aimed at the evaluation to balance the flexibility and rigidity for MIP system to facilitate the mass transfer through the MIP pores without losing the imprinting memory. Results predicted an optimum ratio different to those ratios commonly employed in molecular imprinting within a range of 15.6 to 38.9%. This study also revealed surface response to predict the rebinding of SDIM on MIP.

The post-polymerization approach aims on the modification of binding sites distribution by either chemical or physical means. A good example is the evaluation of the influence of mobile phase composition investigated by Lu et al.[32]. Three kinds of imprinted polymers based on methacrylic acid crosslinked with ethylene glycol dimethacrylate were synthesized. The chromatographic performance was evaluated utilizing acetonitrile, acetic acid, and water as eluents. The investigation considered that acetic acid and water could compete with the carboxylic functional group of MAA and weaken the interactions within the polymer and the template molecule. Results demonstrated that an increase in water contents in the mobile phase did not cause a decrease in selectivity for the imprinted polymer. The MIP system also showed a better separation based on the acetonitrile-buffer mobile phase.

In another example, the potential of chemometrics for the proposal of a mechanism controlling MIP rebinding was considered by Nicholls and collaborators[113]. The influence of temperature and solvent polarity on rebinding was investigated. The synthesized imprinted polymers were based on MAA and EGDMA. Results showed the highest level of specific binding in pure toluene, pure acetonitrile at low temperature, and in 25% of acetonitrile in water at low temperature. Furthermore, they provided a basis for the prediction of MIP-ligand biding. The implications of these findings suggested the requirement of a methodological approach capable of making a relationship between the MIP formation and MIP-ligand recognition to rational design imprinted materials.

CHAPTER 3

3 Motivation and Objectives

With the evident growth in biosensor technology, an innovative approach has been required to develop less expensive material alternative to traditional options. In addition, the construction of a sensor systems with a higher stability compared to its counterparts (i.e. enzyme, antibodies, microorganism) is needed to extend the sensor's applications in an extreme environment (e.g. Mars). Furthermore, essential detection of biological markers is required to prevent chronic diseases. Thus, research objectives will assess both fundamental issues and the utility to predict the recognition capabilities of the sensor system during design phase.

Particular attention will be given establishing a sensor technology for hydrocortisone detection. Hydrocortisone is a biomarker and a key metabolic regulator produced by the adrenal gland (see figure 3.1). It influences the inflammatory response of the body, the glucose's metabolism due to the glyceroneogenesis pathway, and the immune system's functionality. Hydrocortisone counterbalances the effect of insulin by restoring blood glucose to its normal level and by increasing the glycogen stored in the liver, which are ready to support the stress response. Abnormal levels of hydrocortisone influence pathological conditions such as Cushing syndrome, Addison's disease, obesity, neurological conditions associated with constant stress, diabetes, and other syndromes. The detection of

hydrocortisone will prevent and control the medical treatment of these conditions. It is also relevant the detection of hydrocortisone to monitor the therapeutic treatment with corticosteroids drugs in sport medicine and to prevent disease associated with stress. Actually, hydrocortisone is detected by fluorescence assay, radioligand assay, enzyme fragment complementation (EFC), and reversed phase liquid chromatography. Fluorescence, radioactivity, and EFC techniques require the labeling of the template molecule that could interfere with the monitoring process. Much effort has to be devoted to the innovation of analysis techniques. Moreover, the detection of endogenous and exogenous hydrocortisone can be achieved through the development of imprinted hydrogels. The effectiveness of molecular imprinting polymers has demonstrated to be a promising alternative as a sensing device to detect hydrocortisone.

Encouraged by the aforementioned discussion, this research aims for the rational design of hydrogel based-MIPs to be employed as non-invasive biosensors to monitor biological markers and are foreseen as a combined technology with drug delivery systems. With this intention, and choosing hydrocortisone as the model template molecule during the studies with these intentions, the following specific objectives were established:

a. Demonstrate the effectiveness of the MIP complex monitoring method to optimize the hydrogel based-MIP design

b. Elucidate the formation of the functional monomer-template complex before and during MIP synthesis

c. Demonstrate a better understanding of MIP kinetics by comparing the rate of polymerization for imprinting and non-imprinted polymer syntheses; and by investigating the influence of solvent nature (i.e, protic, aprotic) during MIP synthesis

d. Develop thin film hydrogel-based MIPs composed of poly(methacrylic acid) crosslinked with tetra(ethylene glycol) dimethacrylate in aqueous solvent

e. Characterize hydrogel-based MIP to evaluate the optimal monomer/crosslinker ratio and investigate the influence of pH in the MIP's permeability abilities

f. Demonstrate a better understanding of the hydrogel based-MIP binding capacity and their selectivity in aqueous solution.

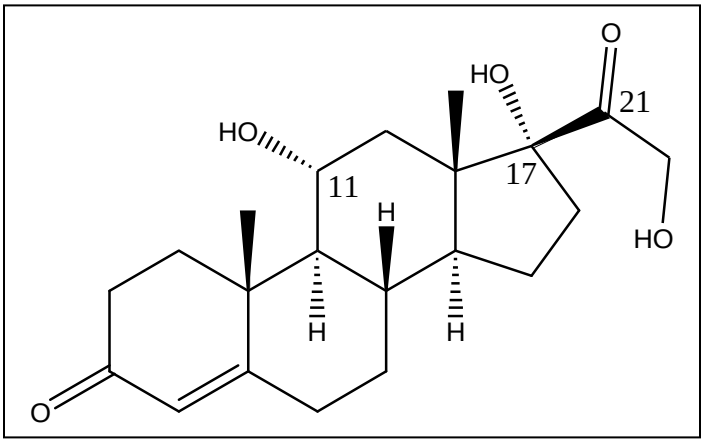

Figure 3.1 Chemical Structure of Hydrocortisone (template molecule)

CHAPTER 4

4 Toward the Rational Design of Molecularly Imprinted Polymers

4.1 Introduction

Molecular imprinting has become an increasingly active field of study for the development of recognition materials of predetermined selectivity. The technique itself and the potential application have been extensively reviewed[3, 48, 69, 70, 78, 80, 102, 114 115].

Although molecular imprinting is conceptually elegant in its simplicity, the molecular level events of the imprinting process are complex in nature. The final performances of MIP and its effectiveness are influenced by several factors during their synthesis such as the type of monomer, the monomer-crosslinker ratio, the template-monomer ratio, the type of initiator, porogen and percentage of dilution, the temperature and pressure of polymerization, the initiation process (e.g. thermal, photochemical), reaction time, and the dimension of the reaction vials[13]. Thus, it appears that a rational design of MIP requires extensive research associated to the imprinting process thermodynamics, the evaluation of the imprinting system via spectroscopic methods, the understanding of the polymerization and the MIP-ligand binding process, and computational studies to elucidate the self assembly of the

functional monomer-template complex, and to optimize the MIP synthesis and recognition abilities.

Some research efforts have been directed towards characterizing and understanding the physical mechanism underlying molecular imprinting process as discussed in detail on chapter 2, sections 2.6, 2.7 and 2.8. The development of a true understanding of the MIP formation and MIP-ligand recognition will assist in the rational design of MIP for specific applications.

Several authors have described the physical factors leading to the formation of functional monomer-template complex and MIP-ligand binding [105, 106, 116]. A vast range of variables play a role in determining the success of imprinting polymerization as previously mentioned. Different approaches have been utilized to predict and optimize the MIP design. These independent efforts have demonstrated the feasibility of the MIP rational design by having a better insight of the molecular imprinting process. Molecular Dynamic (MD) Simulations of the imprinted polymer formation and additional state-of-the-art computational tools are employed to generate a virtual library that will allow the pre-selection of the functional monomer, crosslinker, and porogen employed during MIP synthesis[117]. Essential drawbacks of purely non-experimental approaches are associated with a long time of model and code development and a limited amount of memory for the study performance. The last limitation will define the number of molecules and the volume of the system under evaluation. However, there is another macroscopic effect within the imprinting

process that needs to be assessed through empirical evaluation. The combination of simulation results with an experimental approach will support not only a screening stage; it also reinforces the MIP rational design to obtain a more comprehensive picture of the system of interest.

Another approach to elucidate the imprinting process has focused on understanding the principal aspects that influence the formation of the functional monomer-template complex at the MIP formation stage. Knowledge about the dynamic process of the functional monomer-template association employing spectroscopic techniques is important to understand and possibly predict the behavior of MIPs. Sellenger's group has pioneered the self-assembly evaluation by NMR studies, which is reflected in the Gibbs free energy for the total binding of functional monomer-template complex [118]. Direct evidence has been presented to identify the complex motif and to estimate the association constant of complex formation[10, 30, 119-124]. Nicholls et al. proposed a model for the molecular basis for ligand recognition of MIP by employing NMR spectroscopy[11]. Mizaikoff et al.[108] analyzed the self-assembly mechanism of functional monomer-template complex on the pre-polymeric solution by employing FTIR and NMR spectroscopy. The above-mentioned studies can be considered sensitive methods to identify the magnitude and type of interactions at the MIP complex formation. A further-reaching goal is to combine methods to obtain information related to the functional monomer-template complex's stability through the MIP synthesis.

In order to draw conclusions on how variables relate to the MIP preparation and how they affect their effectiveness during the MIP-ligand rebinding, it is necessary to characterize the imprinting process during polymerization. An interesting study, which evaluates the effect of the template molecule on the polymerization rates and conversion of the imprinting polymerization was reported by Peppas and collaborators [109]. An early lag period was observed on the rate of polymerization followed by a late auto-acceleration during the copolymerization of 2-hydroxyethyl methacrylate (HEMA) and poly(ethylene glycol) dimethacrylate (PEG600DMA). This indicates a complex formation between the functional monomer and the template molecule. Initial attempts were also performed by several groups to confirm that the template-template[12] and functional monomer-template interactions[11] were preserved during the primary stage of the polymerization process using NMR spectroscopy. Collectively, these results provided the basis to hypothesize that a cooperative ligand recognition event in the (-)nicotine-imprinted methacrylic acid-ethylene dimethacrylate copolymers occurs. It is interesting to note the above-mentioned finding must be complemented with empirical evidence that will explain the extent of the solution complexes formed between the monomer and the template during polymerization. In fact, the extent of functional monomer-template interaction in the solution reflects the architecture of the binding site. This piece of information demonstrates MIP can be physically characterized on a molecular level by

spectroscopic methods. Furthermore, a greater interest has to be focused in the development of a method that will correlate MIP formation with MIP-ligand binding.

Despite the fact that understanding the self-assembly of the functional monomer-template complex during the pre-imprinting stage (i.e. MIP formation) will enhance the development of MIP, a number of factors can influence the MIP-ligand rebinding and should be considered (refer to section 2.6). It is clear that molecular level studies of MIP-ligand interactions have aimed the MIP design. Researchers in the field have carefully examined the MIP-ligand binding with FTIR and NMR spectroscopy. Shea et al. demonstrated an effective method for quantitative analysis of interaction sites in the MIP[125]. Related efforts directed to the identification of MIP-ligand binding capacity have recently been undertaken by other authors[31, 126-128]. The adsorption and desorption of the template molecule on imprinted polymers was followed by Surface Enhanced Raman-scattering measurements (SERS)[28].

A significant advance was made to elucidate the imprinting mechanism. This approach will remain an additional value to the molecular imprinting tool-kit in order to optimize the binding sites on MIP materials in an aqueous media. Although MIP synthesis is frequently performed in apolar/aprotic solvents, the use of on a polar solvents has already been investigated yielding MIP with limited performance. It would be suitable to rationally design imprinted materials in mostly polar porogen with binding/release capabilities. The principal purpose is the analytical troubleshooting of significant factors that influence the formation of the functional

monomer-template complex, MIP synthesis, and MIP-ligand rebinding. Progress toward the empirical optimization of the binding/selectivity behavior of MIP will open the doors for the design of a new intelligent target *in situ* sensing device that could be combined with drug delivery systems[129].

At this time, relatively few studies have described the rational design of imprinted hydrogels. This study aims at the evaluation of: 1) functional monomer-template complex formation, 2) polymerization and site formation; and 3) MIP-ligand rebinding. Knowledge of the strength of interaction and complex stoichiometry, evaluation of polymer morphology and complex stability lifetime, and the assessment of MIP-ligand rebinding are necessary for further development of hydrogel based-MIPs with high selectivity and specificity. The interest of this work is to understand how the MAA-hydrocortisone complex formed in solution gives rise to the imprinted sites present in the MIP. In particular the assessment: (i) examined the extent of acetic acid with hydrocortisone which behaves analogously to MAA, (ii) investigated the effect on the magnitude of interactions in dimethylsulfoxide (ε, dielectric constant = 47.2), and ethanol (ε = 24.3), (iii) examined the effect of MAA-hydrocortisone complex formation in the polymerization kinetics, (iv) evaluated the influence of MAA-hydrocortisone complex formation on the resultant imprinted hydrogel morphology. To this end, ^{1}H-Nuclear Magnetic Resonance (NMR) titration and continuous variation studies were performed to identify interaction sites and estimate the apparent affinity during the self-assembly of the complex. Moreover,

Attenuated Total Reflectance Fourier Transform Infrared (ATR-FTIR) studies were performed to monitor molecular imprinting synthesis. Essential information was collected to predict the possible interaction of MIP-ligand rebinding (see chapter 5.0)

Therefore, the comprehensive analysis of self-assembly, polymerization and post-polymerization stage with complementary techniques enable fundamental insights to enhance MIP effectiveness. A successful MIP design must be achieved by making a rapid functional monomer screening, understanding the solvent effect on the imprinting process, identifying the type of interactions present on the MIP processes, and by being familiar with the effect of crosslinker on-site formation. The rational approach described herein particularly focuses on imprinted hydrogels designed in an aqueous media to compromise between rigidity and flexibility for further applications in sensor technology and drug delivery systems.

4.2 Experimental

4.2.1 Materials

All solvents and chemicals were of analytical grade. Methacrylic acid (MAA) was purified in a vacuum prior to use. Hydrocortisone and dimethyl sulfoxide were supplied by Sigma Aldrich (St. Louis, MO, USA). Ethanol (HPLC grade) and acetone (HPLC grade) were obtained from Fisher Scientific (Fair Lawn, New Jersey, USA). Methacrylic acid and tetraethylene glycol dimethacrylate were received from Polysciences (Warrington, Pa, USA). Deuterium oxide (D_2O), dymethyl sulfoxide-d_6, ethanol-d_6, and acetic acid-d_4 were supplied by Wilmad (Buena, NJ, USA). Tetramethylsilane (TMS) was obtained from Wilmad (Buena, NJ, USA). 1-Hydroxyl cyclo hexyl phenyl ketone was purchased from Sigma Aldrich (St. Louis, MO, USA).

4.2.2 Nuclear Magnetic Resonance (NMR) Titration

In order to estimate the magnitude of the interaction between the functional monomer (MAA) and the template molecule (hydrocortisone) in the relevant solvent, NMR titration studies were conducted. This information is essential for the potential prediction of the binding capacities of MIP, monomer and porogen selection, and initial functional monomer-template ratio. It reflects the degree of MAA-hydrocortisone complex at the pre-polymeric mixture. The NMR characterization of functional MAA-hydrocortisone interactions was performed by systematically adding acetic acid-d_4 (monomer analog) to a solution of hydrocortisone (16M) at room

temperature (see figure 4.1). The effect of solvent in the complex formation was evaluated by the use of dymethyl-sulfoxide-d_6, and ethyl alcohol-d_6. The acetic acid-d_4 concentration was varied from 0 to 16 M in the pre-polymeric solution. NMR spectra of the pre-polymeric mixture were recorded on a Bruker Advance 500 MHz spectrometer (B_0 11.74 Tesla), equipped with a broadband detection and QXI-4 detection probes. 1D ^{1}H spectra were acquired with a spectral width of 10330 Hz and 32768 data points. The chemical shift (δ) or relative change in the resonance frequency of the proton in the sample was measured as a function of acetic acid concentration using tetramethylsilane (TMS) as the standard reference. The chemical shifts were measured in protons associated with carbon 11 (4.225 ppm, 4.285 ppm), carbon 17 (5.185 ppm) and carbon 21 (4.669 ppm, 4.658 ppm, 4.657 ppm) during the NMR titration. These protons have been identified as possible interaction points between MAA and hydrocortisone. Apparent disassociation constants were calculated using a non-linear fitting to a one-site model[11] with the software package Origin (version 7.5, Origin Lab, USA). Origin is a software package that provides data analysis and graphing workplaces. It also offers linear and non-linear data fitting methods (e.g., polynomial, Lorentzian, and non-linear least square).

Refer to appendix A and B for calculation example and raw data review.

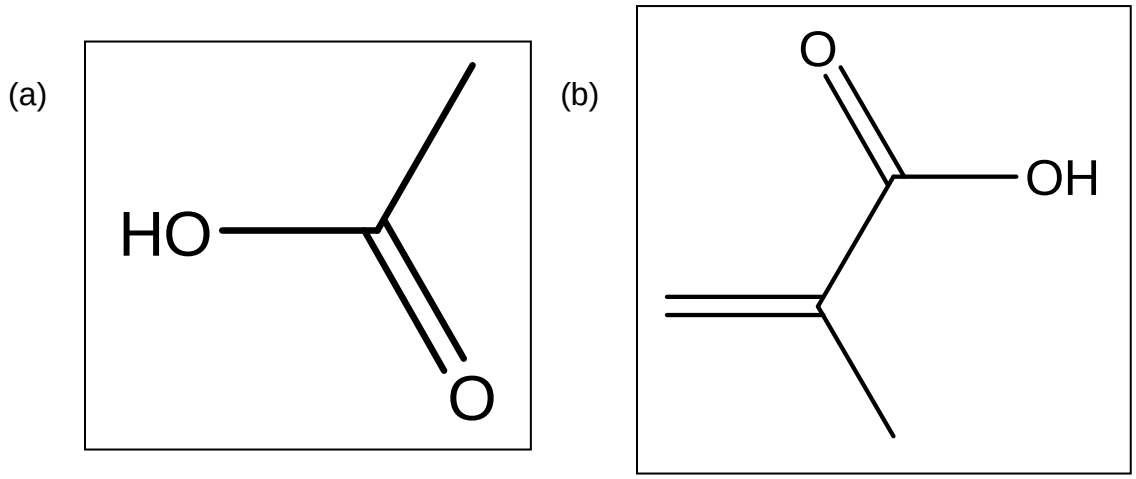

Figure 4.1 Structure of acetic acid (a) and methacrylic acid (b). The presence of carboxylic acid functional groups in both structures promotes interactions that were compared during the functional monomer-template complex assessment.

4.2.3 Continuous Variation Method

The non-covalent interaction for molecular imprinting is limited by the stability of the functional monomer-template complex. The molecular complex's stability in the pre-polymeric mixture can be predicted by modifying the monomer-template ratio in order to move the equilibrium towards the complex formation. To this end, a continuous variation method was conducted using the previously described Bruker Advance 500 MHz spectrometer (B_0 11.74 Tesla). Samples were prepared in dimethyl sulfoxide-d_6 and ethyl alcohol-d_6. The molar fraction of hydrocortisone and functional monomer was systematically varied from 0 to 1.0 with a constant total concentration of 16 M. NMR spectra of the pre-polymeric mixtures were recorded to determine the displacement of chemical shifts in the corresponding protons of possible interactions as previously discussed. A non-linear curve of the suitable property of the system against the MAA-hydrocortisone ratio was examined for discontinuities or abrupt changes of slope corresponding to the stoichiometry of the MAA-hydrocortisone complex[130].

Refer to appendix C and D for calculation example and raw data review.

4.2.4 In situ polymerization by Attenuated Total Reflectance Fourier Transform (ATR-FTIR) Spectroscopy

The structure and local environment of imprinted hydrogels were evaluated by ATR-FTIR studies. The extent of the functional monomer-template complex and its stability's lifetime were monitored during the imprinted synthesis. *In situ* free radical polymerization was performed on ZnSe 45° crystal in an inert environment employing a 1.20±0.30 mW/cm^2 ultraviolet source at room temperature (see figure 4.2). The reaction system was sealed and purged with nitrogen for 10 minutes. Pre-polymeric mixtures were prepared with 1:1 and 1:4 MAA-EGDMA molar ratios to evaluate the influence of complex formation during the imprinted material synthesis. The effect of the solvent nature was studied by performing the hydrogels' synthesis in aqueous (50% wt ethanol solution) and non-aqueous (dimethyl sulfoxide) environments. Spectra were collected every 0.5 minutes with an IR300 ThermoNicolet spectrometer (USA) equipped with a KBr beam splitter and DTGS detector. The spectral range used during the study was 4000-400cm^{-1} with a spectral resolution of 4 cm^{-1}. A comparison peak height versus a common baseline point was performed to estimate the conversion of double bonds.

Refer to appendix E and F for calculation example and raw data review.

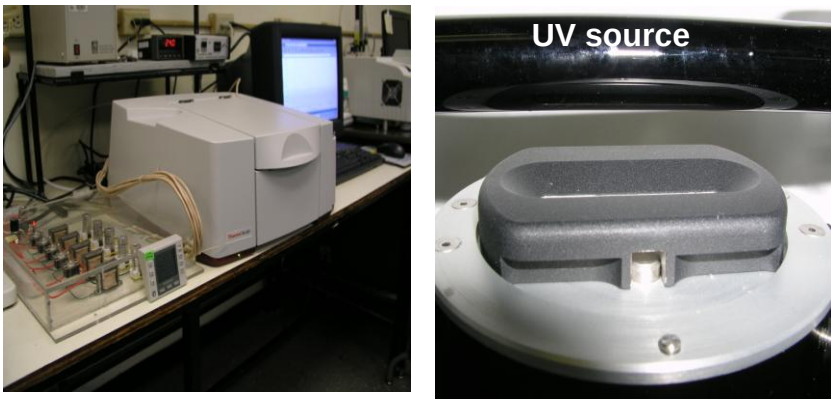

Figure 4.2 In situ polymerization by Attenuated Total Reflectence Fourier Transform Infrared. The polymerization of imprinted and non-imprinted polymers was evaluated in an inert environment. (a) In situ polymerization system, which included a UV source and ATR-FTIR spectrometer.

4.3 Results and Discussion

4.3.1 Self-Assembly Analysis of the Pre-polymeric Mixture for the Prediction of MIP Performance

The self-assembly of functional monomer-template complex has been monitored by estimating the binding constant of the pre-polymeric mixture through spectroscopic techniques (e.g. NMR spectroscopy, FTIR spectroscopy, UV-Vis spectroscopy, fluorescence spectroscopy, Raman spectroscopy, and mass spectrometry) [10-12, 28, 109, 123, 131-134]. In the present study, the formation of the functional monomer-template complex at the molecular level of the imprinting process was evaluated by employing the continuous variation and NMR titration studies. The method of continuous variation, often called Job's method, was employed to determine the stoichiometric coefficients *m* and *n* of the functional monomer-template complex of the type S_mL_n. This information is complementary to the evaluation of the stability or association constant obtained from NMR titrations studies. NMR spectroscopy gives information regarding the nature of the interaction between the functional monomer and the template molecule. The intermolecular interaction of the complex modified the electronic environment of the protons and in the presence of a magnetic field a diamagnetic anisotropy is generated. The induced chemical shift that results from this effect is examined using NMR spectroscopy.

Consequently, the dynamics of the MIP complexes in pre-polymeric solution were predicted.

The determination of the possible stoichiometric relationship of the MAA-hydrocortisone complex was examined with the continuous variation method using acetic acid-d_4 as the monomer analog. The molar fraction of hydrocortisone and acetic acid-d_4 was varied from 0 to 1 with a total constant concentration of 16 M. The Job plot (Fig.4.2) was constructed by evaluating the complex concentration ($\Delta\delta$ x f_t) as a function of the molar fraction of the template (f_t). To understand the quantitative explanation of the Job plot, it is required to develop the expression that represents how the complex concentration varied with the mole fraction. Consider the formation of higher complexes directly from the substrate (S) and ligand (L) , as in

$$mS + nL \leftrightarrow S_m L_n \qquad (4.1)$$

As a result, the overall binding constant (β_{mn}) is defined as

$$\beta_{mn} = \frac{[S_m L_n]}{[S]^m [L]^n} \qquad (4.2)$$

which can also be considered as the overall stability constant (β_{mn}). The overall stability constant is the product of the corresponding binding or association constants (K_{mn}) which result from higher order complexes S_mL_n. Thus, $\beta_{mn}=K_{11}K_{12}$ for a stepwise complex formation.

The mole fraction (f_t) can be defined as

$$f_t = \frac{L_t}{S_t + L_t} = \frac{L_t V}{\upsilon c} \qquad (4.3)$$

where L_t is the total ligand concentration ($Lt=\upsilon_L c/V$). In addition, the mole fraction can be calculated as

$$f_t = \frac{L_t V}{\upsilon c} \qquad (4.4)$$

Combining equation 4.3 and 4.4, it resulted in

$$\frac{L_t}{S_t + L_t} = \frac{L_t V}{\upsilon c} \qquad (4.5)$$

The mass balance equations of the system,

$$S_t = S + m S_m L_n \qquad (4.6)$$

$$L_t = L + n S_m L_n \qquad (4.7)$$

The equations for the method of continuous variation can be expressed as follows by combining equations 4.2 to 4.7,

$$c_f (1 - f_t) = S + m S_m L_n \qquad (4.9)$$

$$c_f f_t = L + n S_m L_n \qquad (4.10)$$

$$\beta_{mn} S^m L^n = S_m L_n \qquad (4.11)$$

where $c_f = \upsilon c/V$. If equation 4.9, 4.10 and 4.11 are combined, they produce

$$\beta_{mn} c_f (1 - f_t) - m S_m L_n \; c_f f_t - n S_m L_n = S_m L_n \qquad (4.12)$$

By differentiating equation 4.12 with respect to f_t and finding the maximum mole fraction (f_{tmax}) of $d[S_mL_n]/df_t=0$ one obtains:

$$\frac{n}{m} = \frac{f_{t\max}}{1 - f_{t\max}} \qquad (4.13)$$

Consequently, the maximum of the continuous variation curves represents the ratio of the molecular complex in solution.

Figure 4.3 illustrates continuous variation curve, which represent the stoichiometry of the MAA-hydrocortisone complex in dimethyl sulfoxide. The concentration of the complex is proportional to the product of f_t x $\Delta\delta$. The Job plot analysis demonstrated a maximum value of the molar fraction (f_{tmax}) of 0.4. It indicates a 1:2 complex formed in solution. The results obtained reflect the relative molecular association, which denote SL_2 stoichiometry. The 1:2 complex is formed by the addition of a second ligand to the 1:1 complexes. The existence of a 1:2 complex suggests the formation of a 1:1 complex, assuming that every complex is formed in a bimolecular process of the following equilibrium:

$$S + L \leftrightarrow SL \qquad (4.14)$$

$$SL + L \leftrightarrow SL_2 \qquad (4.15)$$

Moreover, Job plot results confirm the possibility of the formation of two binding sites during the imprinting process that can promote better affinity during the MIP-ligand rebinding. It has been observed that multiple interaction sites will afford higher complex stability and will promote higher affinity than single functional monomer-template interaction[78]. A two-sites model could be hypothesized based on the results obtained by Mosbach and collaborators. Previous reports associated with artificial antibodies to corticosteroids by molecular imprinting[44, 135] have deduced the implication of various functionalities for hydrocortisone recognition. Mosbach and collaborators have identified the 11-, 17, and 21-OH groups that will directly influence the binding ability of the MIP. These hydroxyl groups are able to act as both hydrogen donor and hydrogen acceptor. Now, it is essential to understand the magnitude of the MAA-hydrocortisone interaction and if these interactions with the carboxyl functionality of the methacrylic acid residues within the MIP will be stabilized during the polymeric synthesis (refer to section 4.3.2).

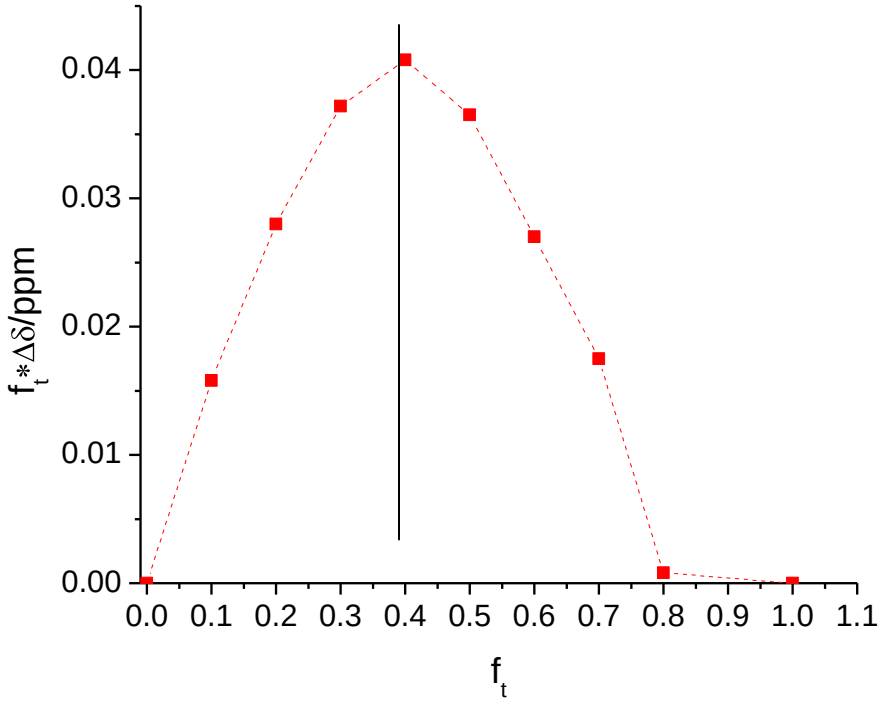

Figure 4.3 ^{1}H Continuous variation method for the complex formation of hydrocortisone with acetic acid-d_4.

In order to evaluate the extent of the MAA-hydrocortisone complex, the dissociation constant was determined through NMR titration. A series of NMR titrations with acetic acid, monomer analog, in a hydrocortisone solution (16 M) was performed to estimate the strength of interaction related to adduct formation with the hydroxyl functional group (i.e. 11-, 17-, and 21-OH group). The effect of the nature of the solvent was evaluated by performing NMR titration on dimethyl sulfoxide-d_6, and ethanol-d_6. As depicted in figure 4.4, initial displacement was observed on the resonance of hydroxyl protons (17-OH, 21-OH) of hydrocortisone at the initial addition of acetic acid. Direct evidence associated with the downfield shift was observed and it is indicative of the interactions between the hydroxyl groups of the template molecule and the carboxylic acid moieties of acetic acid. This result can be confirmed by previous reports[136], which demonstrated that the carboxylic acid-based monomers have been successfully imprinted, recognizing their ability of H-bond donor, H-bond acceptor, ion pair formation and dipole-dipole interactions. In addition, a saturation isotherm as a function of monomer concentration (see Fig. 4.4) enabled the determination of the apparent dissociation constants (K_d) for the complex formation. Table 4.1 summarized the dissociation constant estimated by performing a non-linear fitting with a one-site model.

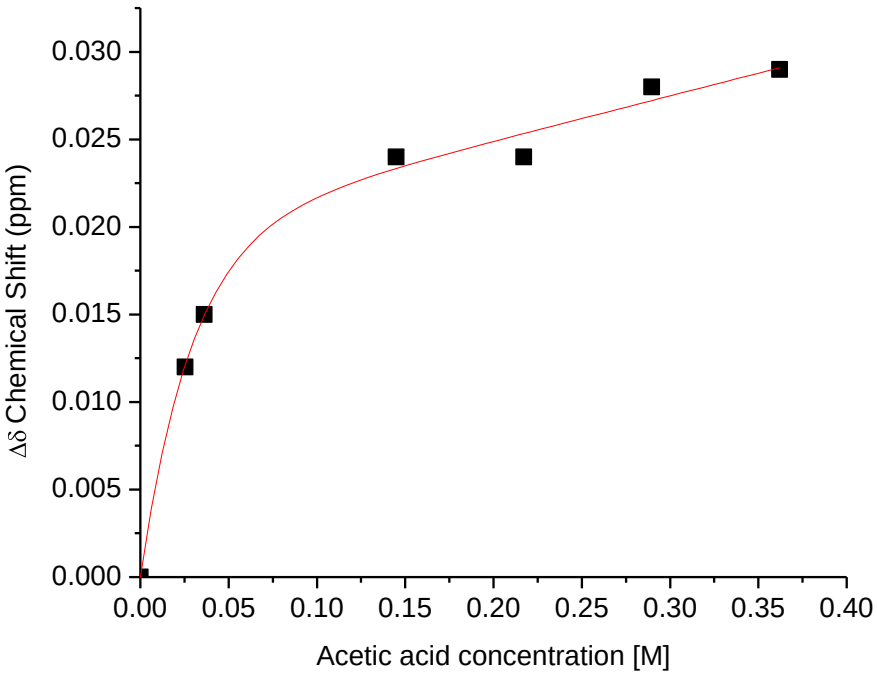

Figure 4.4 Binding isotherms of hydrocortisone/acetic acid complex formation in dimethyl sulfoxide-d_6. A non-linear fitting was performed having a square of Pearson correlation coefficient (R^2) of 0.9899.

TABLE 4.1 Apparent dissociation constant for acetic acid-d_4:hydrocortisone complex

Proton[b]	Dimethyl sulfoxide-d_6 /M	Ethanol-d_6 /M
17-OH	**0.0408±0.003**	**0.5814±0.0.1163**

[b] See figure 3.1 for numbering

The complex's affinity can be related to the magnitude of K_d, which reveals the strength of the functional monomer-template interaction. Naturally, higher dissociation values were observed in ethanol as a result of a higher dielectric constant that is related to the hydrogen bonding capacity of the solvent. Moreover, the magnitudes of the dissociation constants are equivalent to those previously reported for hydrogen bonding[11]. NMR results suggested that the synthesis of an imprinted hydrogel using ethanol as a porogen produced MIPs with binding characteristics of a lower affinity compared to MIPs fabricated with traditional molecular imprinting solvents (i.e. aprotic porogens). However, it demonstrated the feasibility of manufacturing a hydrogel based MIP with imprinting sites recognizing the presence of a MAA-hydrocortisone complex at the pre-polymeric mixture.

Collectively, the continuous variation and Job plot results are qualitative; related with the selectivity and affinity of the resultant MIP and it showed the feasibility for the further development of MIP in more polar solvents. It has been postulated that the MAA-hydrocortisone complex observed at the pre-polymeric mixture would be transformed to a specific binding site. However, the induced

chemical shifts identified in the above-mentioned NMR studies represent the equilibrium average state of a highly dynamic system. The principal objective was to confirm the incorporation of hydrocortisone into the polymer for the formation of imprinted sites. Furthermore, the hypothesis that the functional monomer-template complexes are stable during MIP synthesis to generate imprinted sites was corroborated (refer to section 4.3.2). These results suggested a cooperative effect in the resultant MIP if the multiple interactions observed in the MAA-hydrocortisone complex assemblies were stable during the MIP formation. Moreover, it was concluded that the type and degree of crosslinking and the porogen influenced the association's equilibrium and the absorption-desorption kinetics during MIP rebinding. These factors require rational optimization (refer to chapter 5.0).

4.3.2 Analysis of MIP synthesis

For the further advance to develop materials possessing the responsive properties for sensing and drug delivery applications, molecularly imprinted hydrogels were synthesized by free radical polymerization. The imprinting process was monitored by ATR-FTIR spectroscopy. The main objective was to evaluate inter and intra-molecular changes promoted by functional monomer-template complex formation during the synthesis of molecularly imprinted hydrogels. The synthesis of

imprinted hydrogels was performed in the relevant solvent in varying MAA/EGDMA ratios.

Figure 4.5 demonstrates the imprinted hydrogel spectra of *in situ* polymerization in dimethyl sulfoxide. The spectra show the characteristic absorption peaks of the expected chemical structures (e.g. νC-H = 3000 – 2850 cm^{-1}, νO-H_{MAA}= 3400 -2400 cm^{-1}, νC=O_{MAA}=1710 cm^{-1}, νC=O_{TEGDMA} = 1730 cm^{-1}, νC=C = 1640 cm^{-1}). A medium absorption was observed at frequencies from 3000 to 2840 cm^{-1} that corresponds to sp^3 C-H stretching. The absorption intensity of sp^3 C-H stretching was reduced by performing the synthesis in an aprotic solvent. Moreover, reducing the amount of the crosslinker used in the polymerization feed resulted in a more intensive band absorption at 2500 cm^{-1} due to the O-H stretching of MAA carboxyl moieties. The absorption at 1710 cm^{-1} that corresponds to the carbonyl group (C=O) is strong. Concurrently, the chemical shift of the carboxylic acid vibration at 1710cm^{-1} was observed. These results suggested the formation of interaction sites within the carboxylic acid functional group. The C=C stretching vibration peak at 1640 cm^{-1} confirmed how the polymerization proceeded. The C=C stretching vibration was not employed to estimate the conversion of double bond recognizing this absorption could be affected by the presence of solvent, specifically water, during the polymerization process. Furthermore, the formation of carbonyl salt at 1300 cm^{-1} suggests the formation of cooperative interactions that have the possibility to enhance the stability of the functional monomer-template complex.

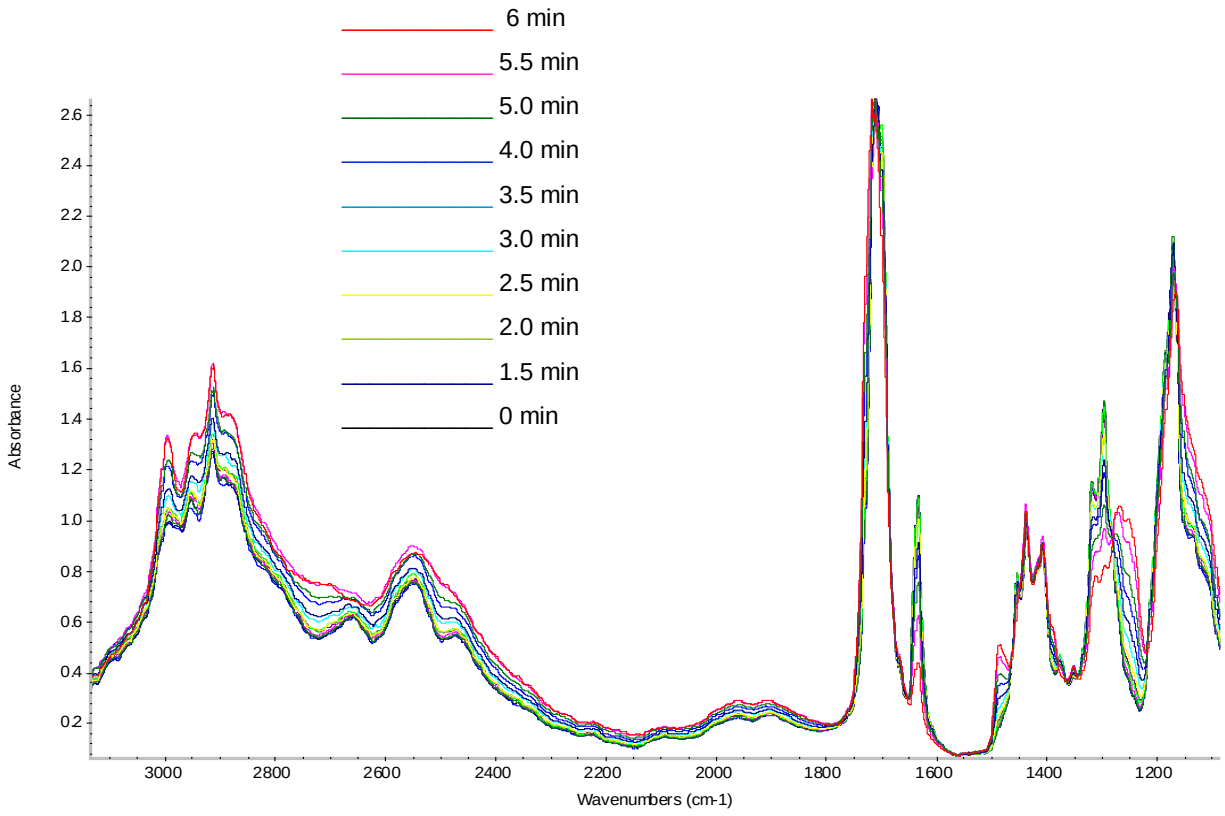

Figure 4.5 ATR-FTIR spectrum of in situ polymerization for 4:1 imprinted hydrogels in a non-aqueous environment (dimethyl sulfoxide). The spectrums were taken before irradiation and after 0.5, 1, 1.5, 2, 2.5, 3, 3.5, 4, 4.5, 5, 5.5, 6 minutes of irradiation by UV light.

The apparent conversion of the double bond, which is directly related with the decrease of absorbance under =CH2 rocking vibration at 1320 cm^{-1}, was calculated as,

$$conversion\ of\ double\ bond = 1 - \frac{\upsilon = CH_2 rocking_t}{\upsilon = CH_2 rocking_0}$$

Herein ν=CH2 $rocking_0$ and ν=CH2 $rocking_t$ are the heights of the absorption peak at 1320 cm^{-1} before and after the exposure for time t. The conversion was monitored to evaluate the effect of the imprinting process in the relevant solvent. The solvent employed was dimethyl sulfoxide and a mixture of 1:1 mass ratio of ethanol and water-d_2. Figure 4.6 illustrates the apparent conversion as a function of time in a non-aqueous (a) and aqueous environment (b), respectively.

As depicted in figure 4.6, the conversion profiles demonstrated the principal steps of chain-growth polymerization: a) the initiation of the active monomer by the association of a free radical initiator species and a single monomer molecule (less than 2 minutes on figure 4.6, (a)), b) the propagation of an active chain by sequential addition of monomers (between 2 to 5 minutes on figure 4.6, (a)); and c) the termination of the rapid growth of polymer chain by the formation of inactive covalent bonds (more than 5 minutes on figure 4.6, (a)). In addition, the imprinting process reduced the conversion of double bounds significantly after 2.5 minutes of polymerization by comparing the imprinted (○) and non-imprinted (□) synthesis.

These results suggested a lower mass transfer of a monomer unit (MAA) due to the MAA-hydrocortiosone complexation. It seems likely that the monomer-template interactions are sustained during polymerization leading to the formation of receptor or imprinted sites. It could be hypothesized that during the MIP synthesis the specificity of the recognition sites could be further developed by changing shapes and introducing an additional functional monomer. This hypothesis is supported by the observation of functional group formation during the MIP synthesis as depicted in figure 4.5. Certainly, the results suggest an influence in the morphology of the imprinted material through the presence of the functional group (MAA) and the template molecule (Hydrocortisone) during the MIP. Similarly, Peppas and collaborators observed a reduction in double bond conversion through the study of the HEMA/Glucose system[109].

The comparison of figures 4.6 (a) and 4.6 (b) showed a higher reduction in the conversion of double bond. The results become evident after the consideration of the solvent effects during the analysis of the propagation of polymer chains. A similar relative effect has been shown by Beuermann and collaborator[137] in the MAA's reactivity depending on the amount of MAA dimers or monomers in solution. A higher polar solvent, such as the mixture of water and ethanol, competes with self-association of the MAA and the polymer chains, the self-association of MAA dimmers and the MAA-hydrocortisone complex. Consequently, the polymer chain's growth and the final shape of the imprinted site are influenced by the presence of the

template molecule (hydrocortisone). However, the in situ polymerization results demonstrated the successful completion of MIP synthesis suggesting the effective fabrication of imprinted hydrogels to extend its application as a targeted drug delivery system[70].

Moreover, the auto-acceleration of non-imprinted and imprinted synthesis was confirmed by observing 3-fold and 6-fold increments of slope magnitude in the sigmodal curve that represent the conversion of the double bond as a function of time, respectively (see figure 4.6 (a) and (b)). A 2-fold reduction in the slope was observed with the introduction of the template molecule by comparing the non-imprinted and imprinted synthesis. The critical conversion at which auto-acceleration begins (i.e. 0.05 for aprotic solvent, and 0.04 for aqueous media) was determined by the intersection of the lines tangent to the conversion versus time curve before and after auto-acceleration[138].

(a)

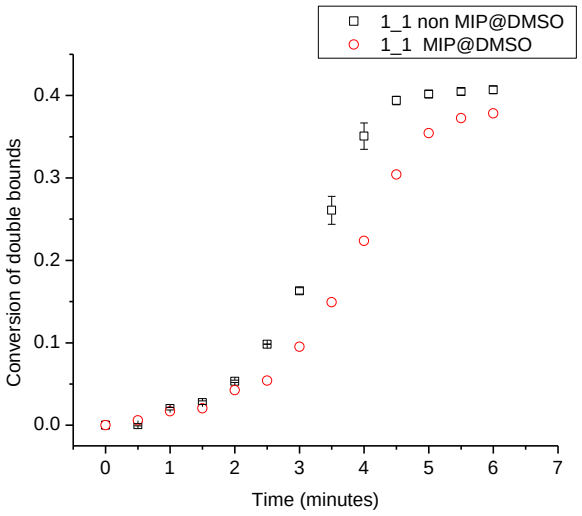

(b)

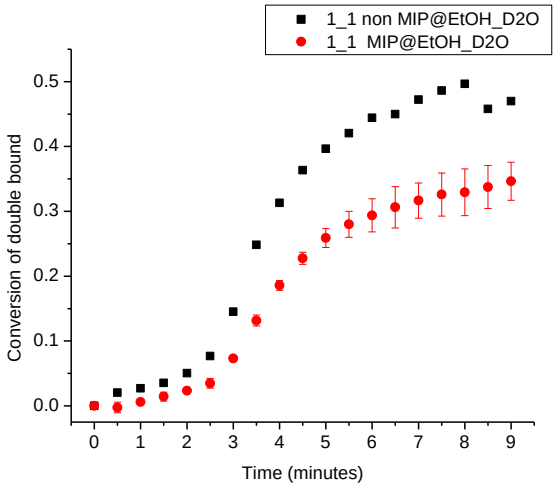

Figure 4.6 Conversion of the double bonds as a function of time for imprinted (○) and non-imprinted (□) hydrogels

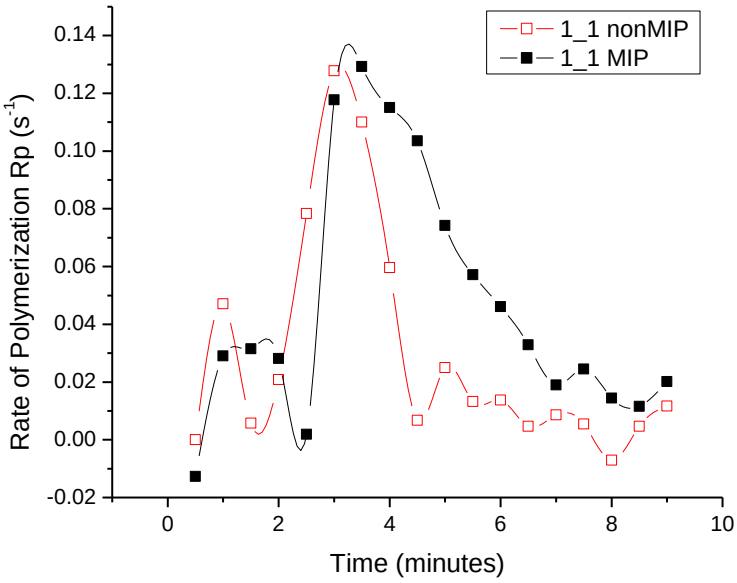

Figure 4.7 Rate of polymerization (R_p) in an aqueous media as a function of time for non-imprinted and imprinted hydrogels

The rate of polymerization (R_p) was estimated to evaluate the effect of complex formation during the imprinted material synthesis. Figure 4.7 shows the rate of polymerization of imprinted (MI) and non-imprinted (non-MI) hydrogels. The imprinted hydrogels demonstrated a lower rate of propagation during the initial 3 minutes of the reaction, which confirms the possible explanation of a lower monomer transfer through the imprinting process. The auto-acceleration effect is also present during the MI and non-MI hydrogels' synthesis. It is suggested that the structural integrity of the MAA-hydrocortisone complex was preserved during the synthesis thus reducing the MAA's mobility that resulted in lower rates of propagation. Higher dissociation rates of the MAA-hydrocortisone complex relative to the propagation rate will not influence the MAA's mobility. Consequently, the rate of propagation will not be reduced. In addition, favorable orientation of the polymer chain during the MIP synthesis produces a higher rate of polymerization in the final steps of the polymer's growth previously observed by the 6-fold slope increment. Consequently, the formation of specific sites with recognition abilities as a result of the functional monomer-template molecule's interactions and by changing the shape during the completion of fully polymerized system is foreseen. As depicted in Figure 4.4, the auto-acceleration is observed at 2.5 minutes for 1:1 MAA:TEGDMA ratio.

4.4 Concluding Remarks

The formation of the MAA-Hydrocortisone complex was elucidated with the Job method and NMR titration studies. The results indicated that, under the relative stoichiometry and concentration employed in this study, methacrylic acid is capable of interacting with hydrocortisone forming complexes, which results in imprinted cavities on molecularly imprinted hydrogels. The presence of 1:2 complexes supports the prediction of high affinity sites in further MIP fabrication. Knowledge of the association constants between the template and the monomer in solution is qualitatively related with the selectivity and affinity of the resultant MIP and it shows the feasibility for the further development of MIP in more polar solvents. The optimization of the functional monomer-template molar ratio, the porogen selection, and the type and degree of crosslinking would lead to a larger fraction of high affinity sites on the MIP.

The synthesis of imprinted hydrogels based on Poly(MAA-TEGDMA) was monitored by ATR-FTIR. In situ polymerization experiments were performed in a variety of solvents that had a direct impact on MIP synthesis. In situ polymerization identified the presence of a functional group in an aqueous media that will promote the formation of imprinted sites. A reduction of the rate of polymerization at the beginning of the imprinted synthesis confirmed the structural integrity of the MAA-hydrocortisone complex already observed from the Job method results. In situ

polymerization results also demonstrated that the monomer-template interactions were not perturbed during the synthesis. It was observed that the arrangement of the carboxyl groups was fixed in space and complementary to the template molecule (hydrocortisone).

In summary, this study clearly demonstrated that monitoring the stability of the functional monomer-template complex before and during the imprinting process provides an in depth insight of the imprinting phenomenon to enhance the MIP design.

CHAPTER 5

5 Molecular Recognition Properties and Characterization of a Hydrogel based-MIP in an Aqueous media

5.1 Introduction

The monitoring of specific clinical markers is highly desirable and has been achieved through the creation of advanced imprinted materials. Imprinted hydrogels are attractive for the production of biomimetic sensors and non-immunogenic synthetic systems as an alternative to biological recognition agents[139]. The molecular imprinting technique provides the means to develop polymeric recognition materials with predetermined ligand selectivity[140]. The imprinted materials are stable, robust, reproducible, and engineerable [141].

The development of the non-covalent approach for imprinting material synthesis in the 1980s and 1990s raised the need of fully understanding the imprinting process to enhance imprinting performance in an aqueous environment. The non-covalent strategy has been used more extensively, recognizing that the synthesis' conditions are compatible with the different solubility of templates and a variety of functional monomers are introduced with the non-covalent method. In addition, high yields can be achieved during the polymer's synthesis using different solvents. Therefore, research into the fundamental aspects of the preparation,

design, and evaluation of an imprinted system is essential to expand hydrogel based-MIPs in an aqueous media. One major challenge in the development of MIPs in an aqueous media is that the presence of polar solvent can disturb the formation of the pre-polymeric complex. As a result, the molecular imprinting of polymers using a non-covalent interaction has been performed mostly in a non-polar solvents[78]. However, the feasibility of generating MIPs in an aqueous buffer has been demonstrated. In addition, imprinted materials have been synthesized traditionally in the presence of a high crosslinking degree in order to fix the orientation of the functional groups and retain their recognition capabilities[80]. Conversely, stimuli-sensitive hydrogel systems are recently under investigation[142] to engineer biomimetic networks with specific reversible-swelling properties. They will provide novel capabilities to MIPs for advanced applications such as drug delivery systems[69] and targeted imprinted matrixes[70]. Furthermore, extending the molecular imprinting technique to biomedical applications required the rational design of an imprinted polymers to optimize the design by selecting functional monomers that promote a better stability of the functional monomer-template complex in a fully aqueous environment. In addition, the MIPs employed for drug delivery systems and target sensor devices should advance in order to reduce the crosslinking agent concentration. Lower crosslinked networks should be optimized in order to retain the integrity of the imprinting sites and to have a good accessibility of the template molecule promoting the MIP-ligand rebinding. Certainly, enhancement in the MIP's

synthesis with lower crosslinking agents extends their applications to drug release systems.

The elusive goal of molecular recognition in hydrogel systems has been reached in certain cases (as discussed in detail in chapter 2 section 4). MIPs prepared with the thermoresponsive hydrogel-based isopropylacrylamide (NIPAm) have been reported for the recognition of pyranine[84]. This system provides the evidence that recognition sites are formed in low crosslinked systems[80]. Additional reports describe several strategies to develop hydrogels as molecular agents for selectively detecting glucose, theophylline, calcium ions, norephedrine, adrenaline, and other significant target molecules[84, 86, 143]. However, it is desirable to fabricate imprinted hydrogels with controlled recognition abilities[142]. The potential to rationally design imprinted hydrogels shows great promise to enhance the binding abilities of hydrogel networks.

This research attempts to further expand the scope of application for hydrogel based-MIPs through the synthesis, characterization and elucidation of the biomimetic recognition of hydrocortisone in molecularly imprinted polymers in an aqueous media. The strategies employed in chapter 4.0 promoted the understanding of the binding abilities of the functional monomer-imprinted complex at the pre-polymeric mixture and during MIP synthesis for the further development of MIPs. In fact, this information assists in the design for the imprinting of biomimetic hydrogel membranes. In this study, hydrogel based-MIPs were synthesized using different

functional monomer/crosslinker ratios for the detection of hydrocortisone in biological fluids. The approach undertaken was to design an intelligent targeted biomimetic membranes that exhibited swelling transitions promoted by external stimuli and with template diffusion abilities that enhanced the MIP-ligand rebinding kinetics. To this end, imprinted and non-imprinted biomimetic membranes were characterized by permeability, swelling, selectivity, and electroconductivity studies. It is important to note that the goal was not to accomplish a better affinity and selectivity compared to traditional densely imprinted polymers, but to form a self-organized active sites that can be controlled and memorized upon gel shrinkage or swelling.

5.2 Experimental

5.2.1 Materials

All solvents and chemicals were of analytical grade. Hydrocortisone was obtained from Sigma Chemical Co. (St. Louis, MO, USA). The photoinitiator was 1-hydroxylphenyl ketone purchased from Sigma Aldrich, Co. (St. Louis, MO, USA). Methacrylic acid (MAA) and tetra(ethylene glycol) dimethacrylate (TEGDMA) were obtained from Polyscience, Inc (Warrington, PA, USA). Methacrylic acid was purified by vacuum distillation prior to use. Ethanol (HPLC grade) was purchased form Fisher Scientific (Fair Lawn, New Jersey, USA). The buffer solutions were prepared

using sodium phosphate monobasic and sodium phosphate dibasic obtained from Fisher Scientific (Fair Lawn, New Jersey, USA).

5.2.2 Biomimetic membrane synthesis

Imprinted and non-imprinted hydrogel networks were polymerized to evaluate their binding and selectivity abilities. Methacylic acid (MAA) and tetra(ethylene glycol) dimethacrylate (TEGDMA) were utilized as the functional monomer and crosslinker, respectively. The molar feed compositions of MAA:TEGDMA used during the synthesis were 4:1, 17:1 and 39:1. A 1:1 mass ratio of ethanol and water was employed as the solvent with a 50% w/w dilution of monomer mixture. The pre-polymeric mixture was purged during 15 minutes with nitrogen to remove dissolved oxygen that acts as a reaction inhibitor. Monomer mixture was casted between microscope slides (75 x 50 x 1 mm) using Teflon® spacers to control thickness (381 μm). Free radical solution polymerization was induced by an ultraviolet source (EFOS Acticure®, Ontario, Canada) with an intensity of 28±2 mW/cm^2. The approximate time of polymerization was 8-10 minutes depending on the amount of crosslinker added. The hydrogel networks were cut into round discs with a 1.5 cm diameter. Similar protocols were employed to produce imprinted hydrogels by incorporating the template molecule (e.g., hydrocortisone, fluorescein) in the pre-polymeric mixture. The template/functional monomer ratio employed during the synthesis of the imprinted gel was 1:4. The hydrogel networks were subsequently

washed with deionized water to remove any un-reacted monomer or oligomers. In the case of imprinted polymers, the template molecule was removed using a 9:1 volumetric ratio mixture of methanol and acetic acid. Imprinted hydrogels were finally washed with deionized water during 7 days. All hydrogel discs were dried under vacuum until they attained a constant weight.

5.2.3 Permeability Studies

Hydrocortisone permeability studies were performed to assess the diffusion characteristics of the imprinted and non-imprinted hydrogel networks as a function of pH (5.5, and 6.0) and MAA:TEGDMA molar ratio (17:1, and 39:1). The presence or absence of the hydrocortisone imprint on the hydrogel networks was indirectly evaluated by assessing the hydrocortisone permeability. Permeation studies were performed on equilibrated swollen hydrogels at 37°C employing a membrane transport system (PermeGear Inc. Hellertown, PA) with a side by side of diffusion cells or half cells (see figure 5.1).

Imprinted and non-imprinted hydrogels were placed between the half cells (7mL of volume). Subsequently, each cell was filled with a buffered solution at the appropriate pH (5.5, 6.0) and ionic strength (0.1 M). A constant concentration gradient was promoted by keeping the hydrocortisone concentration (662 μM) on the donor cell and replenishing the receptor cell with a freshly buffered solution. The effective area of diffusion was 2.54 cm^2. Magnetic stirring (600 rpm) on each reservoir kept the solution well mixed.

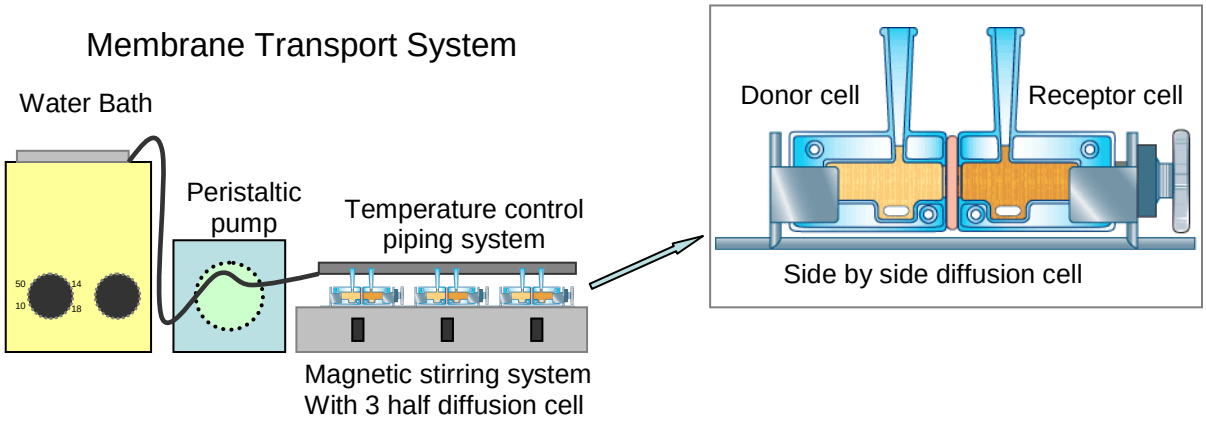

Figure 5.1 Experimental set-up for the permeability studies employing the membrane transport system (PermeGear Inc. Hellertown, PA)

Hydrocortisone concentration was spectrophotometrically determined as a function of time at 242 nm using a PowerWave X UV-Vis spectrophotometer (Bio-tek Instruments, Inc, Winooski, VT). All tests were performed in triplicate. The joint effect of the imprinting technique, pH, and MAA-TEGDMA ratio on the permeability coefficient was evaluated through a 3-factor, 2-level full factorial design. Furthermore, the equality of the permeability coefficient means was tested by a one-way and two-way ANOVA model[144]. The permeability coefficients data was analyzed using MINITAB® (Release 14.13, Minitab, Inc., PA). Counter plot was developed using MINITAB® (Release 14.13, Minitab, Inc., PA).

MINITAB® is a software package that provides a comprehensive set of statistical tools to evaluate the effect of factors on specific response and statistical differences between mean and variance (i.e., one-way ANOVA, two-way ANOVA, t-test).

Refer to appendix G and H for calculation example and raw data review.

5.2.4 Characterization of Hydrogel Networks by Equilibrium Volume Swelling (Q) and Correlation Length (ξ)

The physical properties of imprinted and non-imprinted hydrogels were characterized through buoyancy studies at 37°C in a glutaric acid-sodium hydroxide buffer solution (i.e. swelling medium) with the following pHs: 3.2, 4.0, 4.8, 5.4, 5.8, 6.0, and 7.0. The hydrogel films were weighted in air and n-heptane (non-solvent) at their relaxed state (after crosslinking, but before swelling), dried state (after their completed drying), and swollen state (after equilibrium was attained in the swelling medium). Figure 5.2 illustrates a density kit coupled to a Voyager balance (Ohasu Corp., Pine Brook, NJ) employed to determine the network volume. All tests were performed in triplicate. The equilibrium volume swelling ratio (Q), and mesh size (ξ) were determined as indicated in section 5.3.2. The equality of the Q and ξ means were tested by a one-way and two-way ANOVA model[144], Design and analysis of experiments] using MINITAB® (Release 14.13, Minitab, Inc.,).

Refer to appendix I and J for calculation example and raw data review.

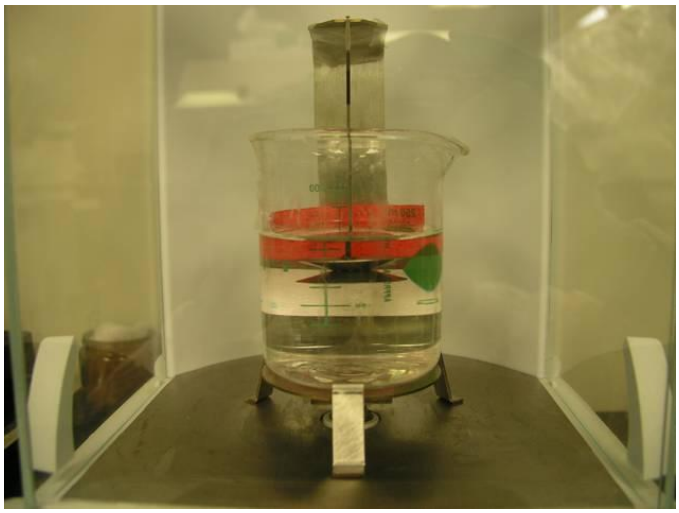

Figure 5.2 Density kit coupled to Voyager balance (Ohasu Corp., Pine Brook,NJ)

5.2.5 Binding studies

The binding capacity of imprinted and non-imprinted hydrogels was determined via batch studies (see figure 5.3). Equilibrated swollen hydrogels (MIP and non-MIP) were immersed in 20 mL of hydrocortisone buffer solution (pH 3.2) at 37°C with a predetermined concentration. The mixture was allowed to equilibrate while stirring (200 rpm) for 24 hours. The remaining concentration at the supernatant was spectrophotometrically analyzed at 242 nm using a PowerWave X UV-Vis spectrophotometer (Bio-tek Instruments, Inc., Winooski, VT).). The hydrocortisone concentration was incremented from 0 to 331 μM. Binding capacity was calculated as described in section 5.3.3. Tests were performed in triplicate.

Refer to appendix K and L for calculation example and raw data review.

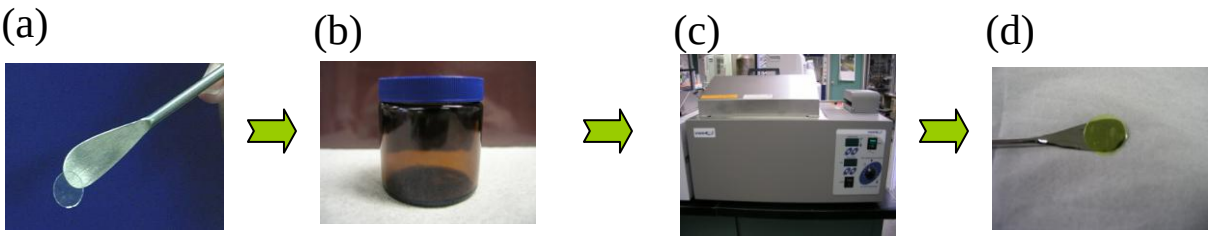

Figure 5.3 Experimental set-up for binding assessment – Imprinted and non-imprinted hydrogels (a) were placed in a 50 mL batch binding beaker (b) with the corresponding buffered solution that contains the template molecule. Batch beakers were incubated in a water bath (PermeGear Inc. Hellertown, PA) at 37°C and 200 rpm. The template molecule incorporation (d) was determined spectrophotometrically

5.2.6 Selectivity Studies

Selectivity of imprinted and non-imprinted hydrogels was evaluated by competitive permeability studies. Imprinted hydrogels with fluorescein template were characterized using a membrane transport system (PermeGear Inc. Hellertown, PA) with a side-by-side diffusion cell previously described in section 5.2.3. Each half-cell was filled with PBS buffered solution (pH 6.0). The donor cell was maintained with a racemic mixture of fluorescein and rhodamine-B, with a 1:1 molar ratio (fluorescein concentration equal to 27 μM). The receptor cell was continuously replenished with fresh buffer. Fluorescein and rhodamine-B concentrations were determined fluometrically at the corresponding excitation (fluorescein 490 nm, rhodamine-B 560 nm) and emission wavelength (fluorescein 520 nm, rhodamine-B 580 nm) using a fluorescence spectophotometer (SpectraMax Gemini EM, Sunnyvale, CA).

5.2.7 Sensitivity Studies of Biomimetic Membranes using Electroconductivity Measurements

A conductometric device for the evaluation of imprinted hydrogel affinity and selectivity was developed[145]. Electroconductivity studies were completed in order to assess the electrochemical activity during the accumulation of the template molecule in the imprinted hydrogels. Electroconductivity measurements were performed at 37°C in a custom-built test cell with two Ag/AgCl electrodes (with a surface area of 1.257cm^2). As a supporting electrolyte, a 0.1 M glutaric acid-sodium hydroxide solution (pH 3.2) was used. Equilibrated swollen imprinted and non-imprinted hydrogels were placed in the custom-built cell with a buffer solution. Hydrocortisone concentration was incremented from 0 to 331 μM to promote changes in conductivity. A small-amplitude alternating voltage was applied to conduct electrochemical studies. The voltage signal was generated by a function generator (Agilent 33120A) and amplified with a custom-built differential amplifier. The output signal was detected by employing a data acquisition board (National Instruments PCI-6052-E) in combination with the software package LabView 6.1 (National Instruments). Electroconductivity variation induced by the interaction of hydrocortisone with the hydrogel structure was recorded as a function of frequency.

In addition, the non-specificity binding capacity of the imprinted membrane was evaluated by measuring the signal induced by fluorescein on the imprinted hydrogel for hydrocortisone. The test was executed as previously discussed by

changing the fluorescein concentration from 0 to 331 μM to promote changes in the electrical signal.

All tests were performed in triplicate. The assessment was performed in collaboration with the Computer and Electrical Engineering Departments of UPRM[145].

Refer to appendix M and N for calculation example and raw data review.

5.3 Results and Discussion

5.3.1 Template Transport in Biomimetic Gels

Permeability studies were conducted to evaluate the feasibility of the MIP-ligand rebinding as a function of the pH and MAA/TEGDMA ratio, recognizing the potential application as a therapeutic monitoring device. It is essential to establish during the polymer design the binding ability and how the hydrogel morphology influences the transport of the template molecule based on the material's porosity (i.e. imprinted site accessibility). The integrity of the recognition sites was investigated by varying the solution pH within the range of operation (pH 3.2 to 7). The permeability coefficient (P) of imprinted and non-imprinted hydrogels was determined using equation (5.1), which considers the steady state mass transfer relation of the system under evaluation, and has been previously described in the literature [146].

$$\ln\left(1-\frac{2c_t}{c_o}\right)=\frac{2A}{V}Pt \qquad (5.1)$$

Here, c_t is the solute concentration in the receptor cell at time t, c_0 is the initial concentration in the donor cell, V is the volume of each half cells (7 mL), and A is the effective permeation area (1.803 cm^2).

Hydrocortisone permeation was measured through swollen hydrogel networks. Figure 5.4 shows the permeability coefficient (P) obtained at the corresponding pH (5.5 and 6.0), and MAA:TEGDMA ratio (17:1, 39:1) for imprinted and non-imprinted polymers. Although the functional monomer:crosslinker ratio employed during this study is higher than normally reported[102], the proposed technique provided significant findings that potentially allowed the affinity and selectivity calibration of MI hydrogel membranes (i.e. the rational adjustment of imprinting factors that influence the MIP's affinity and selectivity). MIP design with a higher functional monomer:crosslinker ratio will extend the potential applications of imprinted materials as biosensors [147].

As depicted in Figure 5.4, the permeability of hydrocortisone in the biomimetic membranes was higher as the MAA:TEGDMA ratio in the polymerization feed was increased. Moreover, a significant increase in the hydrocortisone permeability coefficient was observed with increasing media pH. The lower permeability coefficient values (P within the range of $1.705x10^{-7}$ to $5.352x10^{-7}$ cm/s) observed at pH 5.5 suggest the influence of mesh size and functional monomer interaction on

the hydrocortisone's permeation. A possible explanation is that the permeability of a hydrogel network with a higher MAA:TEGDMA ratio at the polymerization feed contained a more expanded structure which translated into a higher mesh size. In addition, the nature of interaction (i.e. hydrophobic, ion-pairing, hydrogen bonding) between hydrocortisone and the carboxylic group of MAA was modified by medium pH and the combination of different factors of recognition (i.e. stereospecificity, active site shape, recognition site rigidity) influenced the hydrocortisone diffusion through the membrane.

Consequently, lower permeation at lower pH values is expected. A template molecule (cholesterol) with similar functionality has demonstrated higher adsorption capacity of imprinted Poly(MAA-EGDMA) over non-imprinted polymers in gastro-intestinal-mimicking fluid[148].

Furthermore, by comparing the permeability coefficient means, there is strong evidence, as it is well known, that the variability in the permeability coefficient around the average depends on the MAA:TEGDMA ratio (p-values < 0.05, two-way ANOVA). For the 39:1 imprinted hydrogel, the permeation results denoted a value of 4.007×10^{-5} cm/s at pH equal to 6.0, which demonstrated similarity with hydrocortisone permeation through 39:1 non-imprinted hydrogel (p-value = 0.429, 95% CI for the mean is -1.2×10^{-5} to 7.0×10^{-6}, t-test).

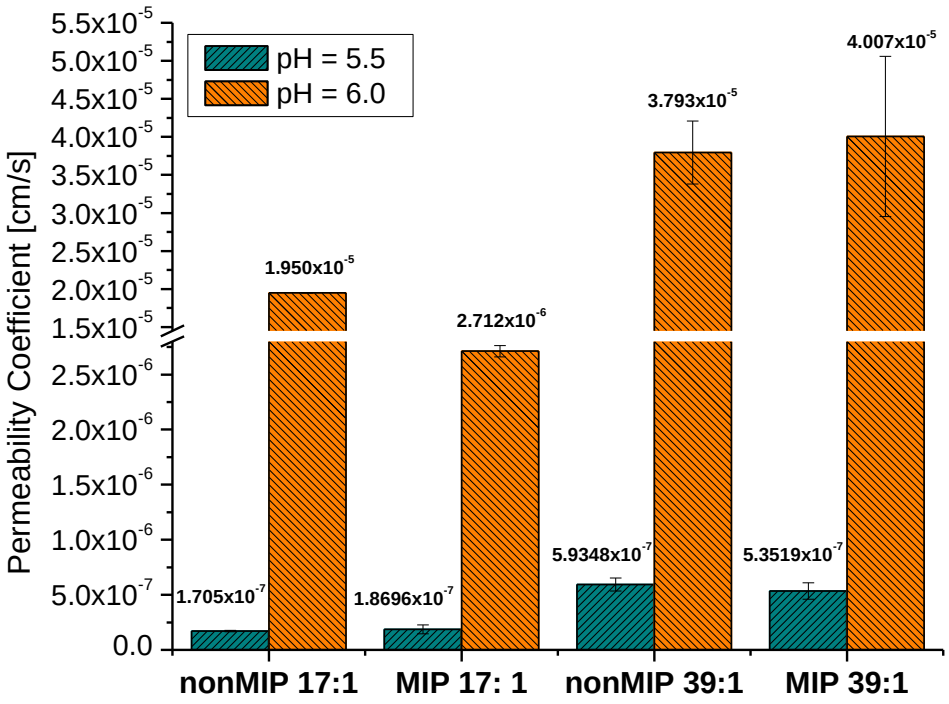

Figure 5.4 The permeability coefficient for hydrocortisone through imprinted and non-imprinted biomimetic membranes [Poly(MAA-TEGDMA)] as a function of pH and MAA:TEGDMA ratio. Vertical bars represent the average values from 3 replicates while error bars represent 3σ (standard deviation).

Regardless, hydrocortisone permeation was significantly reduced (p-value = 0.001 < 0.05, t-test) by employing the 17:1 imprinted hydrogel at a similar pH. This behavior was not observed at a pH equal to 5.5 (p-value > 0.05, two-way ANOVA). Experimental data proposed the contribution of imprinted cavities by employing the 17:1 imprinted membrane at a pH equal to 6.0 that promoted the retention of hydrocortisone on the imprinted network due to the MIP-ligand rebinding. Nevertheless, this effect was not observed on the 39:1 imprinted hydrogel. It was hypothesized that the site's integrity is unstable for the 39:1 imprinted hydrogel, ending on non-specific binding in the hydrogel network. In order to closer investigate the variation of the permeability coefficient as a function of the MAA/TEGDMA ratio and pH for MIP and non-MIP, a contour plot was generated (see Figure 5.5). The interaction between the permeability coefficient and the pH was analyzed using MINITAB®. As expected, figure 5.5 demonstrated that the permeability coefficient is sensitive to the pH and MAA/TEGDMA ratio. The pH influenced the predominant interactions between the hydrocortisone and the carboxyl groups of MAA. Electrostatic and hydrogen bond interactions are directly influenced by the pH range and consequently modified the MIP-ligand rebinding as previously discussed. The MAA/TEGDMA ratio affects the ability of the template molecule to diffuse through the hydrogel network. Certainly, these results indicated that the 17:1 MIP provided a better performance for further detection tests (refer to section 5.3.4). Permeation

results are in agreement with those obtained by Piletsky and collaborators, who evaluated the selective transfer of nucleic acid components through imprinted membranes. The transport of D-Phe through the L-Phe imprinted membrane was higher than the permeability of L-Phe[149]. In addition, Hong et al.[150] reported a decrease in the MIP membrane's permeability as a result of template (THO) binding.

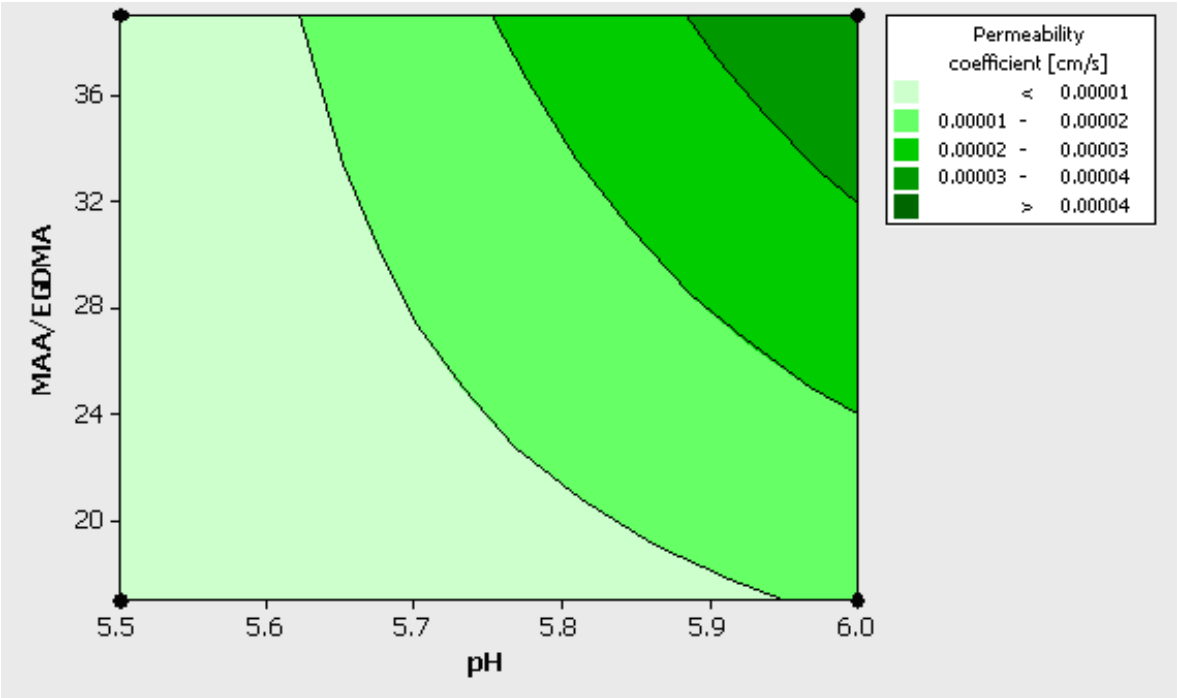

Figure 5.5 Permeability coefficient variation as a function of MAA/TEGDMA ratio and pH for imprinted and non-imprinted biomimetic membranes [Poly(MAA-co-EGDMA)]

Equally important for the rational design of MIPs is the confirmation of the recognition sites' stability by understanding the integrity of the polymeric matrix. To this end the integrity of the imprinted cavity was evaluated by estimating the mesh size or correlation length. The results are detailed in section 5.3.2.

5.3.2 Characterization of Imprinted and Non-imprinted Hydrogels' Morphology

Following the aforementioned results, the morphology of the imprinted structures was studied to understand its influence on the binding capacity of MIP hydrogels. The swelling behavior and correlation length or mesh size (ξ) of imprinted and non-imprinted membranes were evaluated via buoyancy studies. The hydrogel's structure was characterized by the equilibrium volume swelling ratio (Q), the number-average molecular weight between cross-links (M_c), and the correlation length or mesh size (ξ) of the hydrogel network.(see figure 5.6)

The equilibrium-swelling ratio (Q) of the hydrogels was estimated by the determination of the amount of fluid that was incorporated within their structures. It can be represented by,

$$Q = \frac{V_s}{V_d} \qquad (5.2)$$

in which V_s is the volume of a swollen hydrogel and V_d is the volume of a dry hydrogel.

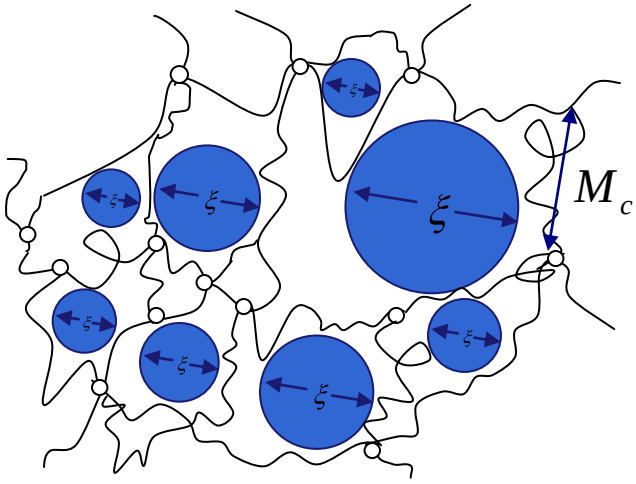

Figure 5.6 Schematic representation of the hydrogel structure

Both volumes were estimated using the buoyancy principle expressed in equation 5.3. The hydrogel's weight was determined in air and in n-heptane to calculate polymer volume as follows:

$$V = \frac{W_a - W_h}{\rho_h} \qquad (5.3)$$

Here, V is the polymer volume, W_a is the polymer weight in air, W_h is the polymer weight in n-heptane, and ρ_h is the density of n-heptane (0.6840 g/cm^3).

Moreover, the correlation length (ξ) of imprinted and non-imprinted hydrogels was estimated to closer investigate the space available between macromolecular chains or mesh size. The variability observed in the swelling ratio of imprinted and non-imprinted polymers translates in changes in the correlation length or mesh size, which represents the linear distance between two adjacent cross-links (see figure 5.3). The correlation length (ξ) was calculated using the equation (5.3):

$$\xi = \upsilon_{2,S}^{-\frac{1}{3}} * l * \sqrt{n} * \sqrt{C_N} \qquad (5.4)$$

where ξ is the correlation length, $\upsilon_{2,s}$ is the swollen polymer volume fraction, *l* is the length of the bond along the polymer backbone (1.54 Å), n is the number of links between two cross-links, and C_N is the Flory characteristic ratio (14.6 for MAA). The number of links between two cross-links (n) was calculated by equation 5.4

$$n = \frac{2M_C}{M_r} \quad (5.5)$$

In equation 5.5, M_r is the molecular weight of the repeating units of which the polymer chain is composed and M_c is the molecular weight between two adjacent crosslinks. The molecular weight between two adjacent cross-links (M_c) can be determined by the Peppas and Merril model[151] (equation 5.6) or by equation (5.7). This is the modification of the Flory-Rehner theory[152] that considers the change of chemical potential due to the presence of electrostatic forces. Peppas and Merril proposed a model to determine M_c in a neutral hydrogel:

$$\frac{1}{\bar{M}_C} = \frac{2}{\bar{M}_n} - \frac{\bar{\upsilon}/V_1 \cdot \ln(1-\upsilon_{2,s}) + \upsilon_{2,s} + \chi_1 \upsilon_{2,s}^{\,2}}{\upsilon_{2,r}\left[\left(\frac{\upsilon_{2,s}}{\upsilon_{2,r}}\right)^{\frac{1}{3}} - \frac{1}{2}\left(\frac{\upsilon_{2,s}}{\upsilon_{2,r}}\right)\right]} \quad (5.6)$$

This expression was modified to consider the anionic interactions present during the swelling of anionic hydrogels that were prepared in the presence of a solvent as follows:

$$\frac{V_1}{4I}\left(\frac{\upsilon_{2,s}^{\,2}}{\bar{\upsilon}}\right)\left(\frac{K_a}{10^{-pH} - K_a}\right) = \left[\ln(1-\upsilon_{2,s}) + \upsilon_{2,s} + \chi_1 \upsilon_{2,s}^{\,2}\right] + \left(\frac{V_1}{\bar{\upsilon}\bar{M}_c}\right)\left(1 - \frac{2\bar{M}_c}{\bar{M}_n}\right)\upsilon_{2,r}\left[\left(\frac{\upsilon_{2,s}}{\upsilon_{2,r}}\right)^{\frac{1}{3}} - \frac{1}{2}\left(\frac{\upsilon_{2,s}}{\upsilon_{2,r}}\right)\right] \quad (5.7)$$

Here, *I* is the ionic strength, K_a is the dissociation constant for the acid, M_n is the molecular weight of the polymer chains prepared under identical conditions, but in the absence of the crosslinking agent, υ is the specific volume for the polymer, V_1 is

the molar volume of the water (18 cm^3/mol), and χ_1 is the Flory polymer–solvent interaction parameter (0.499 for MAA). The relaxed volume fraction ($\upsilon_{2,r}$) and the swollen volume fraction ($\upsilon_{2,r}$) were determined by equations (5.7) and (5.8), respectively.

$$\upsilon_{2,r} = \frac{V_d}{V_r} \qquad (5.8)$$

$$\upsilon_{2,s} = \frac{V_d}{V_s} \qquad (5.9)$$

For the polymer studied in this work, the value of M_n was calculated from equation (5.10)

$$\bar{M}_n = M_0 \frac{k_p [M]}{(f k_d k_t [I])^{1/2}} \qquad (5.10)$$

Here, M_0 is the molecular weight of the monomer, k_p is the kinetic constant of propagation (670 L mol s^{-1}), k_d is the kinetic constant of the decay of the initiator (0.0165 s^{-1}), k_t is the kinetic constant of termination (2.1×10^6 L mol s^{-1}), f is the efficiency of the initiator (0.5), [*M*] and [*I*] are the concentration of the monomer and initiator, respectively. Table 5.1 summarized the parameters used to calculate the mesh size (ξ) and average molecular weight between crosslinker (M_c).

TABLE 5.1 Parameters for the calculation of the mesh size (ξ) and average molecular weight between crosslinker (M_c)

Parameter	Value	Reference
L	1.54 Å	[153]
C_{NMAA}	14.6	[153]
χ_1	0.499	[154]
V_1	18 cm^3 mol^{-1}	[153]
M_0	86.0	[153]
k_p	670 L mol s^{-1}	[153]
k_d	0.0165 s^{-1}	[153]
k_t	2.1x10^6 L mol s^{-1}	[153]
f	0.5	[153]
$[M]$	4.41 M	N/A
$[I]$	4.90 x 10^{-3} M	N/A

A typical equilibrium swelling behavior as a function of a pH within the range of 3.2 to 7.0 for anionic hydrogels is shown in Figure 5.7. The equilibrium volume swelling ratio (Q) increased with a higher media pH for the imprinted and non-imprinted membranes with 4:1, 17:1 and 39:1 MAA:TEGDMA ratio. As the pH increased from 3.2 to 7.0, the equilibrium swelling data demonstrated a 2.9-fold, 3.7-fold, and 5-fold increase of the equilibrium swelling ratio for 4:1, 17:1 and 39:1 biomimetic hydrogels, respectively. The equilibrium volume swelling increased significantly as the MAA:TEGDMA ratio increased. This increment in the MAA:TEGDMA ratio provided the expected trend in the increase of swelling abilities.

It is well understood that the hydrophilic properties of the hydrogel's structure have been increased thus leading to a higher equilibrium degree of swelling. The incorporation of MAA as a functional monomer promoted the ionization of carboxylic groups with the pH increments. The swelling phenomenon can be explained by the thermodynamic equilibrium based on the force of mixing, the ionic nature of the network, and the elastic retractive force of the polymer chains. During the dynamic swelling of the hydrogel in the buffered media, mobile ions diffused from the swelling solution into the hydrogel structure to maintain an electro-neutrality in the swollen hydrogel phase. The rate of ion exchanged creates an additional difference in the osmotic pressure across the hydrogel structure, which produces swelling of the hydrogel network. In addition, the electrostatic repulsion contributes to the swelling kinetics promoted by the presence of ionic moieties in the hydrogel's structure. The equilibrium swelling of the hydrogel is reached when the aforementioned forces are opposed by the retractive force of the polymer chain that depends on hydrogel elasticity. Figure 5.7 also shows a drastic change in the equilibrium swelling ratio near the pH equal to 5 that is consistent with the reported pKa value of MAA detailed in the literature (pK_a 4.7)[155].

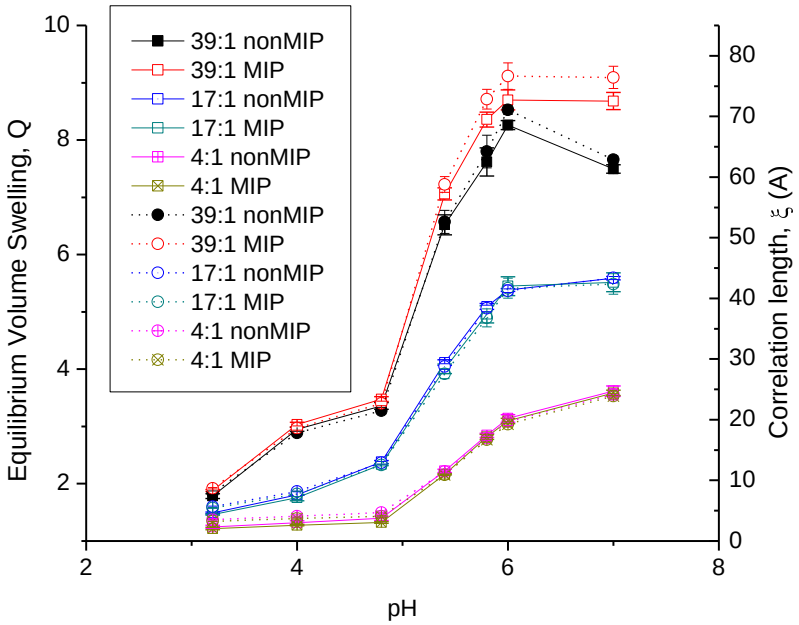

Figure 5.7 Equilibrium volume swelling ratio (Q) [straight line] and correlation length (ξ) [dot lines] of P(MAA-TEGDMA) hydrogels as a function of pH. Each data point represents an average of three replicates and error bars represent 1σ (standard deviation)

The morphology of imprinted and non-imprinted hydrogels is of high interest for the design and optimization of a sensing device to enhance the recognition mechanism associated with the site shape and size. Similar equilibrium swelling behavior was observed by comparing imprinted and non-imprinted hydrogels for the crosslinking ratios evaluated during the study, which suggests equivalence in the polymeric matrix. No statistical difference was observed by comparing the swelling ratio results of MIP and non-MIP (p-values $>$ 0.05 one-way ANOVA). Consequently, it is expected that the imprinted and non-imprinted membrane with the same monomer/crosslinker ratio would embed a similar amount of fluid in the hydrogel network. In this investigation, the influence of mesh size in the MIP's binding capacity was confirmed by estimating the mesh size as a function of the pH and monomer/crosslinker ratio as illustrated in figure 5.7. At a lower pH, the mesh size of imprinted and non-imprinted hydrogels was reduced for the monomer/crosslinker ratios of 4:1, 17:1, and 39:1. The collapsed state (pH 3.2) of imprinted and non-imprinted hydrogels resulted in mesh size average values of 3.25 Å, 5.45 Å, and 7.94 Å for 4:1, 17:1, and 39:1 hydrogels, respectively. Conversely, the uncomplexed membranes (pH 7.0) reflect maximum values of 24.16 Å, 43.63 Å, and 76.42 Å for 4:1, 17:1, and 39:1 hydrogels, respectively. It is evident that the mesh size was directly affected by the degree of crosslinking on the hydrogel network. The trend in mesh size makes the capability to control the imprinted cavities by varying pH

evident. Table 5.2 summarizes the mesh size or correlation length (ξ) results of 4:1, 17:1, and 39:1 imprinted and non-imprinted hydrogels between the pH ranged of 3.2 to 7.0. Similar mesh sizes were observed by comparing the average mesh size of imprinted and non-imprinted hydrogels. 2-sample t-tests demonstrated equivalence between average mesh size (p-value$>$0.05) for the monomer/crosslinker ratio of 4:1 and 17:1 at all pH levels. These results suggest similar average cavity sizes for imprinted and non-imprinted polymers due to the similar nature of the chains formed during the polymerization. Furthermore, equivalence in the morphology for the 17:1 MIP and 17:1 non-MIP confirm the hypothesis that a lower permeation was observed due to the interaction of hydrocortisone with the recognition site. Regardless, the 2-sample t-tests demonstrated a statistical difference between average mesh sizes by comparing 39:1 imprinted and 39:1 non-imprinted hydrogels at pH values higher than pKa of MAA (e.g. 5.4, 5.8, 7.0). These results confirmed the hypothesis that a 39:1 polymeric architecture produced unstable integrity in their recognition sites.

The mesh size (ξ) was correlated with the polymer volume fraction ($\upsilon_{2,s}$) in order to understand the influence of the swelling properties on the binding abilities of the imprinted and non-imprinted hydrogels as a function of the crosslinking ratio. As depicted in figure 5.8 (1), the mesh size (ξ) has a strong positive correlation with the inverted polymer volume fraction ($\upsilon_{2,s}$) reflected by the Pearson correlation coefficient equal to 0.9996 (p-value $<$ 0.001).

TABLE 5.2 Correlation length or mesh size (ξ) of imprinted (MIP) and non-imprinted (non-MIP) hydrogels between pH 3.2 and 7.0. (average ± SD, n = 3)

Hydrogel Crosslinking ratio	**Mesh size ξ (A)**						
	pH 3.2	pH 4.0	pH 4.8	pH 5.4	pH 5.8	pH 6.0	**pH 7.0**
39:1 non-MIP	7.9 (±0.32)	17.8 (±0.28)	21.5 (±0.54)	52.6 (±1.90)	64.2 (±2.70)	71.1 (±0.73)	**62.9 (±0.66)**
39:1 MIP	8.7 (±0.13)	18.6 (±0.36)	22.7 (±0.38)	58.8 (±1.30)	72.9 (±1.62)	76.6 (±2.17)	**76.4 (±1.83)**
17:1 non-MIP	5.6 (±0.11)	8.1 (±0.05)	12.9 (±0.23)	28.8 (±0.47)	38.4 (±0.53)	41.3 (±0.30)	**43.4 (±0.24)**
17:1 MIP	5.5 (±0.08)	7.8 (±0.44)	12.5 (±0.15)	27.6 (±0.80)	36.8 (±1.48)	41.7 (±1.63)	**42.4(±1.69)**
4:1 non-MIP	3.5 (±0.19)	4.1 (±0.22)	4.7 (±0.27)	11.5 (±0.23)	16.9 (±0.33)	19.7 (±0.62)	**24.2 (±0.88)**
4:1 MIP	**3.2 (±0.15)**	**3.7 (±0.08)**	**4.1 (±0.13)**	**10.9 (±0.09)**	**16.7 (±0.39)**	**19.2 (±0.42)**	**23.9 (±0.46)**

The amount of fluid incorporated into the hydrogel network directly promoted the mesh size increment of the non-imprinted hydrogel. These results are in accordance with the linear relationship between the mesh size and the inverse of the polymer volume fraction in the swollen state ($\upsilon_{2,s}$) that has been previously reported by Canal and Peppas[156]. Figure 5.8 (2) illustrates the results near the environmental conditions established during the permeation study. The recognition site's integrity stability of the 17:1 MIP was confirmed by observing network structures with similar mesh size and swelling ratio compared with 17:1 non-MIP (see figure 5.8 (2) data point a and b). However, this behavior was not reflected by the 39:1 hydrogels (i.e. MIP compared with non-MIP), which denotes the unstable characteristic of the imprinted sites (see figure 5.8 (2) data point c and d).

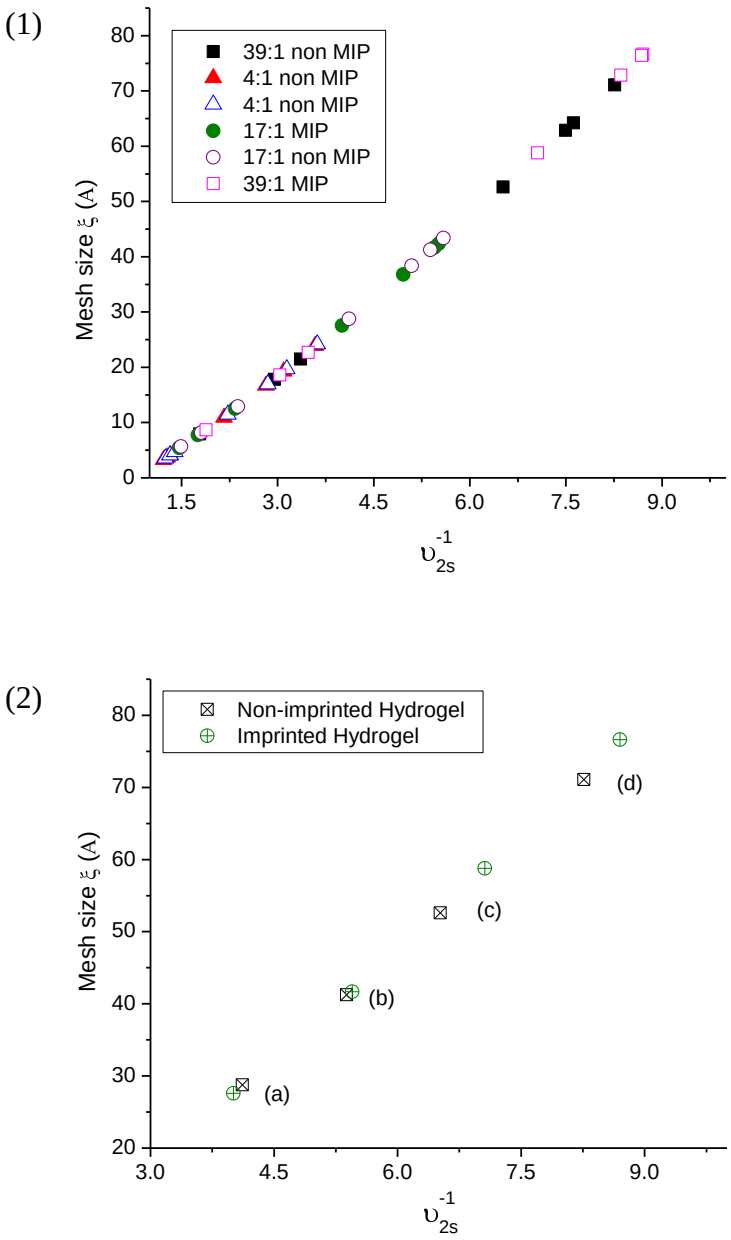

Figure 5.8 Mesh size (ξ) of P(MAA-TEGDMA) imprinted and non-imprinted hydrogels as a function of polymer volume fraction after equilibrium swelling (1). Mesh size (ξ) and polymer volume fraction correlation ($\upsilon_{2,s}$) for the case of permeability study (2): (a) 17:1 hydrogels pH 5.4, (b) 17:1 hydrogels pH 6.0, (c) 39:1 hydrogels pH 5.4, (d) 39:1 hydrogels pH 6.0

The abovementioned results of correlation length, swelling ratio, and permeability studies illustrate the manipulation of hydrogel morphology to enhance the binding abilities of the imprinted hydrogel. The 17:1 imprinted hydrogel demonstrated an effective MIP-ligand rebinding. A possible explanation is that the polymer chain's mobility was reduced, which preserved the stability of the imprinted site. It is anticipated that the affinity and electroconductivity studies reinforced the MIP rational design by allowing the selection of the optimal environmental conditions.

Collectively, the permeation, swelling, and mesh size results demonstrated that the synthesis conditions employed during this study achieved a better size control of the recognition site. Certainly, an advantage is foreseen during the polymeric architecture design of less dense imprinted material because it allowed for the optimization of the monomer/crosslinking ratio. Altogether, these results constituted a valuable piece of information for the rational design of MIPs, resulting in the *in situ* optimization of the MIP-ligand binding process during the post-fabrication phase.

5.3.3 Affinity and Specificity of Imprinted Hydrogels

The binding capabilities of imprinted and non-imprinted membranes were tested via batch studies in a buffer media with a hydrocortisone concentration range of 0 to 331 μM. In order to explore the apparent affinity of hydrocortisone to the predominant hydrophobic interaction, a pH level of 3.2 was selected for the study.

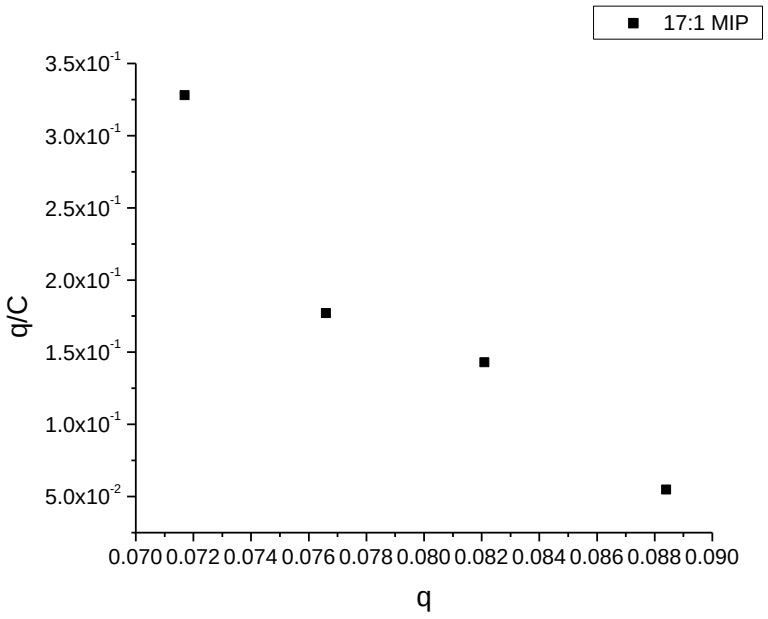

Figure 5.9 Adsorption isotherm in an aqueous media of hydrocortisone to 17:1MIP

Figure 5.9 shows the adsorption isotherm data for the batch rebinding of hydrocortisone to 17:1 MIP. The binding results were fitted to a Langmuir isotherm model. The binding constant (b) was estimated from the slope (15.17309 M^{-1}) of linear regression of the Langmuir isotherm (5.11) and the saturation capacity (q_s = 0.09128) from its intercept (1.385). This equation was employed assuming that the imprinted absorbent contains only one type of site (r^2=0.918).

$$\frac{q}{C} = bq_s - bq \qquad (5.11)$$

where q is the amount of template bounded to the polymer, and C is the amount of template free in the solution. The binding capacities obtained from the adsorption isotherm analysis were lower than the previously reported values[157]. It is known that recognition is more efficient in organic solvents and less in polar solvent. However, these experiments show the affinity of imprinted hydrogels in a swollen state in an aqueous media. Thus, it demonstrated the potential of imprinted hydrogels in an aqueous environment for further applications in intelligent targeted-drug delivery systems. In addition, it was hypothesized that the integrity of the imprinted site is impacted by the MAA/EGDMA ratio, which influenced the mesh size of the polymeric network (refer to table 5.2) and eventually the chain's mobility. The lower the crosslinking ratio, the less the crosslinking agent is incorporated in the

polymeric network structure. As a result, lower crosslinking increased the polymer chain's mobility[158] thus affecting the integrity of the imprinted sites.

Consequently, the affinity of imprinting material can be increased with a higher crosslinking density. However, few reports have demonstrated the binding properties of hydrogel polymers[84, 86, 88]. These experiments indicated that synthetic hydrogels are useful as recognition elements for particular analytes. Further optimization of MIP formulations with high-throughput and combinatorial techniques will provide essential information through this rational design to quickly determine candidates with improved binding properties.

The binding specificity of imprinted and non-imprinted hydrogels was also studied by comparing the permeation capacity of fluorescein and rhodamine-B. Fluorescein was selected as the template molecule for the selectivity studies recognizing that the enantiomers of hydrocortisone are slightly soluble or practically insoluble in water. The main objective was to choose molecules with similar chemical structures, such as fluorescein and rhodamine-B (see figure 5.10), allowing for their comparison. Permeation studies were performed as previously discussed. The permeability coefficient was calculated as described in section 5.3.1. As can be observed in figure 5.10, imprinted hydrogels demonstrated lower fluorescein permeation when compared to non-imprinted hydrogels. The permeation reduction on imprinted hydrogels compared to rhodamine-B permeability is attributed to the interaction of the template molecule (fluorescein) and the hydrogel network. The

data indicated that the biomimetic membrane distinguished fluorescein in a fluorescein-rhodamine mixture, thus demonstrating its ability to operate in a competitive environment. It also confirms that the imprinted sites were functionalized in order to observe the selectivity towards the imprinted template. Results indicated that the molecular imprinting technique was responsible for the specificity of the hydrogel network. The nature and number of interactions between the functional monomer and the template molecule favored the specificity of the biomimetic membrane toward the template molecule[159].

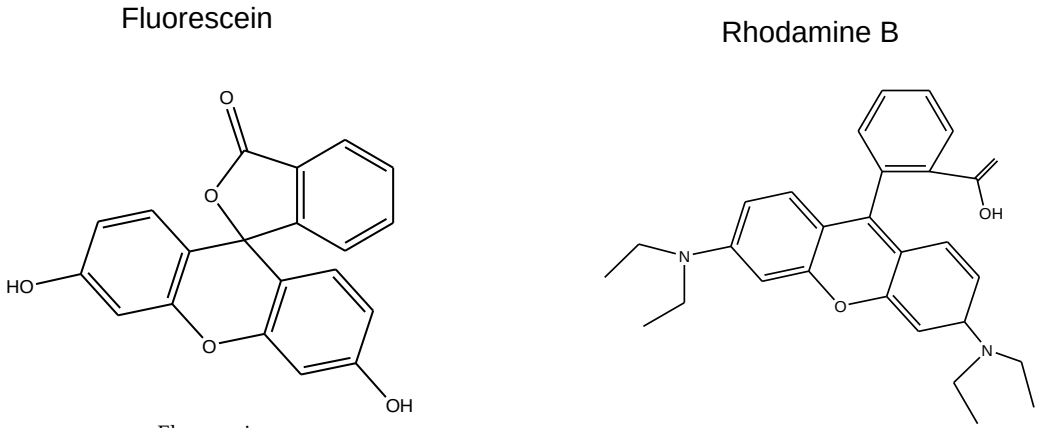

Figure 5.10 Chemical structures of Fluorescein (a) and Rhodamine-B (b).

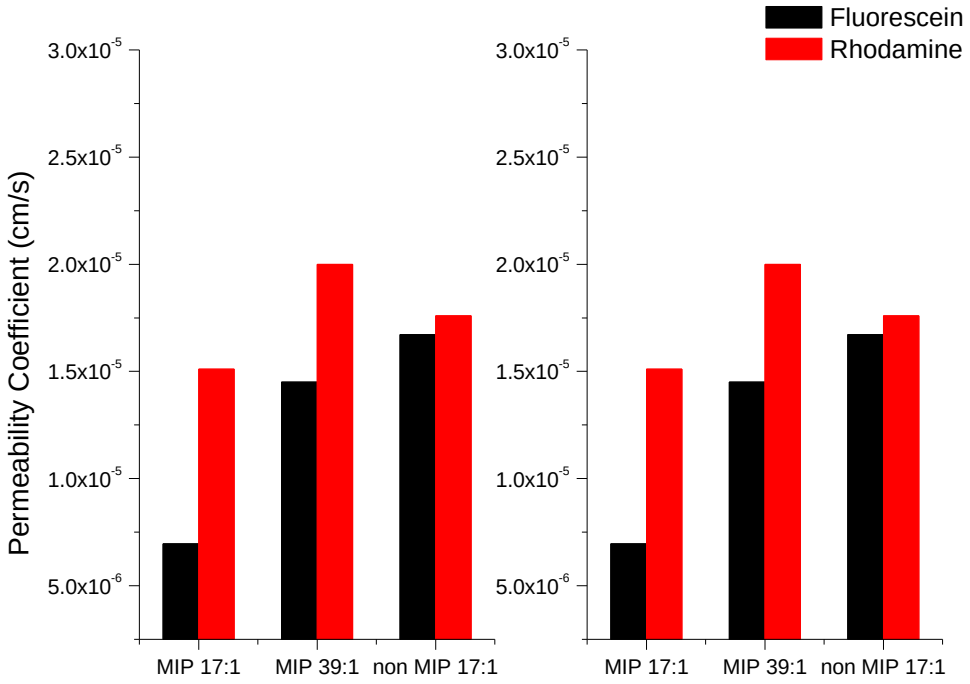

Figure 5.11 Selectivity behavior of Fluorescein-imprinted polymer as a function of MAA-TEGDMA ratio.

5.3.4 Electrochemical Behavior of Imprinted Membranes

The determination of hydrogel electro-conductivity provides vital information regarding the molecular recognition phenomenon on imprinted and non-imprinted hydrogels. Electro-conductivity measures the ability of the material to transport a charge in the presence of an applied electric field[160]. In the present work, the electroactivity of imprinted hydrogels was further evaluated in terms of its eventual clinical application as a targeted sensor device. It also provides information concerning the sensitivity and selectivity of imprinted material.

The electro-conductivity of an imprinted and non-imprinted membrane was monitored by estimating the change in hydrogel resistivity induced by the template molecule. The resistivity (ρ) is inversely proportional to the hydrogel conductivity. Consequently, this parameter measured the ability of the membrane to transport a charge in the presence of an applied electric field. The resistivity was calculated by equation (5.9).

$$\rho = R_{gel} - R_u * \frac{A}{l} \qquad (5.9)$$

Here, R_{gel} is the estimated resistance promoted by the buffer solution and hydrogel network, the R_u is the estimated resistance promoted by the buffer solution, A is the effective cross sectional area (1.14 cm^2), and *l* is the hydrogel thickness (381 μm)[160].

The resistivity behavior of an imprinted and non-imprinted polymer as a function of equilibrium volume swelling and copolymer composition is reflected in the

resistivity studies shown in figure 5.11. Figure 5.11 presents the resistivity of two different compositions (17:1, 39:1) for a non-imprinted polymer in a buffered solution (0.1 M glutaric acid-sodium hydroxide solution). A reduction in the resistivity of the crosslinked hydrogels was observed as the equilibrium volume swelling increases. As depicted in figure 5.12, the results reflected a non-linear correlation with a significant reduction with an equilibrium volume swelling higher than 2. These results are in accordance with studies reported by Sheppard et al[160]. The electrical conductivity (which is inversely proportional to resistivity) of poly(2-hydroxlethyl methacrylate-co-dimethylaminoethyl methacrylate) has been studied as a function of pH. The study reported a significant increase in the conductivity measurement at a water content of 40%. In addition, a higher resistivity in the hydrogel network with a high crosslinking density (17:1) with an equilibrium volume swelling below two (see figure 5.12) was observed. This indicates the idea of ion mobility reduction due to the presence of polymer chains at the collapse state of the hydrogel architecture. The hypothesis was confirmed by evaluating the hydrogel's conductivity in the presence of the template molecule.

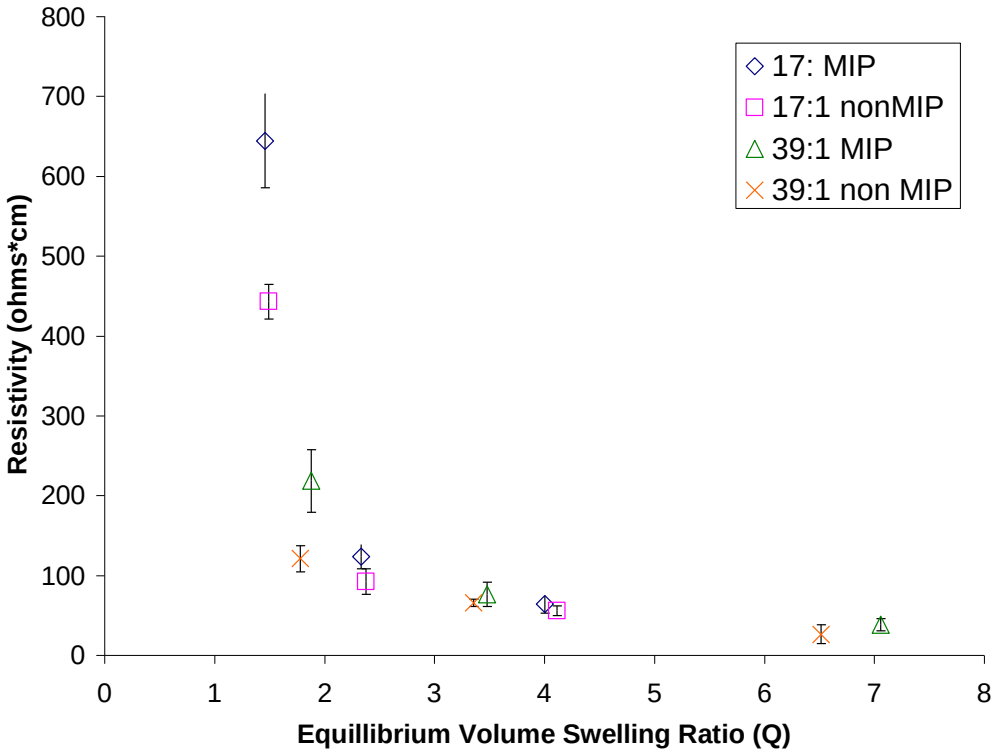

Figure 5.12 Electro-resistivity of biomimetic hydrogels [Poly(MAA-TEGDMA)] as a function of equilibrium volume swelling ratio

In order to understand the effect of the template molecule on the membrane's conductivity, the resistivity (ρ) of imprinted and non-imprinted hydrogels [Poly(MAA-TEGDMA)] was compared in buffered solution (figure 5.13.1) and in a buffered solution containing hydrocortisone (figure 5.13.2). The increment of media pH resulted in higher hydrogel conductivity (lower resistivity). In addition, it was also observed that the resistivity declines by increasing the MAA/EGDMA ratio, resulting in electro-conductivity increments for the imprinted and non-imprinted hydrogel. Figure 5.13.1.a illustrates that the imprinting technique promoted a reduction in hydrogel conductivity. The change in electro-conductivity was attributed to the degree of ion mobility within the hydrogel membrane and in the solution (diffusivity). These facts support the idea that the electrical resistivity of hydrogels as a function of composition provides a sensitive measurement of the swelling state. The swelling capacities of the anionic hydrogels structure are increased by media pH (see figure 5.7) thus providing a larger amount of charge carriers to support electrical conduction. As previously reported in section 5.3.2, the hydrogel's degree of swelling was influenced by the relative concentration of ions within the hydrogel to that in the buffered solution or electrolyte. Higher electro-conductivity (i.e. lower resistivity) resulted in a higher flux of ions due to the electrochemical potential gradient across the membrane promoted by the application of an electric field.

(1)

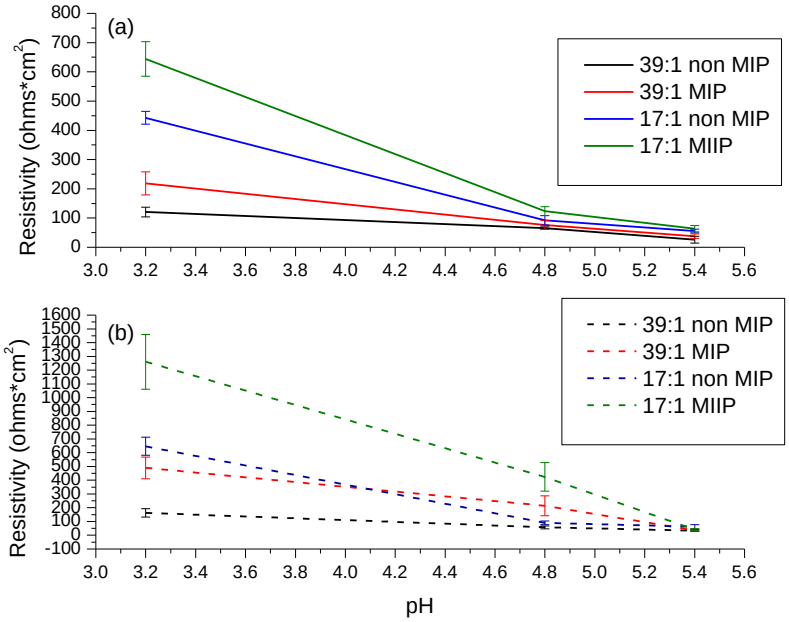

(2)

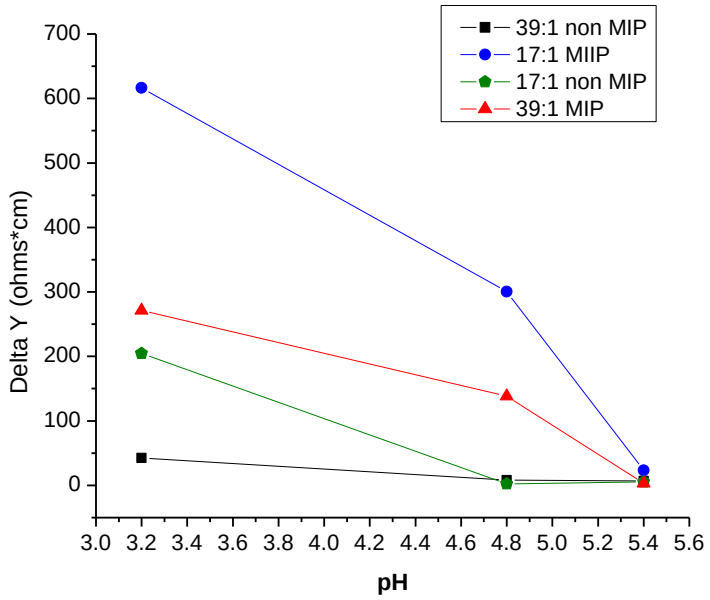

Figure 5.13 Electro-conductivity of imprinted and non-imprinted hydrogels [Poly(MAA-TEGDMA)] as a function of pH obtained in buffered solution [straight lines] and buffered solution of added hydrocortisone (662μM) [dot lines] (1)

It is important to recognize that this hypothesis cannot elucidate the difference in resistivity due to the application of the molecular imprinting technique (imprinted versus non-imprinted hydrogels, refer to figure 5.13.1.b). No statistical difference was observed by comparing the equilibrium-swelling ratio of imprinted and non-imprinted hydrogels. Consequently, this factor did not induce change in membrane resisitivity. A possible explanation for the resistivity increment (electroconductivity reduction) at the collapsed state of the imprinted hydrogel (pH 3.2) is based on a lower mobility of ions in the hydrogel's network due to the presence of a template molecule that remained in the structure after the MIP's synthesis. A low percentage of template molecules in the hydrogel's structure reduced the free volume of water within the gel to a characteristic volume necessary to accommodate transported ions. These results are in agreement to the free volume theory where the major factor controlling the diffusion rate of molecules in the system is the reorganization of the free volume which creates holes through which particles are transferred[161].

The relative effect of MIP-ligand binding is summarized in figure 5.13.1.a. A significant reduction was observed in hydrogel conductivity (p-value < 0.05) in the presence of hydrocortisone at media pH of 3.2 and 4.8. The lower conductivity was indicated by a higher resistivity reading for the imprinted membrane. The non-imprinted membrane demonstrated a higher conductivity (low resistivity) when compared to the imprinted membranes. The higher resistivity values of the imprinted membranes denoted the interaction of hydrocortisone within the hydrogel's structure

as previously discussed. In addition, a linear correlation trend between the resistivity and pH was observed with the imprinted membranes by reflecting higher increments in resistivity value in the presence of a hydrocortisone solution at 4.8 media pH. The most remarkable effect on the hydrogel's electroconductivity resulted with imprinted membranes where the resistivity had a 2-fold (pH 3.2) and 3-fold (pH 4.8) increase at the corresponding media pH.

The response of the imprinted and non-imprinted membranes induced by hydrocortisone binding was evaluated over a range of pH values (3.2, 4.8 and 5.4). The comparison between the response obtained with buffered solutions and buffered solutions with hydrocortisone is represented by delta Y. As depicted in figure 5.13.2, bound hydrocortisone produced a higher delta Y for the imprinted hydrogels. This suggests a decrease in the ion diffusion across the polymer interface due to the presence of the template molecule in the imprinted cavities, as formerly described. Variations in hydrogel electroconductivity (i.e. higher delta Y) were most significant on the 17:1 imprinted hydrogel. These findings are consistent with the permeability results previously reported in section 5.3.1. The 17:1 imprinted hydrogel also generated the most remarkable signal at pH 3.2 (see figure 5.13.2).

The performance of biomimetic membranes as a function of hydrocortisone concentration was evaluated and compared with a competitive ligand (fluorescein). Figure 5.13 shows that the biomimetic membrane's conductivity was reduced inversely proportional to the template's concentration. The signal obtained with the

imprinted hydrogel was 1.7-fold and 8.7-fold higher than those obtained with the non-imprinted hydrogel for 60μM and 240μM of hydrocortisone concentration, respectively. Therefore, the imprinted hydrogel demonstrated a higher sensitivity and affinity toward the template molecule when compared to a non-imprinted hydrogel. However, an increment on hydrogel conductivity was observed proportional to fluorescein concentration as shown in figure 5.13, which is an inverse response of the biomimetic membrane. The response induced by fluorescein suggested that the incorporation of these molecules modified the hydrogel's structure thus promoting a more swollen hydrogel, which increased its electroconductivity. As previously demonstrated in figure 5.12, the hydrogel's resistivity strongly declines with the increased equilibrium volume swelling. Therefore, a possible explanation of the higher conductivity induced by flourescein is a conformational reorganization of the hydrogel network that resulted from its interaction with the biomimetic membrane (see figure 5.15). The hydrogel's swelling ratio increased producing resistivity reduction in accordance of present expected standards. Piletsky et al.[162] also measured the electro-resistance of sialic acid-imprinted polymers and observed swelling of the empty imprinted cavities resulting from the solvation of the boronic acid sites.

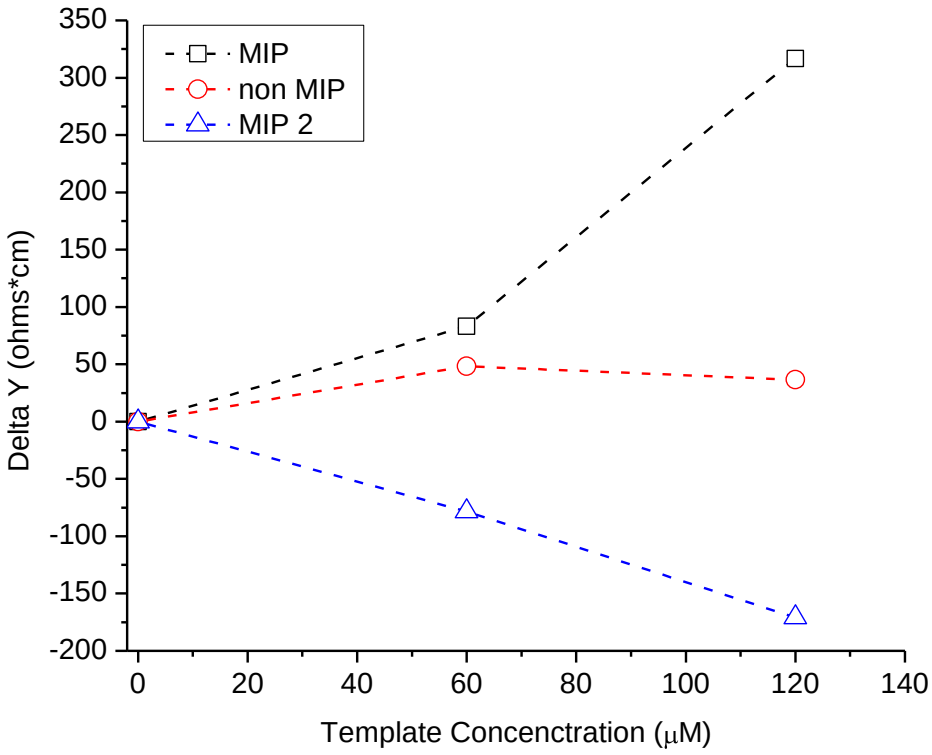

Figure 5.14 Detection signal induced by the template adsorption on imprinted (□) and non-imprinted (○) biomimetic hydrogels [Poly(MAA-TEGDMA)] in buffer solution at pH equal to 3.2 : (template hydrocortisone). Response curve induced by fluorescein adsorption in an imprinted biomimetic hydrogel (△)

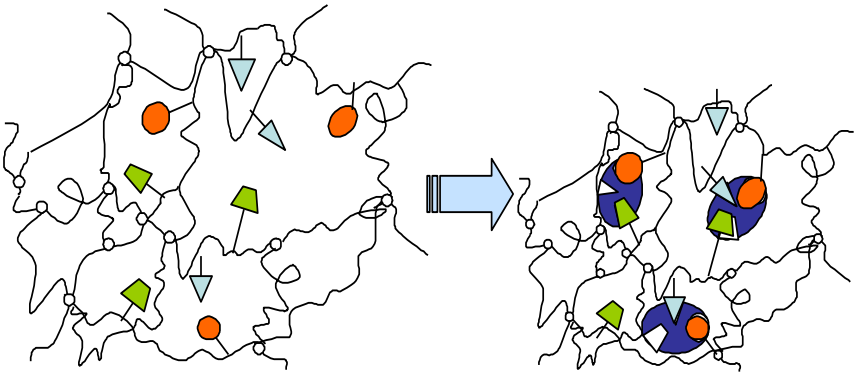

Figure 5.15 Induced fit in imprinted hydrogel structures.

The imprinted cavities were functionalized to bind the template molecule, which produced a variation in its binding capacity that was indirectly measured via electroconductivity studies. The obtained results are satisfactory, in terms that the molecular imprinting technique produced binding sites in a water-swollen state. The presence of water during the MIP synthesis can disrupt the hydrogen bonds formed in between the functional monomer and template. It has been observed that the recognition properties of MIP prepared in organic solvents have a higher affinity compared to those synthesized in an aqueous media, as previously discussed. Regardless, more efforts have to be made in the MIP synthesis in an aqueous media in order to have fully compatible MIPs with biological analytes. Several efforts have reported that the molecular recognition phenomenon in an aqueous media resulted from a number of weak interactions acting in a concerted fashion which promotes the re-binding of the template molecule[72]. The results indicated that hydrogel-based MIPs synthesized in an aqueous media have recognition and specificity abilities towards the template molecule at their swollen-state. Therefore, it was confirmed that the targeting device response can be tuned to a pre-selected analyte using imprinted hydrogels in an aqueous media.

5.4 Closing Remarks

In the present work, it was possible to obtain a hydrogel based-MIP via free radical polymerization in an aqueous environment by using methacrylic acid and ethylene glycol dimethacrylate as the functional monomer and cross-linker, respectively. Swelling and correlation length results indicated that the diffusion of the template molecule (hydrocortisone) through the hydrogel network was enhanced by the swelling process. This work presents the binding capacity of imprinted gels by observing change in hydrogel permeation and conductivity. Collectively, permeability, affinity, selectivity, and electrochemical results suggest that the imprinted cavities were correctly functionalized and shaped to allow the diffusion of the template molecule through the imprinted gel and its effective interaction. The 17:1 MAA/TEGDMA hydrogel membrane confirmed to be a biomimetic network with specific sites for hydrocortisone recognition and showed at the same time good diffusion abilities. The hydrogel based-MIP developed in this study demonstrated a sensitivity to distinguish, with good accuracy, differences in hydrocortisone content in an aqueous media. It was demonstrated that the response was tuned to a pre-selected analyte using the molecular imprinting technique for hydrogel materials in an aqueous media.

In summary, the aforementioned results are in accordance with the direct evidence of adduct formation between the carboxylic groups of the monomer analog and hydrocortisone previously reported in the NMR titration studies and Job Plot

method. The complex formation during the imprinted synthesis was confirmed by ATR-FTIR results. This indicates that it is suitable to predict the binding abilities of the system studied. Certainly, these findings provide quantitative information for the MIP's rational design.

The latter approach confirmed that the detection and selectivity of an imprinted hydrogel based in poly(MAA-co-EGDMA) is possible and provides a definitive impetus to develop sensor devices for detecting hydrocortisone or other biological markers (i.e. transaminase[50], glucose[163], cholesterol[148, 164-166], and human serum albumin[89, 167]). Furthermore, the rapid, low cost, and robustness of imprinted biomimetic membranes may enable the novel design of *in vitro* diagnostic systems. Hydrogel-based imprinted sensors demonstrated their ability to quantitatively measure hydrocortisone and aid the patient and healthcare professional to monitor the clinical treatment of hydrocortisone-drug usage or stress level diseases.

CHAPTER 6

6 Conclusions and Recommendations

6.1 Closing Remarks

Overall, the work performed in chapter 4 illustrates the formation of an MAA-hydrocortisone complex in the pre-polymeric mixture. The effect of the selected solvent for synthesis during the imprinting was measured through the determination of the association constant using NMR titration studies. The presence of an imprinted site with a higher binding affinity through the observation of 1:2 complex equilibrium was predicted. NMR titration and Job plot analysis demonstrated to be an essential technique to confirm the presence of a solution adduct and the stability of a functional monomer-template complex[108, 123, 132, 134]. Furthermore, in situ polymerization was employed using ATR-FTIR spectroscopy to assess the imprinting process[168]. The rate of polymerization was found to be lower during the molecular imprinting synthesis due to the presence of the MAA-hydrocortisone complex. This suggests that the structural integrity of the MAA-hydrocortisone complex was preserved during the synthesis. Certainly, the imprinted sites are created and are present in the hydrogel polymeric network. The monitoring of the imprinting synthesis through in situ polymerization allows the evaluation of the rate of propagation relative to the rate of dissociation to confirm the stability of the MAA-hydrocortisone complex. In summary, this work established the present and the

future of imprinted materials in the development of tools that predict and control the optimization and design of the next generation of engineered MIP.

Through the work performed in chapter 5, a substantially better understanding of the MIP-ligand rebinding phenomenon was reached. In this work the molecular imprinting technique was applied to fabricate hydrogel networks based on poly(MAA-co-EGDMA), which shows recognition properties towards hydrocortisone in an aqueous environment. The affinity of the recognition sites of equilibrated hydrogels was evaluated by monitoring the transport of hydrocortisone through non-porous biomimetic hydrogels. This particular study demonstrated the recognition abilities of hydrogel networks at a swollen state of imprinted hydrogels with a 17:1 MAA:TEGDMA ratio. Swelling trends demonstrated a similar amount of accessible interaction sites on imprinted and non-imprinted membranes, which supports the initial hypothesis that a reduction in hydrocortisone permeation resulted from the MIP-ligand rebinding due to the presence of complementary recognition sites. The template rebinding capacity of the imprinted hydrogels was confirmed by binding studies. The results revealed the presence of affinity sites in the imprinted hydrogels. In addition, this study describes that the electrical resistivity depends on the equilibrium swelling of the imprinted membrane. Certainly, the response change of imprinted hydrogels was induced by the MIP-ligand rebinding process as shown in the electrochemical behavior of the imprinted hydrogel. The 17:1 imprinted gel exhibited an elevated sensitivity to discriminate differences in concentration of target

hydrocortisone. Collectively these results indicated that imprinted hydrogels are provident materials for the development of intelligent targeting systems such as sensing devices or in combination with drug delivery interfaces. In conclusion, novel imprinted methodology to optimize the MIP-ligand binding will bring similar materials to the marketplace of biomedicine applications[169, 170].

6.2 Future Perspective

As discussed previously in Chapter 4.0, the relative stioichiometry of the functional monomer-template complex was accurately monitored by the continuous variation method. In addition, the magnitude of association was estimated by NMR titration study. Findings suggested that the binding abilities of imprinted hydrogels can be predicted by monitoring the functional monomer-template complex. In this study, the use of hydrocortisone as a template solution required the synthesis of an imprinted polymer having a pre-polymeric saturated solution of hydrocortisone. However, the assessment of complex formation was extended by varying the template's concentration in the pre-polymeric solution. The functional monomer-template ratio at the pre-polymeric phase was estimated in order to enhance the MIP's fabrication.

In addition, the work discussed in chapter 4 demonstrated the advantage of using ATR-FTIR spectroscopy to examine the polymerization of imprinted hydrogels. A better understanding of the structural integrity of imprinted sites during MIP

polymerization was accomplished. It remains necessary, however, to evaluate the effect of template concentration in the MIP morphology. This will allow for the design of homogeneous imprinted material. As a consequence, a better distribution of binding sites will be obtained during the MIP design. A study of the effect of polymerization techniques on MIP synthesis[137, 168] is recommended. Various polymerization alternatives such as living polymerization[96, 171-173] have been reported.

As previously mentioned, the collective results obtained in chapter 5 demonstrated successful imprinting in a hydrogel network and its ability to detect hydrocortisone. The evaluation of the structural integrity of the imprinted sites and their accessibility provides new insights about the degree of molecular recognition that resulted from the molecular imprinting process and the following efforts that still have to be done. High throughput permeation studies would be helpful for the optimization of MIP performance. Thus, using techniques that would allow the simultaneous evaluation of vast crosslinking agent alternatives and the functional monomer-crosslinker ratio during the MIP synthesis will advance the MIP design. It may be useful to expand permeation and affinity studies with several solvents as a function of dielectric constant to reinforce the binding abilities of MIP. It would allow for the accurate assessment of the mechanism underlying the ligand recognition of the MIP's system. It remains necessary to correlate the affinity of the imprinted sites at the MIP-ligand rebinding with the association of the MIP's complex formation. The

idea is to quantitatively relate the pre-polymeric complex's stability with the selectivity and affinity distribution of the resultant MIP.

It would also be interesting to focus future studies on dynamic electrochemical evaluations for the better understanding of the mass transfer limitations and the amount of binding sites present in the MIP's morphology. Findings of higher resistivity values due to the presence of hydrocortisone after MIP synthesis suggest it would be necessary to develop more effective methods of template removal, which enhance the template extraction after MIP synthesis. It would also be interesting to focus future studies to develop a predicted model of resistivity to understand the relative importance of various components that inversely influence the resistivity (i.e. solution mobilities of the ions and the mobility within the gel inclined by its swelling state). The idea is to provide a semi-quantitative description of the observed behavior which supports or rejects the hypothesis that the resistivity was impacted by the presence of the template molecule[174].

An additional recommendation is to develop a prototype of biosensors based on imprinting technology to evaluate the challenge for their commercialization. It is essential to enhance the interaction between the imprinted material and the transducer. To this end, the polymerization should be performed over the surface of the transducer. Equally important is to evaluate different MIP morphologies to improve the template diffusion and consequently the sensor response time. The objective is to design MIPs as alternatives to biological receptors for the marketplace.

The robustness of the MIP sensors justifies their application in implantable devices, biotechnological processes, space, and deep water detection [175]. The rational design proposed and evaluated in this dissertation is considered an essential tool to achieve the integration of polymer network with lower crosslinking agent with transducers in the biosensor fabrication.

Finally, it remains necessary to focus future studies in MIP design for macromolecules such as enzymes (i.e. transaminase[50], glucose[163], cholesterol[148, 164-166], human serum albumin[89, 167]) relevant on the molecular recognition of biological system. The rational design illustrated in this dissertation should be merged with combinatorial techniques[176], chemometrics[113], and computational screening[177] techniques. The novel design of MIP, which increases the quantity and affinity of imprinted sites, may be relevant to future work on imprinted devices from the bench to the market.

6.3 Literature Cited

1. Haupt, K.; Mosbach, K., Molecularly imprinted polymers and their use in biomimetic sensors. *Chemical Reviews* **2000,** 100, (7), 2495-2504.
2. Malhotra, B.; Chaubey, A., Biosensors for clinical diagnostics industry. *Sensor and Actuators B-Chemical* **2003,** 91, (1-3), 117-127.
3. Piletsky, S.; Alcock, S.; Turner, A., Molecular imprinting: at the edge of the third millennium. *Trends in Biotechnology* **2001,** 19, (1), 9-12.
4. Dickert, F.; Hayden, O.; Lieberzeit, P.; Haderspoeck, C.; Bindeus, R.; Palfinger, C.; Wirl, B., Nano- and micro-structuring of sensor materials - from molecule to cell detection. *Synthetic Metals* **2003,** 138, (1-2), 65-69.
5. Kanekiyo, Y.; Ono, Y.; Inoue, K.; Sano, M.; Shinkai, S., 'Molecular-imprinting' in polyion complexes which creates the 'memory' for the AMP template. *J. of the Chem. Soc.-Perkin Transactions 2* **1999**, (3), 557-561.
6. Sanjonz, P.; Kele, M.; Zhong, G.; Sellergren, B.; Guiochon, G., Study of thermodynamics and mass tranfer kinetics of two enantiomers on a polymeric imprineted stationary phase. *J. Chromatogr. A* **1998,** 810, 1-17.
7. Takeuchi, T.; Fukuma, D.; Matsui, J., Combinatorial molecular imprinting: An approach to synthetic polymer receptors. *Anal. Chem.* **1999,** 71, (2), 285-290.
8. Holroyd, S.; Groves, P.; Searle, M.; Gerhard, U.; Williams, D., Rational Design and Biding of Modified Cell-Wall Peptides to Vancomycin-group Antibiotics - Factorizing Free-Energy Contributions to Binding. *Tetrahedron* **1993,** 49, (41), 9171-9182.
9. Li, Z.; Day, M.; Ding, J.; Faid, K., Synthesis and characterization of functional methacrylate copolymers and their application in molecular imprinting. *Macromolecules* **2005,** 38, (7), 2620-2625.
10. Andersson, H.; Nicholls, I., Spectroscopic evaluation of molecular imprinting polymerization systems. *Biorg. Chem.* **1997,** 25, (3), 203-211.
11. Karlsson, J.; Karlsson, B.; Andersson, L.; Nicholls, I., The roles of template complexation and ligand binding conditions on recognition in bupivacaine molecularly imprinted polymers. *Analyst* **2004,** 129, (5), 456-462.
12. Svenson, J.; Karlsson, J.; Nicholls, I., H-1 nuclear magnetic resonance study of the molecular imprinting of (-)-nicotine: template self-association, a molecular basis for cooperative ligand binding. *J. Chromatogr A* **2004,** 1024, (1-2), 39-44.

13. Karim, K.; Breton, F.; Rouillon, R.; Piletska, E.; Guerreiro, A.; Chianella, I.; Piletsky, S., How to find effective functional monomers for effective molecularly imprinted polymers? *Advanc. Drug Deliv. Rev.* **2005,** 57, (12), 1795-1808.
14. Wulff, G., Molecular imprinting in crosslinked polymers - The role of the binding sites. *Molecular Crystals and Liquid Crystals Science and Technology Section A-Molecular Crystals and Liquid Crystals* **1996,** 276, 1-6.
15. Andersson, L., Molecular imprinting: developments and applications in the Anal. Chem. field. *J. Chromatogr. B* **2000,** 745, (1), 3-13.
16. Mosbach, K.; Yu, Y.; Andersch, J.; Ye, L., Generation of new enzyme inhibitors using imprinted binding sites: The anti-idiotypic approach, a step toward the next generation of molecular imprinting. *J. Amer. Chem. Soc,* **2001,** 123, (49), 12420-12421.
17. Scheller, F.; Wollenberger, U.; Warsinke, A.; Lisdat, F., Research and development in biosensors. *Current Opinion in Biotechnology* **2001,** 12, (1), 35-40.
18. Mathew, J.; Buchardt, O., Molecular Imprinting Approach for the Recognition Of Adenine in Aqueous-Medium and Hydrolisis of Adenosine 5'-triphosphate. *Bioconjugate Chemistry* **1995,** 6, (5), 524-528.
19. Mosbach, K., Toward the next generation of molecular imprinting with emphasis on the formation, by direct molding, of compounds with biological activity (biomimetics). *Anal. Chim. Acta* **2001,** 435, (1), 3-8.
20. Anonymous, *Chem. Eng. News* **1949,** 27, 913.
21. Wulff, G., *Angew. Chem.* **1972,** 84, 364.
22. Mosbach, K.; Sellergren, B.; Andersson, L., Imprinted of Amino Acid Derivatives in Macropourus Polymers. *Tetrahedron Letters* **1984,** 25, (45), 5211-5214.
23. Belokon, Y.; Tararov, V. I.; Savel'eva, T.; Vorob'ev, M.; Vitt, S.; Sizoy, V.; Sukhacheva, N.; Vasil'ev, G.; Belikov, V., *Makromol.Chem.* **1983,** 184, 2213.
24. Spivak, D.; Campbell, J., Systematic study of steric and spatial contributions to molecular recognition bynon-covalent imprinted polymers. *Analyst* **2001,** 126, (6), 793-797.
25. Baggiani, C.; Anfossi, L.; Giovannoli, C.; Tozzi, C., Binding properties of 2,4,5-trichlorophenoxyacetic acid-imprinted polymers prepared with different molar ratios between template and functional monomer. *Talanta* **2004,** 62, (5), 1029-1034.
26. Lin, J.; Nakagama, T.; Uchiyama, K.; Hobo, T., Temperature effect on chiral recognition of some amino acids with molecularly imprinted polymer filled capillary electrochromatography. *Biomed. Chromatogr.* **1997,** 11, (5), 298-302.
27. Zander, A.; Findlay, P.; Renner, T.; Sellergren, B.; Swietlow, A., Analysis of nicotine and its oxidation products in nicotine chewing gum by a molecularly imprinted solid phase extraction. *Anal. Chem.* **1998,** 70, (15), 3304-3314.
28. Kostrewa, S.; Emgenbroich, M.; Klockow, D.; Wulff, G., Surface-enhanced Raman scattering on molecularly imprinted polymers in water. *Macromolecular Chem. and Phys.* **2003,** 204, (3), 481-487.

29. Takeuchi, T.; Haginaka, J., Separation and sensing based on molecular recognition using molecularly imprinted polymers. *J. Chromatogr.. B-Analytical Technologies in the Biomedical and Life Sciences* **1999,** 728, (1), 1-20.
30. Takeuchi, T.; Dobashi, A.; Kimura, K., Molecular imprinting of biotin derivatives and its application to competitive binding assay using nonisotopic labeled ligands. *Anal. Chem.* **2000,** 72, (11), 2418-2422.
31. Liu, X.; Dordick, J., Sugar acrylate-based polymers as chiral molecularly imprintable hydrogels. *J. Polym. Sci, Part A-Polymer Chemistry* **1999,** 37, (11), 1665-1671.
32. Lu, Y.; Li, C.; Liu, X.; Huang, W., Molecular recognition through the exact placement of functional groups on non-covalent molecularly imprinted polymers. *J. Chromatogr. A* **2002,** 950, (1-2), 89-97.
33. Baggiani, C.; Giraudi, G.; Giovannoli, C.; Trotta, F.; Vanni, A., Chromatographic characterization of molecularly imprinted polymers binding the herbicide 2,4,5-trichlorophenoxyacetic acid. *J. Chromatogr. A* **2000,** 883, (1-2), 119-126.
34. Yang, D.; Ju, M.; Maeda, A.; Hayashi, K.; Toko, K.; Lee, S.; Kunitake, T., Design of highly efficient receptor sites by combination of cyclodextrin units and molecular cavity in TiO2 ultrathin layer. *Biosensors & Bioelectronics* **2006,** 22, (3), 388-392.
35. Fu, Q.; Sanbe, H.; Kagawa, C.; Kunimoto, K.; Haginaka, J., Uniformly sized molecularly imprinted polymer for (S)-nilvadipine. Comparison of chiral recognition ability with HPLC chiral stationary phases based on a protein. *Anal. Chem.* **2003,** 75, (2), 191-198.
36. Marx, S.; Avnir, D.; Fireman-Shoresh, S., General Method for Chiral imprinting Sol-Gel Thin Films Exhibiting Enatioselectivity. *Chem. Mater.* **2003,** 15, 3607-3613.
37. Nicholls, I.; Andersson, H.; Knutsson, M., Novel chiral recognition elements for molecularly imprinted polymers preparation. *J. Mol. Recogn* **1998,** 11, 87-90.
38. Rashid, B.; Briggs, R.; Hay, J.; Stevenson, D., Preliminary evaluation of a molecular imprinted polymer for solid-phase extraction of tamoxifen. *Anal. Commun.* **1997,** 34, (10), 303-305.
39. Minura, N.; Matsumoto, T.; Bulgarevish, E.; Hu, M.; Rachkov, A., Molecularly imprinted polymers prepared in aqueous solution selective for [Sar1,Ala8]angiotensin II. *Anal. Chim. Acta* **2004,** 504, 191-197.
40. Vidyasankar, S.; Ru, M.; Arnold, F., Molecularly imprinted ligand-exchange adsorbents for the chiral separation of underivatized amino acids. *J. Chromatogr. A* **1997,** 775, (1-2), 51-63.
41. Piletsky, S.; Panasyuk, T.; Piletskaya, E.; Nicholls, I.; Ulbricht, M., Receptor and transport properties of imprinted polymer membranes - a review. *J. Membr. Sci.* **1999,** 157, (2), 263-278.

42. Vlatakis, G.; Aandersson, L.; Muller, R.; Mosbach, K., Drug Assay using Antibody Mimics made by Molecularl Imprinting. *Nature* **1993,** 361, (6413), 645-647.
43. Andersson, L., Application of molecular imprinting to the development of aqueous buffer and organic solvent based radioligand binding assays for (S)-propranolol. *Anal. Chem.* **1996,** 68, (1), 111-117.
44. Ansell, R.; Ramstrom, O.; Mosbach, K., Towards artificial antibodies prepared by molecular imprinting. *Clinical Chem.* **1996,** 42, (9), 1506-1512.
45. Haupt, K.; Dzgoev, A.; Mosbach, K., Assay system for the herbicide 2,4-dichlorophenoxyacetic acid using a molecularly imprinted polymer as an artificial recognition element. *Anal. Chem.* **1998,** 70, (3), 628-631.
46. Tada, M.; Iwasawa, Y., Design of molecular-imprinting metal-complex catalysts. *J. Mol. Catal. A-Chemical* **2003,** 199, (1-2), 115-137.
47. Suzuki, A.; Tada, M.; Sasaki, T.; Shido, T.; Iwasawa, Y., Design of catalytic sites at oxide surfaces by metal-complex attaching and molecular imprinting techniques. *J. Mol. Catal. A-Chemical* **2002,** 182, (1), 125-136.
48. Bruggemann, O.; Haupt, K.; Ye, L.; Yilmaz, E.; Mosbach, K., New configurations and applications of molecularly imprinted polymers. *J. Chromatogr. A* **2000,** 889, (1-2), 15-24.
49. Toorisaka, E.; Uezu, K.; Goto, M.; Furusaki, S., A molecularly imprinted polymer that shows enzymatic activity. *Biochem. Eng. J.* **2003,** 14, (2), 85-91.
50. Svenson, J.; Zheng, N.; Nicholls, I., A molecularly imprinted polymer-based synthetic transaminase. *J. Amer. Chem. Soc.* **2004,** 126, (27), 8554-8560.
51. Meng, Z.; Sode, K., The molecular reaction vessels for a transesterification process created by molecular imprinting technique. *J. Mol. Recogn.* **2005,** 18, (3), 262-266.
52. Ciardelli, G.; Silvestri, D.; Cristallini, C.; Barbani, N.; Giusti, P., The relevance of the transfer of molecular information between natural and synthetic materials in the realisation of biomedical devices with enhanced properties. *J. Biomat. Sci. -Polymer Edition* **2005,** 16, (2), 219-236.
53. Piletsky, S.; Turner, A., Electrochemical sensors based on molecularly imprinted polymers. *Electroanalysis* **2002,** 14, (5), 317-323.
54. Cheong, S.; McNiven, S.; Rachkov, K.; Levi, R.; Yano, K.; Karube, I., Testosterone receptor binding mimic constructed using molecular imprinting. *Macromolecules* **1997,** 30, (5), 1317-1322.
55. Kriz, D.; Kempe, M.; Mosbach, K., Introduction of molecularly imprinted polymers as recognition elements in conductometric chemical sensors. *Sensors and Actuators B-Chemical* **1996,** 33, (1-3), 178-181.
56. KRIZ, D.; RAMSTROM, O.; SVENSSON, A.; MOSBACH, K., Introducing Biomimetic Sensors based on Molecularly Imprinted Polymers as Recognition Elements. *Anal. Chem.* **1995,** 67, (13), 2142-2144.
57. Zayats, M.; Lahav, M.; Kharitonov, A.; Willner, I., Imprinting of specific molecular recognition sites in inorganic and organic thin layer membranes

associated with ion-sensitive field-effect transistors. *Tetrahedron* **2002,** 58, (4), 815-824.
58. Dickert, F.; Lieberzeit, P.; Miarecka, S.; Mann, K.; Hayden, O.; Palfinger, C., Synthetic receptors for chemical sensors - subnano- and micrometre patterning by imprinting techniques. *Biosens. & Biolectron.* **2004,** 20, (6), 1040-1044.
59. Xi, F.; Wu, J.; Lin, X., Novel nylon-supported organic-inorganic hybrid membrane with hierarchical pores as a potential immobilized metal affinity adsorbent. *J. Chormatogr. A* **2006,** 1125, (1), 38-51.
60. Ciardelli, G.; Cioni, B.; Cristallini, C.; Barbani, N.; Silvestri, D.; Giusti, P., Acrylic polymeric nanospheres for the release and recognition of molecules of clinical interest. *Biosens. & Biolectron.* **2004,** 20, (6), 1083-1090.
61. Suarez-Rodriguez, J.; Diaz-Garcia, M., Fluorescent competitive flow-through assay for chloramphenicol using molecularly imprinted polymers. *Biosens. & Biolectron.* **2001,** 16, (9-12), 955-961.
62. Der Lee, Y.; Joseph, A.; Lin, C.; Huang, H., Photo-litographically impregnated and molecularly imprinted polymers thin film for biosensor applications. *J. Chromatogr. A* **2004,** 1027, 263-268.
63. Matsui, J.; Akamatsu, K.; Nishiguchi, S.; Miyoshi, D.; Nawafune, H.; Tamaki, K.; Sugimoto, N., Composite of Au nanoparticles and molecularly imprinted polymer as a sensing material. *Anal. Chem.* **2004,** 76, (5), 1310-1315.
64. Karube, I.; Piletsky, S.; Piletskaya, E.; Elgerma, A.; Yano, K., Atrazine sensing by molecurly imprinted membranes. *Biosens. & Biolectron.* **1995,** 10, 959-964.
65. Shimitzu, K.; Greene, N., Colorimetric Molecularly Imprinted Polymer Sensor Array using Dye Displacement. *J. Amer. Chem. Soc.* **2005,** 127, 5695-5700.
66. Hoffman, A., Hydrogels for biomedical applications. *Adv. Drug Deliver. Rev.* **2002,** 54, (1), 3-12.
67. Allender, C.; Richardson, C.; Woodhouse, B.; Heard, C.; Brain, K., Pharmaceutical applications for molecularly imprinted polymers. *Intern. J. Pharm.* **2000,** 195, (1-2), 39-43.
68. Peppas, N.; Oral, E.; Huang, Y.; Bures, P., Surface Modifications and Molecular Imprinting of Polymers in medical and pharmaceutical applications. *J. Control. Release* **2001,** 72, 25-33.
69. Cunliffe, D.; Kirby, A.; Alexander, C., Molecularly imprinted drug delivery systems. *Adv. Drug Deliv. Rev.* **2005,** 57, (12), 1836-1853.
70. Sellergren, B.; Allender, C., Molecularly imprinted polymers: A bridge to advanced drug delivery. *Adv. Drug Deliv. Rev.* **2005,** 57, (12), 1733-1741.
71. Whitcombe, M.; Vulfson, E., Imprinted polymers. *Adv. Mater.* **2001,** 13, (7), 467-+.
72. Ramstrom, O.; Ansell, R., Molecular imprinting technology: Challenges and prospects for the future. *Chirality* **1998,** 10, (3), 195-209.

73. Sellergren, B., Imprinted chiral stationary phases in high-performance liquid chromatography. *J. Chromatogr. A* **2001,** 906, (1-2), 227-252.
74. Cormack, P.; Mosbach, K., Molecular imprinting: recent developments and the road ahead. *Reactive & Functional Polymers* **1999,** 41, (1-3), 115-124.
75. Mosbach, K.; Ramstrom, O., The emerging technique of molecular imprinting and its future impact on biotechnology. *Bio-Technology* **1996,** 14, (2), 163-170.
76. Martin-Esteban, A., Molecularly imprinted polymers: new molecular recognition materials for selective solid-phase extraction of organic compounds. *Fresenius J. Anal. Chem.* **2001,** 370, 795-802.
77. Andersson, L., Molecular imprinting for drug bioanalysis - A review on the application of imprinted polymers to solid-phase extraction and binding assay. *J. Chromatogr. B* **2000,** 739, (1), 163-173.
78. Haupt, K.; Mosbach, K., Plastic antibodies: developments and applications. *Trens Biotechnol.***1998,** 16, (11), 468-475.
79. Haupt, K.; Mayes, A.; Mosbach, K., Herbicide assay using an imprinted polymer based system analogous to competitive fluoroimmunoassays. *Anal. Chem.* **1998,** 70, (18), 3936-3939.
80. Byrne, M.; Park, K.; Peppas, N., Molecular imprinting within hydrogels. *Adv. Drug Deliv. Rev.* **2002,** 54, (1), 149-161.
81. Peppas, N.; KHARE, A., Preparation, Sructure and Diffusional Behavior of Hydrogels in Controlled-Release. *ADV. DRUG DELIV. REV.* **1993,** 11, (1-2), 1-35.
82. Kashyap, N.; Kumar, N.; Kumar, M., Smart Gels for Drug Delivery Applications. *Drug Delivery Technology* **2004,** 4, 32-39.
83. Peppas, N.; Huang, Y.; Torres-Lugo, M.; Ward, J.; Zhang, J., Physicochemical, foundations and structural design of hydrogels in medicine and biology. *Annual Rev. Biomed. Eng.* **2000,** 2, 9-29.
84. Tanaka, T., Frustration in Polymer Conformation in Gels and Minization through Molecular Imprinting. *Physical Review Letters* **2000,** 85, (23), 5000 - 5003.
85. Alvarez-Lorenzo, C.; Yanez, F.; Barreiro-Iglesias, R.; Concheiro, A., Imprinted soft contact lenses as norfloxacin delivery systems. *J. Control. Release* **2006,** 113, (3), 236-244.
86. Parmpi, P.; Kofinas, P., Biomimetic glucose recognition using molecularly imprinted polymer hydrogels. *Biomaterials* **2004,** 25, (10), 1969-1973.
87. Oral, E.; Peppas, N., Responsive and recognitive hydrogels using star polymers. *J. Biomed. Mater. Res. PART A* **2004,** 68A, (3), 439-447.
88. Peppas, N.; Oral, E., Hydrophilic Molecular Imprinting poly(hydroxyethyl-methacrylate) polymers. *J. Biomed. Mater. Res. PART A* **2006,** 78, (A), 205-210.
89. Demirel, G.; Ozcetin, G.; Turan, E.; Caykara, T., pH/temperature-sensitive imprinted ionic poly (N-tert-butylacrylamide-co-acrylamide/maleic acid) hydrogels for bovine serum albumin. *Macromolecular Bioscience* **2005,** 5, (10), 1032-1037.
90. Chapiro, A., *Pure and Appl. Chem.* **1981,** 53, 643.
91. Wulff, G.; Kemmere, R.; Veitmeier, J.; Poll, H., *Nouv J Chim* **1982,** 6, 681.

92. Wulff, G.; Veitmeier, J.; Poll, H., *Makromol.Chem.* **1987,** 188, 731.
93. Wulff, G., *Angew. Chem.Int. Ed. Engl.* **1995,** 34, 1812.
94. Perez-Moral, N.; Mayes, A., Direct rapid synthesis of MIP beads in SPE cartridges. *Biosens.. & Biolectron..* **2006,** 21, (9), 1798-1803.
95. March, J., *Advanced Organic Chemistry*. John Wiley & Son: 1992.
96. Perez-Moral, N.; Mayes, A., Comparative study of imprinted polymer particles prepared by different polymerisation methods. *Anal. Chim. Acta* **2004,** 504, (1), 15-21.
97. Kempe, M.; Mosbach, K., Separation of Amino-Acids, Peptides and Proteines on Molecularly Imprinted Stationary Phases. *J. Chromatogr. A* **1995,** 691, (1-2), 317-323.
98. Zou, H.; Huang, X.; Chen, X.; Luo, Q.; Kong, L., Molecular imprinted monolithic stationary phase for liquid chromatographic separation of enantiomers and diasteromers. *J. Chormatogr. A* **2003,** 984, 273-282.
99. Flores, A.; Cunliff, D.; Whitcombe, M.; Vulfson, E., Imprinted polymers prepared by aqueous suspension polymerization. *J. Appl. Polym. Sci.* **2000,** 77, (8), 1841-1850.
100. Mandler, D.; Turyan, I.; Marx, S.; Shustak, G., Application of Sol Gel Technology for Electroanalytical Sensing. *Electroanalysis* **2003,** 15, 398-408.
101. Sergeyeva, T.; Piletsky, S.; Piletska, E.; Brovko, O.; Karabanova, L.; Sergeeva, L.; El'skaya, A.; Turner, A., In situ formation of porous molecularly imprinted polymer membranes. *Macromolecules* **2003,** 36, (19), 7352-7357.
102. Cormack, P.; Elorza, A., Molecularly imprinted polymers: synthesis and characterisation. *J. Chromatogr. B-Analytical Technologies in the Biomedical and Life Sciences* **2004,** 804, (1), 173-182.
103. Sherrington, D., Preparation, structure and morphology of polymer supports. *Chem. Commun.* **1998**, 2278-2286.
104. Schmidt, R.; Mosbach, K.; Haupt, K., A simple method for spin-coating molecularly imprinted polymer films of controlled thickness and porosity. *Adv. Mater.* **2004,** 16, (8), 719-+.
105. Nicholls, I.; Adbo, K.; Andersson, H.; Andersson, P.; Ankarloo, J.; Hedin-Dahlstrom, J.; Jokela, P.; Karlsson, J.; Olofsson, L.; Rosengren, J.; Shoravi, S.; Svenson, J.; Wikman, S., Can we rationally design molecularly imprinted polymers? *Anal. Chim. Acta* **2001,** 435, (1), 9-18.
106. Nicholls, I., Towards the rational design of molecularly imprinted polymers. *J. Mol. Recogn.* **1998,** 11, (1-6), 79-82.
107. Sellergren, B.; Lepisto, M.; Mosbach, K., *J Amer Chem Soc* **1988,** 110, 5853.
108. Molinelli, A.; O'Mahony, J.; Nolan, K.; Smyth, M.; Jakusch, M.; Mizaikoff, B., Analyzing the mechanisms of selectivity in biomimetic self-assemblies via IR and NMR spectroscopy of prepolymerization solutions and molecular dynamics simulations. *Anal. Chem.* **2005,** 77, (16), 5196-5204.
109. Oral, E.; Peppas, N., Dynamic studies of molecular imprinting polymerizations. *Polymer* **2004,** 45, (18), 6163-6173.

110. Sellegren, B.; Shea, K., Origin of Peak Asymmetry and the Effect of Temperature on Solute Retention in Enantiomer Separations on Imprinted Chiral Stationary Phases. *J. Chormatogr. A* **1995,** 690, (1), 29-39.
111. El-Toufaili, F.; Visnjevski, A.; Bruggemann, O., Screening combinatorial libraries of molecularly imprinted polymer films casted on membranes in single-use membrane modules. *J. Chromatogr. B-Analytical Technologies in the Biomedical and Life Sciences* **2004,** 804, (1), 135-139.
112. Davies, M.; De Biasi, V.; Perrett, D., Approaches to the rational design of molecularly imprinted polymers. *Anal. Chim. Acta* **2004,** 504, (1), 7-14.
113. Rosengren, A.; Karlsson, J.; Andersson, P.; Nicholls, I., Chemometric models of template-molecularly imprinted polymer binding. *Anal. Chem.* **2005,** 77, (17), 5700-5705.
114. Alvarez-Lorenzo, C.; Concheiro, A., Molecularly imprinted polymers for drug delivery. *J. Chromatogr. B-Analytical Technologies in the Biomedical and Life Sciences* **2004,** 804, (1), 231-245.
115. van Nostrum, C., Molecular imprinting a new tool for drug innovation. *Drug Discovery Today: Technology* **2005,** 2, 119-124.
116. Holroyd, S.; Groves, P.; Searle, M.; Gerhard, U.; Williams, D., Rational Design and Binding of Modified Cell-Wall Peptides to Vancomycin-group Antibiotics - Factorizing Free-Energy Contributions to Binding. *Tetrahedron* **1993,** 49, (41), 9171-9182.
117. Ciardelli, G.; Giusti, P.; Bronco, S.; Cappelli, C.; Monti, S., Towards the design of highly selective recognition sites into molecular imprinting polymers: A computational approach. *Biosens. & Bioelectron.* **2006,** 22, 153-163.
118. Sellergren, B., Noncovalent molecular imprinting: Antibody-like molecular recognition in polymeric network materials. *Trac-Trends in Anal. Chem.* **1997,** 16, (6), 310-320.
119. Matsui, J.; Kubo, H.; Takeuchi, T., Design and preparation of molecularly imprinted atrazine-receptor polymers: Investigation of functional monomers and solvents. *Anal. Sci.* **1998,** 14, (4), 699-702.
120. Katz, A.; Davis, M., Investigations into the mechanisms of molecular recognition with imprinted polymers. *Macromolecules* **1999,** 32, (12), 4113-4121.
121. Xiwen, H.; Jie, Z., Study of the nature of recognition in molecularly imprinted polymer selective for 2-aminopyridine. *Anal. Chim. Acta* **1999,** 381, 85-91.
122. Lubke, C.; Lubke, M.; Whitcombe, M.; Vulfson, E., Imprinted polymers prepared with stoichiometric template-monomer complexes: Efficient binding of ampicillin from aqueous solutions. *Macromolecules* **2000,** 33, (14), 5098-5105.
123. Idziak, L.; Benrebouh, A.; Deschamps, F., Simple NMR experiments as a means to predict the performance of an anti-17 alpha-ethynylestradiol molecularly imprinted polymer. *Anal. Chim. Acta* **2001,** 435, (1), 137-140.
124. Lu, Y.; Li, C.; Zhang, H.; Liu, X., Study on the mechanism of chiral recognition with molecularly imprinted polymers. *Anal. Chim. Acta* **2003,** 489, (1), 33-43.

125. Shea, K. J.; Sasaki, D. Y., An Analysis of Small-Molecule Binding to Functionalized Synthetic Polymers by ^{13}C CP/MAS NMR and FT-IR Spectroscopy. *J. Amer. Chem. Soc.* **1991,** 113, 4109-4120.
126. Kobayashi, T.; Wang, H.; Fujii, N., Molecular imprint membranes of polyacrylonitrile copolymers with different acrylic acid segments. *Anal. Chim. Acta* **1998,** 365, (1-3), 81-88.
127. Mohr, G.; Citterio, D.; Demuth, C.; Fehlmann, M.; Jenny, L.; Lohse, C.; Moradian, A.; Nezel, T.; Rothmaier, M.; Spichiger, U., Reversible chemical reactions as the basis for optical sensors used to detect amines, alcohols and humidity. *J. Mater. Chem.* **1999,** 9, (9), 2259-2264.
128. Yoshida, M.; Hatate, Y.; Uezu, K.; Goto, M.; Furusaki, S., Chiral-recognition polymer prepared by surface molecular imprinting technique. *Colloids and Surfaces A-Physicochemical and Engineering Aspects* **2000,** 169, (1-3), 259-269.
129. Spivak, D., Optimization, evaluation, and characterization molecularly imprinted polymers. *Adv. Drug Deliv. Rev.* **2005,** 57, 1779-1794.
130. Connors, K., *Binding Constants -The Measurements of Molecular Complex Stability*. John Wiley & Sons: 1987.
131. Svenson, J.; Andersson, H.; Piletsky, S.; Nicholls, I., Spectroscopic studies of the molecular imprinting self-assembly process. *J. Mol. Recogn.* **1998,** 11, (1-6), 83-86.
132. Sasaki, D.; Alam, T., Solid-state P-31 NMR study of phosphonate binding sites in guanidine-functionalized, molecular imprinted silica xerogels. *Chem. Mater.* **2000,** 12, (5), 1400-1407.
133. Sipahigil, O.; Torres-Lugo, M.; Peppas, N., FTIR spectroscopic analysis of protein/carrier interactions in novel protein delivery systems. *Stp. Pharma Sciences* **2002,** 12, (6), 345-350.
134. Dykes, G.; Smith, D.; Caragheorgheopol, A., NMR and ESR investigations of the interaction between a carboxylic acid and an amine at the focal point of L-lysine based dendritic branches. *Organ. & Biomol. Chem.* **2004,** 2, (6), 922-926.
135. Ramstrom, O.; Ye, L.; Mosbach, K., Artificial antibodies to corticosteroids prepared by molecular imprinting. *Chemistry & Biology* **1996,** 3, (6), 471-477.
136. Mayes, A.; Whitcombe, M., Synthetic strategies for the generation of molecularly imprinted organic polymers. *Adv. Drug Deliv. Rev.* **2005,** 57, 1742-1778.
137. Beuermann, S.; Paquet, D. A.; McMinn, J. H.; Hutchinson, R. A., Propagation Kinetics of Methacrylic Acid Study by Pulse-Laser Polymerization. *Macromolecules* **1997,** 30, 194-197.
138. Bowman, C. N.; Elliott, J. E., Effect of primary cyclization on Free Radical Polymerization Kinetics: Modeling Approach. *Macromolecules* **2002,** 35, 7125-7131.
139. Allender, C., Molecularly Imprinted Polymers: Technology and Applications. *Adv. Drug Deliv. Rev.* **2005,** 57, 1731-1732.

140. Sellergren, B., *Molecularly Ijmprinted Polymers Man-Made Mimics of Antibodies and Their Applications in Anal. Chem*. 2nd ed.; 2001; Vol. 23, p 557.
141. Hillberg, A.; Brain, K.; Allender, C., Molecular imprinted polymer sensors: Implications for therapeutics. *Adv. Drug Deliv. REV.* **2005,** 57, (12), 1875-1889.
142. Peppas, N.; Hilt, J.; Khademhosseini, A.; Langer, R., Hydrogels in biology and medicine: From molecular principles to bionanotechnology. *Adv. Mater.* **2006,** 18, (11), 1345-1360.
143. Watanabe, M.; Akahoshi, T.; Tabata, Y.; Nakayama, D., Molecular Specific Swelling Change of Hydrogels in Accordance with the Concentration of Guest Molecules. *J. Amer. Chem. Soc* **1998,** 120, 5577-5578.
144. Montgomery, D. C., *Design and Analysis of Experiments*. Fourth Ediciton ed.; John Wiley & Son, Inc.: 1997; p 704.
145. Ortega, C.; Juan, E. Electrical Studies of Cross-linked Methacrylic acid Hydrogels for Biosensors Applications base on Statistical Analyses. University of Puerto Rico, Mayaguez, 2007.
146. Peppas, N.; Bell, C., Water, solute and protein diffusion in physiologically responsive hydrogels of poly(methacrylic acid-g-ethylene glycol). *Biomaterials* **1996,** 17, 1206-1218.
147. Ju, H.; Lin, J., Electrochemical and chemiluminescent immunosensors for tumor markers. *Biosens. & Bioelectron.* **2004,** 20, (8), 1461-1470.
148. Sellergren, B., Imprinted polymer for selective adsorption of cholesterol. *Chem. Mater.* **1998,** 10, 4037-4046.
149. Piletsky, S.; Dubei, I.; Fredroyak, D.; Kukhar, V., Substrate-selective polymeric membranes:selective transfer of nucleic acid components. *Biopolym. Kletka.* **1990,** 6, 55.
150. Hong, J.; Anderson, P.; Qian, J.; Martin, C., Selectively-Permeable Ultrathin Film Composite Membrane Based on Molecularly-Imprinted Polymers. *Chem. Mater.* **1998,** 10, 1029-1033.
151. Peppas, N.; Merril, E., Crosslinked poly(vinyl alcohol) hydrogels as swelling elastic networks. *J. App. Polym. Sci.* **1977,** 21, 1763-1770.
152. Flory, P.; Rehner, J., Statistical Mechanics of Cross-Linked Polymer Networks II. Swelling. *J. Chem. Phys.* **1949,** 11, 521.
153. Peppas, N.; Tanya am Ende, M., Transport of ionizable drugs and proteins in crosslinked poly(acrylic acid) and poly(acrylic acid-co-2-hydroxyethyl methacrylate) hydrogels. *J. App. Polym. Sci.* **1996,** 99, 673-685.
154. Kim, B.; Peppas, N., Synthesis and characterization of pH-sensitive glycopolymers for oral drug delivery systems. *J. Biomater. Sci.-Polymer Edition* **2002,** 13, (11), 1271-1281.
155. Herber, S.; Olthuis, W.; Bergveld, P., A swelling hydrogel-based Pco2 Sensor. *Sensors and Actuators B-Chemical* **2003,** 91, 378-382.
156. Canal, T.; Peppas, N., Correlation Between Mesh Size and Equilibrium Degree of Swelling of Polymeric Networks. *J. Biomed. Mater. Res.* **1989,** 23, 1183-113.

157. Syu, M.; Nia, Y., An alleosteric model for the bidingin of bilirubin to the bilirubin imprinted poly(methacrylic acid-co-ethylene glycol dimethacrylate). *Anal. Chim. Acta* **2005,** 539, 97-106.
158. Garcia, D.; Katimbe, I.; Escobar, J.; Bada, N.; Casquero, J.; Hernaez, E., Synthesis and characterization of poly(methacylic acid) hydrogels for metoclopramide delivery. *Eur. Polym. J.* **2004,** 40, 1637-1643.
159. Wulff, G.; Vietmeier, J.; Poll, H., Enzyme analogue build polymers 22. Influence of the nature of the crosslinking agent on the performance of imprinted polymers in racemic resolution. *Makromol.Chem.* **1987,** 188, 731-740.
160. Sheppard, N.; Lesho, M.; Tucker, R.; SalehiHad, S., Electrical conductivity of pH-responsive hydrogels. *J. Biomater. Sci.-Polymer Edition* **1997,** 8, (5), 349-362.
161. Masaro, L.; Zhu, X. X., Physical Models for diffusions for polymers solutions, gels and solid. *Prog. Poly. Sci* **1999,** 24, 731-775.
162. Piletsky, S.; Piletskaya, E.; Panasyuk, T.; El'skaya, A.; Levi, R.; Karube, I.; Wulff, G., Imprinted membranes for sensor technology: Opposite behavior of covalently and noncovalently imprinted membranes. *Macromolecules* **1998,** 31, (7), 2137-2140.
163. Lowe, C.; Domschke, A.; Smith, D.; Zeng, J.; James, K.; Karangu, N.; Blyth, J.; Xiaoping, Y.; Hussain, A.; Lee, M.; Sartain, F.; Marshall, A.; Satyamoorthy, K., Holographic glucose sensors. *Biosens. & Bioelectron.* **2005,** 20, (8), 1602-1610.
164. Gore, M.; Karmalkar, R.; Kulkarni, M., Enhanced capacities and selectivities for cholesterol in aqueous media by molecular imprinting: role of novel cross-linkers. *J. Chromatogr. B-Analytical Technologies in the BIomedical and LIfe Sciences* **2004,** 804, (1), 211-221.
165. Hwang, C.; Lee, W., Chromatographic characteristics of cholesterol-imprinted polymers prepared by covalent and non-covalent imprinting methods. *J. Chromatogr. A* **2002,** 962, (1-2), 69-78.
166. Whitcombe, M.; Rodriguez, M.; Villar, P.; Vulfson, E., A New Method for the Introduction of Recognition Site Functionality into Polymers Prepared by Molecular Imprinting - Synthesis and Characterization of Polymeric Receptors for Cholesterol. *J. Amer. Chem. Soc.* **1995,** 117, (27), 7105-7111.
167. Bossi, A.; Speghini, A.; Turner, A.; Piletsky, S.; Bonini, F., Surface imprinted beads for the recognition of human serum albumin. *Bioesens. & Bioelectron.* **2005,** 22, (9-10), 2322-2328.
168. Schneider, F.; Piletsky, S.; Piletska, E.; Guerreiro, A.; Ulbricht, M., Comparison of thin-layer and bulk MIPs synthesized by photoinitiated in situ crosslinking polymerization from the same reaction mixtures. *J. Appl. Polym. Sci.* **2005,** 98, (1), 362-372.
169. Wilson, G.; Gifford, R., Biosensors for real-time in vivo measurements. *Biosens. & Bioelectron.* **2005,** 20, (12), 2388-2403.

170. Wang, P.; Xu, G.; Qin, L.; Xu, Y.; Li, Y.; Li, R., Cell-based biosensors and its application in biomedicine. *Sensors and Actuators B-Chemical* **2005,** 108, (1-2), 576-584.
171. Peppas, N.; Shahar, A.; Ward, J., Kinetics of living radical polymerizations of multifuctional monomers. *Polymer* **2002,** 43, 1745-1752.
172. Bai, R.; Hua, D.; Sun, W.; Lu, W.; Pan, C., Study on controled/livin free-radical polymerization of methyl acrilate in the presence of benzyl 9H-carbazole-9-carbodithioate under thermal condition. *Eur. Polym. J.* **2005,** 41, 1674-1680.
173. Pinto, J.; Lima, E.; Cunningham, M.; Lenzy, M., Producing Bimodal Molecular Weight Distribution Polymer Resins Using Living and Conventional Free-Radical POlymerization. *Industrial & Engineering Chemistry Research* **2005,** 44, 2568-2578.
174. Zhu, X. X.; Masaro, L., Physical models of diffusion for polymer solutions, gels and solids. *Progress Polym. Sci.* **1999,** 24, 731-775.
175. Piletsky, S., MIP Sensors. In Turner, N., Ed. New Devlopment in MIP Technology: Cardiff, 2006; pp 97-116.
176. Potyrailo, R., Polymeric Sensor Materials: Toward an Alliance of Combinatorial and Rational Design Tools? *Angew. Chem. Int. Ed.* **2006,** 45, 702-723.
177. Dineiro, Y.; Menendez, M.; Blanco-Lopez, M.; Lobo-Castanon, M.; Miranda-Ordieres, A.; Tunon-Blanco, P., Computational approach to the rational design of molecularly imprinted polymers for voltammetric sensing of homovanillic acid. *Anal. Chem.* **2005,** 77, (20), 6741-6746.

6.4 Appendices

Appendix A – NMR Titration Study Calculation Example
Appendix B – NMR Titration Study Raw Data
Appendix C – Continuous Variation Study Calculation Example
Appendix D – Continuous Variation Study Raw Data
Appendix E – Conversion of Double Bond and Polymerization Rate Calculation Example
Appendix F – Conversion of Double Bond and Polymerization Rate Raw Data
Appendix G – Permeability Study Calculation Example
Appendix H – Permeability Study Raw Data
Appendix I – Swelling and Correlation Length Study Calculation Example
Appendix J – Swelling and Correlation Length Study Raw Data
Appendix K – Binding Study Calculation Example
Appendix L – Binding Study
Appendix M– Electrochemical Study Calculation Example
Appendix N – Electrochemical Study Raw Data

Appendix A – NMR Titration Study Calculation Example

1. The corresponding peaks of interactions were identified using COSY

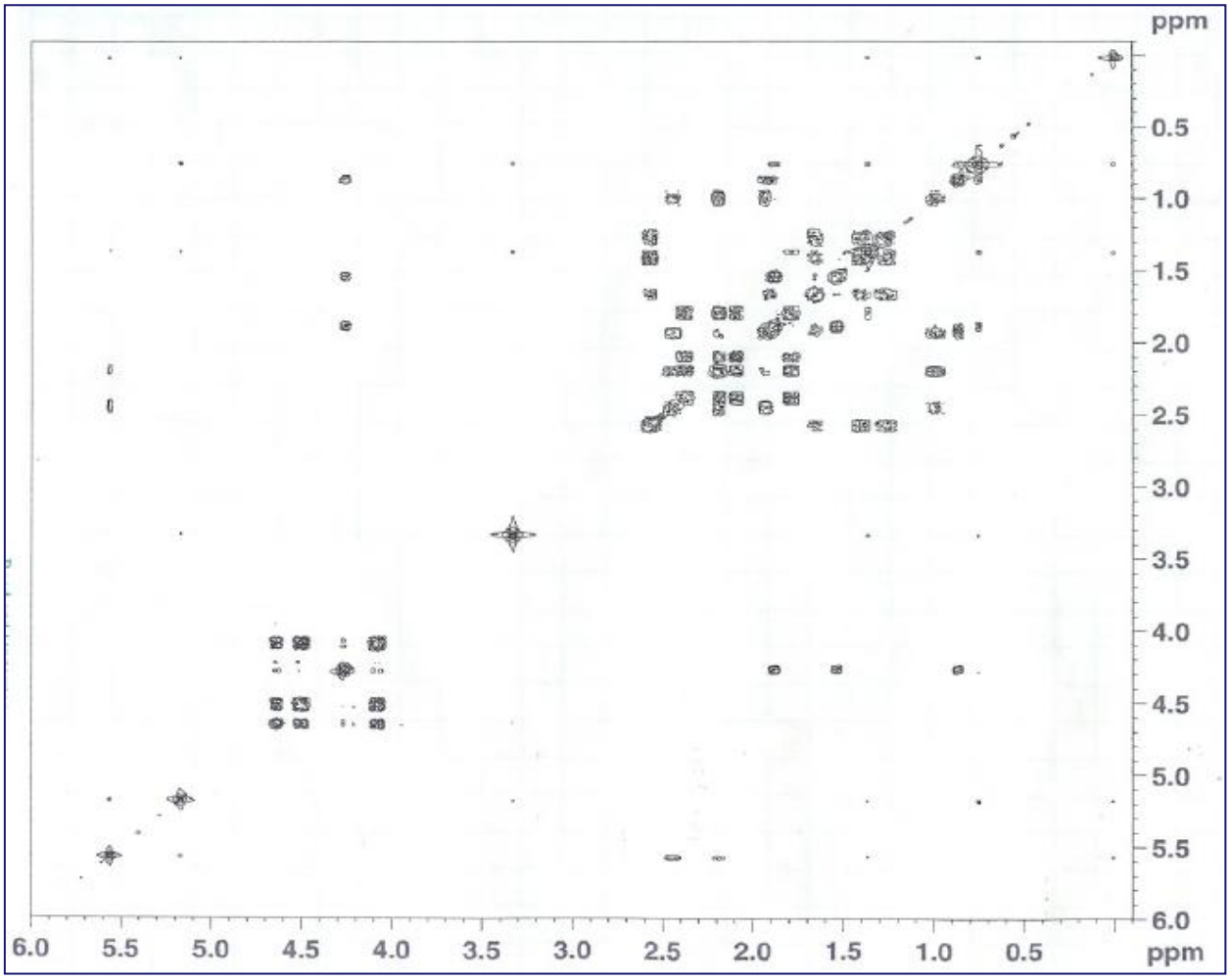

Figure 1. COSY for Hydrocortisone

2. The sample spectra were generated

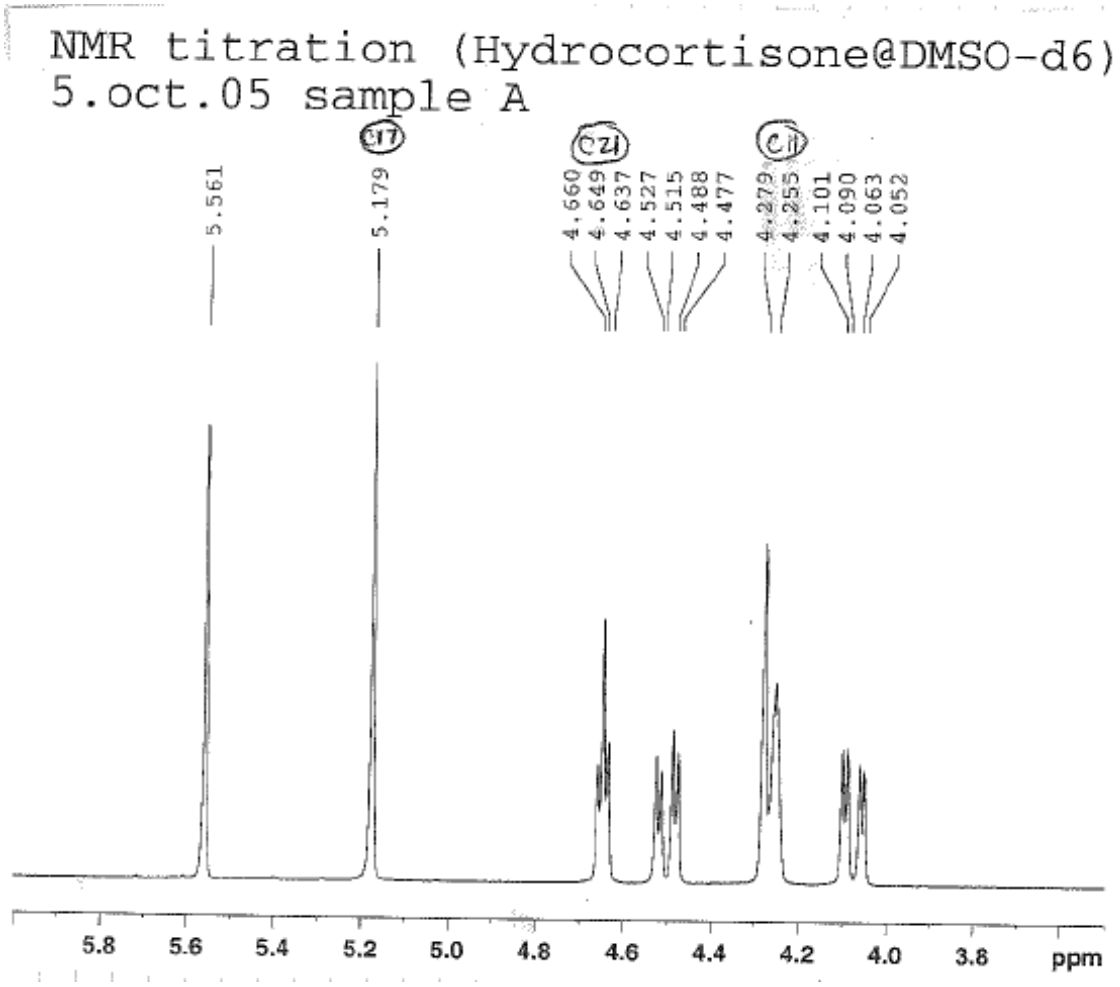

Figure 2- NMR titration spectra for sample A

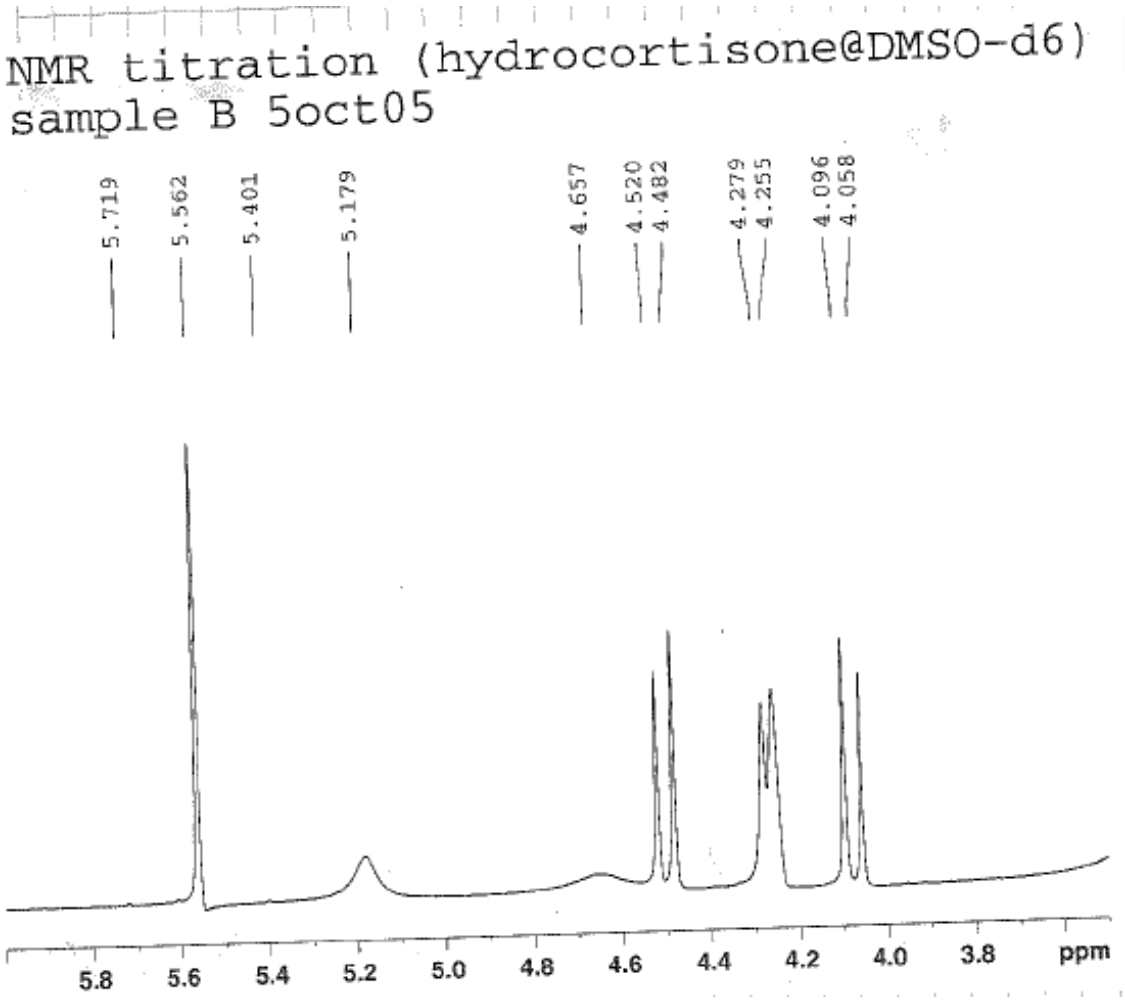

Figure 2 NMR titration spectra for sample B

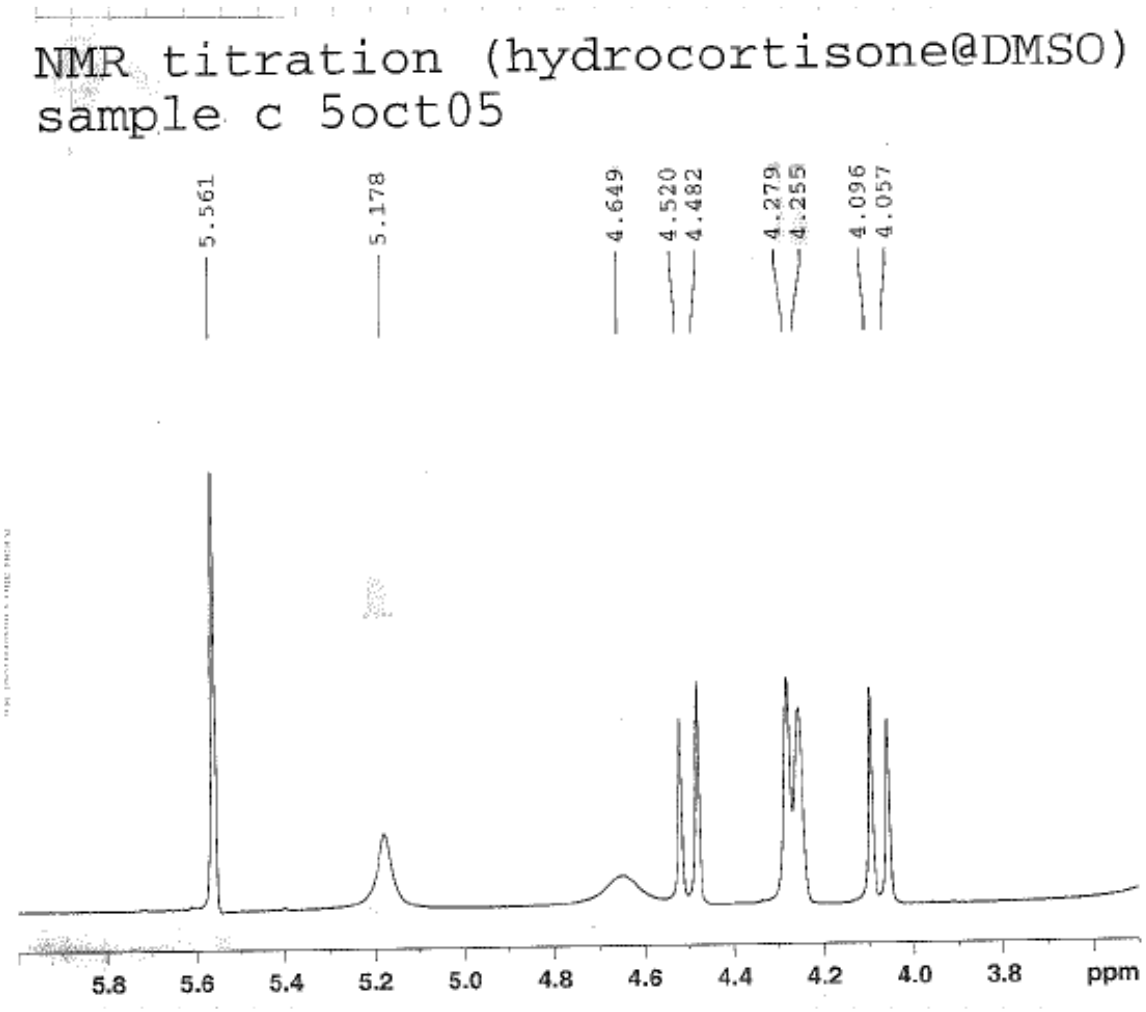

Figure 3 NMR titration spectra for sample C

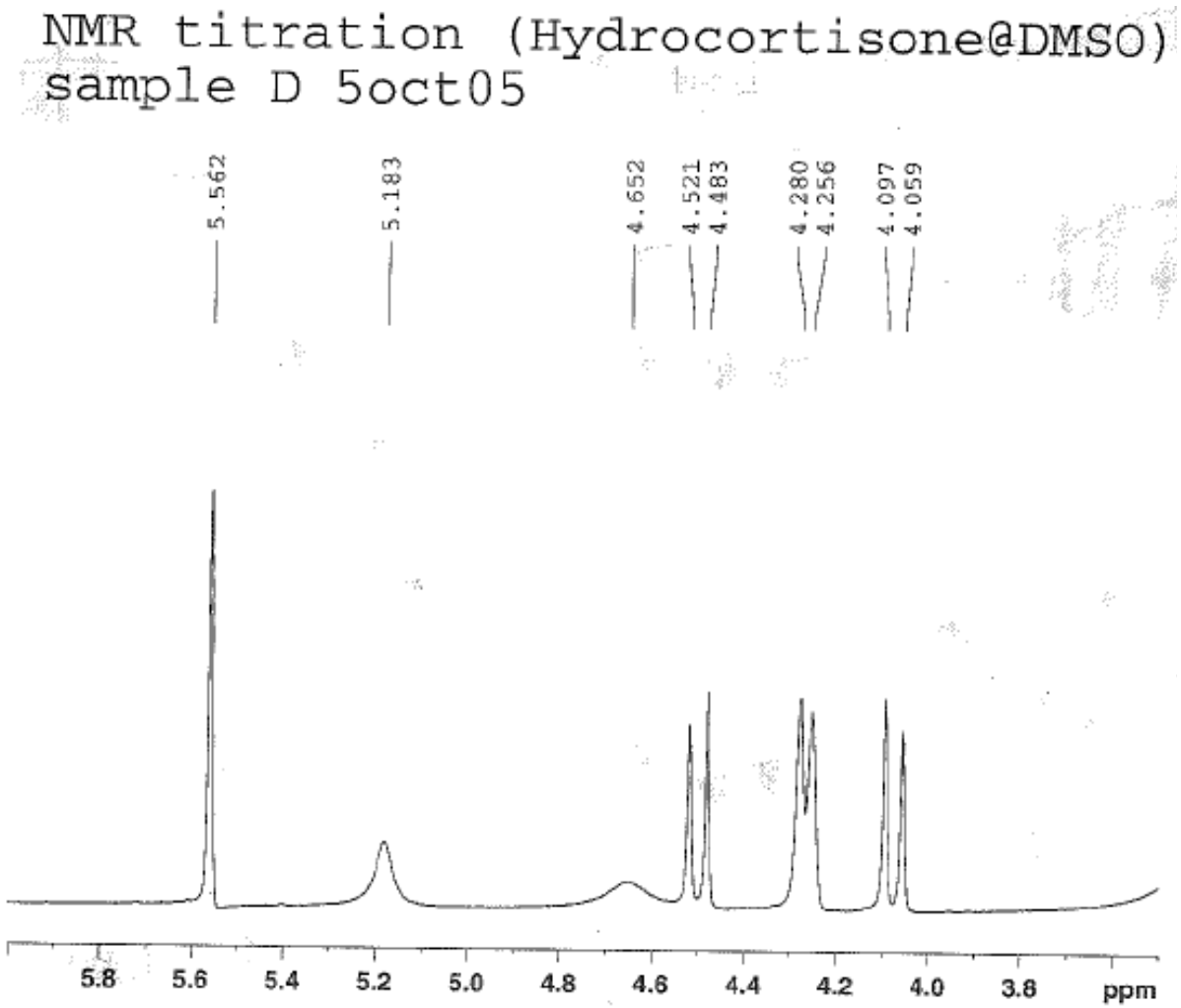

Figure 4 NMR titration spectra for sample D

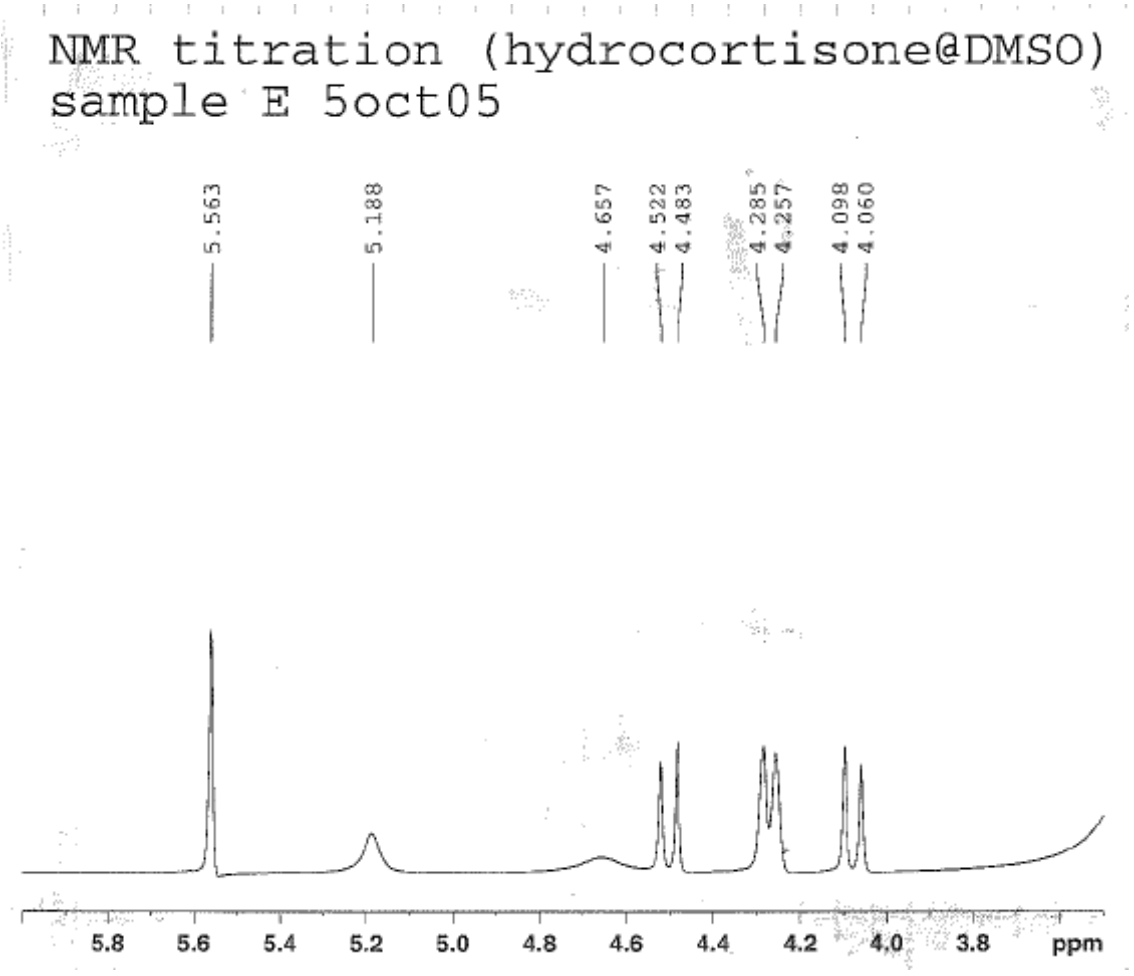

Figure 5. NMR titration spectra for sample E

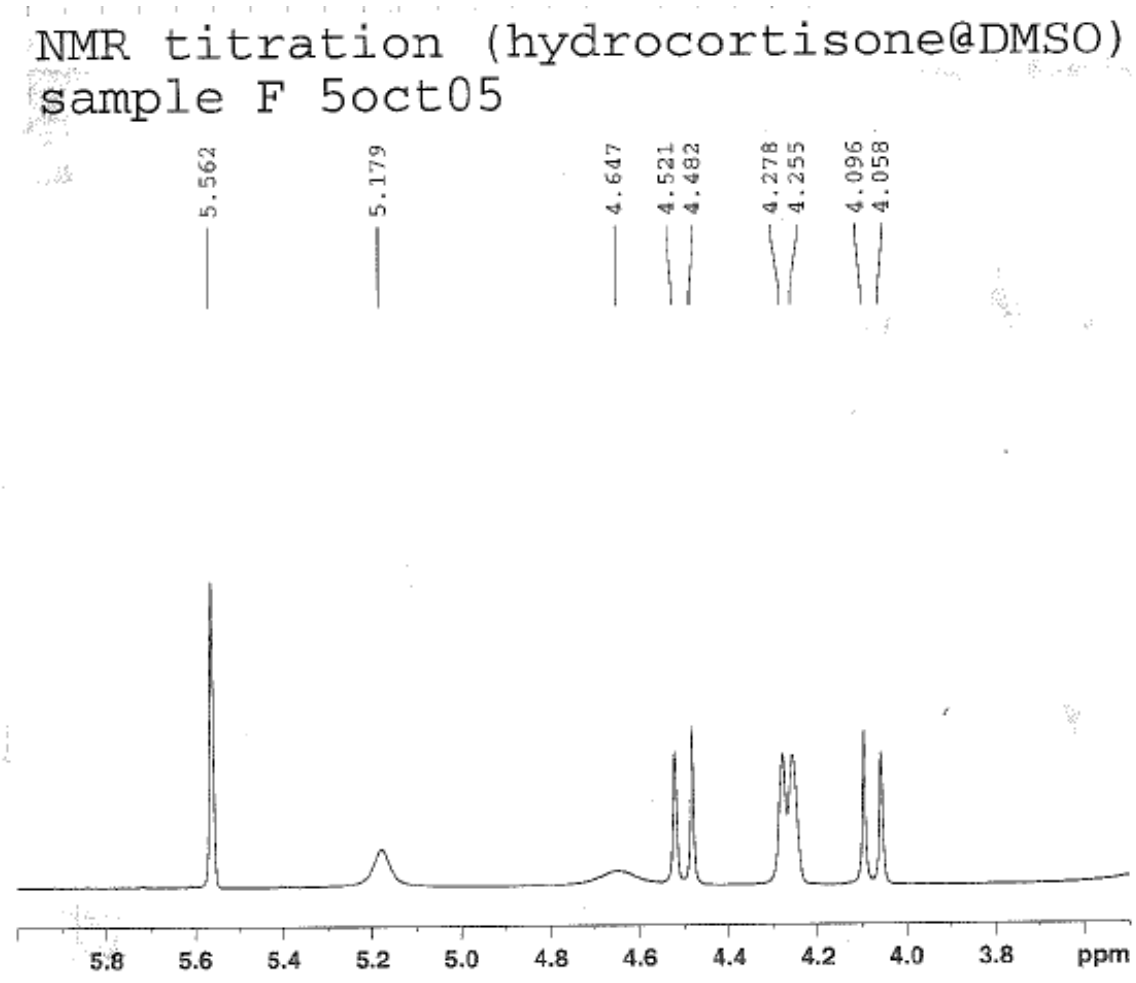

Figure 6. NMR titration spectra for sample F

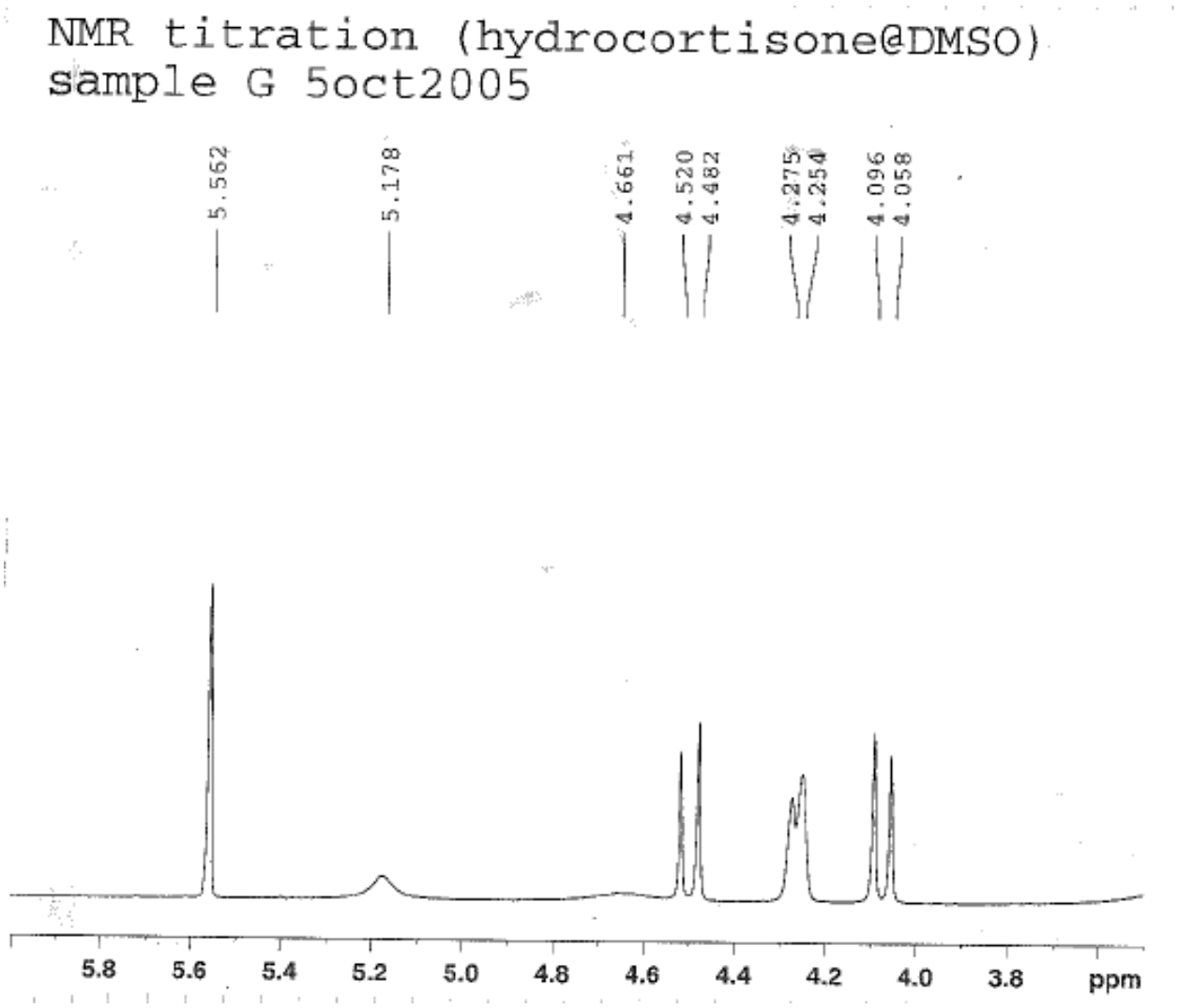

Figure 7. NMR titration spectra for sample G

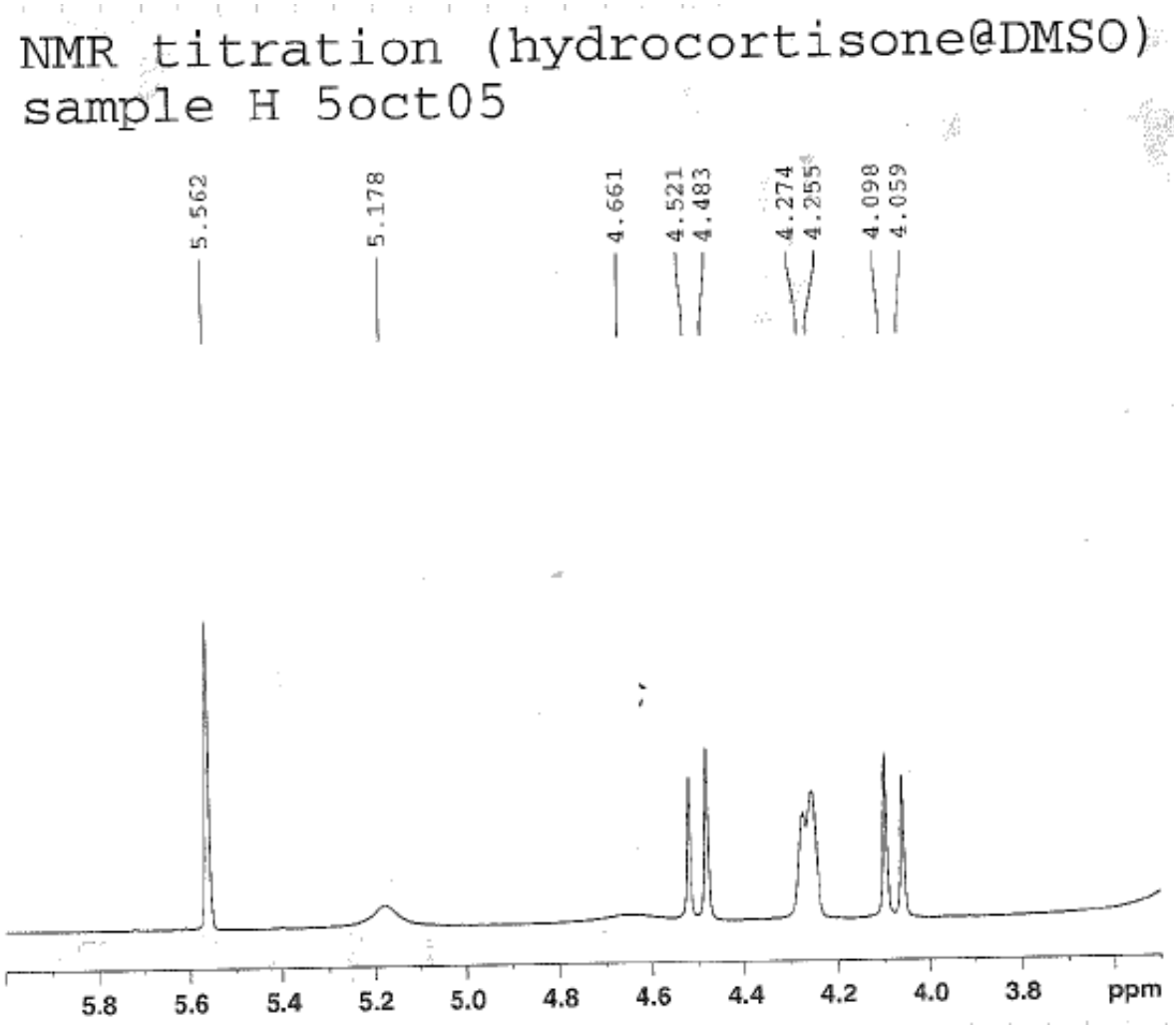

Figure 8 NMR titration spectra for sample H

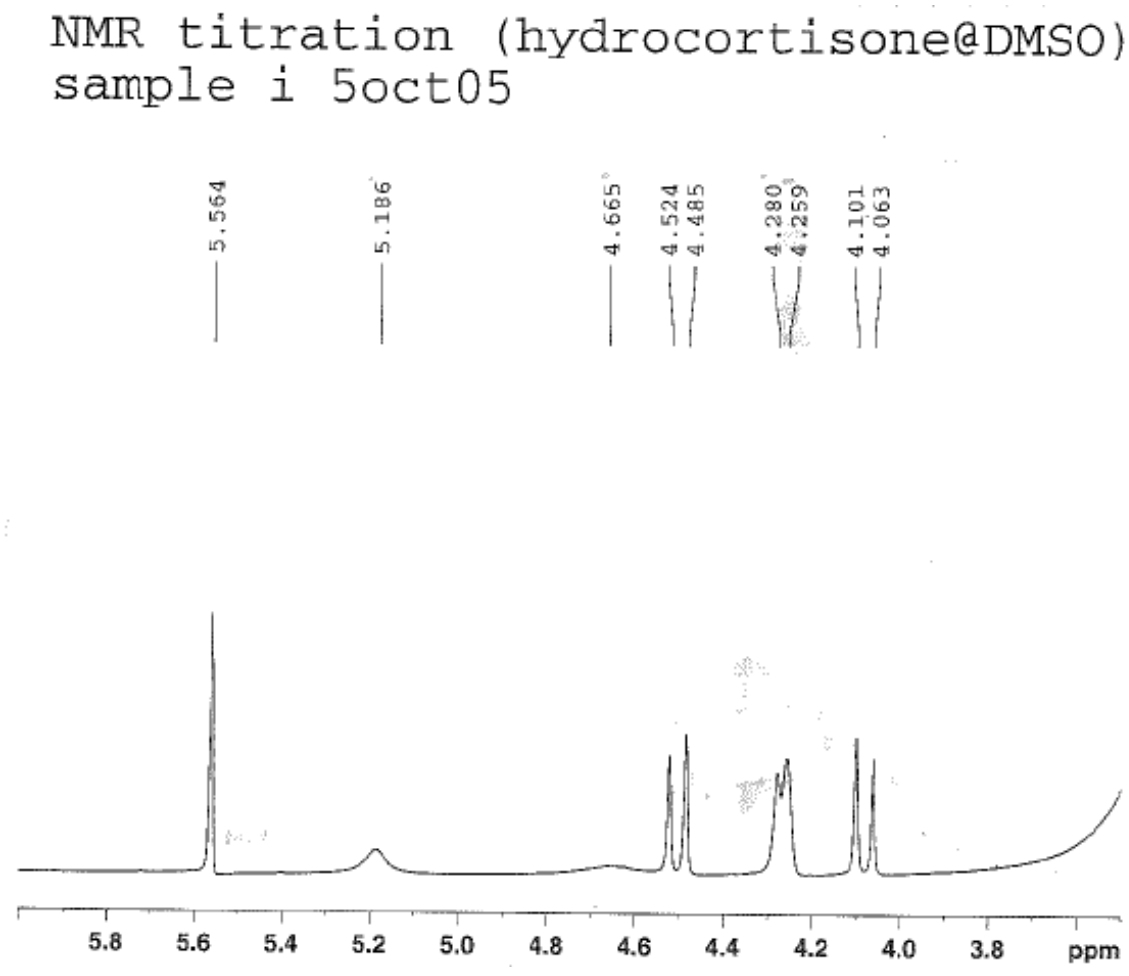

Figure 9 NMR titration spectra of sample I

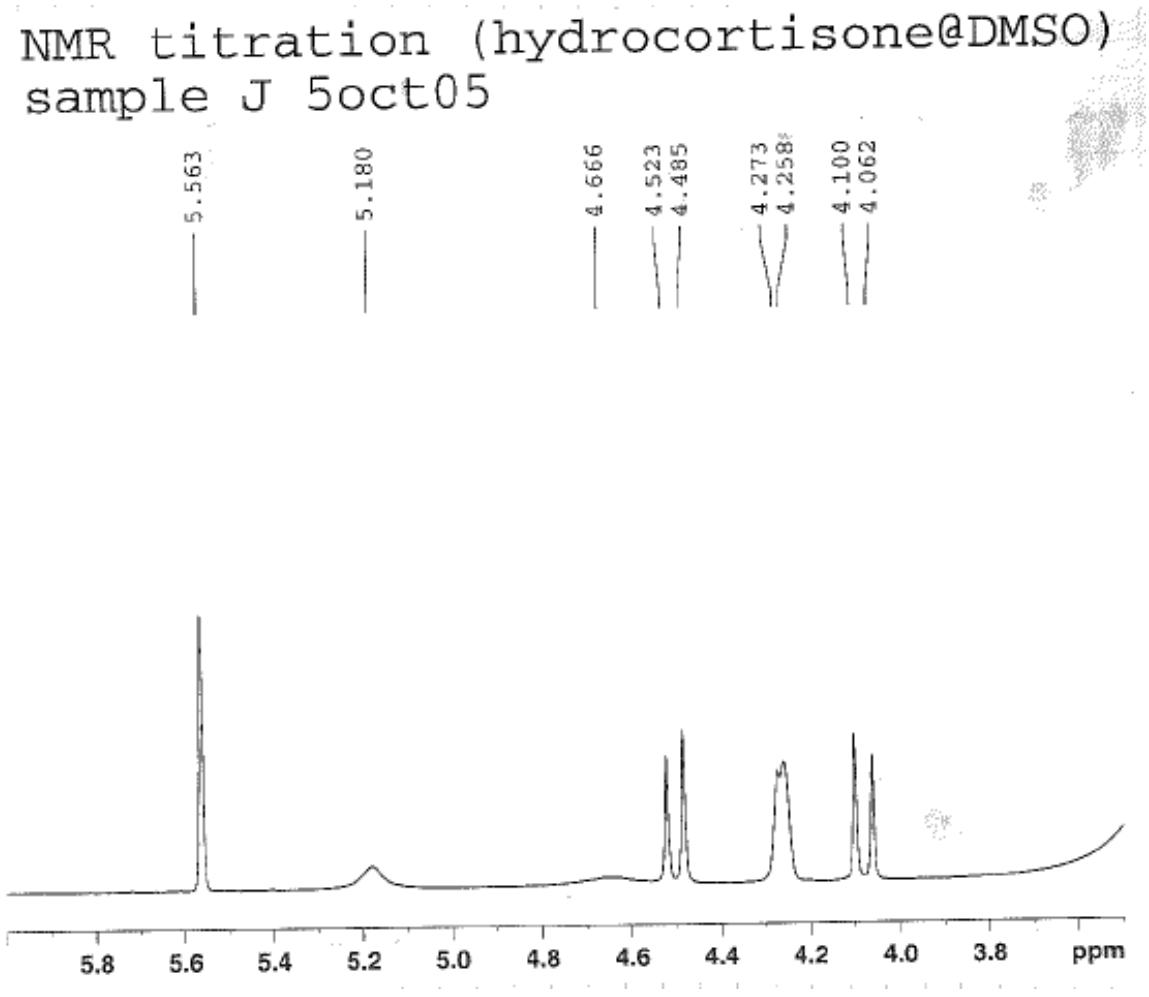

Figure 10 NMR titration Spectra for Smaple J

3. The chemical shift were estimated to generate NMR titration curve (refer to Chapter 4)

Appendix B – NMR Titration Study Raw Data

Table 1 NMR titration Hydrocortisone @ Ethanol

HAc [uL]	Acetit acid Concentration [M]	H17
0.0	0	5.275
0.5	0.018103448	5.285
0.7	0.025344828	5.294
1.0	0.036206897	5.287
1.5	0.054310345	5.287
2.0	0.072413793	5.293
4.0	0.144827586	5.319
6.0	0.217241379	5.321
8.0	0.289655172	5.339
10.0	0.362068966	5.366

Table 2

HAc [uL]	Acetit acid Concentration [M]	Change in Chemical Shift
0.0	0	0
0.5	0.018103448	0.01
0.7	0.025344828	0.019
1.0	0.036206897	0.012
4.0	0.144827586	0.012
6.0	0.217241379	0.018
8.0	0.289655172	0.044
10.0	0.362068966	0.046

Table 3 NMR titration Hydrocortisone @ DMSO

HAc [uL]	Acetit acid Concentration [M]	H17
0.0	0	5.185
0.5	0.018103448	5.189
0.7	0.025344828	5.189
1.0	0.036206897	5.185
1.5	0.054310345	5.185
2.0	0.072413793	5.186
4.0	0.144827586	5.186
6.0	0.217241379	5.184
8.0	0.289655172	5.182
10.0	0.362068966	5.183

Table 4

HAc [uL]	Acetit acid Concentration [M]	Change in Chemical Shift	
0.0	0	0.000	0
1.0	0.036206897	0.000	0.011
1.5	0.054310345	0.004	0.012
2.0	0.072413793	0.004	0.015
4.0	0.144827586	0.003	0.015
8.0	0.289655172	0.005	0.015
10.0	0.362068966	0.007	0.017

Appendix C – Continuous Variation Study Calculation Example

1. Samples were prepared promoting the variation of the hydrocortisone/monomer ratio (0 to 1)

2. The sample spectra were generated

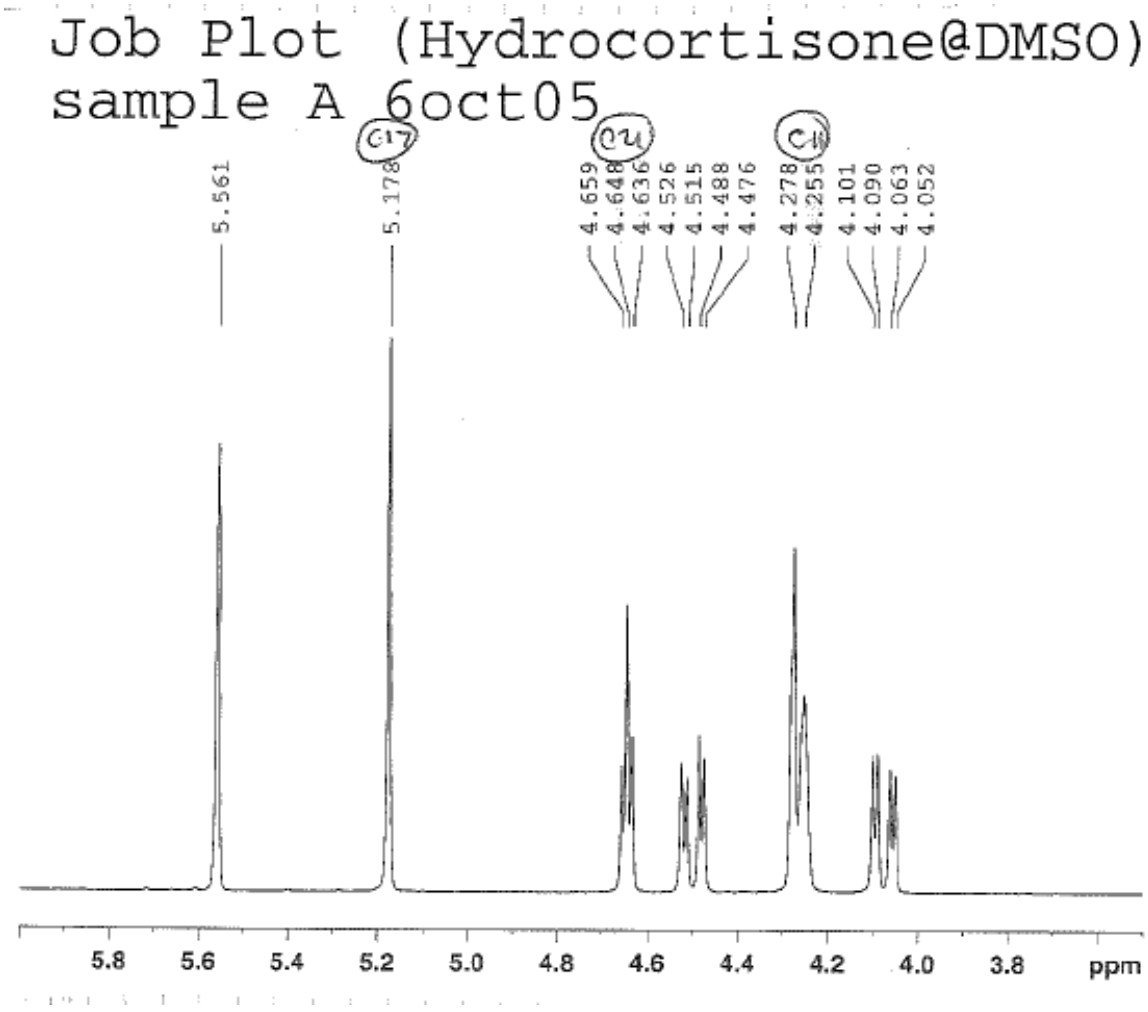

Figure 1 Job plot spectra of sample A

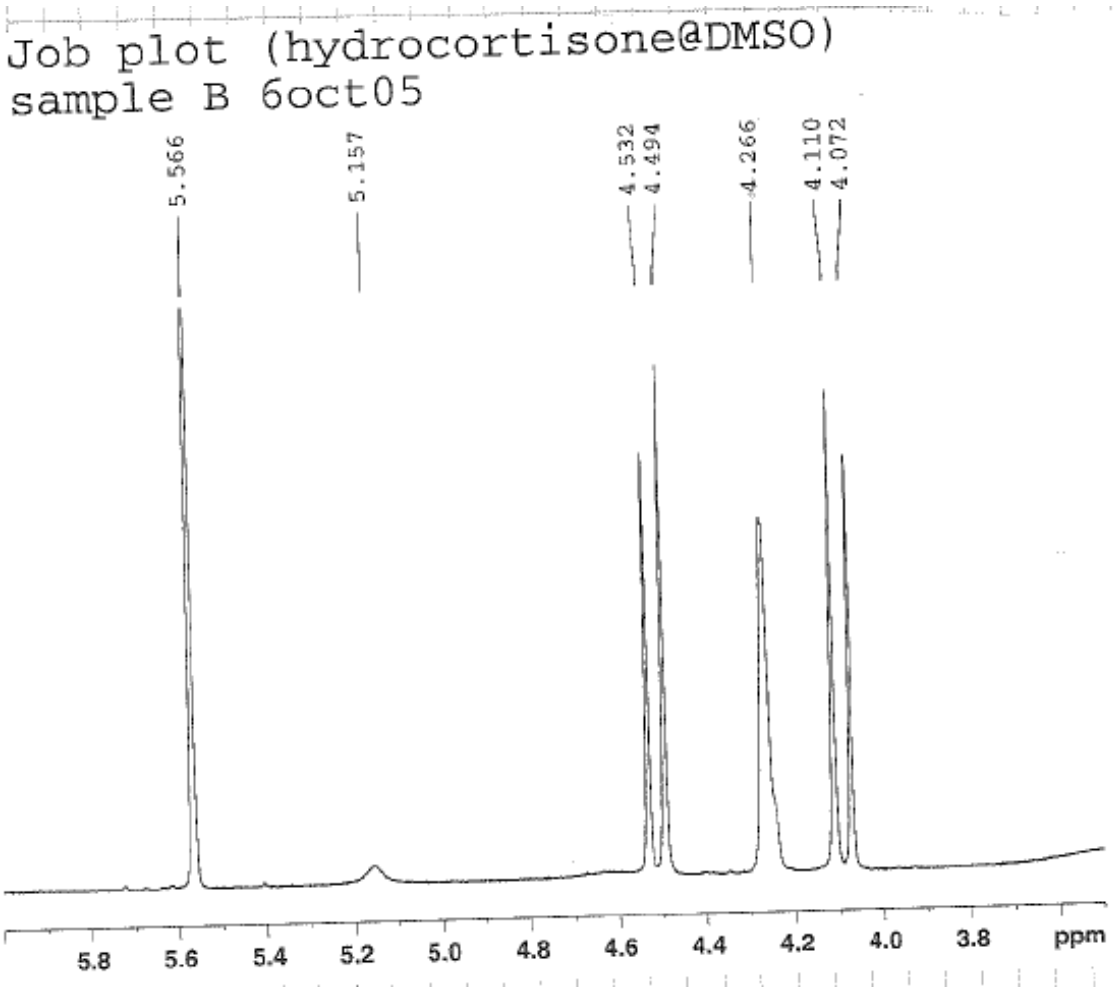

Figure 2 Job plot spectra of sample B

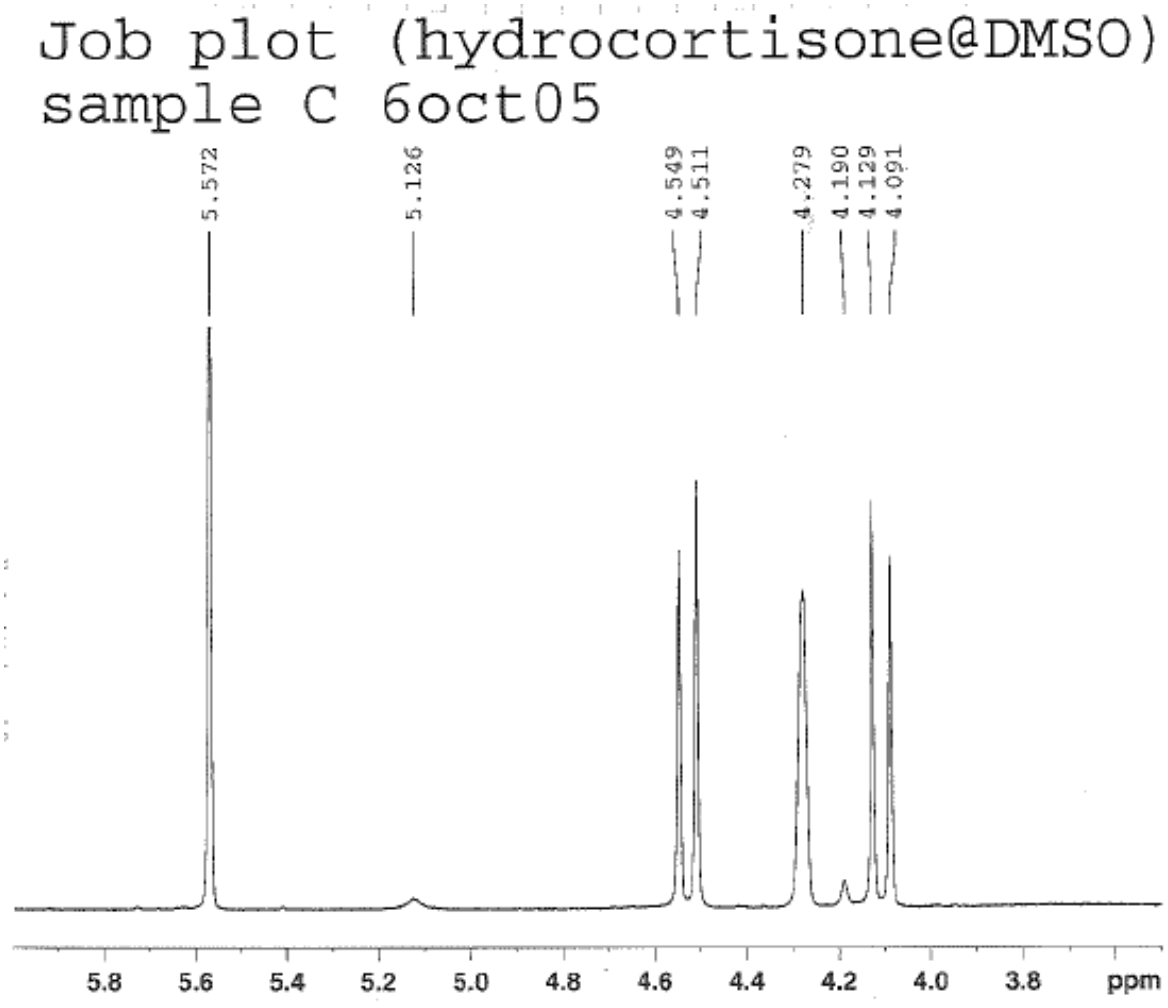

Figure 3 Job plot spectra of sample C

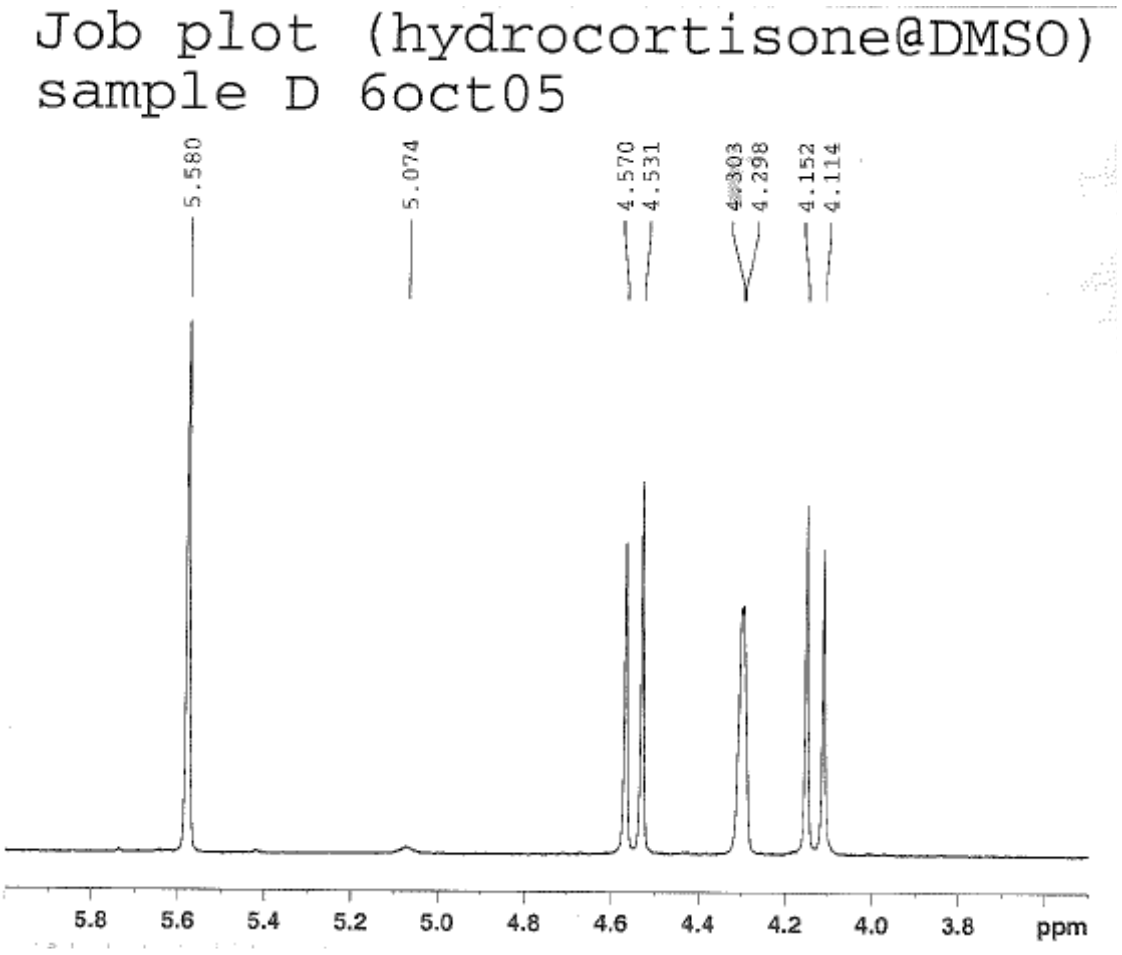

Figure 4 Job plot spectra of sample D

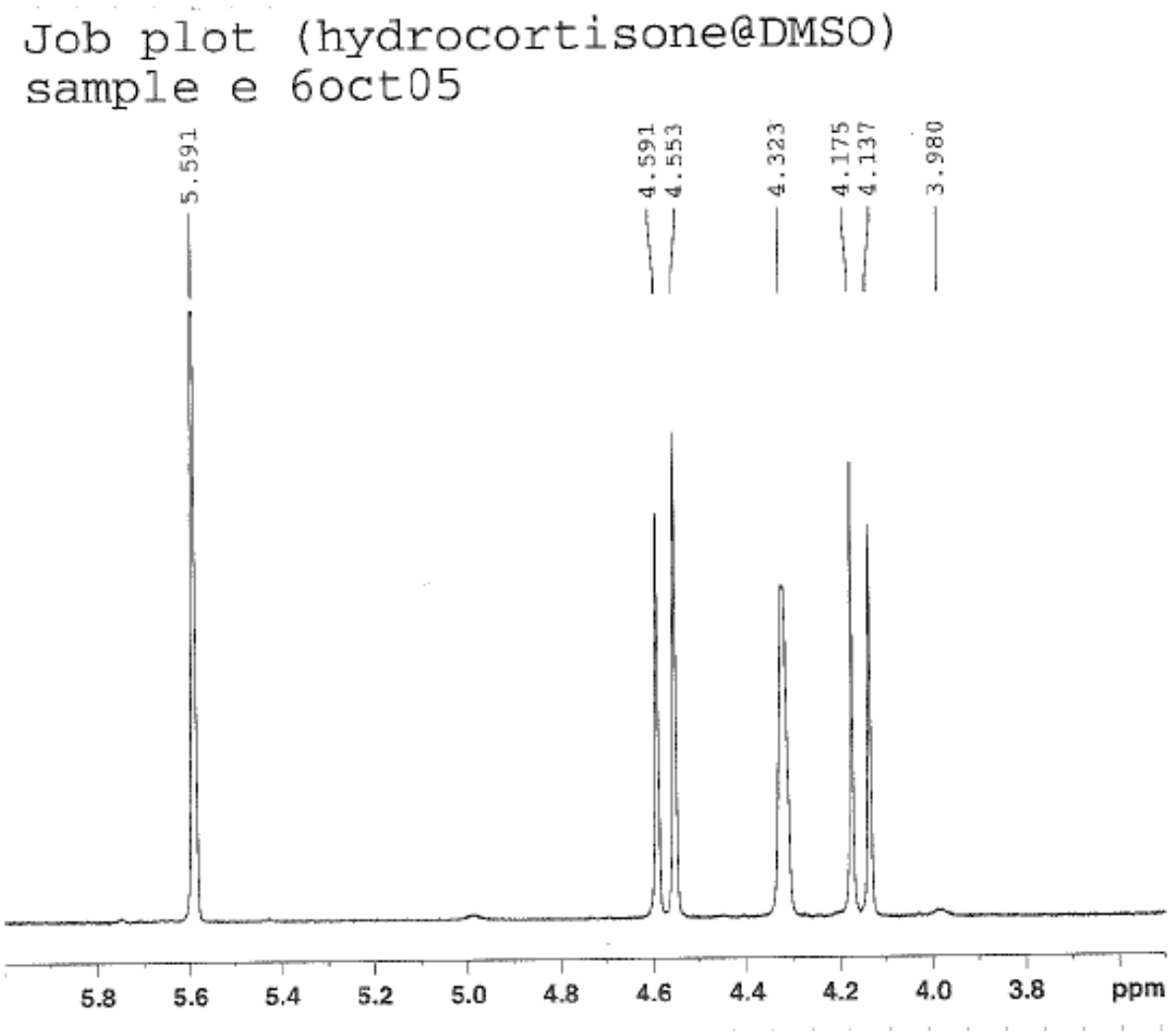

Figure 5 Job plot spectra of sample E

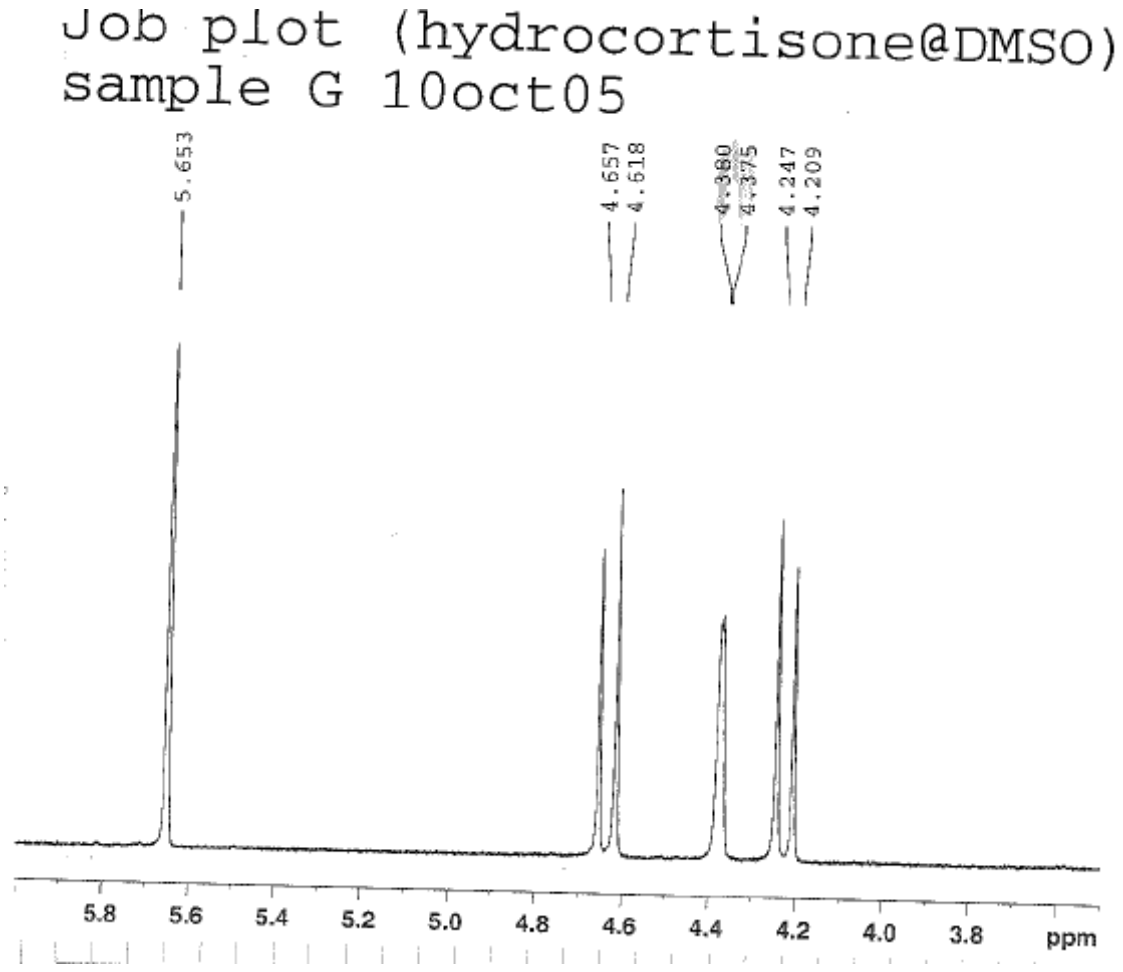

Figure 6. Job plot spectra of sample G

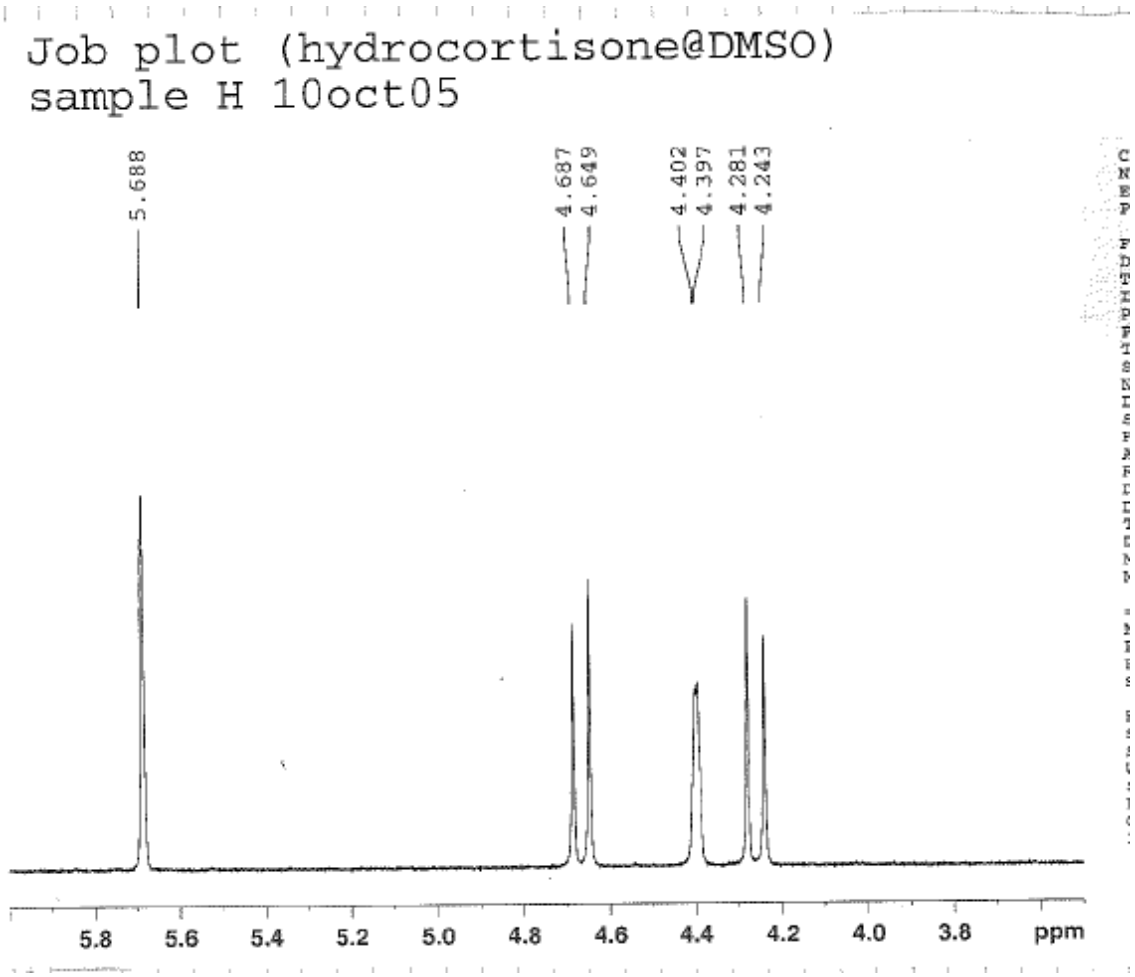

Figure 7. Job plot spectra of sample H

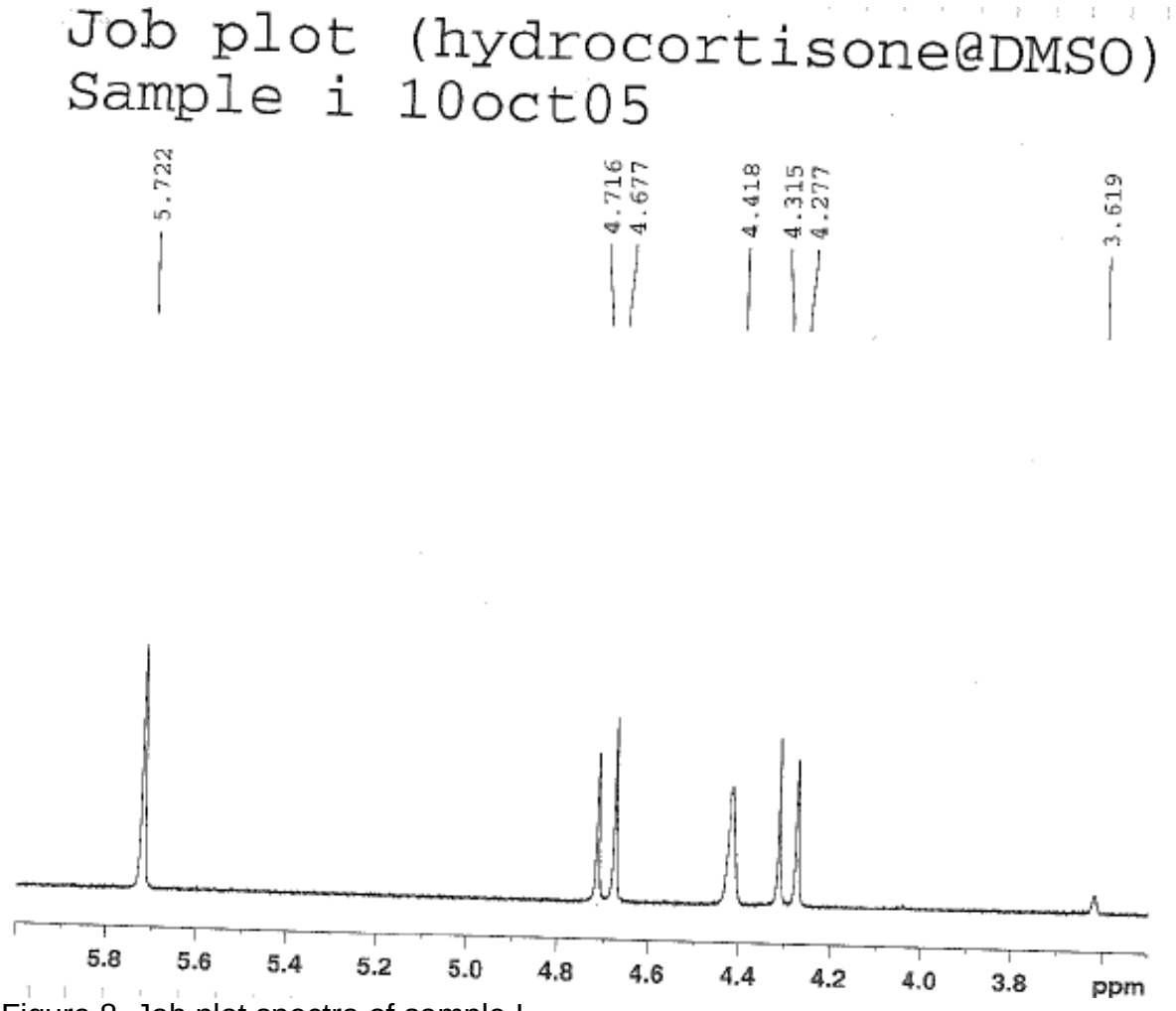

Figure 8. Job plot spectra of sample I

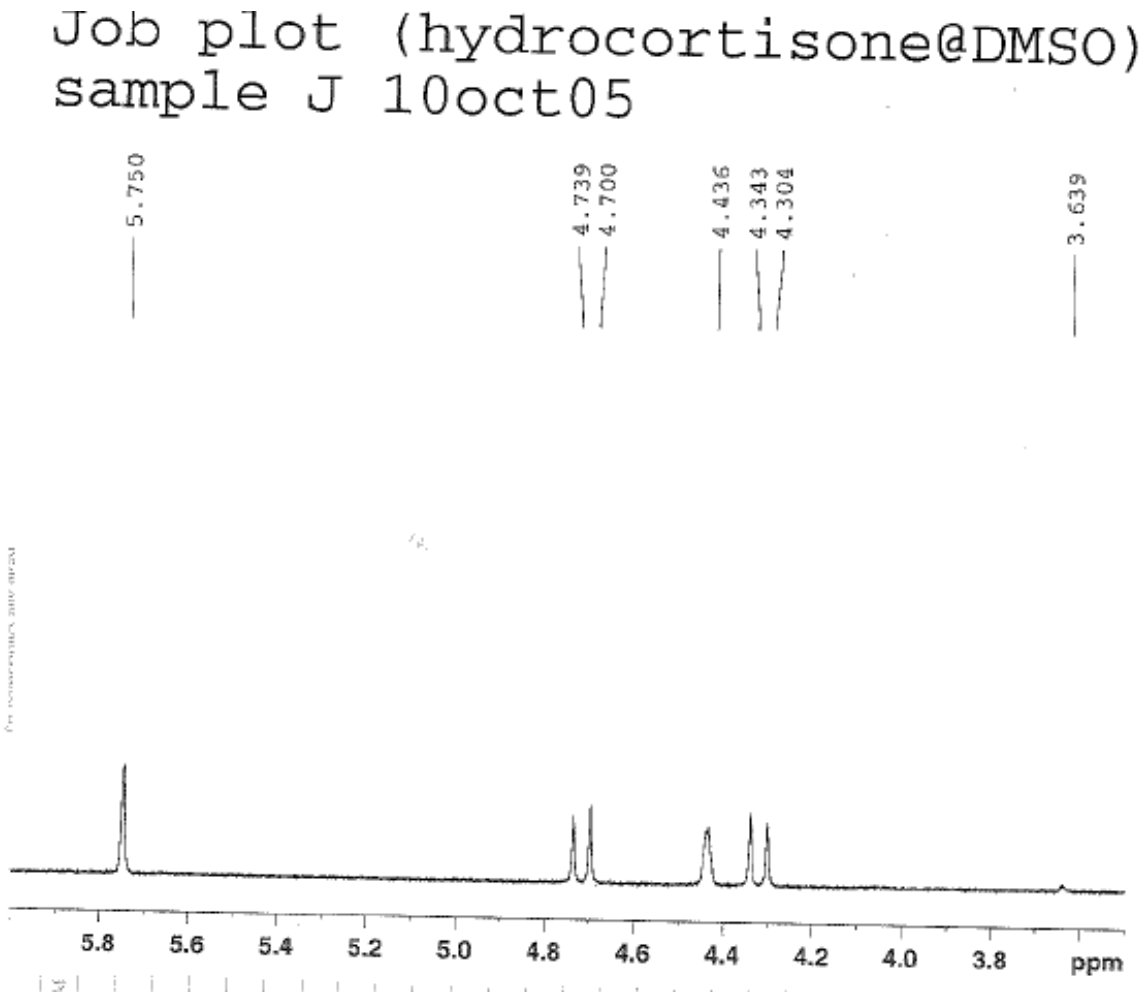

Figure 9. Job plot spectra of sample J

Appendix D – Continuous Variation Study Raw Data

Ft Hyd	C17	ft* C17
0	4.278	0
0.1	4.436	0.0158
0.2	4.418	0.028
0.3	4.402	0.0372
0.4	4.38	0.0408
0.5	4.351	0.0365
0.6	4.323	0.027
0.7	4.303	0.0175
0.8	4.279	0.0008
0.9	4.266	0.0108
1	4.278	0

Appendix E – Conversion of Double Bond and Polymerization Rate Calculation Example

1. Samples were prepared at the corresponding monomer/crosslinker ratio for imprinted and non imprinted synthesis.

2. ATR-FTIR spectra were generated as a function of time. The height of the –CH2 rocking vibration was measure using the ThermoNicolet software

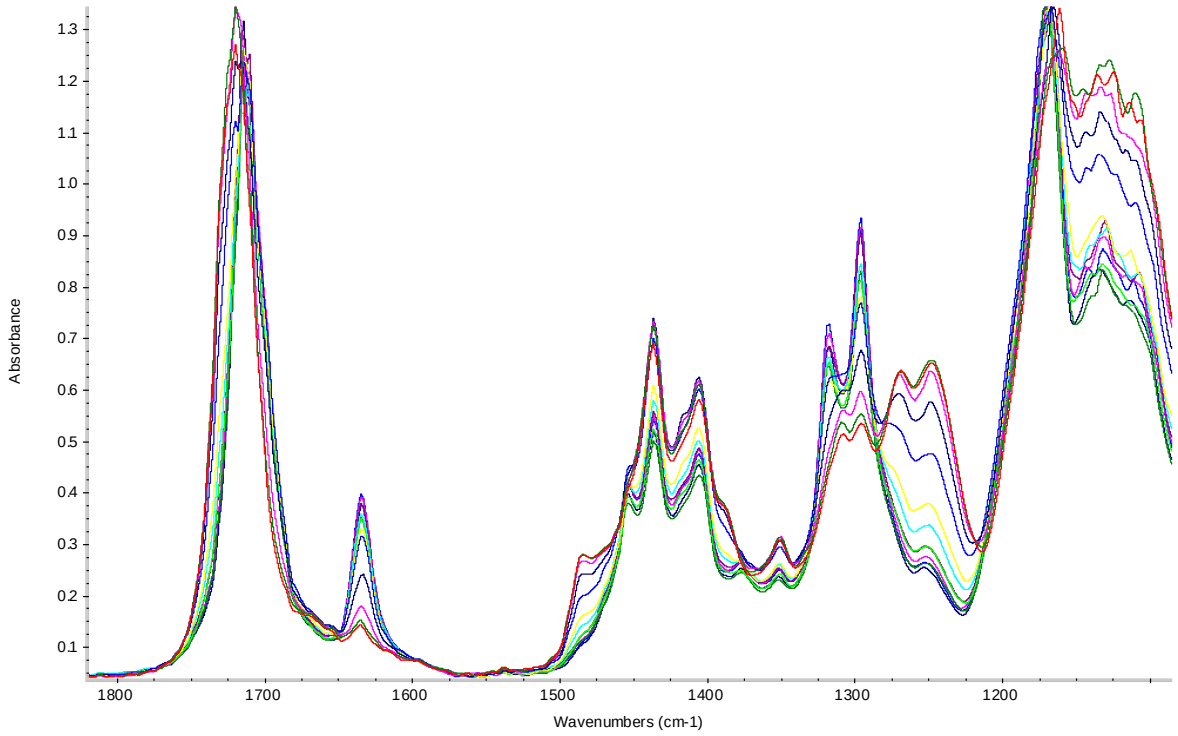

Figure 1. FTIR spectra for 1_1 MIP EtOH_D20

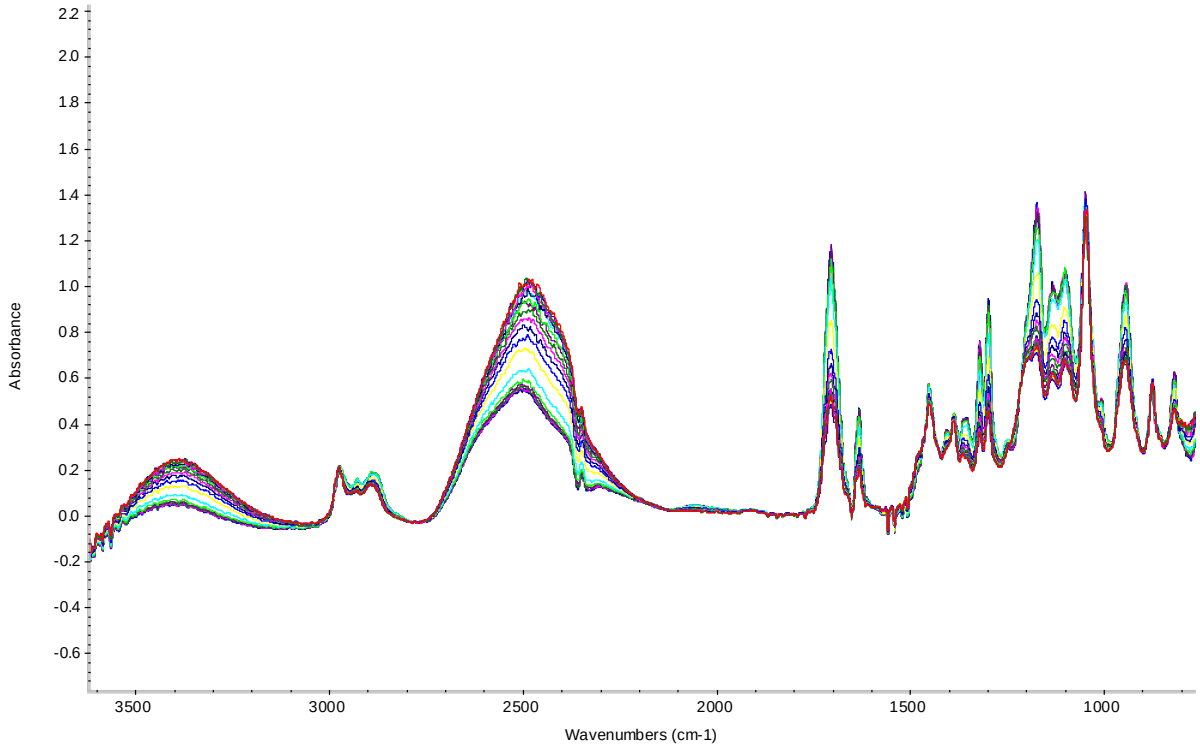

Figure 2. FTIR spectra for 1_1 non MIP EtOH_D20

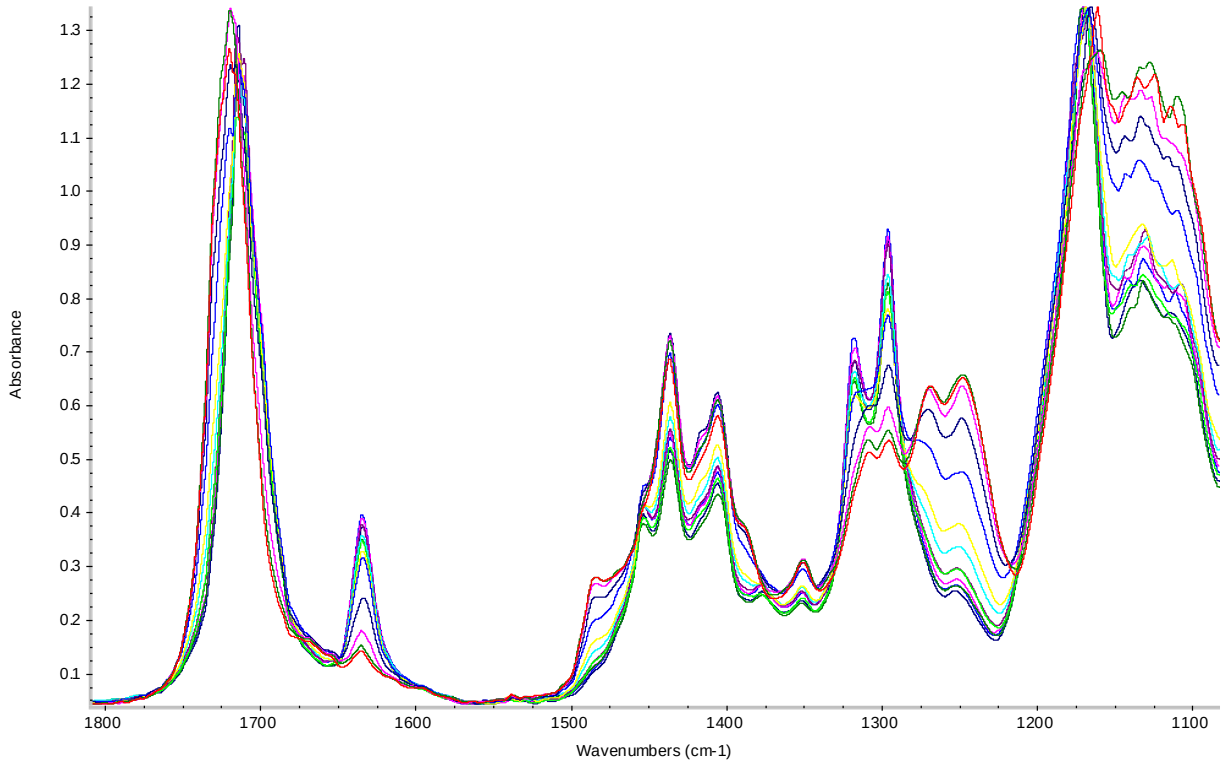

Figure 3. FTIR spectra for 1_1 MIP DMSO

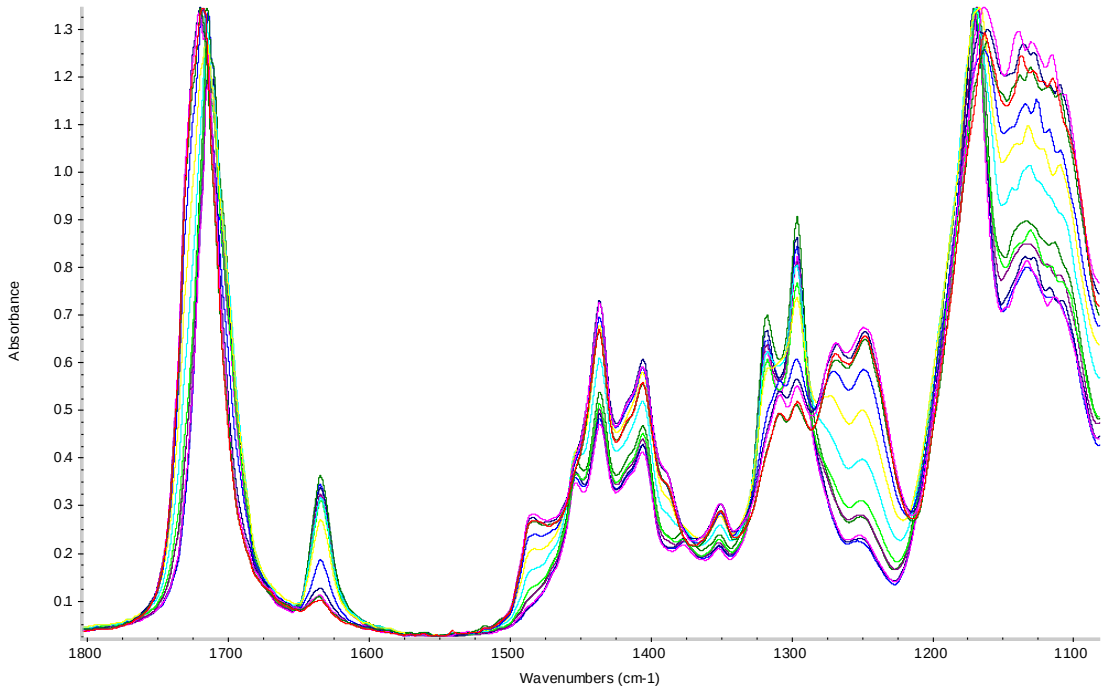

Figure 4. FTIR spectra for 1_1 non MIP DMSO

Appendix F – Conversion of Double Bond and Polymerization Rate Raw Data

Table 1 1 1 MIP@Etoh

	Height -CH2 Rocking				
time (min)	R1	R2	R3	R4	R5
0	0.8324	0.7384	0.7021	0.7112	0.8185
0.5	0.8377	0.7315	0.6988	0.7057	0.8293
1	0.8256	0.7384	0.6919	0.6828	0.8226
1.5	0.8125	0.7299	0.6832	0.6615	0.8064
2	0.8008	0.7257	0.6691	0.6077	0.7948
2.5	0.8000	0.6987	0.6269	0.4950	0.7410
3	0.7510	0.6703	0.5734	0.3693	0.6731
3.5	0.6972	0.6288	0.5221	0.2882	0.6115
4	0.6493	0.5852	0.4924	0.2603	0.6194
4.5	0.6062	0.5496	0.4669	0.3137	0.6308
5	0.5753	0.5275	0.4513	0.2989	0.6423
5.5	0.5515	0.5150	0.4421	0.2858	0.6300
6	0.5323	0.5056	0.4442	0.2707	0.6042
6.5	0.5186	0.4968	0.4342		0.5859
7	0.5107	0.4913	0.4542		0.5593
7.5	0.5005	0.4825	0.5029		0.5461
8	0.4945	0.4843	0.4910		0.5354
8.5	0.4897	0.4746	0.4892		0.5328
9	0.4813	0.4666	0.4640		0.5328
9.5			0.4484		0.5041
10			0.4203		0.4760

Table 2

Conversion of Double bound					
time (min)	R1	R2	R3	R4	R5
0	0	0	0	0	0
0.5	-0.00637	0.009345	0.0047	0.007733	-0.01319
1	0.008169	0	0.014528	0.039933	-0.00501
1.5	0.023907	0.011511	0.026919	0.069882	0.014783
2	0.037963	0.017199	0.047002	0.145529	0.028955
2.5	0.038924	0.053765	0.107107	0.303993	0.094685
3	0.09779	0.092226	0.183307	0.480737	0.177642
3.5	0.162422	0.148429	0.256374	0.594769	0.252902
4	0.219966	0.207476	0.298675	0.633999	0.24325
4.5	0.271744	0.255688	0.334995	0.558915	0.229322
5	0.308866	0.285618	0.357214	0.579724	0.215272
5.5	0.337458	0.302546	0.370318	0.598144	0.230299
6	0.360524	0.315276	0.367327	0.619376	0.26182
6.5	0.376982	0.327194	0.38157	1	0.284178
7	0.386473	0.334642	0.353084	1	0.316677
7.5	0.398727	0.34656	0.28372	1	0.332804
8	0.405935	0.344122	0.300669	1	0.345877
8.5	0.411701	0.357259	0.303233	1	0.349053
9	0.421792	0.368093	0.339125	1	0.349053
9.5			0.361345		0.384117
10			0.401367		0.418448

Table 3

time (min)	Average	SDV
0	0	0
0.5	-0.00273	0.014799
1	0.017462	0.031779
1.5	0.042333	0.038961
2	0.087242	0.08243
2.5	0.199339	0.148003
3	0.329189	0.21432
3.5	0.423836	0.241737
4	0.438624	0.276301
4.5	0.394118	0.233057
5	0.397498	0.257707
5.5	0.414222	0.260105
6	0.440598	0.25283
6.5	0.642089	0.506162
7	0.658338	0.483182
7.5	0.666402	0.471779
8	0.672938	0.462535
8.5	0.674527	0.460289
9	0.674527	0.460289

Table 4

time (min)	R1	Rp instantantaneo R2
0		
0.5	-0.01273	0.018689
1	0.029073	-0.01869
1.5	0.031475	0.023023
2	0.028111	0.011376
2.5	0.001922	0.073131
3	0.117732	0.076923
3.5	0.129265	0.112405
4	0.115089	0.118093
4.5	0.103556	0.096425
5	0.074243	0.059859
5.5	0.057184	0.033857
6	0.046132	0.02546
6.5	0.032917	0.023835
7	0.018981	0.014897
7.5	0.024507	0.023835
8	0.014416	-0.00488
8.5	0.011533	0.026273
9	0.020183	0.021668

Table 5 1 1 non MIP @ EtOH

time (min)	Height -CH2 Rocking		
	R1	R2	R3
0	0.7686	0.6496	0.7559
0.5	0.7686	0.6517	0.7480
1	0.7505	0.6433	0.7489
1.5	0.7483	0.6501	0.7299
2	0.7403	0.6499	0.7184
2.5	0.7102	0.6326	0.6894
3	0.6611	0.5953	0.6278
3.5	0.6188	0.5578	0.5407
4	0.5959	0.5272	0.4868
4.5	0.5933	0.4953	0.4489
5	0.5837	0.5030	0.4220
5.5	0.5786	0.4735	0.4017
6	0.5733	0.4821	0.3820
6.5	0.5715	0.4785	0.3820
7	0.5682	0.4611	0.3823
7.5	0.5661	0.4446	0.3631
8	0.5688	0.4422	0.3536
8.5	0.5670	0.4339	0.3463
9	0.5625	0.4182	0.3637

Table 6

time (min)	Conversion of Double bound		
	R1	R2	R3
0	0	0	0
0.5	0	-0.00323	0.010451
1	0.023549	0.009698	0.00926
1.5	0.026412	-0.00077	0.034396
2	0.03682	-0.00046	0.04961
2.5	0.075982	0.02617	0.087975
3	0.139865	0.08359	0.169467
3.5	0.1949	0.141318	0.284694
4	0.224694	0.188424	0.355999
4.5	0.228077	0.237531	0.406138
5	0.240567	0.225677	0.441725
5.5	0.247203	0.27109	0.468581
6	0.254098	0.257851	0.494642
6.5	0.25644	0.263393	0.494642
7	0.260734	0.290179	0.494245
7.5	0.263466	0.315579	0.519645
8	0.259953	0.319273	0.532213
8.5	0.262295	0.33205	0.541871
9	0.26815	0.356219	0.518852

Table 7

time (min)	R1	Rp instantantaneo R2	R3
0			
0.5	0	-0.00647	0.020902
1	0.047098621	0.025862	-0.00238
1.5	0.005724694	-0.02094	0.050271
2	0.02081707	0.000616	0.030427
2.5	0.078324226	0.053264	0.07673
3	0.127764767	0.11484	0.162985
3.5	0.110070258	0.115456	0.230454
4	0.059588863	0.094212	0.142611
4.5	0.006765548	0.098214	0.100278
5	0.024980484	-0.02371	0.071173
5.5	0.013270882	0.090825	0.053711
6	0.013791309	-0.02648	0.052123
6.5	0.004683841	0.011084	0
7	0.008587041	0.053571	-0.00079
7.5	0.005464481	0.0508	0.0508
8	-0.007025761	0.007389	0.025136
8.5	0.004683841	0.025554	0.019315
9	0.011709602	0.048337	-0.04604

Table 8 1 1 non MIP @ DMSO

time (min)	Height -CH2 Rocking R1	R2
0	0.8700	0.8843
0.5	0.8834	0.8757
1	0.8576	0.8421
1.5	0.8472	0.8475
2	0.8226	0.8049
2.5	0.7669	0.7508
3	0.6813	0.6729
3.5	0.5846	0.5478
4	0.4817	0.4434
4.5	0.4278	0.4132
5	0.4209	0.4039
5.5	0.4189	0.3996
6	0.4136	0.3989

Table 9

	Conversion of Double bound		
time (min)	R1	R2	R3
0	0	0	#DIV/0!
0.5	-0.0154	0.009725	#DIV/0!
1	0.014253	0.047721	#DIV/0!
1.5	0.026207	0.041615	#DIV/0!
2	0.054483	0.089789	#DIV/0!
2.5	0.118506	0.150967	#DIV/0!
3	0.216897	0.239059	#DIV/0!
3.5	0.328046	0.380527	#DIV/0!
4	0.446322	0.498586	#DIV/0!
4.5	0.508276	0.532738	#DIV/0!
5	0.516207	0.543255	#DIV/0!
5.5	0.518506	0.548117	#DIV/0!
6	0.524598	0.548909	

Table 10

		Rp instantantaneo
time (min)	R1	R2
0		
0.5	-0.0308	0.01945
1	0.05931	0.075992
1.5	0.023908	-0.01221
2	0.056552	0.096347
2.5	0.128046	0.122357
3	0.196782	0.176185
3.5	0.222299	0.282936
4	0.236552	0.236119
4.5	0.123908	0.068303
5	0.015862	0.021034
5.5	0.004598	0.009725
6	0.012184	0.001583

Table 11

time (min)	Area -CH2 Rocking R1	R2	R3
0	0.8568	0.8981	
0.5	0.8524	0.8828	
1	0.8195	0.8649	
1.5	0.7891	0.8635	
2	0.7184	0.8277	
2.5	0.6288	0.8297	
3	0.5104	0.7798	
3.5	0.4411	0.6976	
4	0.4227	0.6179	
4.5	0.4232	0.5357	
5	0.4236	0.4827	
5.5	0.3716	0.423	
6	0.3637	0.4596	

Table 12

time (min)	Conversion of Double bound R1	R2
0	0	0
0.5	0.005135	0.017036
1	0.043534	0.036967
1.5	0.079015	0.038526
2	0.161531	0.078388
2.5	0.266106	0.076161
3	0.404295	0.131723
3.5	0.485177	0.223249
4	0.506653	0.311992
4.5	0.506069	0.403519
5	0.505602	0.462532
5.5	0.566293	0.529006
6	0.575514	0.488253

Table 13

time (min)	R1	Rp instantantaneo R2
0		
0.5	0.010271	0.034072
1	0.076797	0.039862
1.5	0.070962	0.003118
2	0.165033	0.079724
2.5	0.20915	-0.00445
3	0.276377	0.111123
3.5	0.161765	0.183053
4	0.042951	0.177486
4.5	-0.00117	0.183053
5	-0.00093	0.118027
5.5	0.121382	0.132947
6	0.018441	0.08151

Appendix G – Permeability Study Calculation Example

1. A correlation between hydrocortisone concentration and absorbance was performed developing a calibration curve (refer to raw data in table 3)

2. The change in the reservoir concentration was measure using UV spectroscopy at 242 nm (refer to raw data in table 4)

3. The concentration of hydrocortisone was estimated by changing the absorbance of the solution to hydrocortisone concentration (refer to raw data in table 5)

4. The accumulative concentration of hydrocortisone was estimated to generate a graph using the following equation

$$\ln\left(1-\frac{2c_t}{c_o}\right)=\frac{2A}{V}Pt \qquad \text{(equation G.1)}$$

Refer to raw data in table 13.

Figure 1 illustrates the behavior of equation G.1.

5. The permeability coefficient was estimated from the slope obtained form figure1. This procedure was repeated for each polymer recipe at the corresponding pH of evaluation.

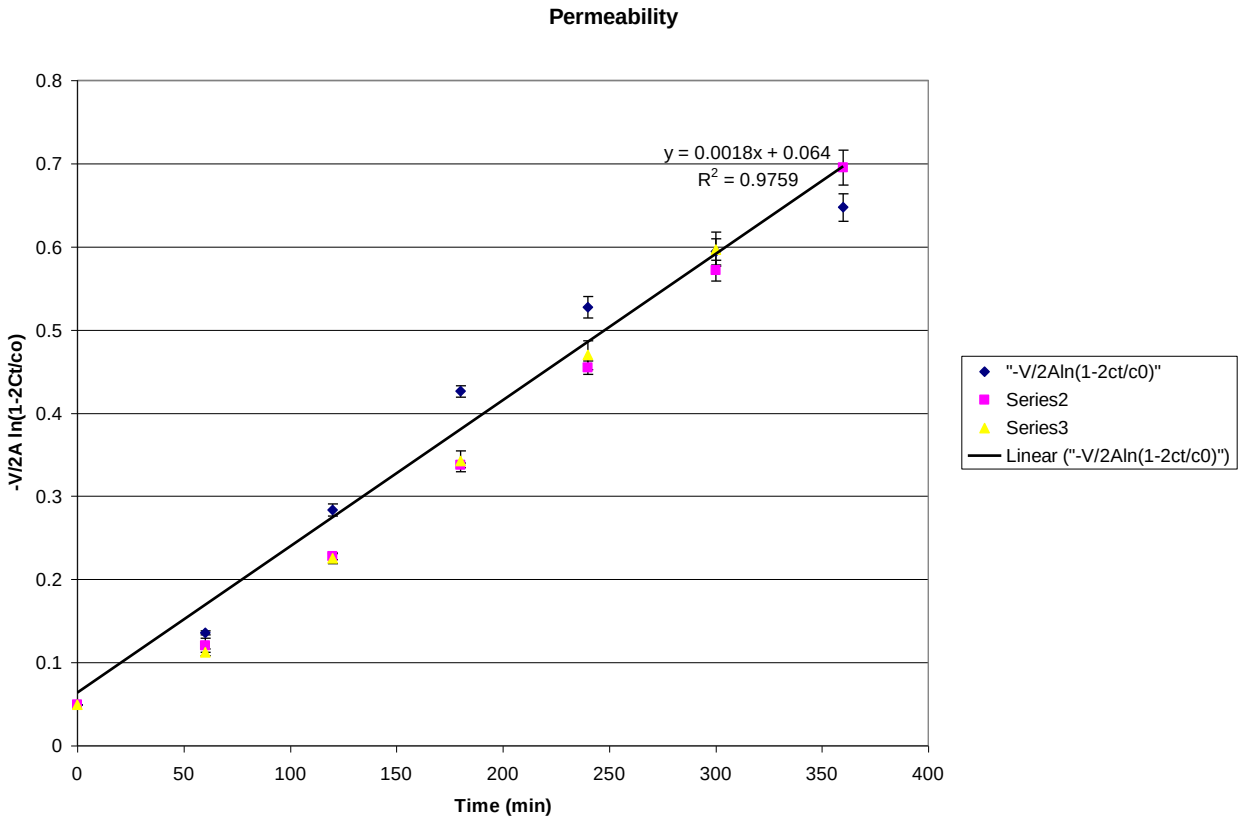

Figure 1. Permeability data as a function of time using equation G.1

Appendix H – Permeability Study Raw Data

Table 1

Hydrogel Type	Impirinting	MAA/EGDMA	pH	Replicate no.	Permeability coefficient [cm/s]	DOE run
nonMIP 17:1	no	17	5.5	1	1.68912E-07	15
nonMIP 17:1	no	17	5.5	2	1.70000E-07	20
nonMIP 17:1	no	17	5.5	3	1.72622E-07	21
MIP 17: 1	yes	17	5.5	1	1.89124E-07	4
MIP 17: 1	yes	17	5.5	2	1.72622E-07	14
MIP 17: 1	yes	17	5.5	3	1.99124E-07	16
nonMIP 39:1	no	39	5.5	1	5.75000E-07	6
nonMIP 39:1	no	39	5.5	2	6.13889E-07	8
nonMIP 39:1	no	39	5.5	3	5.91556E-07	19
MIP 39:1	yes	39	5.5	1	5.19444E-07	5
MIP 39:1	yes	39	5.5	2	5.22222E-07	10
MIP 39:1	yes	39	5.5	3	5.63889E-07	12
nonMIP 17:1	no	17	6.0	1	1.95000E-05	9
nonMIP 17:1	no	17	6.0	2	1.95000E-05	17
nonMIP 17:1	no	17	6.0	3	1.94981E-05	18
MIP 17: 1	yes	17	6.0	1	2.73132E-06	3
MIP 17: 1	yes	17	6.0	2	2.70583E-06	11
MIP 17: 1	yes	17	6.0	3	2.69950E-06	13
nonMIP 39:1	no	39	6.0	1	3.87817E-05	1
nonMIP 39:1	no	39	6.0	2	3.86667E-05	2
nonMIP 39:1	no	39	6.0	3	3.63333E-05	22
MIP 39:1	yes	39	6.0	1	3.68833E-05	7
MIP 39:1	yes	39	6.0	2	3.95000E-05	23
MIP 39:1	yes	39	6.0	3	4.38333E-05	24

Table 2

Hydrogel Type	pH	Average Permeability coefficient [cm/s]	SDEV Permeability coefficient [cm/s]	3*SDEV
nonMIP 17:1	5.5	1.70511E-07	1.90692E-09	5.72076E-09
MIP 17: 1	5.5	1.86957E-07	1.33834E-08	4.01502E-08
nonMIP 39:1	5.5	5.93481E-07	1.95158E-08	5.85475E-08
MIP 39:1	5.5	5.35185E-07	2.48969E-08	7.46907E-08
nonMIP 17:1	6.0	1.94994E-05	1.08157E-09	3.24471E-09
MIP 17: 1	6.0	2.71222E-06	1.68453E-08	5.05358E-08
nonMIP 39:1	6.0	3.79272E-05	1.38155E-06	4.14464E-06
MIP 39:1	6.0	4.00722E-05	3.51016E-06	1.05305E-05

Table 3 Calibration Curve of permeability study (January 4, 2006)

	Absorbancia				
Conc. [mg/mL]	R1	R2	R3	Average	sdev
0.12	3.014	2.696	2.948	2.886	0.167821
0.06	1.672	1.603	1.584	1.619667	0.046307
0.03	0.823	0.788	0.796	0.802333	0.018339
0.015	0.409	0.39	0.392	0.397	0.01044
0.0075	0.198	0.191	0.193	0.194	0.003606
0.00375	0.095	0.091	0.092	0.092667	0.002082
0.001875	0.053	0.043	0.045	0.047	0.005292

Table 4

R1		Absorbancia	
tiempo (hr)	A	B	C
0	0.003	0.004	0.004
1	0.153	0.16	0.159
2	0.227	0.234	0.238
3	0.213	0.213	0.211
4	0.146	0.156	0.158
5	0.107	0.111	0.112
6	0.092	0.093	0.093

Table 5

R1		Concentración	
tiempo (hr)	A	B	C
0	0.003	0.003	0.003
1	0.004846	0.005134	0.005093
2	0.007888	0.008176	0.008341
3	0.007313	0.007313	0.007231
4	0.004559	0.00497	0.005052
5	0.002956	0.00312	0.003161
6	0.002339	0.00238	0.00238

Table 6

R1		Concentración		Average	Sdev
tiempo (hr)	A	B	C		
0	0.003	0.003	0.003	0.003	0
1	0.007846	0.008134	0.008093	0.008025	0.000156
2	0.015735	0.01631	0.016434	0.01616	0.000373
3	0.023048	0.023623	0.023664	0.023445	0.000345
4	0.027606	0.028593	0.028716	0.028305	0.000608
5	0.030562	0.031713	0.031877	0.031384	0.000717
6	0.032901	0.034093	0.034257	0.03375	0.00074

Table 7

R2		Absorbancia	
tiempo (hr)	A	B	C
0	0.003	0.004	0.004
1	0.15	0.129	0.13
2	0.172	0.184	0.186
3	0.168	0.181	0.181
4	0.171	0.183	0.181
5	0.164	0.171	0.172
6	0.159	0.173	0.173

Table 8

R2		Concentración	
tiempo (hr)	A	B	C
0	0.003	0.003	0.003
1	0.004723	0.00386	0.003901
2	0.005627	0.006121	0.006203
3	0.005463	0.005997	0.005997
4	0.005586	0.00608	0.005997
5	0.005299	0.005586	0.005627
6	0.005093	0.005669	0.005669

Table 9

R2		Concentración		Average	Sdev
tiempo (hr)	A	B	C		
0	0.003	0.003	0.003	0.003	0
1	0.007723	0.00686	0.006901	0.007161	0.000487
2	0.013351	0.012981	0.013104	0.013145	0.000188
3	0.018814	0.018978	0.019101	0.018964	0.000144
4	0.0244	0.025058	0.025099	0.024852	0.000392
5	0.029699	0.030644	0.030726	0.030356	0.000571
6	0.034792	0.036313	0.036395	0.035833	0.000903

Table 10

R3		Absorbancia	
tiempo (hr)	A	B	C
0	0.003	0.004	0.004
1	0.118	0.127	0.129
2	0.187	0.191	0.192
3	0.177	0.193	0.186
4	0.184	0.191	0.193
5	0.177	0.178	0.184
6	0.478	0.471	0.477

Table 11

R3		Concentración	
tiempo (hr)	A	B	C
0	0.003	0.003	0.003
1	0.003408	0.003778	0.00386
2	0.006244	0.006409	0.00645
3	0.005833	0.006491	0.006203
4	0.006121	0.006409	0.006491
5	0.005833	0.005874	0.006121
6	0.018206	0.017918	0.018165

Table 12

R3		Concentración		Average	Sdev
tiempo (hr)	A	B	C		
0	0.003	0.003	0.003	0.003	0
1	0.006408	0.006778	0.00686	0.006682	0.000241
2	0.012652	0.013186	0.01331	0.013049	0.00035
3	0.018485	0.019677	0.019513	0.019225	0.000646
4	0.024606	0.026085	0.026003	0.025565	0.000832
5	0.030439	0.03196	0.032124	0.031507	0.000929
6	0.048645	0.049878	0.050289	0.049604	0.000856

Table 13

R1					
time [min]	"-V/2Aln(1-2ct/c0)"				
	A	B	C	average	sdev
0	0.049606	0.049606	0.049606	0.049606	9.31323E-10
60	0.132496	0.13753	0.13681	0.135612	0.002722143
120	0.275393	0.286238	0.288569	0.2834	0.007031499
180	0.417872	0.429537	0.430373	0.425928	0.006988557
240	0.512237	0.533271	0.535916	0.527141	0.012975079
300	0.575938	0.601317	0.604969	0.594075	0.015812471
360	0.627861	0.654862	0.658616	0.647113	0.016778468

Table 14

R2 time [min]	"-V/2Aln(1-2ct/c0)"				
	A	B	C	average	sdev
0	0.0496	0.0496	0.0496	0.049606	9.31323E-10
60	0.1303	0.1153	0.1160	0.120576	0.008466073
120	0.2311	0.2243	0.2266	0.227324	0.003455058
180	0.3341	0.3373	0.3397	0.337045	0.002799257
240	0.4454	0.4589	0.4598	0.454696	0.008065558
300	0.5571	0.5777	0.5795	0.571467	0.012459625
360	0.6709	0.7062	0.7081	0.695034	0.020952485

Table 15

R3 time [min]	"-V/2Aln(1-2ct/c0)"				
	A	B	C	average	sdev
0	0.0496	0.0496	0.0496	0.049606	9.31323E-10
60	0.1075	0.1139	0.1153	0.112257	0.004162433
120	0.2183	0.2281	0.2303	0.225571	0.006399614
180	0.3278	0.3509	0.3477	0.342125	0.012539346
240	0.4496	0.4802	0.4785	0.469464	0.017212452
300	0.5732	0.6068	0.6105	0.596833	0.020514827
360	1.0185	1.0527	1.0642	1.045116	0.023755595

Table 16

time [min]	**"-V/2Aln(1-2ct/c0)"**	
	AVERAGE	STDEV
0	0.04960609	9.31323E-10
60	0.122814782	0.011837397
120	0.245431724	0.032893149
180	0.368365788	0.049914721
240	0.483767121	0.038282075
300	0.58745831	0.013917012
360	0.671073563	0.033885327

Table 17 Calibration Curve of permeability study (January 9, 2006)

	Absorbancia				
Conc. [mg/mL]	R1	R2	R3	Average	sdev
0.12	2.722	2.722	2.662	2.702	0.034641
0.06	1.418	1.393	1.387	1.399333	0.016442
0.03	0.69	0.682	0.683	0.685	0.004359
0.015	0.338	0.334	0.335	0.335667	0.002082
0.0075	0.166	0.162	0.16	0.162667	0.003055
0.00375	0.077	0.08	0.077	0.078	0.001732
0.001875	0.035	0.036	0.036	0.035667	0.000577

Table 18

R1	Absorbancia		
tiempo (hr)	A	B	C
0	0.001	0.003	0.002
1	0.016	0.019	0.018
2	0.223	0.229	0.233
3	0.108	0.114	0.114
4	0.099	0.102	0.105
5	0.103	0.108	0.11
6	0.108	0.113	0.114

Table 19

R1	Concentración		
tiempo (hr)	A	B	C
0	0.003	0.003	0.003
1	0.000688	0.00082	0.000776
2	0.009814	0.010079	0.010255
3	0.004744	0.005009	0.005009
4	0.004347	0.00448	0.004612
5	0.004524	0.004744	0.004832
6	0.004744	0.004965	0.005009

Table 20

R1		Concentración		Average	Sdev
tiempo (hr)	A	B	C		
0	0.003	0.003	0.003	0.003	0
1	0.003688	0.00382	0.003776	0.003761	6.73E-05
2	0.013502	0.013899	0.014031	0.013811	0.000275
3	0.018246	0.018908	0.01904	0.018731	0.000425
4	0.022593	0.023387	0.023652	0.023211	0.000551
5	0.027117	0.028131	0.028484	0.027911	0.00071
6	0.031861	0.033096	0.033492	0.032816	0.000851

Table 21

R2		Absorbancia	
tiempo (hr)	A	B	C
0	0.001	0.003	0.002
1	0.156	0.134	0.136
2	0.18	0.192	0.193
3	0.176	0.189	0.189
4	0.179	0.191	0.189
5	0.172	0.178	0.18
6	0.167	0.18	0.18

Table 22

R2		Concentración	
tiempo (hr)	A	B	C
0	0.003	0.003	0.003
1	0.00686	0.00589	0.005979
2	0.007919	0.008448	0.008492
3	0.007742	0.008315	0.008315
4	0.007874	0.008404	0.008315
5	0.007566	0.00783	0.007919
6	0.007345	0.007919	0.007919

Table 23

R2		Concentración		Average	Sdev
tiempo (hr)	A	B	C		
0	0.003	0.003	0.003	0.003	0
1	0.00986	0.00889	0.008979	0.009243	0.000536
2	0.017779	0.017338	0.01747	0.017529	0.000226
3	0.025521	0.025653	0.025786	0.025653	0.000132
4	0.033395	0.034057	0.034101	0.033851	0.000395
5	0.040961	0.041887	0.042019	0.041623	0.000577
6	0.048307	0.049806	0.049938	0.04935	0.000906

Table 24

R3		Absorbancia	
tiempo (hr)	A	B	C
0	0.001	0.003	0.002
1	0.124	0.132	0.134
2	0.195	0.2	0.2
3	0.184	0.201	0.194
4	0.192	0.2	0.202
5	0.185	0.186	0.193
6	0.493	0.499	0.5

Table 25

R3		Concentración	
tiempo (hr)	A	B	C
0	0.003	0.003	0.003
1	0.005449	0.005802	0.00589
2	0.00858	0.0088	0.0088
3	0.008095	0.008844	0.008536
4	0.008448	0.0088	0.008888
5	0.008139	0.008183	0.008492
6	0.021719	0.021983	0.022027

Table 26

R3		Concentración		Average	Sdev
tiempo (hr)	A	B	C		
0	0.003	0.003	0.003	0.003	0
1	0.008449	0.008802	0.00889	0.008714	0.000233
2	0.017029	0.017603	0.017691	0.017441	0.000359
3	0.025124	0.026447	0.026226	0.025933	0.000709
4	0.033572	0.035247	0.035115	0.034645	0.000931
5	0.041711	0.04343	0.043607	0.042916	0.001047
6	0.063429	0.065413	0.065634	0.064826	0.001214

Table 27

R1 time [min]	"-V/2Aln(1-2ct/c0)"				
	A	B	C	average	sdev
0	0.049606	0.049606	0.049606	0.049606	9.31323E-10
60	0.061158	0.063388	0.062644	0.062397	0.001135129
150	0.233881	0.241195	0.243639	0.239571	0.005077582
210	0.323165	0.335941	0.338506	0.332538	0.008217606
270	0.408715	0.424744	0.430116	0.421192	0.011134068
330	0.501888	0.523397	0.530934	0.51874	0.015072717
390	0.604609	0.632246	0.641213	0.626023	0.019079223

Table 28

R2 time [min]	"-V/2Aln(1-2ct/c0)"				
	A	B	C	average	sdev
0	0.0496	0.0496	0.0496	0.049606	9.31323E-10
60	0.1680	0.1508	0.1524	0.157064	0.00950164
120	0.3142	0.3058	0.3083	0.309407	0.004327866
180	0.4685	0.4713	0.4740	0.471252	0.002746892
240	0.6390	0.6540	0.6550	0.649366	0.008975949
300	0.8181	0.8412	0.8445	0.834627	0.014384449
360	1.0092	1.0506	1.0543	1.038075	0.025038853

Table 29

R3 time [min]	"-V/2Aln(1-2ct/c0)"				
	A	B	C	average	sdev
0	0.0496	0.0496	0.0496	0.049606	9.31323E-10
60	0.1431	0.1493	0.1508	0.147714	0.004105487
120	0.2999	0.3108	0.3125	0.307726	0.006853786
180	0.4603	0.4878	0.4832	0.477096	0.014732026
240	0.6430	0.6814	0.6783	0.667563	0.021316891
300	0.8368	0.8803	0.8848	0.867313	0.026523101
360	1.4734	1.5434	1.5513	1.522704	0.042859227

Table 30 Calibration Curve of permeability study (January 28, 2006)

	Absorbancia				
Conc. [mg/mL]	R1	R2	R3	Average	sdev
0.12	2.528	2.515	2.471	2.504667	0.029872
0.06	1.273	1.26	1.256	1.263	0.008888
0.03	0.617	0.616	0.617	0.616667	0.000577
0.015	0.302	0.3	0.301	0.301	0.001
0.0075	0.148	0.147	0.148	0.147667	0.000577
0.00375	0.071	0.069	0.072	0.070667	0.001528
0.001875	0.032	0.033	0.034	0.033	0.001

Table 31

R1	Absorbancia		
tiempo (hr)	A	B	C
0	0.000	0.001	0.000
1	0.142	0.147	0.147
2	0.177	0.179	0.181
3	0.17	0.169	0.169
4	0.16	0.163	0.164
5	0.155	0.162	0.163
6	0.152	0.16	0.162

Table 32

R1	Concentración		
tiempo (hr)	A	B	C
0	0.003	0.003	0.003
1	0.006363	0.006601	0.006601
2	0.008031	0.008126	0.008222
3	0.007697	0.00765	0.00765
4	0.007221	0.007364	0.007411
5	0.006983	0.007316	0.007364
6	0.00684	0.007221	0.007316

Table 33

R1	Concentración			Average	Sdev
tiempo (hr)	A	B	C		
0	0.003	0.003	0.003	0.003	0
1	0.009363	0.009601	0.009601	0.009522	0.000138
2	0.017394	0.017728	0.017823	0.017648	0.000225
3	0.025091	0.025377	0.025473	0.025314	0.000198
4	0.032312	0.032741	0.032884	0.032646	0.000298
5	0.039295	0.040057	0.040248	0.039867	0.000504
6	0.046134	0.047278	0.047564	0.046992	0.000757

Table 34

R2		Absorbancia	
tiempo (hr)	A	B	C
0	0.000	0.001	0.000
1	0.136	0.142	0.139
2	0.161	0.162	0.166
3	0.152	0.156	0.157
4	0.145	0.153	0.153
5	0.149	0.155	0.156
6	0.134	0.135	0.142

Table 35

R2		Concentración	
tiempo (hr)	A	B	C
0	0.003	0.003	0.003
1	0.006077	0.006363	0.00622
2	0.007268	0.007316	0.007507
3	0.00684	0.00703	0.007078
4	0.006506	0.006887	0.006887
5	0.006697	0.006983	0.00703
6	0.005982	0.006029	0.006363

Table 36

R2		Concentración		Average	Sdev
tiempo (hr)	A	B	C		
0	0.003	0.003	0.003	0.003	0
1	0.009077	0.009363	0.00922	0.00922	0.000143
2	0.016345	0.016679	0.016727	0.016584	0.000208
3	0.023185	0.023709	0.023805	0.023566	0.000334
4	0.029691	0.030596	0.030692	0.030326	0.000552
5	0.036387	0.037579	0.037722	0.037229	0.000733
6	0.042369	0.043608	0.044085	0.043354	0.000886

Table 37

R3		Absorbancia	
tiempo (hr)	A	B	C
0	0.000	0.001	0.000
1	0.116	0.122	0.123
2	0.134	0.141	0.142
3	0.132	0.14	0.14
4	0.132	0.134	0.134
5	0.161	0.17	0.172
6	0.129	0.135	0.137

Table 38

R3		Concentración	
tiempo (hr)	A	B	C
0	0.003	0.003	0.003
1	0.005124	0.00541	0.005457
2	0.005982	0.006315	0.006363
3	0.005886	0.006268	0.006268
4	0.005886	0.005982	0.005982
5	0.007268	0.007697	0.007793
6	0.005743	0.006029	0.006125

Table 39

R3		Concentración		Average	Sdev
tiempo (hr)	A	B	C		
0	0.003	0.003	0.003	0.003	0
1	0.008124	0.00841	0.008457	0.00833	0.00018
2	0.014105	0.014725	0.01482	0.01455	0.000388
3	0.019992	0.020992	0.021088	0.020691	0.000607
4	0.025878	0.026974	0.027069	0.02664	0.000662
5	0.033146	0.034672	0.034862	0.034227	0.00094
6	0.03889	0.040701	0.040987	0.040192	0.001137

Table 40

R1 time [min]	"-V/2Aln(1-2ct/c0)"				
	A	B	C	average	Sdev
0	0.049606	0.049606	0.049606	0.049606	9.31323E-10
60	0.159169	0.163394	0.163394	0.161986	0.002439268
120	0.306822	0.313204	0.315031	0.311686	0.004309662
180	0.459616	0.465529	0.467504	0.464216	0.004104324
240	0.614662	0.62427	0.627484	0.622139	0.006671358
300	0.777245	0.795847	0.800525	0.791206	0.012314586
360	0.950753	0.981333	0.989053	0.973713	0.020255115

Table 41

R2 time [min]	"-V/2Aln(1-2ct/c0)"				
	A	B	C	average	sdev
0	0.0496	0.0496	0.0496	0.049606	9.31323E-10
60	0.1541	0.1592	0.1566	0.15664	0.002528963
120	0.2869	0.2932	0.2941	0.291413	0.003933998
180	0.4206	0.4313	0.4332	0.428388	0.006772655
240	0.5569	0.5767	0.5788	0.570807	0.01204947
300	0.7079	0.7360	0.7394	0.727785	0.017302811
360	0.8533	0.8849	0.8971	0.878445	0.02259126

Table 42

R3 time [min]	"-V/2Aln(1-2ct/c0)"				
	A	B	C	average	sdev
0	0.0496	0.0496	0.0496	0.049606	9.31323E-10
60	0.1373	0.1424	0.1432	0.140967	0.003164712
120	0.2450	0.2565	0.2583	0.253265	0.007205663
180	0.3571	0.3768	0.3787	0.370832	0.011960673
240	0.4759	0.4989	0.5009	0.491892	0.013868851
300	0.6334	0.6681	0.6725	0.657991	0.021418814
360	0.7674	0.8117	0.8188	0.799292	0.027815569

Table 43 Calibration Curve of permeability study (February 8, 2006)

	Absorbancia				
Conc. [mg/mL]	R1	R2	R3	Average	Sdev
0.12	2.408	2.394	2.353	2.385	0.028583
0.06	1.215	1.201	1.198	1.204667	0.009074
0.03	0.589	0.588	0.589	0.588667	0.000577
0.015	0.289	0.286	0.288	0.287667	0.001528
0.0075	0.141	0.141	0.142	0.141333	0.000577
0.00375	0.068	0.066	0.069	0.067667	0.001528
0.001875	0.031	0.031	0.032	0.031333	0.000577

Table 44

R1		Absorbancia	
tiempo (hr)	A	B	C
0	0.000	0.000	0.004
1	0.164	0.167	0.17
2	0.184	0.194	0.2
3	0.186	0.19	0.188
4	0.179	0.185	0.187
5	0.17	0.188	0.176
6	0.171	0.175	0.187

Table 45

R1		Concentración	
tiempo (hr)	A	B	C
0	0.003	0.003	0.003
1	0.007843	0.007993	0.008144
2	0.008844	0.009345	0.009645
3	0.008944	0.009145	0.009044
4	0.008594	0.008894	0.008994
5	0.008144	0.009044	0.008444
6	0.008194	0.008394	0.008994

Table 46

R1		Concentración		Average	Sdev
tiempo (hr)	A	B	C		
0	0.003	0.003	0.003	0.003	0
1	0.010843	0.010993	0.011144	0.010993	0.00015
2	0.019688	0.020338	0.020789	0.020271	0.000554
3	0.028632	0.029483	0.029833	0.029316	0.000618
4	0.037226	0.038377	0.038828	0.038144	0.000826
5	0.045369	0.047422	0.047271	0.046688	0.001144
6	0.053563	0.055815	0.056266	0.055215	0.001448

Table 47

R2		Absorbancia	
tiempo (hr)	A	B	C
0	0.000	0.000	0.004
1	0.131	0.135	0.135
2	0.149	0.153	0.156
3	0.145	0.163	0.157
4	0.145	0.153	0.168
5	0.141	0.147	0.151
6	0.138	0.14	0.142

Table 48

R2		Concentración	
tiempo (hr)	A	B	C
0	0.003	0.003	0.003
1	0.006192	0.006392	0.006392
2	0.007092	0.007293	0.007443
3	0.006892	0.007793	0.007493
4	0.006892	0.007293	0.008043
5	0.006692	0.006992	0.007193
6	0.006542	0.006642	0.006742

Table 49

R2		Concentración		Average	Sdev
tiempo (hr)	A	B	C		
0	0.003	0.003	0.003	0.003	0
1	0.009192	0.009392	0.009392	0.009325	0.000116
2	0.016284	0.016684	0.016835	0.016601	0.000285
3	0.023176	0.024478	0.024327	0.023994	0.000712
4	0.030068	0.03177	0.032371	0.031403	0.001194
5	0.03676	0.038763	0.039563	0.038362	0.001444
6	0.043302	0.045405	0.046305	0.045004	0.001541

Table 50

R3		Absorbancia	
tiempo (hr)	A	B	C
0	0.000	0.000	0.004
1	0.106	0.113	0.148
2	0.131	0.142	0.166
3	0.137	0.137	0.14
4	0.13	0.133	0.132
5	0.123	0.128	0.153
6	0.132	0.134	0.152

Table 51

R3		Concentración	
tiempo (hr)	A	B	C
0	0.003	0.003	0.003
1	0.00494	0.005291	0.007042
2	0.006192	0.006742	0.007943
3	0.006492	0.006492	0.006642
4	0.006141	0.006292	0.006242
5	0.005791	0.006041	0.007293
6	0.006242	0.006342	0.007243

Table 52

R3		Concentración		Average	Sdev
tiempo (hr)	A	B	C		
0	0.003	0.003	0.003	0.003	0
1	0.00794	0.008291	0.010042	0.008758	0.001126
2	0.014132	0.015033	0.017986	0.015717	0.002016
3	0.020624	0.021524	0.024628	0.022259	0.002101
4	0.026765	0.027816	0.030869	0.028483	0.002132
5	0.032556	0.033857	0.038162	0.034858	0.002934
6	0.038798	0.040199	0.045405	0.041467	0.003481

Table 53

R1 time [min]	"-V/2Aln(1-2ct/c0)"				
	A	B	C	average	sdev
0	0.049606	0.049606	0.049606	0.049606	9.31323E-10
60	0.185562	0.188259	0.19096	0.188261	0.002699006
120	0.351116	0.363867	0.372743	0.362575	0.010871219
180	0.534106	0.552439	0.560037	0.548861	0.013330703
240	0.727652	0.755094	0.765937	0.749561	0.019732971
300	0.930572	0.985203	0.981154	0.965643	0.03043994
360	1.158436	1.226014	1.239814	1.208088	0.043550018

Table 54

time [min]	**"-V/2Aln(1-2ct/c0)"**	
	AVERAGE	STDEV
0	0.04960609	9.31323E-10
60	0.165102274	0.020663581
120	0.309871822	0.046377377
180	0.46275808	0.076573379
240	0.625138097	0.112304145
300	0.797920531	0.150893948
360	0.987124568	0.202806104

Table 55 Calibration Curve of permeability study (February 9, 2006)

	Absorbancia				
Conc. [mg/mL]	R1	R2	R3	Average	sdev
0.12	2.551	2.577	2.59	2.572667	0.019858
0.06	1.292	1.309	1.32	1.307	0.014107
0.03	0.631	0.644	0.648	0.641	0.008888
0.015	0.309	0.315	0.321	0.315	0.006
0.0075	0.151	0.151	0.159	0.153667	0.004619
0.00375	0.074	0.073	0.075	0.074	0.001
0.001875	0.035	0.033	0.034	0.034	0.001

Table 56

R1		Absorbancia	
tiempo (hr)	A	B	C
0	0.000	0.000	0.002
1	0.037	0.034	0.033
2	0.086	0.093	0.092
3	0.096	0.099	0.101
4	0.096	0.098	0.098
5	0.091	0.089	0.094
6	0.092	0.095	0.098

Table 57

R1		Concentración	
tiempo (hr)	A	B	C
0	0.003	0.005	0.006
1	0.001485	0.001346	0.001299
2	0.003758	0.004083	0.004037
3	0.004222	0.004362	0.004454
4	0.004222	0.004315	0.004315
5	0.00399	0.003898	0.00413
6	0.004037	0.004176	0.004315

Table 58

R1		Concentración		Average	Sdev
tiempo (hr)	A	B	C		
0	0.003	0.003	0.003	0.003	0
1	0.004485	0.006346	0.007299	0.006043	0.001431
2	0.008243	0.010429	0.011336	0.010003	0.00159
3	0.012465	0.01479	0.01579	0.014349	0.001706
4	0.016688	0.019105	0.020105	0.018633	0.001757
5	0.020678	0.023003	0.024235	0.022639	0.001806
6	0.024715	0.027179	0.02855	0.026815	0.001943

Table 59

R3		Absorbancia	
tiempo (hr)	A	B	C
0	0.000	0.000	0.002
1	0.029	0.033	0.032
2	0.072	0.078	0.077
3	0.121	0.124	0.127
4	0.106	0.109	0.111
5	0.098	0.101	0.101
6	0.079	0.09	0.083

Table 60

R3		Concentración	
tiempo (hr)	A	B	C
0	0.003	0.005	0.006
1	0.001114	0.001299	0.001253
2	0.003109	0.003387	0.003341
3	0.005382	0.005522	0.005661
4	0.004686	0.004826	0.004918
5	0.004315	0.004454	0.004454
6	0.003434	0.003944	0.003619

Table 61

R3		Concentración		Average	Sdev
tiempo (hr)	A	B	C		
0	0.003	0.003	0.003	0.003	0
1	0.004114	0.006299	0.007253	0.005889	0.001609
2	0.007222	0.009686	0.010594	0.009167	0.001744
3	0.012605	0.015208	0.016254	0.014689	0.001879
4	0.017291	0.020033	0.021173	0.019499	0.001995
5	0.021606	0.024488	0.025627	0.023907	0.002072
6	0.02504	0.028432	0.029246	0.027573	0.002231

Table 62

R1					
time [min]	"-V/2Aln(1-2ct/c0)"				
	A	B	C	average	sdev
0	0.049606	0.049606	0.049606	0.049606	9.31323E-10
60	0.07463	0.106449	0.122958	0.101346	0.024564992
120	0.139438	0.178136	0.194426	0.170667	0.02824459
180	0.2149	0.257723	0.276435	0.249686	0.031545375
240	0.293384	0.339779	0.359296	0.33082	0.033856932
300	0.370562	0.416969	0.442015	0.409849	0.036254527
360	0.451859	0.503193	0.532353	0.495801	0.040752602

Table 63

R3 time [min]	"-V/2Aln(1-2ct/c0)" A	B	C	average	sdev
0	0.0496	0.0496	0.0496	0.049606	9.31323E-10
60	0.0683	0.1056	0.1222	0.098715	0.027565993
120	0.1216	0.1649	0.1811	0.155871	0.03074346
180	0.2174	0.2655	0.2852	0.256044	0.034849759
240	0.3049	0.3579	0.3803	0.347694	0.038759457
300	0.3890	0.4472	0.4707	0.435617	0.042085825
360	0.4585	0.5298	0.5473	0.511896	0.047021341

Table 64 Calibration Curve of permeability study (February 27, 2006)

	Absorbancia				
Conc. [mg/mL]	R1	R2	R3	Average	sdev
0.12	2.553	2.521	2.518	2.530667	0.019399
0.06	1.298	1.258	1.298	1.284667	0.023094
0.03	0.634	0.621	0.641	0.632	0.010149
0.015	0.31	0.305	0.315	0.31	0.005
0.0075	0.149	0.147	0.152	0.149333	0.002517
0.00375	0.071	0.069	0.07	0.07	0.001
0.001875	0.031	0.031	0.032	0.031333	0.000577

Table 65

R1	Absorbancia		
tiempo (hr)	A	B	C
0	0.000	0.000	0.002
1	0.09	0.097	0.098
2	0.108	0.111	0.113
3	0.11	0.115	0.116
4	0.108	0.113	0.115
5	0.102	0.108	0.108
6	0.105	0.106	0.107

Table 66

R1		Concentración	
tiempo (hr)	A	B	C
0	0.003	0.005	0.006
1	0.003945	0.004275	0.004322
2	0.004794	0.004935	0.005029
3	0.004888	0.005124	0.005171
4	0.004794	0.005029	0.005124
5	0.004511	0.004794	0.004794
6	0.004652	0.0047	0.004747

Table 67

R1		Concentración		Average	Sdev
tiempo (hr)	A	B	C		
0	0.003	0.003	0.003	0.003	0
1	0.006945	0.009275	0.010322	0.008848	0.001729
2	0.011739	0.01421	0.015352	0.013767	0.001847
3	0.016627	0.019334	0.020523	0.018828	0.001997
4	0.021421	0.024364	0.025646	0.02381	0.002166
5	0.025932	0.029157	0.03044	0.02851	0.002323
6	0.030584	0.033857	0.035187	0.033209	0.002369

Table 68

R1					
time [min]	"-V/2Aln(1-2ct/c0)"				
	A	B	C	average	sdev
0	0.049606	0.049606	0.049606	0.049606	9.31323E-10
60	0.116816	0.157618	0.176236	0.150223	0.030392312
120	0.201709	0.246955	0.26821	0.238958	0.033964021
180	0.292234	0.344227	0.367498	0.334653	0.038534862
240	0.38527	0.444649	0.471109	0.433676	0.043959136
300	0.477045	0.545408	0.573274	0.531909	0.049514518
360	0.576427	0.649485	0.679971	0.635294	0.053210889

Appendix I – Swelling and Correlation Length Studies Calculation Example

1. The weight in are and in heptane was measured using the density kit.
2. The following equations were employed to calculate the equilibrium swelling

$$V = \frac{W_a - W_h}{\rho_h}$$

$$Q = \frac{V_s}{V_d}$$

$$\upsilon_{2,r} = \frac{V_d}{V_r}$$

$$\upsilon_{2,s} = \frac{V_d}{V_s}$$

$$n = \frac{2M_C}{M_r}$$

$$\bar{M}_n = M_0 \frac{k_p [M]}{(f k_d k_t [\,]}^{1/2}$$

$$\xi = \upsilon_{2,S}^{-\frac{1}{3}} * l * \sqrt{n} * \sqrt{C_N}$$

$$\frac{1}{\bar{M}_C} = \frac{2}{\bar{M}_n} - \frac{(\rho/V_1)[\ln(1-\upsilon_{2,s}) + \upsilon_{2,s} + \chi_1 \upsilon_{2,s}^{\,2}]}{\upsilon_{2,r}\left[\left(\frac{\upsilon_{2,s}}{\upsilon_{2,r}}\right)^{\frac{1}{3}} - \frac{1}{2}\left(\frac{\upsilon_{2,s}}{\upsilon_{2,r}}\right)\right]}$$

Refer to raw data for details

Appendix J – Swelling and Correlation Length Studies Raw Data

Table 1.

Vg,r (relaxed volume)	Wair (g)	Wliq (g)	aux density (g/cm3)	Volume (cm3)
39:1 nonMIP P1-A1	0.0508	0.0230	0.6840	0.0406
39:1 nonMIP P1-A3	0.0499	0.0226	0.6840	0.0399
39:1 nonMIP P1-A6	0.0490	0.0226	0.6840	0.0386
39:1 MIP P1-A3	0.0484	0.0220	0.6840	0.0386
39:1 MIP P1-A1	0.0499	0.0227	0.6840	0.0398
39:1 MIP P1-A2	0.0557	0.0251	0.6840	0.0447
17:1 nonMIP P1-A1	0.0459	0.0210	0.6840	0.0364
17:1 nonMIP P1-A2	0.0511	0.0230	0.6840	0.0411
17:1 nonMIP P1-A3	0.0468	0.0213	0.6840	0.0373
17:1 MIP P1-A1	0.0427	0.0194	0.6840	0.0341
17:1 MIP P1-A2	0.0463	0.0213	0.6840	0.0365
17:1 MIP P1-A3	0.0444	0.0206	0.6840	0.0348
4:1 nonMIP P1-A5	0.0608	0.0251	0.6840	0.0522
4:1 nonMIP P1-A3	0.0602	0.0249	0.6840	0.0516
4:1 nonMIP P1-A4	0.0575	0.0239	0.6840	0.0491
4:1 MIP P1-A3	0.0608	0.0250	0.6840	0.0523
4:1 MIP P1-A1	0.0606	0.0246	0.6840	0.0526
4:1 MIP P1-A2	0.0656	0.0265	0.6840	0.0572

Table 2

Vd (Dry volume)	Wair (g)	Wliq (g)	aux density (g/cm3)	Volume (cm3)
39:1 nonMIP P1-A1	0.0444	0.0226	0.6840	0.0319
39:1 nonMIP P1-A3	0.0439	0.0222	0.6840	0.0317
39:1 nonMIP P1-A6	0.0426	0.0212	0.6840	0.0313
39:1 MIP P1-A3	0.0385	0.0188	0.6840	0.0288
39:1 MIP P1-A1	0.0387	0.0188	0.6840	0.0291
39:1 MIP P1-A2	0.0423	0.0207	0.6840	0.0316
17:1 nonMIP P1-A1	0.0395	0.0203	0.6840	0.0281
17:1 nonMIP P1-A2	0.0436	0.0220	0.6840	0.0316
17:1 nonMIP P1-A3	0.0412	0.0210	0.6840	0.0295
17:1 MIP P1-A1	0.0388	0.0196	0.6840	0.0281
17:1 MIP P1-A2	0.0415	0.0207	0.6840	0.0304
17:1 MIP P1-A3	0.0399	0.0199	0.6840	0.0292
4:1 nonMIP P1-A5	0.0422	0.0196	0.6840	0.0330
4:1 nonMIP P1-A3	0.0404	0.0192	0.6840	0.0310
4:1 nonMIP P1-A4	0.0395	0.0184	0.6840	0.0308
4:1 MIP P1-A3	0.0410	0.0188	0.6840	0.0325
4:1 MIP P1-A1	0.0399	0.0184	0.6840	0.0314
4:1 MIP P1-A2	0.0425	0.0198	0.6840	0.0332

Table 3

Vs (equillibrium swelling volume) pH=3.2	Wair (g)	Wliq (g)	aux density (g/cm3)	Volume (cm3)
39:1 nonMIP P1-A1	0.0688	0.0296	0.6840	0.0573
39:1 nonMIP P1-A3	0.0690	0.0296	0.6840	0.0576
39:1 nonMIP P1-A6	0.0702	0.0330	0.6840	0.0544
39:1 MIP P1-A3	0.0657	0.0284	0.6840	0.0545
39:1 MIP P1-A1	0.0651	0.0280	0.6840	0.0542
39:1 MIP P1-A2	0.0718	0.0309	0.6840	0.0598
17:1 nonMIP P1-A1	0.0521	0.0233	0.6840	0.0421
17:1 nonMIP P1-A2	0.0582	0.0263	0.6840	0.0466
17:1 nonMIP P1-A3	0.0546	0.0243	0.6840	0.0443
17:1 MIP P1-A1	0.0507	0.0224	0.6840	0.0414
17:1 MIP P1-A2	0.0548	0.0245	0.6840	0.0443
17:1 MIP P1-A3	0.0530	0.0239	0.6840	0.0425
4:1 nonMIP P1-A5	0.0504	0.0229	0.6840	0.0402
4:1 nonMIP P1-A3	0.0488	0.0219	0.6840	0.0393
4:1 nonMIP P1-A4	0.0479	0.0214	0.6840	0.0387
4:1 MIP P1-A3	0.0491	0.0222	0.6840	0.0393
4:1 MIP P1-A1	0.0469	0.0211	0.6840	0.0377
4:1 MIP P1-A2	0.0509	0.0227	0.6840	0.0412

Table 4

Vs (equillibrium swelling volume) pH=4.0	Wair (g)	Wliq (g)	aux density (g/cm3)	Volume (cm3)
39:1 nonMIP P1-A1	0.1049	0.0407	0.6840	0.0939
39:1 nonMIP P1-A3	0.1033	0.0399	0.6840	0.0927
39:1 nonMIP P1-A6	0.1045	0.0406	0.6840	0.0934
39:1 MIP P1-A3	0.0971	0.0378	0.6840	0.0867
39:1 MIP P1-A1	0.0979	0.0379	0.6840	0.0877
39:1 MIP P1-A2	0.1090	0.0425	0.6840	0.0972
17:1 nonMIP P1-A1	0.0616	0.0268	0.6840	0.0509
17:1 nonMIP P1-A2	0.0676	0.0287	0.6840	0.0569
17:1 nonMIP P1-A3	0.0640	0.0275	0.6840	0.0534
17:1 MIP P1-A1	0.0593	0.0250	0.6840	0.0501
17:1 MIP P1-A2	0.0615	0.0263	0.6840	0.0515
17:1 MIP P1-A3	0.0621	0.0263	0.6840	0.0523
4:1 nonMIP P1-A5	0.0527	0.0236	0.6840	0.0425
4:1 nonMIP P1-A3	0.0513	0.0231	0.6840	0.0412
4:1 nonMIP P1-A4	0.0504	0.0220	0.6840	0.0415
4:1 MIP P1-A3	0.0511	0.0228	0.6840	0.0414
4:1 MIP P1-A1	0.0491	0.0219	0.6840	0.0398
4:1 MIP P1-A2	0.0531	0.0238	0.6840	0.0428

Table 5

Vs (equillibrium swelling volume) pH=4.8	Wair (g)	Wliq (g)	aux density (g/cm3)	Volume (cm3)
39:1 nonMIP P1-A1	0.1203	0.0482	0.6840	0.1054
39:1 nonMIP P1-A3	0.1210	0.0485	0.6840	0.1060
39:1 nonMIP P1-A6	0.1217	0.0484	0.6840	0.1072
39:1 MIP P1-A3	0.1145	0.0456	0.6840	0.1007
39:1 MIP P1-A1	0.1137	0.0454	0.6840	0.0999
39:1 MIP P1-A2	0.1257	0.0500	0.6840	0.1107
17:1 nonMIP P1-A1	0.0796	0.0334	0.6840	0.0675
17:1 nonMIP P1-A2	0.0874	0.0366	0.6840	0.0743
17:1 nonMIP P1-A3	0.0826	0.0345	0.6840	0.0703
17:1 MIP P1-A1	0.0760	0.0314	0.6840	0.0652
17:1 MIP P1-A2	0.0832	0.0348	0.6840	0.0708
17:1 MIP P1-A3	0.0810	0.0339	0.6840	0.0689
4:1 nonMIP P1-A5	0.0549	0.0243	0.6840	0.0447
4:1 nonMIP P1-A3	0.0540	0.0239	0.6840	0.0440
4:1 nonMIP P1-A4	0.0523	0.0224	0.6840	0.0437
4:1 MIP P1-A3	0.0532	0.0236	0.6840	0.0433
4:1 MIP P1-A1	0.0506	0.0225	0.6840	0.0411
4:1 MIP P1-A2	0.0543	0.0241	0.6840	0.0442

Table 6

Vs (equillibrium swelling volume) pH=5.4	Wair (g)	Wliq (g)	aux density (g/cm3)	Volume (cm3)
39:1 nonMIP P1-A1	0.2309	0.0869	0.6840	0.2105
39:1 nonMIP P1-A3	0.2309	0.0869	0.6840	0.2105
39:1 nonMIP P1-A6	0.2170	0.0818	0.6840	0.1977
39:1 MIP P1-A3	0.2206	0.0837	0.6840	0.2001
39:1 MIP P1-A1	0.2246	0.0840	0.6840	0.2056
39:1 MIP P1-A2	0.2479	0.0932	0.6840	0.2262
17:1 nonMIP P1-A1	0.1321	0.0523	0.6840	0.1167
17:1 nonMIP P1-A2	0.1459	0.0582	0.6840	0.1282
17:1 nonMIP P1-A3	0.1388	0.0554	0.6840	0.1219
17:1 MIP P1-A1	0.1298	0.0515	0.6840	0.1145
17:1 MIP P1-A2	0.1396	0.0559	0.6840	0.1224
17:1 MIP P1-A3	0.1298	0.0515	0.6840	0.1145
4:1 nonMIP P1-A5	0.0842	0.0346	0.6840	0.0725
4:1 nonMIP P1-A3	0.0818	0.0340	0.6840	0.0699
4:1 nonMIP P1-A4	0.0803	0.0334	0.6840	0.0686
4:1 MIP P1-A3	0.0828	0.0346	0.6840	0.0705
4:1 MIP P1-A1	0.0796	0.0333	0.6840	0.0677
4:1 MIP P1-A2	0.0848	0.0356	0.6840	0.0719

Table 7

Vs (equillibrium swelling volume) pH=5.8	Wair (g)	Wliq (g)	aux density (g/cm3)	Volume (cm3)
39:1 nonMIP P1-A1	0.2757	0.1036	0.6840	0.2516
39:1 nonMIP P1-A3	0.2577	0.0965	0.6840	0.2357
39:1 nonMIP P1-A6	0.2577	0.0965	0.6840	0.2357
39:1 MIP P1-A3	0.2627	0.0986	0.6840	0.2399
39:1 MIP P1-A1	0.2625	0.0985	0.6840	0.2398
39:1 MIP P1-A2	0.2937	0.1101	0.6840	0.2684
17:1 nonMIP P1-A1	0.1625	0.0636	0.6840	0.1446
17:1 nonMIP P1-A2	0.1800	0.0710	0.6840	0.1594
17:1 nonMIP P1-A3	0.1682	0.0655	0.6840	0.1501
17:1 MIP P1-A1	0.1586	0.0627	0.6840	0.1402
17:1 MIP P1-A2	0.1739	0.0681	0.6840	0.1547
17:1 MIP P1-A3	0.1586	0.0627	0.6840	0.1402
4:1 nonMIP P1-A5	0.1075	0.0441	0.6840	0.0927
4:1 nonMIP P1-A3	0.1037	0.0427	0.6840	0.0892
4:1 nonMIP P1-A4	0.1018	0.0416	0.6840	0.0880
4:1 MIP P1-A3	0.1052	0.0428	0.6840	0.0912
4:1 MIP P1-A1	0.1013	0.0416	0.6840	0.0873
4:1 MIP P1-A2	0.1100	0.0450	0.6840	0.0950

Table 8

Vs (equillibrium swelling volume) pH=6.0	Wair (g)	Wliq (g)	aux density (g/cm3)	Volume (cm3)
39:1 nonMIP P1-A1	0.2864	0.1077	0.6840	0.2613
39:1 nonMIP P1-A3	0.2864	0.1077	0.6840	0.2613
39:1 nonMIP P1-A6	0.2864	0.1077	0.6840	0.2613
39:1 MIP P1-A3	0.2715	0.1021	0.6840	0.2477
39:1 MIP P1-A1	0.2736	0.1025	0.6840	0.2501
39:1 MIP P1-A2	0.3068	0.1145	0.6840	0.2811
17:1 nonMIP P1-A1	0.1710	0.0672	0.6840	0.1518
17:1 nonMIP P1-A2	0.1916	0.0753	0.6840	0.1700
17:1 nonMIP P1-A3	0.1786	0.0704	0.6840	0.1582
17:1 MIP P1-A1	0.1682	0.0664	0.6840	0.1488
17:1 MIP P1-A2	0.1848	0.0722	0.6840	0.1646
17:1 MIP P1-A3	0.1848	0.0722	0.6840	0.1646
4:1 nonMIP P1-A5	0.1174	0.0481	0.6840	0.1013
4:1 nonMIP P1-A3	0.1141	0.0464	0.6840	0.0990
4:1 nonMIP P1-A4	0.1111	0.0444	0.6840	0.0975
4:1 MIP P1-A3	0.1162	0.0473	0.6840	0.1007
4:1 MIP P1-A1	0.1103	0.0448	0.6840	0.0958
4:1 MIP P1-A2	0.1203	0.0491	0.6840	0.1041

Table 9

Vs (equillibrium swelling volume) pH=7.0	Wair (g)	Wliq (g)	aux density (g/cm3)	Volume (cm3)
39:1 nonMIP P1-A1	0.2611	0.0990	0.6840	0.2370
39:1 nonMIP P1-A3	0.2611	0.0990	0.6840	0.2370
39:1 nonMIP P1-A6	0.2611	0.0990	0.6840	0.2370
39:1 MIP P1-A3	0.2756	0.1047	0.6840	0.2499
39:1 MIP P1-A1	0.2743	0.1045	0.6840	0.2482
39:1 MIP P1-A2	0.3076	0.1168	0.6840	0.2789
17:1 nonMIP P1-A1	0.1792	0.0719	0.6840	0.1569
17:1 nonMIP P1-A2	0.2001	0.0800	0.6840	0.1756
17:1 nonMIP P1-A3	0.1894	0.0759	0.6840	0.1659
17:1 MIP P1-A1	0.1774	0.0707	0.6840	0.1560
17:1 MIP P1-A2	0.1950	0.0773	0.6840	0.1721
17:1 MIP P1-A3	0.1774	0.0707	0.6840	0.1560
4:1 nonMIP P1-A5	0.1353	0.0558	0.6840	0.1162
4:1 nonMIP P1-A3	0.1323	0.0540	0.6840	0.1145
4:1 nonMIP P1-A4	0.1293	0.0525	0.6840	0.1123
4:1 MIP P1-A3	0.1343	0.0547	0.6840	0.1164
4:1 MIP P1-A1	0.1287	0.0526	0.6840	0.1113
4:1 MIP P1-A2	0.1395	0.0570	0.6840	0.1206

Table 10

	v2,r	v2,s						
		pH=3.2	pH=4.0	pH=4.8	pH=5.4	pH=5.8	pH=6.0	pH=7.0
39:1 nonMIP P1-A1	0.7842	0.5561	0.3396	0.3024	0.1514	0.1267	0.1220	0.1345
39:1 nonMIP P1-A3	0.7949	0.5508	0.3423	0.2993	0.1507	0.1346	0.1214	0.1339
39:1 nonMIP P1-A6	0.8106	0.5753	0.3349	0.2920	0.1583	0.1328	0.1198	0.1320
39:1 MIP P1-A3	0.7462	0.5282	0.3322	0.2859	0.1439	0.1200	0.1163	0.1153
39:1 MIP P1-A1	0.7316	0.5364	0.3317	0.2914	0.1415	0.1213	0.1163	0.1172
39:1 MIP P1-A2	0.7059	0.5281	0.3248	0.2853	0.1396	0.1176	0.1123	0.1132
17:1 nonMIP P1-A1	0.7711	0.6667	0.5517	0.4156	0.2406	0.1941	0.1850	0.1789
17:1 nonMIP P1-A2	0.7687	0.6771	0.5553	0.4252	0.2463	0.1982	0.1857	0.1799
17:1 nonMIP P1-A3	0.7922	0.6667	0.5534	0.4200	0.2422	0.1967	0.1867	0.1780
17:1 MIP P1-A1	0.8240	0.6784	0.5598	0.4305	0.2452	0.2002	0.1886	0.1799
17:1 MIP P1-A2	0.8320	0.6865	0.5909	0.4298	0.2485	0.1966	0.1847	0.1767
17:1 MIP P1-A3	0.8403	0.6873	0.5587	0.4246	0.2554	0.2086	0.1776	0.1874
4:1 nonMIP P1-A5	0.6331	0.8218	0.7766	0.7386	0.4556	0.3565	0.3261	0.2843
4:1 nonMIP P1-A3	0.6006	0.7881	0.7518	0.7043	0.4435	0.3475	0.3131	0.2708
4:1 nonMIP P1-A4	0.6280	0.7962	0.7430	0.7057	0.4499	0.3505	0.3163	0.2747
4:1 MIP P1-A3	0.6201	0.8253	0.7845	0.7500	0.4606	0.3558	0.3222	0.2789
4:1 MIP P1-A1	0.5972	0.8333	0.7904	0.7651	0.4644	0.3601	0.3282	0.2825
4:1 MIP P1-A2	0.5806	0.8050	0.7747	0.7517	0.4614	0.3492	0.3188	0.2752

Table 11

Equillibrium volume swelling ratio Q							
	pH=3.2	pH=4.0	pH=4.8	pH=5.4	pH=5.8	pH=6.0	pH=7.0
39:1 nonMIP P1-A1	1.7982	2.9450	3.3073	6.6055	7.8945	8.1972	7.4358
39:1 nonMIP P1-A3	1.8157	2.9217	3.3410	6.6359	7.4286	8.2350	7.4700
39:1 nonMIP P1-A6	1.7383	2.9860	3.4252	6.3178	7.5327	8.3505	7.5748
39:1 MIP P1-A3	1.8934	3.0102	3.4975	6.9492	8.3299	8.5990	8.6751
39:1 MIP P1-A1	1.8643	3.0151	3.4322	7.0653	8.2412	8.5980	8.5327
39:1 MIP P1-A2	1.8935	3.0787	3.5046	7.1620	8.5000	8.9028	8.8333
17:1 nonMIP P1-A1	1.5000	1.8125	2.4063	4.1563	5.1510	5.4063	5.5885
17:1 nonMIP P1-A2	1.4769	1.8009	2.3519	4.0602	5.0463	5.3843	5.5602
17:1 nonMIP P1-A3	1.5000	1.8069	2.3812	4.1287	5.0842	5.3564	5.6188
17:1 MIP P1-A1	1.4740	1.7865	2.3229	4.0781	4.9948	5.3021	5.5573
17:1 MIP P1-A2	1.4567	1.6923	2.3269	4.0240	5.0865	5.4135	5.6587
17:1 MIP P1-A3	1.4550	1.7900	2.3550	3.9150	4.7950	5.6300	5.3350
4:1 nonMIP P1-A5	1.2168	1.2876	1.3540	2.1947	2.8053	3.0664	3.5177
4:1 nonMIP P1-A3	1.2689	1.3302	1.4198	2.2547	2.8774	3.1934	3.6934
4:1 nonMIP P1-A4	1.2559	1.3460	1.4171	2.2227	2.8531	3.1611	3.6398
4:1 MIP P1-A3	1.2117	1.2748	1.3333	2.1712	2.8108	3.1036	3.5856
4:1 MIP P1-A1	1.2000	1.2651	1.3070	2.1535	2.7767	3.0465	3.5395
4:1 MIP P1-A2	1.2423	1.2907	1.3304	2.1674	2.8634	3.1366	3.6344

Table 12

Average Equillibrium volume swelling ratio Q							
	pH=3.2	pH=4.0	pH=4.8	pH=5.4	pH=5.8	pH=6.0	pH=7.0
39:1 nonMIP	1.7841	2.9509	3.3579	6.5197	7.6186	8.2609	7.4935
39:1 MIP	1.8837	3.0346	3.4781	7.0589	8.3571	8.6999	8.6804
17:1 nonMIP	1.4923	1.8068	2.3798	4.1150	5.0938	5.3823	5.5892
17:1 MIP	1.4619	1.7563	2.3349	4.0057	4.9588	5.4485	5.5170
4:1 nonMIP	1.2472	1.3213	1.3970	2.2241	2.8452	3.1403	3.6170
4:1 MIP	1.2180	1.2769	1.3236	2.1640	2.8170	3.0956	3.5865

Table 13

STDEV Equillibrium volume swelling ratio Q							
	pH=3.2	pH=4.0	pH=4.8	pH=5.4	pH=5.8	pH=6.0	pH=7.0
39:1 nonMIP	0.040560978	0.032566	0.060726138	0.175579	0.244547	0.079823337	0.072408299
39:1 MIP	0.016823026	0.038236	0.039931908	0.106546	0.131509	0.175682858	0.150403683
17:1 nonMIP	0.01336459	0.005788	0.027227048	0.049468	0.053039	0.024964029	0.029318553
17:1 MIP	0.010481753	0.055409	0.01748192	0.083091	0.149069	0.16674499	0.165549433
4:1 nonMIP	0.027100825	0.030188	0.037238019	0.030035	0.036657	0.066025769	0.090048214
4:1 MIP	0.021835556	0.012945	0.014444023	0.009314	0.043676	0.045561828	0.0474197

Table 14

Determination of Number Average Molecular weight of the monomer (Mn)			
M:C ratio	**17_1**	**39_1**	**4_1**
Mn	872740.5744	983919.9	561457.3

Table 15

Determination of	*Molecular weight between crosslinker (Mc)*			
Peppas-Merril equiation		1/Mc=a-b/c		
	M:C ratio	**17_1**	**39_1**	**4_1**
A	**2/Mn**	2.29E-06	2.03E-06	3.56E-06

Table 16

b	pH=3.2	pH=4.0	pH=4.8	pH=5.4	pH=5.8	pH=6.0	pH=7.0
39:1 nonMIP P1-A1	-0.005515	-0.000962	-0.000654	-7.2E-05	-4.15E-05	-3.69E-05	-4.99E-05
39:1 nonMIP P1-A3	-0.005315	-0.000988	-0.000633	-7.1E-05	-5E-05	-3.64E-05	-4.92E-05
39:1 nonMIP P1-A6	-0.006281	-0.000919	-0.000583	-8.27E-05	-4.79E-05	-3.49E-05	-4.71E-05
39:1 MIP P1-A3	-0.004539	-0.000894	-0.000544	-6.15E-05	-3.51E-05	-3.19E-05	-3.1E-05
39:1 MIP P1-A1	-0.00481	-0.000889	-0.000579	-5.84E-05	-3.63E-05	-3.19E-05	-3.26E-05
39:1 MIP P1-A2	-0.004538	-0.00083	-0.000541	-5.6E-05	-3.3E-05	-2.87E-05	-2.94E-05
17:1 nonMIP P1-A1	-0.011282	-0.0053	-0.001899	-0.000308	-0.000156	-0.000134	-0.00012
17:1 nonMIP P1-A2	-0.012054	-0.00543	-0.002057	-0.000332	-0.000166	-0.000135	-0.000122
17:1 nonMIP P1-A3	-0.011282	-0.005362	-0.00197	-0.000315	-0.000162	-0.000137	-0.000118
17:1 MIP P1-A1	-0.012156	-0.0056	-0.002148	-0.000328	-0.000171	-0.000142	-0.000122
17:1 MIP P1-A2	-0.012789	-0.006907	-0.002135	-0.000342	-0.000162	-0.000133	-0.000116
17:1 MIP P1-A3	-0.012855	-0.005558	-0.002047	-0.000374	-0.000195	-0.000118	-0.000139
4:1 nonMIP P1-A5	-0.030646	-0.022808	-0.017908	-0.002648	-0.001132	-0.00084	-0.000534
4:1 nonMIP P1-A3	-0.024556	-0.019468	-0.014433	-0.002406	-0.001039	-0.000734	-0.000455
4:1 nonMIP P1-A4	-0.025885	-0.018412	-0.014558	-0.002531	-0.001069	-0.000759	-0.000477
4:1 MIP P1-A3	-0.031366	-0.023984	-0.01925	-0.002751	-0.001124	-0.000807	-0.000501
4:1 MIP P1-A1	-0.033124	-0.02493	-0.021191	-0.002833	-0.001172	-0.000858	-0.000523
4:1 MIP P1-A2	-0.027406	-0.022533	-0.019453	-0.002769	-0.001056	-0.000779	-0.00048

Table 17

c		pH=3.2	pH=4.0	pH=4.8	pH=5.4	pH=5.8	pH=6.0	pH=7.0
	39:1 nonMIP P1-A1	0.29874	0.18338	0.16178	0.07288	0.05876	0.05612	0.06319
	39:1 nonMIP P1-A3	0.29655	0.18477	0.15978	0.07228	0.06308	0.05564	0.06265
	39:1 nonMIP P1-A6	0.30900	0.18025	0.15514	0.07638	0.06176	0.05446	0.06134
	39:1 MIP P1-A3	0.28377	0.17972	0.15289	0.06926	0.05563	0.05352	0.05295
	39:1 MIP P1-A1	0.28704	0.17961	0.15635	0.06817	0.05661	0.05376	0.05426
	39:1 MIP P1-A2	0.28188	0.17603	0.15331	0.06754	0.05494	0.05193	0.05243
	17:1 nonMIP P1-A1	0.34691	0.29609	0.22621	0.12565	0.09815	0.09275	0.08920
	17:1 nonMIP P1-A2	0.35086	0.29767	0.23144	0.12908	0.10058	0.09324	0.08978
	17:1 nonMIP P1-A3	0.34889	0.29775	0.22857	0.12614	0.09921	0.09332	0.08820
	17:1 MIP P1-A1	0.35659	0.30195	0.23427	0.12722	0.10061	0.09379	0.08871
	17:1 MIP P1-A2	0.36066	0.31737	0.23382	0.12900	0.09832	0.09135	0.08667
	17:1 MIP P1-A3	0.36168	0.30188	0.23093	0.13292	0.10518	0.08703	0.09277
	4:1 nonMIP P1-A5	0.36307	0.35501	0.34668	0.24436	0.19400	0.17743	0.15386
	4:1 nonMIP P1-A3	0.34573	0.33968	0.32975	0.23712	0.18906	0.17040	0.14658
	4:1 nonMIP P1-A4	0.35701	0.34629	0.33716	0.24141	0.19077	0.17203	0.14847
	4:1 MIP P1-A3	0.35861	0.35222	0.34554	0.24607	0.19356	0.17532	0.15096
	4:1 MIP P1-A1	0.34981	0.34477	0.34088	0.24647	0.19567	0.17867	0.15331
	4:1 MIP P1-A2	0.33955	0.33602	0.33265	0.24403	0.18977	0.17354	0.14932

Table 18

Mc		pH=3.2	pH=4.0	pH=4.8	pH=5.4	pH=5.8	pH=6.0	pH=7.0
	39:1 nonMIP P1-A1	54.17	190.51	247.15	1009.86	1412.78	1514.99	1263.30
	39:1 nonMIP P1-A3	55.79	186.91	252.38	1015.98	1257.39	1523.38	1270.58
	39:1 nonMIP P1-A6	49.19	196.14	265.95	921.33	1285.19	1556.24	1298.63
	39:1 MIP P1-A3	62.51	200.90	280.64	1123.25	1577.74	1673.22	1700.64
	39:1 MIP P1-A1	59.67	201.87	269.79	1163.69	1553.31	1680.11	1656.60
	39:1 MIP P1-A2	62.11	212.12	283.29	1202.56	1657.63	1805.62	1779.75
	17:1 nonMIP P1-A1	30.75	55.86	119.09	407.39	630.09	693.42	740.14
	17:1 nonMIP P1-A2	29.10	54.81	112.50	388.16	605.12	688.24	733.20
	17:1 nonMIP P1-A3	30.92	55.52	116.02	400.33	611.14	677.68	744.39
	17:1 MIP P1-A1	29.33	53.91	109.04	388.06	585.99	659.55	723.28
	17:1 MIP P1-A2	28.20	45.94	109.49	376.92	606.56	685.87	747.89
	17:1 MIP P1-A3	28.13	54.31	112.78	355.42	538.29	739.14	665.27
	4:1 nonMIP P1-A5	11.85	15.56	19.36	92.26	171.30	211.14	288.00
	4:1 nonMIP P1-A3	14.08	17.45	22.84	98.52	181.83	232.03	321.61
	4:1 nonMIP P1-A4	13.79	18.81	23.16	95.36	178.32	226.49	310.63
	4:1 MIP P1-A3	11.43	14.69	17.95	89.40	172.05	217.18	300.77
	4:1 MIP P1-A1	10.56	13.83	16.09	86.97	166.91	208.06	292.83
	4:1 MIP P1-A2	12.39	14.91	17.10	88.12	179.56	222.65	310.90

Table19

Average Mc							
	pH=3.2	pH=4.0	pH=4.8	pH=5.4	pH=5.8	pH=6.0	pH=7.0
39:1 nonMIP	53.05	191.19	255.16	982.39	1318.45	1531.54	1277.50
39:1 MIP	61.43	204.96	277.90	1163.17	1596.22	1719.65	1712.33
17:1 nonMIP	30.26	55.40	115.87	398.63	615.45	686.45	739.24
17:1 MIP	28.55	51.39	110.43	373.47	576.94	694.85	712.15
4:1 nonMIP	13.24	17.27	21.79	95.38	177.15	223.22	306.75
4:1 MIP	11.46	14.48	17.04	88.16	172.84	215.96	301.50

Table 20

SDEV Mc							
	pH=3.2	pH=4.0	pH=4.8	pH=5.4	pH=5.8	pH=6.0	pH=7.0
39:1 nonMIP	3.436867	4.648895	9.703219	52.96795	82.86053	21.80063	18.65535
39:1 MIP	1.537607	6.218032	7.152183	39.65693	54.56301	74.52999	62.40097
17:1 nonMIP	1.003328	0.538101	3.299687	9.726207	13.03076	8.022693	5.65053
17:1 MIP	0.673226	4.717596	2.04119	16.59437	35.02346	40.54945	42.42374
4:1 nonMIP	1.214043	1.628422	2.109651	3.130519	5.361222	10.82524	17.14069
4:1 MIP	0.914766	0.571073	0.932835	1.216626	6.363982	7.369219	9.058256

Table 21

Average Number of linkes between two-crosslinks (n)							
	pH=3.2	pH=4.0	pH=4.8	pH=5.4	pH=5.8	pH=6.0	pH=7.0
39:1 nonMIP	1.23	4.44	5.93	22.82	30.63	35.58	29.67
39:1 MIP	1.43	4.76	6.46	27.02	37.08	39.95	39.78
17:1 nonMIP	0.70	1.29	2.69	9.26	14.30	15.95	17.17
17:1 MIP	0.66	1.19	2.57	8.68	13.40	16.14	16.54
4:1 nonMIP	0.31	0.40	0.51	2.22	4.12	5.19	7.13
4:1 MIP	0.27	0.34	0.40	2.05	4.01	5.02	7.00

Table 22

SDEV Number of linkes between two-crosslinks (n)							
	pH=3.2	pH=4.0	pH=4.8	pH=5.4	pH=5.8	pH=6.0	pH=7.0
39:1 nonMIP	0.079834	0.107988	0.225394	1.230382	1.924751	0.506403	0.433341
39:1 MIP	0.035717	0.144437	0.166137	0.921183	1.267434	1.731243	1.4495
17:1 nonMIP	0.023306	0.012499	0.076648	0.225928	0.302689	0.186358	0.131255
17:1 MIP	0.015638	0.109584	0.047414	0.385467	0.813553	0.941915	0.985453
4:1 nonMIP	0.028201	0.037826	0.049005	0.072718	0.124535	0.251457	0.398158
4:1 MIP	0.021249	0.013265	0.021669	0.028261	0.147828	0.171178	0.210412

Table 23

Average Correlation length or mesh size (□) nm							
	pH=3.2	pH=4.0	pH=4.8	pH=5.4	pH=5.8	pH=6.0	pH=7.0
39:1 nonMIP	0.793675	1.78224	2.149469	5.261308	6.41969	7.109469	6.285509
39:1 MIP	0.869867	1.862616	2.269768	5.879078	7.28576	7.663985	7.642125
17:1 nonMIP	0.564864	0.814662	1.29145	2.875182	3.835933	4.126271	4.336204
17:1 MIP	0.545005	0.776878	1.252866	2.757918	3.680309	4.167802	4.236897
4:1 nonMIP	0.351785	0.409614	0.46865	1.145579	1.694835	1.965955	2.41568
4:1 MIP	0.324774	0.370895	0.407275	1.091433	1.668492	1.924618	2.388443

Table 24

SDEV Correlation length or mesh size (□) nm							
	pH=3.2	pH=4.0	pH=4.8	pH=5.4	pH=5.8	pH=6.0	pH=7.0
39:1 nonMIP	0.031857	0.028208	0.053749	0.189714	0.26958	0.07344	0.066087
39:1 MIP	0.013481	0.036007	0.037919	0.129805	0.162275	0.217074	0.182913
17:1 nonMIP	0.011078	0.004817	0.023322	0.046595	0.053783	0.030466	0.024094
17:1 MIP	0.007713	0.044183	0.014688	0.080472	0.148982	0.163872	0.169018
4:1 nonMIP	0.018834	0.02247	0.027085	0.023957	0.032964	0.061604	0.087742
4:1 MIP	0.014869	0.008484	0.012551	0.009014	0.039315	0.042324	0.046379

Table 25

Average Correlation length or mesh size (□) A							
	pH=3.2	pH=4.0	pH=4.8	pH=5.4	pH=5.8	pH=6.0	pH=7.0
39:1 nonMIP	7.936753	17.8224	21.49469	52.61308	64.1969	71.09469	62.85509
39:1 MIP	8.698671	18.62616	22.69768	58.79078	72.8576	76.63985	76.42125
17:1 nonMIP	5.648644	8.146623	12.9145	28.75182	38.35933	41.26271	43.36204
17:1 MIP	5.450051	7.768777	12.52866	27.57918	36.80309	41.67802	42.36897
4:1 nonMIP	3.517849	4.096142	4.686504	11.45579	16.94835	19.65955	24.1568
4:1 MIP	3.247743	3.708952	4.072755	10.91433	16.68492	19.24618	23.88443

Table 26

SDEV Correlation length or mesh size (□) A							
	pH=3.2	pH=4.0	pH=4.8	pH=5.4	pH=5.8	pH=6.0	pH=7.0
39:1 nonMIP	0.318568	0.282082	0.537485	1.897141	2.695797	0.734402	0.660865
39:1 MIP	0.134808	0.360071	0.379186	1.298049	1.622753	2.170741	1.829125
17:1 nonMIP	0.110781	0.048173	0.233216	0.46595	0.537833	0.304658	0.240939
17:1 MIP	0.077125	0.441825	0.146882	0.804724	1.489817	1.638724	1.690179
4:1 nonMIP	0.188339	0.224696	0.270853	0.239566	0.329636	0.616042	0.877418
4:1 MIP	0.148691	0.084838	0.125506	0.090142	0.393145	0.42324	0.463792

Appendix G – Binding Study Calculation Example

1. The concentration of Hydrocortisone in the batch solution was estimated using a calibration curve generated y UV spectroscopy at 242 nm
2. The Langmuir isotherm was employed to calculate the amount of hydrocortisone that remains in the solution

$$\frac{q}{C} = bq_s - bq \quad \text{(equation G.1)}$$

3. Refer to raw data in table 1

Appendix H – Binding Study Raw Data

Table 1

	Bounded	Bounded/Free
MIP	0.0717	0.328
	0.0766	0.177
	0.0821	0.143
	0.0884	0.0548

Appendix I – Electrochemical Study Calculation Example

1. The resistivity of imprinted and non-imprinted polymers was measured

2. It was calculated using the following equation

$$\rho = \left(R_{gel} - R_u\right) * \frac{A}{l} \quad \textbf{(equation I.1)}$$

3. Refer to raw data in table 1.

4. The Delta Y was estimated by calculating the difference between the resistivity of the polymer at the buffer and with the buffer in the presence of hydrocortisone. (refer to raw data in table 3)

Appendix J – Electrochemical Study Raw Data

Table 1

Hydrogel Type	Composition	Resistivity @ pH =3.2	Resistivity @ pH =4.8	Resistivity @ pH =5.4	Swelling @ pH =3.2	Swelling @ pH =4.8	Swelling @ pH =5.4
non MIP	39:1 nonMIP R1	101.211	67.638	41.071	1.79817	3.30734	6.6055
non MIP	39:1 nonMIP R2	137.377	62.903	21.7417	1.81567	3.34101	6.6359
non MIP	39:1 nonMIP R3	125.275	64.715	17.5776	1.73832	3.42523	6.3178
MIP	39:1 MIP R1	253.884	60.03	47.9379	1.8934	3.49746	6.9492
MIP	39:1 MIP R2	166.096	97.317	33.0831	1.86432	3.43216	7.0653
MIP	39:1 MIP R3	238.728	73.954	35.5755	1.89352	3.50463	7.162
non MIP	17:1 nonMIP R1	441.351	72.993	57.1271	1.5	2.40625	4.1563
non MIP	17:1 nonMIP R2	451.731	108.018	60.7907	1.47685	2.35185	4.0602
non MIP	17:1 nonMIP R3	441.801	100	52.2122	1.5	2.38119	4.1287
MIP	17:1 MIP R1	705.215	108.208	66.5865	1.47396	2.32292	4.0781
MIP	17:1 MIP R2	639.499	119.029	74.4944	1.45673	2.32692	4.024
MIP	17:1 MIP R3	588.408	142.512	50.4904	1.455	2.355	3.915

Table 2

Hydrogel Type	Composition	Buffer	pH	Average Resistance (ohms) (450 samples)	Resistance Standard Deviation (450 samples)	Average Resistivity (ohms*cm) (450 samples)	Standard Deviation (450 samples)
non-MIP	17/1	Plain	3.2	14.74	0.73	442.6422	21.9219
non-MIP	17/1	Plain	4.8	3.07	0.54	92.1921	16.2162
non-MIP	17/1	Plain	5.4	1.85	0.21	55.5555	6.3063
non-MIP	39/1	Plain	3.2	4.02	0.55	120.7206	16.5165
non-MIP	39/1	Plain	4.8	2.17	0.15	65.1651	4.5045
non-MIP	39/1	Plain	5.4	0.87	0.39	26.1261	11.7117
non-MIP	17/1	Saturated	3.2	21.55	2.19	647.1465	65.7657
non-MIP	17/1	Saturated	4.8	2.99	0.44	89.7897	13.2132
non-MIP	17/1	Saturated	5.4	2.03	0.55	60.9609	16.5165
non-MIP	39/1	Saturated	3.2	5.43	1.00	163.0629	30.03
non-MIP	39/1	Saturated	4.8	1.9	0.33	57.057	9.9099
non-MIP	39/1	Saturated	5.4	1.098	0.15	32.97294	4.5045
MIP	17/1	Plain	3.2	21.45	1.97	644.1435	59.1591
MIP	17/1	Plain	4.8	4.11	0.5	123.4233	15.015
MIP	17/1	Plain	5.4	2.12	0.36	63.6636	10.8108
MIP	39/1	Plain	3.2	7.27	1.31	218.3181	39.3393
MIP	39/1	Plain	4.8	2.53	0.51	75.9759	15.3153
MIP	39/1	Plain	5.4	1.26	0.25	37.8378	7.5075
MIP	17/1	Saturated	3.2	41.98	6.64	1260.6594	199.3992
MIP	17/1	Saturated	4.8	14.12	3.46	424.0236	103.9038
MIP	17/1	Saturated	5.4	1.34	0.28	40.2402	8.4084
MIP	39/1	Saturated	3.2	16.3	2.61	489.489	78.3783
MIP	39/1	Saturated	4.8	7.13	2.40	214.1139	72.072
MIP	39/1	Saturated	5.4	1.15	0.20	34.5345	6.006

Table 3

	pH	Delta Y (Rbinding - Rgel)
17:1 MIP	3.2	616.5159
17:1 MIP	4.8	300.6003
17:1 MIP	5.4	23.4234
17:1 non MIP	3.2	204.5043
17:1 non MIP	4.8	2.4024
17:1 non MIP	5.4	5.4054
39:1 MIP	3.2	271.1709
39:1 MIP	4.8	138.138
39:1 MIP	5.4	3.3033
39:1 non MIP	3.2	42.3423
39:1 non MIP	4.8	8.1081
39:1 non MIP	5.4	6.84684